

Journal of Polymer Science **Part A-2: Polymer Physics**

Board of Editors: H. Mark · C. G. Overberger · T. G. Fox

Advisory Editors:

R. M. Fuoss · J. J. Hermans · H. W. Melville · G. Smets

Editor: T. G. Fox **Associate Editors:** E. F. Casassa · H. Markovitz

Advisory Board:

G. Allen	G. Gee	S. Krimm	R. Simha
F. R. Anderson	A. N. Gent	M. Kurata	W. P. Slichter
W. O. Baker	W. E. Gibbs	R. F. Landel	T. L. Smith
H. Benoit	S. Gratch	P. H. Lindenmeyer	W. O. Statton
F. A. Bovey	C. A. J. Hoeve	L. Mandelkern	R. S. Stein
A. M. Bueche	J. D. Hoffman	B. Maxwell	W. H. Stockmayer
R. H. Cole	R. E. Hughes	L. Nielsen	M. Takayanagi
H. Eisenberg	H. D. Keith	A. Peterlin	A. V. Tobolsky
J. D. Ferry	A. Keller	R. S. Porter	K. Wolf
E. W. Fischer	A. J. Kovacs	F. Price	B. Wunderlich
P. J. Flory	G. Kraus	G. V. Schulz	
H. Fujita	W. R. Krigbaum	A. R. Shultz	

The Journal of Polymer Science is published in four sections as follows: Part A-1, Polymer Chemistry, monthly; Part A-2, Polymer Physics, monthly; Part B, Polymer Letters, monthly; Part C, Polymer Symposia, irregular.

Published monthly by Interscience Publishers, a Division of John Wiley & Sons, Inc., covering one volume annually. Publication Office at 20th and Northampton Sts., Easton, Pa. 18042. Executive, Editorial, and Circulation Offices at 605 Third Avenue, New York, N.Y. 10016. Second-class postage paid at Easton, Pa. Subscription price, \$325.00 per volume (including Parts A-1, B, and C). Foreign postage \$15.00 per volume (including Parts A-1, B, and C).

Copyright © 1971 by John Wiley & Sons, Inc. All rights reserved. No part of this publication may be reproduced by any means, nor transmitted, nor translated into a machine language without the written permission of the publisher.

Optical Anisotropy of Polymer Chains and Markov Processes. I. Polyethylene

BERNARD LEMAIRE and GEORGES FOURCHE, *Centre de Recherches Paul Pascal, Domaine Universitaire, 33 Talence, France*

Synopsis

A study of the average molecular optical anisotropy ($\langle \gamma^2 \rangle$) of tetrahedral lattice polyethylene chains of any length has been carried out by using Markov processes. The results of this treatment include simplified models of polymer chains, as well as more elaborate models, which are in current use.

INTRODUCTION

The anisotropy of the molecular polarizability (optical anisotropy) γ^2 can be defined¹ by the expression

$$\gamma^2 = \frac{1}{2}[(\alpha_{XX} - \alpha_{YY})^2 + (\alpha_{YY} - \alpha_{ZZ})^2 + (\alpha_{ZZ} - \alpha_{XX})^2] + 3(\alpha_{XY}^2 + \alpha_{YZ}^2 + \alpha_{ZX}^2) \quad (1)$$

where the quantities α_{XX} , α_{YY} , etc. are the components of the molecular polarizability tensor α with respect to cartesian molecular fixed axes X , Y , Z . It is known that the molecular optical anisotropy is a quantity which is very sensitive to conformations of polymers in solution. Thus, a statistical calculation of the average molecular optical anisotropy $\langle \gamma^2 \rangle$ of polymer chains has been undertaken. Calculations of $\langle \gamma^2 \rangle$ for linear chains were recently carried out by direct enumeration of all molecular conformations^{1,2} and by matrix methods.³⁻⁶ The relation between Markov processes and the conformational statistics of chains has been developed⁷ previously for simple cases, in connection with studies of average dimensions and dipole moments. Therefore, in the present work (as outlined in a previous note⁸) a method of evaluation of $\langle \gamma^2 \rangle$ by using Markov processes is presented first for a simple chain, polyethylene (PE), and then for a somewhat more complex chain, polyoxyethylene (POE). In order to give an overall view of the method used in this work, a comparative study of molecular optical anisotropy of these chains is carried out for various models. Three models of molecular chains will be considered successively, corresponding to: (1) equally probable internal rotations (first-order Markov chain), (2) independent internal rotations (second-order Markov chain), (3) interdependent internal rotations (third-order Markov process). The treatment in this paper will be limited to the special but important

case of tetrahedral lattice chains. However, a possibility of extension of the results, for nonlattice chains, will be indicated. Finally, it will be pointed out that certain conditional probabilities derived here could be useful in the simulation of lattice chains.

A general, Markov process of order r can be characterized by the relation (2):

$$\begin{aligned} \Pr(X_n = \theta_n / X_{n-1} = \theta_{n-1}, \dots, X_1 = \theta_1) \\ = \Pr(X_n = \theta_n / X_{n-1} = \theta_{n-1}, \dots, X_{n-r} = \theta_{n-r}) \\ = f(\theta_n, \theta_{n-1}, \dots, \theta_{n-r}, n) \end{aligned} \quad (2)$$

in which X_n is the state of the system at time n , θ_n is a possible outcome of X_n , and the slant bar (/) stands for "knowing that." When $r = 1$, the process is called a simple Markov process. If the probabilities in eq. (2) are independent of n , one is dealing with a finite Markov chain of order r ; when $r = 1$, this chain is a simple finite Markov chain.

It is important to note that in a discrete Markov process the changes of state, or "transitions," occur at successive moments, whereas in a real polymer chain the states of all the elements, i.e., the various conformations of all the monomer units, exist simultaneously. Consequently, the conformations of all real chains in solution do not have a Markov character.^{7,9} However, it will be shown in this study that it is always possible to define, on the basis of the real statistics of the molecule, a probabilistic model of the chain to which can be applied the results of the general theory of Markov processes.

PHYSICAL MODEL AND BASIC EQUATIONS

In the present treatment the usual assumption of additivity of bond polarizabilities will be made. The validity of this assumption has been discussed at length. However, from numerous results obtained in this laboratory^{1,2,10-13} it appears that it is a good approximation for molecules in dilute solution.

Consider a polyethylene chain $\text{H}-(\text{CH}_2)_{n+1}\text{H}$ in which the carbon skeleton comprises n C—C bonds. Such a chain is composed only of C—C and C—H single bonds, which, from the optical point of view, have essentially axial symmetry. In order to simplify the optical problem it will be assumed that in these molecules all valence angles are tetrahedral. It can be shown^{14,15} that under these conditions the chain is equivalent to a molecule containing only C—C bonds, each one possessing an optical anisotropy equal to $\Gamma = \gamma_{\text{CC}} - 2\gamma_{\text{CH}}$, where $\gamma_{\text{CC}} = \alpha_{\text{CC}}^{\parallel} - \alpha_{\text{CC}}^{\perp}$ and $\gamma_{\text{CH}} = \alpha_{\text{CH}}^{\parallel} - \alpha_{\text{CH}}^{\perp}$, are, respectively, the optical anisotropies of the C—C and C—H bonds. $\alpha_{\text{CC}}^{\parallel}$, $\alpha_{\text{CH}}^{\parallel}$, $\alpha_{\text{CC}}^{\perp}$, and $\alpha_{\text{CH}}^{\perp}$ are the principal optical polarizabilities parallel and perpendicular to the bonds considered. Finally, the molecular deformations will be described by using the theory of rotational isomers,¹⁶ in which each conformation of the molecule is characterized by a series of rota-

tion angles, $\varphi_3, \varphi_4, \dots, \varphi_n$, associated with successive bonds in the chain. The angle φ_j is the dihedral angle between the planes defined by the pairs of bonds $(j-2, j-1)$ and $(j-1, j)$. It is known that in polyethylene each C—C bond can exist in three isomeric states one *trans* (*t*) and two *gauche* (*g* and *g'*), corresponding to the internal rotation angles $0, +120^\circ$, and -120° , with respect to the preceding bond pair.

On the basis of the model just described the molecular optical anisotropy γ^2 of a rigid conformation of the molecule is given by^{14,15}

$$\gamma^2 = \left[\frac{4}{3} (n_1^2 + n_2^2 + n_3^2 + n_4^2) - (n^2/3) \right] \Gamma^2 \quad (3)$$

in which n_1, \dots, n_4 are the numbers of C—C bonds parallel, respectively, to each of the four directions belonging to the set $\Omega = \{1, 2, 3, 4\}$, of a reference system of the molecule represented by the diagonals of a cube. As the average values of n_i^2 are independent of i , one can write

$$\langle \gamma^2 \rangle = [(16/3) \langle n_1^2 \rangle - (n^2/3)] \Gamma^2 \quad (4)$$

It is necessary to rewrite eq. (4) in terms of probability. The rotation at time j of a given bond of the chain about the previous bond will represent the result of a trial denoted by a number to indicate the direction adopted by this bond, i.e., an element of the finite set Ω . The state of internal rotation of the j -th bond, which is its direction relative to the molecular reference system (the cube diagonals), will be designated by Y_j . In general, the state at time j of a set of r successive bonds can be represented by the r -uplet

$$X_j = (Y_{j-r+1}, Y_{j-r+2}, \dots, Y_j)$$

Let A_j be a random variable which is equal to unity when the event $\{Y_j = 1\}$ is realized and zero otherwise, where $1 \leq j \leq n$. Then, we have

$$\begin{aligned} n_1 &= \sum_{j=1}^n A_j \\ n_1^2 &= \sum_j A_j^2 + 2 \sum_{j < k} A_j A_k \\ \langle n_1^2 \rangle &= \sum_j \langle A_j^2 \rangle + 2 \sum_{j < k} \langle A_j A_k \rangle \\ \langle n_1^2 \rangle &= \sum_j \text{Pr}(Y_j = 1) + 2 \sum_{j < k} \text{Pr}(Y_j = 1 \text{ and } Y_k = 1) \end{aligned} \quad (5)$$

EQUALLY PROBABLE INTERNAL ROTATIONS

In this section a very simplified chain model will be presented in order to illustrate the calculation of $\langle \gamma^2 \rangle$. Suppose that the various positions resulting from internal rotations of all of the bonds of the chain are equally probable. Then, each bond can assume with probability $1/3$ each of the three positions $0, +120^\circ$, and -120° . Thus, since the bonds are numbered

in arbitrary order, each can take with equal probability any one of the three directions other than that of the preceding bond. The numbers identifying these directions are members of the set Ω .

This model is essentially equivalent to that known as the freely rotating model.¹⁷ However, in the present model the choice of tetrahedral angles and of the three internal rotation angles 0 , $+120^\circ$, and -120° allows the chain configuration to be described on the basis of a tetrahedral lattice. It will be found that the general molecular configuration can be studied by a simple Markov chain (order 1). Thus, the internal rotational state of the j th bond is represented by $X_j = (Y_j)$.

Let the compound events be defined by

$$\{X_j = a\} = \{X_j = 1\}$$

and (6)

$$\{X_j = b\} = \bigcup_{\alpha=2}^4 \{X_j = \alpha\}$$

where the symbol U has the probabilistic sense of union and the event $\{X_j = b\}$, for example, indicates that the random variable X_j is in the state 2, 3, or 4, representing the corresponding direction of the j -th bond. These states will be described symbolically by $a = (1)$ and $b = \bigcup_{\alpha=2}^4 (\alpha)$, respectively.

The various transition probabilities corresponding to states a and b are given by

$$\left. \begin{aligned} \Pr(X_{j+1} = a/X_j = a) &= P_{aa} = 0 & \Pr(X_{j+1} = b/X_j = a) &= P_{ab} = 1 \\ \Pr(X_{j+1} = a/X_j = b) &= P_{ba} = 1/3 & \Pr(X_{j+1} = b/X_j = b) &= P_{bb} = 2/3 \end{aligned} \right\} \quad (7)$$

and the related matrix, which is of the form

$$\mathbf{P} = \begin{bmatrix} P_{aa} & P_{ab} \\ P_{ba} & P_{bb} \end{bmatrix} = \begin{bmatrix} 0 & 1 \\ 1/3 & 2/3 \end{bmatrix} \quad (8)$$

characterizes a simple and a regular Markov chain for the states a and b . If it is noted that

$$\Pr(Y_j = 1 \text{ and } Y_k = 1) = \Pr(X_j = a \text{ and } X_k = a) = \Pr(X_j = a) \Pr(X_k = a/X_j = a)$$

$$\Pr(Y_j = 1) = \Pr(X_j = a) = \frac{1}{4} \quad \forall j$$

and that

$$\Pr(X_k = a/X_j = a) = [\mathbf{P}^{k-j}]_{11}$$

where the subscripts identify the (1, 1) element of the matrix product. Then eq. (5) becomes

$$\langle n_1^2 \rangle = \frac{n}{4} + \frac{1}{2} [\mathbf{P} \mathbf{S}_{n-1}]_{11} \quad V_n \geq 1 \quad (9)$$

where \mathbf{S}_n is defined by

$$\mathbf{S}_n = \sum_{j=1}^n \sum_{k=j}^n \mathbf{P}^{k-j} \quad V_n \geq 1$$

and

$$\mathbf{S}_0 = \mathbf{0}$$

Utilizing specific properties^{18,19} of regular stochastic matrix one can show that

$$\mathbf{S}_n = \frac{n^2 \mathbf{P}^*}{2} + n[\mathbf{Z} - (\mathbf{P}^*/2)] + (\mathbf{Z} - \mathbf{Z}^2) + (\mathbf{P}^{n+1} \mathbf{Z}^2 - \mathbf{P}^*) \quad (10)$$

where

$$\mathbf{P}^* = \lim_{n \rightarrow \infty} \mathbf{P}^n$$

and

$$\mathbf{Z} = [\mathbf{I}_2 - (\mathbf{P} - \mathbf{P}^*)]^{-1}$$

These last matrices have the form

$$\mathbf{P}^* = \begin{vmatrix} \frac{1}{4} & \frac{3}{4} \\ \frac{1}{4} & \frac{3}{4} \end{vmatrix}$$

and

$$\mathbf{Z} = \begin{vmatrix} 13/16 & 3/16 \\ 1/16 & 15/16 \end{vmatrix} \quad (11)$$

By developing eq. (9) with the aid of the expression for \mathbf{S}_{n-1} obtained from eq. (10), one obtains

$$\langle n_1^2 \rangle = \frac{n^2}{16} + \frac{3n}{32} + \frac{9}{128} + (\mathbf{P}^{n+1} \mathbf{Z}^2 - \mathbf{P}^*)_{11} \quad (12)$$

Finally, by substitution of eq. (12) in eq. (4) the average molecular optical anisotropy of the chain becomes

$$\langle \gamma^2 \rangle / \Gamma^2 = \frac{n}{2} + \frac{3}{8} + \frac{16}{3} (\mathbf{P}^{n+1} \mathbf{Z}^2 - \mathbf{P}^*)_{11} \quad V_n \geq 1 \quad (13)$$

A number of comments can be made concerning the above results: (1) since

$$\mathbf{P}^{n+1} \mathbf{Z}^2 = \mathbf{P}^*$$

the asymptotic behavior of $\langle \gamma^2 \rangle$ can be easily obtained for large values of n ; (2) by diagonalization of \mathbf{P} one could obtain in this particular case the much simpler form^{17,20}

$$\langle \gamma^2 \rangle / \Gamma^2 = \frac{n}{2} + \frac{3}{8} \left[1 - \left(-\frac{1}{3} \right)^n \right]$$

however, the diagonalization method would lead to less general results than eq. (13).

INDEPENDENT INTERNAL ROTATION*

It will be assumed here that internal rotations of the various bonds of the chain in their valence cones are not equally probable. These rotations are hindered by the interactions between different atoms in the molecule. Accordingly, a probability which takes into account these interaction forces must be attributed to each of the states of internal rotation, 0 , $+120^\circ$, and -120° (t , g , and g').

If it is assumed that each of the internal rotation angles $\varphi_3, \varphi_4, \dots, \varphi_n$ is independent of its neighbor, the total energy, $E(\varphi_3, \varphi_4, \dots, \varphi_n)$ of a given molecular conformation can be expressed in the form

$$E(\varphi_3, \varphi_4, \dots, \varphi_n) = \sum_{j=3}^n E(\varphi_j) \quad (14)$$

This assumption is equivalent to considering, along the chain, successive elementary sequences of three bonds of energy $E(\varphi_j)$. Thus, only interactions between groups of nonbonded atoms separated by three bonds of the molecular skeleton are considered.

Probabilistic Analysis of the Chain

Statistical Weights. The statistical weight of a given conformation of the chain can be defined by a product $u_3 u_4 \dots u_n$ of statistical weights, where

$$u_j = \exp \{ -E(\varphi_j) / RT \}$$

with R the gas constant and T the absolute temperature. On the basis of the preceding hypotheses these statistical weights are mutually independent. The *trans* form of the elementary unit of three bonds will be chosen as the reference state and arbitrarily assigned a statistical weight of unity.

* The treatment presented here is somewhat different from and more general than that of Lemaire et al.⁸

The states g and g' thus have a statistical weight $\sigma = \exp \{-\Delta E_\sigma/RT\}$, where ΔE_σ is the difference in energy between a given *gauche* isomer and the *trans* form. Consequently, the respective probabilities of *trans* and *gauche* forms along the chain become

$$\Pr(t) = 1/(1 + 2\sigma) = p$$

and (15)

$$\Pr(g) = \Pr(g') = \sigma/(1 + 2\sigma) = q$$

where

$$p + 2q = 1$$

These probabilities are independent of the chain length.

Markov Chain. It has just been shown that the general configuration of the molecular chain can be uniquely described by the conformations t , g , and g' of the groups of three successive bonds. The characterization of any of these elementary conformations for a bond j relative to the reference system (diagonals of a cube) evidently necessitates the knowledge of the direction numbers of the two bonds $j - 2, j - 1$ adjacent to it.

From the probabilistic point of view the molecular chain behaves as a second-order Markov chain. It will be shown that such a chain can be reduced to a simple one.

Let $X_j = (Y_{j-1}, Y_j)$ represent the internal rotational state of bonds $j - 1$ and j . The transition from the state X_j to the state X_{j+1} , if it is allowed, defines one of the various conformations t , g , or g' described previously. Consider, in schematic notation, the states

$$\begin{aligned} a &= \underset{\alpha=2}{U}^4(\alpha, 1) \\ b &= \underset{\substack{\alpha, \beta=2 \\ \alpha \neq \beta}}{U}^4(\alpha, \beta) \\ c &= \underset{\alpha=2}{U}^4(1, \alpha) \end{aligned} \quad (16)$$

where the event $\{X_j = a\}$, for example, indicates that the random variable X_j is in the state (2, 1), or (3, 1), or (4, 1). A state of the type a , b , or c will be designated by E_j , that is $E_j \in \{a, b, c\}$. The theorem on conditional probabilities yields the relation

$$\begin{aligned} \Pr(X_{j+1} = E_{j+1}/X_j = E_j, \dots, X_i = E_i) \\ = \frac{\Pr(X_i = E_i, \dots, X_j = E_j, X_{j+1} = E_{j+1})}{\Pr(X_i = E_i, \dots, X_j = E_j)} \end{aligned} \quad 2 \leq i \leq j - 1 \quad (17)$$

In passing to the statistical weight of the corresponding conformation and designating by ϵ_j^k any conformation of the set of bonds j to k , one can write the above ratio as

$$\frac{\left(\sum_{\epsilon_3^j/X_i=E_i, \dots, X_j=E_j} u_3 u_1 \dots u_j\right) \left(\sum_{\epsilon_{j+1}^{j+1}/X_j=E_j, X_{j+1}=E_{j+1}} u_{j+1}\right) \times \left(\sum_{\epsilon_{j+2}^n/X_{j+1}=E_{j+1}} u_{j+2} u_{j+3} \dots u_n\right)}{\left(\sum_{\epsilon_3^j/X_i=E_i, \dots, X_j=E_j} u_3 u_1 \dots u_j\right) \left(\sum_{\epsilon_{j+1}^n/X_j=E_j} u_{j+1} u_{j+2} \dots u_n\right)} \quad (18)$$

Then eq. (17) becomes, for $2 \leq i \leq j - 1$

$$\begin{aligned} \Pr(X_{j+1} = E_{j+1}/X_j = E_j, \dots, X_i = E_i) &= \frac{\sum_{\epsilon_{j+1}^{j+1}/X_j=E_j, X_{j+1}=E_{j+1}} u_{j+1}}{1 + 2\sigma} \\ &= \Pr(X_{j+1} = E_{j+1}/X_j = E_j) \end{aligned} \quad (19)$$

It is seen that these probabilities are independent of i and j , and that one is concerned with a simple Markov chain.

The matrix of the transition probabilities can be written

$$\mathbf{P} = \begin{vmatrix} P_{aa} & P_{ab} & P_{ac} \\ P_{ba} & P_{bb} & P_{bc} \\ P_{ca} & P_{cb} & P_{cc} \end{vmatrix} = \begin{vmatrix} 0 & 0 & 1 \\ q & p + q & 0 \\ p & 2q & 0 \end{vmatrix} \quad (20)$$

For $q \neq 0$ this matrix characterizes a simple and regular Markov chain for the two-bond states a, b , and c .

Average Molecular Optical Anisotropy

From symmetry considerations, which are independent of all hypotheses concerning intramolecular interactions in the chain, one has

$$\Pr(Y_j = 1) = \Pr(X_j = a) = \frac{1}{4}$$

and

$$\Pr(Y_{j-1} = 1) = \Pr(X_j = c) = \frac{1}{4}$$

From eq. (5) one can write $V_n \geq 3$,

$$\begin{aligned} \langle n_1^2 \rangle &= \frac{n}{4} + 2 \sum_{k=2}^n \Pr(Y_1 = 1 \text{ and } Y_k = 1) \\ &\quad + 2 \sum_{j=2}^{n-1} \sum_{k=j+1}^n \Pr(Y_j = 1 \text{ and } Y_k = 1) \end{aligned} \quad (21)$$

and, by expressing eq. (21) in terms of the matrix \mathbf{P} one finds for $q \neq 0$

$$\langle n_1^2 \rangle = \frac{n}{4} + \frac{1}{2} [\mathbf{P}\mathcal{S}_{n-1}]_{11} \quad V_n \geq 1 \quad (22)$$

After further developments one obtains for $q \neq 0$

$$\langle n_1^2 \rangle = \frac{n^2}{16} + n \left(\frac{\mathbf{Z}_{11}}{2} - \frac{5}{16} \right) + \frac{1}{2} (\mathbf{Z} - \mathbf{Z}^2)_{11} + \frac{1}{2} (\mathbf{P}^{n+1}\mathbf{Z}^2 - \mathbf{P}^*)_{11} \quad (23)$$

with

$$\mathbf{P}^* = \begin{bmatrix} 1 & 1 & 1 \\ 4 & 2 & 4 \\ 1 & 1 & 1 \\ 4 & 2 & 4 \\ 1 & 1 & 1 \\ 4 & 2 & 4 \end{bmatrix}$$

and

$$\mathbf{Z} = \frac{1}{4q} \begin{bmatrix} 7q+2 & 3q-2 & 3q+2 \\ 4 & 2 & 4 \\ 7q-2 & 3q+2 & 3q-2 \\ 4 & 2 & 4 \\ 2-5q & 7q-2 & 7q+2 \\ 4 & 2 & 4 \end{bmatrix} \quad (24)$$

Finally, carrying out the indicated calculations one finds the expression

$$\langle \gamma^2 \rangle / \Gamma^2 = \frac{2-3q}{6q} n + \frac{9q^2+12q-4}{24q^2} + \frac{8}{3} (\mathbf{P}^{n+1}\mathbf{Z}^2 - \mathbf{P}^*)_{11} \quad (25)$$

A number of comments can be made concerning the above results:

We have

$$\lim_{n \rightarrow \infty} \mathbf{P}^{n+1}\mathbf{Z}^2 = \mathbf{P}^*$$

if one puts $p = q = 1/3$ in eq. (25), one finds results corresponding to the first-order case.

For $q = 0$ the chain is entirely extended, and γ^2 can be calculated from eq. (3). In this case a summation formula can be established which leads to an expression in n^2 . However, the two cases $q = 0$ and $q \neq 0$ are fundamentally different and cannot be treated by the same method.

Finally, it should be noted that the form of eq. (25) is particularly convenient for programming numerical calculations, as this expression involves only matrix multiplication.

INTERDEPENDENT INTERNAL ROTATIONS

In a real molecular chain, forces act between all pairs of atoms. Hence, all quantities which depend on interatomic forces are interdependent. In particular, the potential functions for internal rotations about the various

bonds should be interdependent. A reasonable approximation is to assume that the potential energy for rotation about a given bond depends only on the rotational states of nearest-neighboring bonds. Then, the total energy $E(\varphi_3, \varphi_1, \dots, \varphi_n)$ of a given configuration of the molecule can be written in the form

$$E(\varphi_3, \varphi_1, \dots, \varphi_n) = \sum_{j=3}^n E(\varphi_{j-1}, \varphi_j) \quad (26)$$

where it is noted that the first term in the summation is a function of only one angle, because of the absence of a preceding bond at the end of the chain. This result leads to successive consideration of sequences of four bonds along the chain and of energy $E(\varphi_{j-1}, \varphi_j)$. Thus, interactions among groups of atoms separated by three and four bonds of the molecular skeleton are included.

Probabilistic Analysis of the Chain

Statistical Weights. The statistical weight of a given chain conformation will again be defined as the product $u_3 u_4 \dots u_n$ of interdependent statistical weights such that $u_j = \exp \{ -E(\varphi_{j-1}, \varphi_j)/RT \}$. It was noted above that each sequence of three bonds can adopt three different conformations because of the threefold periodicity of the potential function. Hence, in a unit of four bonds it will be necessary to consider nine different conformations. The completely *trans* form will be arbitrarily chosen as the reference state and assigned a statistical weight of unity. Thus, the following statistical weights will be assigned to the conformations of three bonds: $1(t)$ and $\sigma(g, g')$. For four bonds the corresponding weights are $1(tt, tg, tg', gt, g't)$, $\xi(gg, g'g')$ and $\omega(gg', g'g)$. The unit statistical weight for the conformations t and tt result directly from the choice of the reference state. But the assignment of the same unit statistical weight to the conformations tg, tg', gt , and $g't$ implies that the corresponding energies between atoms separated by four bonds are essentially the same as in the conformation tt .

The statistical weights are given by the appropriate Boltzmann factors,

$$\begin{aligned} \sigma &= \exp \{ -\Delta E_\sigma / RT \} \\ \xi &= \exp \{ -\Delta E_\xi / RT \} \end{aligned} \quad (27)$$

and

$$\omega = \exp \{ -\Delta E_\omega / RT \}$$

where ΔE_σ , ΔE_ξ , and ΔE_ω are the energy differences between the various conformations and the reference state. The set of the statistical weights of the various conformations of a sequence of four bonds of the chain is represented by the matrix

$$\mathbf{U} = \begin{vmatrix} u_{tt} & u_{tg} & u_{tg'} \\ u_{gt} & u_{gg} & u_{gg'} \\ u_{g't} & u_{g'g} & u_{g'g'} \end{vmatrix} = \begin{vmatrix} 1 & \sigma & \sigma \\ 1 & \sigma\xi & \sigma\omega \\ 1 & \sigma\omega & \sigma\xi \end{vmatrix} \quad (28)$$

For the sequence of the three bonds at the beginning of the chain, the corresponding statistical weights are given by the first row of the matrix of eq. (28).

For $j \geq 3$, the states t , g , and g' of the j th bond are represented by the symbols $\{X_j = t\}$, $\{X_j = g\}$, and $\{X_j = g'\}$, respectively.

By definition let $p_t^{j,n}$, $p_g^{j,n}$, and $p_{g'}^{j,n}$ be the statistical weights taken over the set of bond conformations in the interval j to n , such that $X_{j-1} = t$, $X_{j-1} = g$, and $X_{j-1} = g'$, respectively. Then one finds that, respectively,

$$\begin{aligned} p_t^{j,n} &= \sum_{\epsilon_j^n / X_{j-1} = t} u_j u_{j+1} \dots u_n \\ p_g^{j,n} &= \sum_{\epsilon_j^n / X_{j-1} = g} u_j u_{j+1} \dots u_n \\ p_{g'}^{j,n} &= \sum_{\epsilon_j^n / X_{j-1} = g'} u_j u_{j+1} \dots u_n \end{aligned} \quad (29)$$

The properties of the interdependent model allow one to write the following recursion relation:

$$(p_t^{j,n}, p_g^{j,n}, p_{g'}^{j,n})_T = \mathbf{U}(p_t^{j+1,n}, p_g^{j+1,n}, p_{g'}^{j+1,n})_T \quad (30)$$

where the subscript T denotes the transpose. Successive application of this recursion relation yields

$$(p_t^{j,n}, p_g^{j,n}, p_{g'}^{j,n})_T = \mathbf{U}^{n-j+1}(1, 1, 1)_T \quad (31)$$

A quantity which will be of interest later is the ratio

$$p_g^{j,n}/p_t^{j,n} = p_{g'}^{j,n}/p_t^{j,n} = \delta^{j,n}$$

which can be obtained either by direct calculation by using eq. (31) or analytically by diagonalizing \mathbf{U} . In the latter case

$$\delta^{j,n} = \frac{1}{1 - \lambda_2 \lambda_3 (\lambda_3^{n-j+1} - \lambda_2^{n-j+1}) / (\lambda_3^{n-j+2} - \lambda_2^{n-j+2})} \quad (32)$$

where $\lambda_{2,3} = 1/2(\sigma\xi + \sigma\omega + 1 \pm \{(\sigma\xi + \sigma\omega - 1)^2 + 8\sigma\}^{1/2})$

are two of the eigenvalues of \mathbf{U} . The plus and minus signs distinguish λ_2 from λ_3 .

Conditional Probabilities. In order to evaluate the transition matrix of the chain it is necessary to calculate the conditional probabilities of the type $\Pr(X_{j+1} = t/X_j = t)$, $\Pr(X_{j+1} = g/X_j = t)$, etc. By using relation (17) and a decomposition analogous to that in eq. (18) the following relation can be written

$$\Pr(X_{j+1} = t/X_j = t) = p_t^{j+2,n}/p_t^{j+1,n}$$

and aided by eq. (30) one obtains

$$\Pr(X_{j+1} = t/X_j = t) = p_j = \frac{1}{1 + 2\sigma\delta^{j+2,n}} \quad (33a)$$

In a similar manner it can be shown that

$$\Pr(X_{j+1} = g/X_j = t) = \Pr(X_{j+1} = g'/X_j = t) = q_j = \frac{\sigma\delta^{j+2,n}}{1 + 2\sigma\delta^{j+2,n}} \quad (33b)$$

$$\Pr(X_{j+1} = t/X_j = g) = \Pr(X_{j+1} = t/X_j = g') = r_j = \frac{1}{1 + \sigma(\xi + \omega)\delta^{j+2,n}} \quad (33c)$$

$$\begin{aligned} \Pr(X_{j+1} = g/X_j = g) &= \Pr(X_{j+1} = g'/X_j = g') \\ &= s_j = \frac{\sigma\xi\delta^{j+2,n}}{1 + \sigma(\xi + \omega)\delta^{j+2,n}} \end{aligned} \quad (33d)$$

$$\begin{aligned} \Pr(X_{j+1} = g/X_j = g') &= \Pr(X_{j+1} = g'/X_j = g) \\ &= t_j = \frac{\sigma\omega\delta^{j+2,n}}{1 + \sigma(\xi + \omega)\delta^{j+2,n}} \end{aligned} \quad (33e)$$

Furthermore

$$\Pr(X_3 = t) = x_3 = \frac{1}{1 + 2\sigma\delta^{4,n}} \quad (34)$$

and

$$\Pr(X_3 = g) = \Pr(X_3 = g') = y_3 = \frac{\sigma\delta^{4,n}}{1 + 2\sigma\delta^{4,n}}$$

The transition probabilities of eq. (33), from a given state of bond j to another state of the bond $j + 1$ depend not only on the conformation of these bonds, but also on the conformation of bonds posterior to bond $j + 1$ through the term $\delta^{j+2,n}$. These probabilities are furthermore, functions of the position in the chain of the bond involved, and thus, contrary to the case of independent rotations, are not constant.

Markov Processes. The general configuration of the molecular chain has been studied by using the set of elementary conformations of four bonds, as described by eq. (28). Consequently, in order to know if a given bond j belongs to one of these various conformations it is necessary to mark in the reference system the directions of the three bonds $j - 3$, $j - 2$, and $j - 1$, which fall adjacent to it. Thus, the system is described by a third-order Markov process, which, as will be shown, can be reduced to the simple case.

Let the triplet $X_j = (Y_{j-2}, Y_{j-1}, Y_j)$ represent the internal rotation state of the corresponding bonds. The passage from the triplet X_j to the triplet X_{j+1} , if allowed, defines one of the four bond conformations which has just been discussed.

Consider the following states:

$$\begin{aligned}
 a &= \overset{4}{U}_{\substack{\alpha, \beta = 2 \\ \alpha \neq \beta}} (\alpha, \beta, 1) \\
 b &= \overset{4}{U}_{\alpha = 2} (1, \alpha, 1) \\
 c &= \overset{4}{U}_{\substack{\alpha, \beta = 2 \\ \alpha \neq \beta}} (\alpha, \beta, \alpha) \\
 d &= \overset{4}{U}_{\substack{\alpha, \beta, \gamma = 2 \\ \alpha \neq \beta \\ \beta \neq \gamma \\ \alpha \neq \gamma}} (\alpha, \beta, \gamma) \\
 e &= \overset{4}{U}_{\substack{\alpha, \beta = 2 \\ \alpha \neq \beta}} (1, \alpha, \beta) \\
 f &= \overset{4}{U}_{\substack{\alpha, \beta = 2 \\ \alpha \neq \beta}} (\alpha, 1, \beta) \\
 h &= \overset{4}{U}_{\alpha = 2} (\alpha, 1, \alpha)
 \end{aligned} \tag{35}$$

Let E_j represent a state of type a , or b , ..., or f , or h ; thus $E_j \in \{a, b, \dots, f, h\}$. Considering the four-bond interaction model adopted earlier, it can be seen that the decomposition of eq. (18) is still valid here, but for the states E_j that have just been defined. Thus one has for $3 \leq i \leq j - 1$,

$$\begin{aligned}
 \Pr(X_{j+1} = E_{j+1}/X_j = E_j, \dots, X_i = E_i) \\
 &= \frac{\left(\sum_{\epsilon_{j+1}^{j+1}/X_j = E_j, X_{j+1} = E_{j+1}} u_{j+1} \right) \left(\sum_{\epsilon_{j+2}^n/X_{j+1} = E_{j+1}} u_{j+2} u_{j+3} \dots u_n \right)}{\sum_{\epsilon_{j+1}^n/X_j = E_j} u_{j+1} u_{j+2} \dots u_n} \\
 &= \Pr(X_{j+1} = E_{j+1}/X_j = E_j)
 \end{aligned} \tag{36}$$

It is seen, then, that one is concerned with a simple Markov process. Equation (36) allows the calculation of the different transition probabilities of this process, viz.,

$$\begin{aligned}
 \Pr(X_{j+1} = f/X_j = a) &= \sigma(\xi + \omega) p_\theta^{j+2, n} / p_\theta^{j+1, n} \\
 &= \frac{\sigma(\xi + \omega) \delta^{j+2, n}}{1 + \sigma(\xi + \omega) \delta^{j+2, n}} \\
 &= s_j + t_j, \\
 \Pr(X_{j+1} = e/X_j = h) &= 2\sigma p_\theta^{j+2, n} / p_t^{j+1, n} \\
 &= \frac{2\sigma \delta^{j+2, n}}{1 + 2\sigma \delta^{j+2, n}} \\
 &= 2q_j
 \end{aligned} \tag{37}$$

The seventh-order transition matrix \mathbf{P}_j , from states of bond j to states of bond $j + 1$ is written in the form

$$\mathbf{P}_j = \begin{pmatrix} p_{aa;j} & p_{ab;j} & \dots & \dots & \dots & p_{ah;j} \\ p_{ba;j} & p_{bb;j} & \dots & \dots & \dots & p_{bh;j} \\ \dots & \dots & \dots & \dots & \dots & \dots \\ \dots & \dots & \dots & \dots & \dots & \dots \\ \dots & \dots & \dots & \dots & \dots & \dots \\ \dots & \dots & \dots & \dots & \dots & \dots \\ \dots & \dots & \dots & \dots & \dots & \dots \\ \dots & \dots & \dots & \dots & \dots & \dots \\ \dots & \dots & \dots & \dots & \dots & \dots \\ \dots & \dots & \dots & \dots & \dots & \dots \\ p_{ha;j} & \dots & \dots & \dots & \dots & p_{hh;j} \end{pmatrix} \\
 = \begin{pmatrix} 0 & 0 & 0 & 0 & 0 & s_j + t_j & r_j \\ 0 & 0 & 0 & 0 & 0 & 2q_j & p_j \\ q_j & 0 & p_j & q_j & 0 & 0 & 0 \\ s_j & 0 & r_j & t_j & 0 & 0 & 0 \\ t_j & 0 & r_j & s_j & 0 & 0 & 0 \\ 0 & r_j & 0 & 0 & s_j + t_j & 0 & 0 \\ 0 & p_j & 0 & 0 & 2q_j & 0 & 0 \end{pmatrix} \tag{38}$$

It should be noted that this matrix is modified by a translation along the chain and is not constant as n varies. Furthermore, it characterizes a simple Markov process for the three-bond states a, b, \dots, f, h .

Average Molecular Optical Anisotropy

For $n \geq 4$, eq. (5) can be written in the form,

$$\langle n_1^2 \rangle = \frac{n}{4} + 2 \sum_{k=2}^n \Pr(Y_1 = 1 \text{ and } Y_k = 1) + 2 \sum_{k=3}^n \Pr(Y_2 = 1 \text{ and } Y_k = 1) \\
 + 2 \sum_{j=3}^{n-1} \sum_{k=j+1}^n \Pr(Y_j = 1 \text{ and } Y_k = 1) \tag{39}$$

The method of evaluating each summation in eq. (39) can be illustrated by considering the last term on the right-hand side. A well known property of Markov processes allows one to write for $j < k$

$$(\mathbf{P}_j \mathbf{P}_{j+1} \dots \mathbf{P}_{k-1})_{ab} = \Pr(X_k = b / X_j = a)$$

The *a priori* probability vector at time j , which can be written

$$\mathbf{Q}_j = [\Pr(X_j = a), \dots, \Pr(X_j = f), \Pr(X_j = h)] \tag{40}$$

has the property

$$\mathbf{Q}_j = \mathbf{Q}_{j-1}\mathbf{P}_{j-1} = \mathbf{Q}_3\mathbf{P}_3\mathbf{P}_4 \dots \mathbf{P}_{j-1} = \mathbf{Q}_3\mathbf{P}_2\mathbf{P}_3\mathbf{P}_4 \dots \mathbf{P}_{j-1} \quad (41)$$

where the matrix $\mathbf{P}_2 = \mathbf{I}_7$ is equal to a seventh-order unit matrix. Hence $V_{j,k}$ such that $3 \leq j < k$,

$$\Pr(Y_j = 1 \text{ and } Y_k = 1) = \mathbf{Q}_3\mathbf{P}_2\mathbf{P}_3\mathbf{P}_4 \dots \mathbf{P}_{j-1}\mathbf{M}\mathbf{P}_j\mathbf{P}_{j+1} \dots \mathbf{P}_{k-1}\mathbf{V} \quad (42)$$

where

$$\mathbf{M} = \begin{pmatrix} 1 & 0 & 0 & \cdot & \cdot & \cdot & 0 \\ 0 & 1 & 0 & \cdot & \cdot & \cdot & 0 \\ 0 & 0 & 0 & \cdot & \cdot & \cdot & 0 \\ \cdot & \cdot & \cdot & \cdot & \cdot & \cdot & \cdot \\ \cdot & \cdot & \cdot & \cdot & \cdot & \cdot & \cdot \\ \cdot & \cdot & \cdot & \cdot & \cdot & \cdot & \cdot \\ 0 & 0 & 0 & \cdot & \cdot & \cdot & 0 \end{pmatrix}$$

and

$$\mathbf{V} = \begin{pmatrix} 1 \\ 1 \\ 0 \\ \cdot \\ \cdot \\ \cdot \\ 0 \end{pmatrix}$$

(43)

are, respectively, a square seventh-order matrix and a seventh-order column vector. Similarly, if one defines

$$\begin{aligned} \mathbf{L}_3 &= [0, \Pr(X_3 = b), 0, 0, \Pr(X_3 = e), 0, 0] \\ \mathbf{L}_3' &= [0, 0, 0, 0, 0, \Pr(X_3 = f), \Pr(X_3 = h)] \end{aligned} \quad (44)$$

one finds that

$$\Pr(Y_1 = 1 \text{ and } Y_k = 1) = \mathbf{L}_3\mathbf{P}_2\mathbf{P}_3\mathbf{P}_4 \dots \mathbf{P}_{k-1}\mathbf{V}$$

and

$$\Pr(Y_2 = 1 \text{ and } Y_k = 1) = \mathbf{L}_3'\mathbf{P}_2\mathbf{P}_3\mathbf{P}_4 \dots \mathbf{P}_{k-1}\mathbf{V}$$

Thus,

$$\begin{aligned} \langle n_1^2 \rangle &= \frac{n}{4} + 2 \left\{ \sum_{k=3}^n (\mathbf{L}_3 + \mathbf{L}_3')\mathbf{P}_2\mathbf{P}_3\mathbf{P}_4 \dots \mathbf{P}_{k-1}\mathbf{V} \right. \\ &\quad \left. + \sum_{j=3}^{n-1} \sum_{k=j+1}^n \mathbf{Q}_j\mathbf{P}_2\mathbf{P}_3 \dots \mathbf{P}_{j-1}\mathbf{M}\mathbf{P}_j \dots \mathbf{P}_{k-1}\mathbf{V} \right\} \quad (46) \end{aligned}$$

It has been shown by a recursion relation that the sums in braces can be

generated identically in the following manner:

$$\left\{ \right\} = [(\mathbf{L}_3 + \mathbf{L}_3' + \mathbf{Q}_3\mathbf{M} - \mathbf{Q}_3), \mathbf{Q}_3, \mathbf{O}] \left[\prod_{j=3}^{n-1} \mathbf{H}_j \right] \begin{vmatrix} \mathbf{V} \\ \mathbf{O}_T \\ \mathbf{V} \end{vmatrix} \quad (47)$$

where

$$\begin{aligned} \mathbf{Q}_3 &= (y_3/2, x_3/4, x_3/2, y_3/2, y_3/2, y_3/2, x_3/4) \\ \mathbf{L}_3 &= (0, x_3/4, 0, 0, y_3/2, 0, 0) \\ \mathbf{L}_3' &= (0, 0, 0, 0, 0, y_3/2, x_3/4) \\ \mathbf{O} &= (0, 0, 0, 0, 0, 0, 0) \end{aligned} \quad (48)$$

$$\mathbf{H}_j = \begin{vmatrix} \mathbf{P}_j & \mathbf{O}_7 & \mathbf{I}_7 \\ \mathbf{P}_j\mathbf{M} & \mathbf{P}_j & \mathbf{O}_7 \\ \mathbf{O}_7 & \mathbf{O}_7 & \mathbf{I}_7 \end{vmatrix} \quad (49)$$

\mathbf{O}_7 and \mathbf{O}_T being, respectively, a square null, seventh-order matrix and a seventh-order null column vector. The matrices \mathbf{H}_j are thus of order 21. Noting that for $j \geq 3$, $\mathbf{Q}_j\mathbf{V} = \text{Pr}(X_j = a) + \text{Pr}(X_j = b) = \text{Pr}(Y_j = 1) = 1/4$, one can incorporate the term $n/4$ of eq. (46) in the matrix product by taking

$$\begin{aligned} \mathbf{W}' &= 2 \{ [(\mathbf{L}_3 + \mathbf{L}_3' - (\mathbf{Q}_3/2)], \mathbf{Q}_3, [(3\mathbf{Q}_3/2) - \mathbf{L}_3 - \mathbf{L}_3'] \} \\ \mathbf{W} &= \begin{vmatrix} \mathbf{V} \\ \mathbf{O}_T \\ \mathbf{V} \end{vmatrix} \end{aligned} \quad (50)$$

thus, for $n \geq 3$ the expression for the average molecular optical anisotropy becomes

$$\langle \gamma^2 \rangle / \Gamma^2 = \frac{16}{3} \mathbf{W}' \left[\prod_{j=2}^{n-1} \mathbf{H}_j \right] \mathbf{W} - (n^2/3) \quad (51)$$

A number of comments can be made concerning the above results. It is seen that in this case, unlike those of first and second order, it is not possible to employ a summation formula to reduce the sums appearing in eq. (46). In effect, in the third-order case the matrices \mathbf{P}_j depend on n . Thus, the final result has been expressed in the form of a product of matrices \mathbf{H}_j which can be easily evaluated for numerical calculations.

With $\xi = \omega = 1$, that is, $\delta^{j+2, n} = 1$ in eq. (51), one obtains the results corresponding to the second-order case. Furthermore, if, in addition, $\sigma = 1$, the results are those of the first-order case.

GENERAL REMARKS

The results just established essentially relate to the tetrahedral lattice. However the conditional probabilities of eq. (33) can be extended to the case in which each bond j introduces m distinct values $\varphi_j^{(1)}, \varphi_j^{(2)}, \dots,$

$\varphi_j^{(m)}$ of the internal rotation angle. The set of the statistical weights corresponding to the rotation of the j th bond of the molecule will be represented by the m -order matrix \mathbf{U}_j , of which the element of row r and column s will be written

$$u_{j,rs} = e^{-E(\varphi_{j-1}^{(r)}, \varphi_j^{(s)})/RT}$$

In an analogous manner to eq. (29) we define the following quantities:

$$p_r^{j,n} = \sum_{\epsilon_j^n / \varphi_{j-1} = \varphi_{j-1}^{(r)}} u_j u_{j+1} \dots u_n \quad (52)$$

It can be shown that

$$(p_1^{j,n}, p_2^{j,n}, \dots, p_m^{j,n})_T = (\mathbf{U}_{j-1} \mathbf{U}_j \dots \mathbf{U}_{n-1})(1, 1, \dots, 1)_T \quad (53)$$

and similarly to eqs. (33), (34) one has

$$\Pr(\varphi_{j+1} = \varphi_{j+1}^{(s)} / \varphi_j = \varphi_j^{(r)}) = u_{j+1,rs} p_s^{j+2,n} / p_r^{j+1,n} V_j \geq 3 \quad (54)$$

$$\Pr(\varphi_3 = \varphi_3^{(s)}) = p_s^{4,n} / \sum_{r=1}^m p_r^{4,n} \quad (55)$$

The set of conditional probabilities of eq. (54) will be represented in a matrix \mathbf{G}_j of order m . These probabilities can be easily obtained with the aid of relation (53) in which only statistical weight matrices appear.

At this stage of our development it would be possible to express the average molecular optical anisotropy of a chain in a form sensibly equivalent to the matrix method. It is known^{3,4} that the average molecular optical anisotropy $\langle \gamma^2 \rangle$ of polymer chains can be written as a sum of two terms; the first is easily obtained, and the second can be schematically written as:

$$\sum_{j < k} \langle f(\varphi_j) \cdot f(\varphi_{j+1}) \dots f(\varphi_{k-1}) \rangle$$

where each function $f(\varphi_j)$ is a ninth-order matrix. By using the theorem on conditional probabilities, the average can be expressed in the form:

$$\langle \quad \rangle = \sum_{\varphi_{j-1}, \varphi_j, \dots, \varphi_{k-1}} \Pr(\varphi_{j-1}) \prod_{i=j}^{k-1} \Pr(\varphi_i / \varphi_{i-1}) f(\varphi_i) \quad (56)$$

Let \mathbf{F}_j be defined as a pseudodiagonal matrix in which the r th element is $f(\varphi_j^{(r)})$. Later, \mathbf{F}_j will be formally considered as a matrix of order m . Let \mathbf{Q}_j be the *a priori* probability vector at time j , such as

$$\mathbf{Q}_j = [\Pr(\varphi_j = \varphi_j^{(1)}), \Pr(\varphi_j = \varphi_j^{(2)}), \dots, \Pr(\varphi_j = \varphi_j^{(m)})]$$

and \mathbf{S} the m -column vector $(1, 1, \dots, 1)_T$.

Finally, eq. (56) can be expressed in the form

$$\mathbf{Q}_{j-1} (\mathbf{G}_{j-1} \mathbf{F}_{j-1}) (\mathbf{G}_j \mathbf{F}_j) \dots (\mathbf{G}_{k-2} \mathbf{F}_{k-2}) \mathbf{S} \quad (57)$$

The summation $\sum_{j < k} \langle \quad \rangle$ may be generated identically by taking a matrix product as illustrated in eq. (51).

At last, another remark can be made. It must be noticed that conditional probabilities of eq. (33) corresponding to the case of interdependence allow one to simulate on a computer the step by step generation of the various conformations of a chain with their corresponding probabilities. Such a simulation can be useful to study the excluded volume effect (as-

TABLE I
Values of $\langle \gamma^2 \rangle / \Gamma^2$ Calculated with the Aid of Markov Processes
for the Various Models of Internal Rotation^{a, b}

n	$\langle \gamma^2 \rangle / \Gamma^2$		
	Equiprobability ^c	Independence ^d	Interdependence ^e
1	1	1	1
2	1.3333	1.3333	1.3333
3	1.8888	2.5445	2.5445
4	2.3703	3.3252	3.3863
5	2.8765	4.5202	4.7865
6	3.3744	5.4692	5.8278
7	3.8751	6.6228	7.2429
8	4.3749	7.6427	8.3807
9	4.8750	8.7661	9.7752
10	5.3749	9.8184	10.9640
11	5.8750	10.9239	12.3337
12	6.3749	11.9920	13.5536
13	6.8750	13.0875	14.9025
14	7.3750	14.1635	16.1431
15	7.8750	15.2537	17.4761
16	8.3750	16.3337	18.7311
17	8.8750	17.4211	20.0524
18	9.3750	18.5032	21.3176
19	9.8750	19.5891	22.6304
20	10.3750	20.6723	23.9029
.	.	.	.
.	.	.	.
.	.	.	.
30	15.3750	31.5160	36.8198
.	.	.	.
.	.	.	.
.	.	.	.
40	20.3750	42.3592	49.7311
.	.	.	.
.	.	.	.
.	.	.	.
50	25.3750	53.2025	62.6414

^a The number of C-C bonds is n . Tetrahedral valence angles have been assumed and the internal rotation angle is $\varphi = 0, \pm 120^\circ$.

^b The matrix method⁶ gives results in perfect agreement with the values in this table for the same choice of parameters.

^c By eq. (13).

^d By eq. (25): at 25°C, $\sigma = 0.3633$, i.e., $p = 0.5791$ and $q = 0.2104$.

^e By eq. (51): at 25°C, $\sigma = 0.3633$, $\sigma\omega = 0.0147$, and $\xi = 1$, [to be substituted in eqs. (33) and (34)].

sumed to be generally weak²¹ on the molecular optical anisotropy. The generation of the chain in a tetrahedral lattice allows interesting simplifications in the evaluation of $\langle \gamma^2 \rangle$ because this computation is equivalent to counting of the bonds according to the four directions of the lattice.

NUMERICAL RESULTS AND DISCUSSION

Comparison of experimental and theoretical values of the average molecular optical anisotropy of polyethylene chains has been made previously.^{1,4} Hence, the numerical results given here will be limited to a few illustrative values of $\langle \gamma^2 \rangle / \Gamma^2$ calculated for each of the three chain models that has been developed. The following energy parameters have been chosen:⁵ $\Delta E_\sigma = -RT \ln \sigma = 600$ cal/mole, $\Delta E_\xi \approx 0$, $\Delta E_\omega = -RT \ln \omega = 1900$ cal/mole; for a temperature of 25°C, $\sigma = 0.3633$; $\sigma\xi = \sigma$, $\sigma\omega = 0.01471$, from which can be obtained the various transition probabilities needed to calculate $\langle \gamma^2 \rangle$ for the two later models considered. The numerical results up to $n = 50$ are summarized in Table I. It has been verified that these numerical results are in excellent agreement with those obtained by the matrix method⁵ and the same choice of parameters.

The ratio $\langle \gamma^2 \rangle / n\Gamma^2$ is plotted in Figure 1 as a function of n for the different models of internal rotation studied. It is evident that only curves 2 and 3, which correspond to models of hindered internal rotation, exhibit values of $\langle \gamma^2 \rangle / n\Gamma^2$ which increase with n , in agreement with experiment. Hence, the model of curve 1 should be eliminated.

It is known,^{1,5} however, that the model of curve 3, which takes into account the interdependence of internal rotations, yields the best agreement with the ensemble of experimental results. It can also be seen in Figure 1 that the effect of including correlations between internal rotation angles of nearest-neighbor bonds is to increase the values of $\langle \gamma^2 \rangle / n\Gamma^2$ by about 20% (for $n \gg 1$) compared with the results for independent internal rotations.

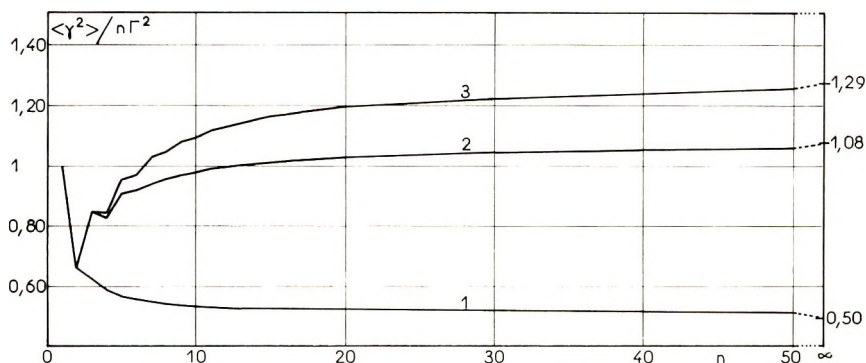


Fig. 1. Curves for (1) a chain with tetrahedral valence angles and equally probable internal rotations; (2) the model for independent internal rotations and (3) that for interdependent internal rotations.

This result can be explained in the following manner. The elimination from the chain of all *gauche* conformations containing the sterically unacceptable sequences gg' and $g'g$ [$\omega \approx 0$ in eq. (28)] favors the extended conformations which are rich in *trans* bonds, and results in an increase in the anisotropy of the chain. By using eq. (3) it can be shown that the *trans* form of a molecule of given length n is much more anisotropic, other things being equal, than any of the corresponding *gauche* forms.

CONCLUSIONS

By use of Markov processes, the average molecular optical anisotropy $\langle \gamma^2 \rangle$ of tetrahedral-lattice polyethylene chains has been calculated as an explicit function of various parameters which define the statistics of a molecular chain of any length. The analysis developed here presents for the first time, the treatment of $\langle \gamma^2 \rangle$ with the aid of Markov processes, for various models, from the simplest to the most sophisticated of those in current use. The study of these models emphasizes the importance of the condition of interdependence. It also provides a basis for the comparison of the effects obtained under the same conditions for other conformational properties of chains such as end-to-end distance,^{9a} for example.

In this work all numerical calculations are performed by relatively straightforward programming of matrix products. In the case of interdependence, the only one of real interest, the matrices considered here are of order 21 versus 24^4 or 33^3 in the matrix methods. Thus the computational difficulties of these different methods are sensibly equivalent for the cases considered in this paper. However, since the matrix method appears to be of more general utility, the possibility of extension of our results has been shown in this paper.

Finally the present study indicates how, the equivalence between the conformational statistics of chains and the corresponding problem of the theory of Markov processes must be understood. In particular, in the case of a real chain, for which it is necessary to take into consideration the interdependence of the internal rotations, it is found that eqs. (33) allow this effect to be represented by mutually dependent consecutive (rather than simultaneous) events. This idea may help to explain certain comments found in the literature.^{9b}

References

1. P. Bothorel, *J. Colloid Sci.*, **27**, 529 (1968).
2. G. Fourche, *J. Chim. Phys.*, **65**, 1500 (1968).
3. R. L. Jernigan and P. J. Flory, *J. Chem. Phys.*, **47**, 1999 (1967).
4. K. Nagai, *J. Chem. Phys.*, **47**, 4690 (1967).
5. G. Fourche and P. Bothorel, *J. Chim. Phys.*, **66**, 54 (1969).
6. G. Fourche, *J. Chim. Phys.*, **66**, 320 (1969).
7. T. M. Birshtein and O. B. Ptitsyn, *Conformations of Macromolecules*, Interscience, New York, 1966.
8. B. Lemaire, G. Fourche, F. Roger, and P. Bothorel, *C.R. Acad. Sci. (Paris)*, **C**, **268**, 1103 (1969).

9. P. J. Flory, *Statistical Mechanics of Chain Molecules*, Interscience, New York, 1969, (a) p. 147; (b) pp. 89-93.
10. A. Unanue and P. Bothorel, *Bull. Soc. Chim. France*, **1964**, 573.
11. A. Unanue and P. Bothorel, *Bull. Soc. Chim. France*, **1965**, 2827.
12. C. Clement and P. Bothorel, *J. Chim. Phys.*, **61**, 1282 (1964).
13. P. Foulani and C. Clement, *Bull. Soc. Chim. France*, **1969**, 3462.
14. R. P. Smith and E. M. Mortensen, *J. Chem. Phys.*, **32**, 502 (1960).
15. C. Clement and P. Bothorel, *J. Chim. Phys.*, **61**, 1262 (1964).
16. M. V. Volkenstein, *Configurational Statistics of Polymeric Chains*, Interscience, New York, 1963.
17. H. Benoit, *C.R. Acad. Sci. (Paris)*, **236**, 687 (1953).
18. P. Gordon, *Théorie des chaînes de Markov finies et ses applications*, Dunod, Paris, 1965.
19. J. G. Kemeny and J. L. Snell, *Finite Markov Chains*, Van Nostrand, New York, 1960.
20. R. P. Smith, *J. Chem. Phys.*, **44**, 2543 (1966).
21. V. N. Tsvetkov, V. E. Bychkova, S. M. Savvon, and N. K. Nekrasov, *Vysokomol. Soedin.*, **1**, 1407 (1959); *Polym. Sci. USSR*, **1**, 584 (1960).

Received July 14, 1970

Revised October 15, 1970

Optical Anisotropy of Polymer Chains and Markov Processes. II. Polyoxyethylene

BERNARD LEMAIRE and GEORGES FOURCHE, *Centre de Recherches Paul Pascal, Domaine Universitaire, 33 Talence, France*

Synopsis

A comparative study of the average molecular optical anisotropy ($\langle \gamma^2 \rangle$) of the polyoxyethylene chain, $R-O-(CH_2CH_2O)_nR$ where $R = CH_3, H$ and n is the degree of polymerization of the molecule, was carried out for the different internal rotational models considered in Part I of this series. In particular, the results obtained show that the condition of interdependence between internal rotational angles of nearest-neighboring bonds increases the average molecular optical anisotropy by about 4% ($n \gg 1$), compared with the case of independent rotations. This increase is much weaker than in polyethylene chains, for which it is about 20% under analogous conditions.

Introduction

The procedure for calculating the average molecular optical anisotropy which was developed in Part I¹ will now be applied to polyoxyethylene (POE) chains, having the general formula $R-O-(CH_2CH_2O)_nR$, where $R = CH_3, H$ and n is the degree of polymerization. The definitions and notations, as well as the results, of Part I will be used in this treatment. Thus calculations of the same type as in Part I need not be developed. Furthermore the same physical model will be employed.

It is generally assumed^{2,3} that in POE the angle φ which characterizes the internal rotation state of a given bond, can have values 0, $+120^\circ$, and -120° , corresponding to the *trans* (*t*), *gauche* (*g*), and *gauche prime* (*g'*) positions, respectively. Furthermore, in POE all valence angles are very close to the tetrahedral values,^{2,4} allowing certain simplifications⁵ to be made in the calculation of the molecular optical anisotropy.

From the point of view of optical anisotropy, the POE chain behaves as if it were made up solely of C-C, C-O, and O-R bonds, each having an optical anisotropy equal,^{6,7} respectively to $\Gamma = \gamma_{CC} - 2\gamma_{CH}$, $S_{CO} = \gamma_{CO} - \gamma_{CH}$, and γ_{OR} (γ_{CC} , γ_{CO} , γ_{OR} , and γ_{CH} being the optical anisotropies of bonds C-C, C-O, O-R, and C-H). If one considers a chain of poly(oxyethylene dimethyl ether) (POEM), ($R = CH_3$), one can show⁶ that $\gamma_{OCH_3} \equiv S_{CO}$; and, for poly(oxyethylene glycol) (POEG), ($R = H$), $\gamma_{OR} = \gamma_{OH}$, the optical anisotropy of the O-H bond.

General Equations

The molecular optical anisotropy γ^2 of a rigid conformation of the POE chain is written^{6,7}

$$\begin{aligned} \gamma^2 = & \left[\frac{4}{3}(n_1^2 + n_2^2 + n_3^2 + n_4^2) - \frac{n^2}{3} \right] \Gamma^2 \\ & + \left[\frac{4}{3}(p_1^2 + p_2^2 + p_3^2 + p_4^2) - \frac{4n^2}{3} \right] S_{CO}^2 \\ & + \left[\frac{4}{3}(r_1^2 + r_2^2 + r_3^2 + r_4^2) - \frac{4}{3} \right] \gamma_{OR}^2 \\ & + \left[\frac{8}{3}(n_1 p_1 + n_2 p_2 + n_3 p_3 + n_4 p_4) - \frac{4n^2}{3} \right] \Gamma S_{CO} \\ & + \left[\frac{8}{3}(n_1 r_1 + n_2 r_2 + n_3 r_3 + n_4 r_4) - \frac{4n}{3} \right] \Gamma \gamma_{OR} \\ & + \left[\frac{8}{3}(p_1 r_1 + p_2 r_2 + p_3 r_3 + p_4 r_4) - \frac{8n}{3} \right] S_{CO} \gamma_{OR} \quad (1) \end{aligned}$$

in which $n_1, n_2, n_3,$ and n_4 are the numbers of C-C bonds parallel to directions 1, 2, 3, and 4, respectively, of a molecular reference system represented by the diagonals of a cube, and p_1, p_2, p_3, p_4 and r_1, r_2, r_3, r_4 are the corresponding numbers relative to C-O and O-R bonds. As the average values $\langle n_i^2 \rangle, \langle p_i^2 \rangle,$ etc., are independent of the direction i , one can write:

$$\begin{aligned} \langle \gamma^2 \rangle = & \left[\frac{16}{3} \langle n_1^2 \rangle - \frac{n^2}{3} \right] \Gamma^2 + \left[\frac{16}{3} \langle p_1^2 \rangle - \frac{4n^2}{3} \right] S_{CO}^2 + \left[\frac{16}{3} \langle r_1^2 \rangle - \frac{4}{3} \right] \gamma_{OR}^2 \\ & + \left[\frac{32}{3} \langle n_1 p_1 \rangle - \frac{4n^2}{3} \right] \Gamma S_{CO} + \left[\frac{32}{3} \langle n_1 r_1 \rangle - \frac{4n}{3} \right] \Gamma \gamma_{OR} + \left[\frac{32}{3} \langle p_1 r_1 \rangle - \frac{8n}{3} \right] \\ & \times S_{CO} \gamma_{OR} \quad (2) \end{aligned}$$

In the reference system of the molecule the state of the μ th bond of the skeleton, i.e., the number representing the direction adopted by this bond, will be designated by Y_μ . If A_μ is a random variable equal to unity when the event $\{Y_\mu = 1\}$ is realized and zero in the other cases, for $1 \leq \mu \leq 3n + 2$, one has

$$n_1 = \sum_{j=1}^n A_{3j} \quad (3)$$

$$p_1 = \sum_{j=1}^n A_{3j-1} + \sum_{k=2}^{n+1} A_{3k-2} \quad (4)$$

$$r_1 = A_1 + A_{3n+2} \quad (5)$$

Then, for the average values.

$$\langle n_1^2 \rangle = \sum_j \langle A_{3j}^2 \rangle + \sum_{j \neq j'} \langle A_{3j} A_{3j'} \rangle \quad (6)$$

$$\begin{aligned} \langle p_1^2 \rangle = \sum \langle A_{3j-1}^2 \rangle + \sum_{k'} \langle A_{3k-2}^2 \rangle + \sum_{j \neq j'} \langle A_{3j-1} A_{3j'-1} \rangle \\ + \sum_{k \neq k'} \langle A_{3k-2} A_{3k'-2} \rangle + 2 \sum_{j,k} \langle A_{3j-1} A_{3k-2} \rangle \end{aligned} \quad (7)$$

$$\langle r_1^2 \rangle = \langle A_1^2 \rangle + \langle A_{3n+2}^2 \rangle + 2 \langle A_1 A_{3n+2} \rangle \quad (8)$$

$$\langle n_1 p_1 \rangle = \sum_{j,j'} \langle A_{3j} A_{3j'-1} \rangle + \sum_{j,k'} \langle A_{3j} A_{3k-2} \rangle \quad (9)$$

$$\langle n_1 r_1 \rangle = \sum_j (\langle A_1 A_{3j} \rangle + \langle A_{3j} A_{3n+2} \rangle) \quad (10)$$

$$\begin{aligned} \langle p_1 r_1 \rangle = \sum_j (\langle A_1 A_{3j-1} \rangle + \langle A_{3j-1} A_{3n+2} \rangle) \\ + \sum_{k'} (\langle A_1 A_{3k-2} \rangle + \langle A_{3k-2} A_{3n+2} \rangle) \end{aligned} \quad (11)$$

and, by introducing the corresponding probabilities, we have

$$\langle n_1^2 \rangle = \sum_j \Pr(Y_{3j} = 1) + \sum_{j \neq j'} \Pr(Y_{3j} = 1 \text{ and } Y_{3j'} = 1) \quad (6')$$

$$\begin{aligned} \langle p_1^2 \rangle = \sum \Pr(Y_{3j-1} = 1) + \sum_{k'} \Pr(Y_{3k-2} = 1) + \sum_{j \neq j'} \Pr(Y_{3j-1} = 1 \\ \text{and } Y_{3j'-1} = 1) + \sum_{k \neq k'} \Pr(Y_{3k-2} = 1 \text{ and } Y_{3k'-2} = 1) \\ + 2 \sum_{j,k} \Pr(Y_{3j-1} = 1 \text{ and } Y_{3k-2} = 1) \end{aligned} \quad (7')$$

$$\begin{aligned} \langle r_1^2 \rangle = \Pr(Y_1 = 1) + \Pr(Y_{3n+2} = 1) \\ + 2 \Pr(Y_1 = 1 \text{ and } Y_{3n+2} = 1) \end{aligned} \quad (8')$$

$$\langle n_1 p_1 \rangle = \sum_{j,j'} \Pr(Y_{3j} = 1 \text{ and } Y_{3j'} = 1) + \sum_{j,k'} \Pr(Y_{3j} = 1 \text{ and } Y_{3k-2} = 1) \quad (9')$$

$$\begin{aligned} \langle n_1 r_1 \rangle = \sum_j [\Pr(Y_1 = 1 \text{ and } Y_{3j} = 1) \\ + \Pr(Y_{3j} = 1 \text{ and } Y_{3n+2} = 1)] \end{aligned} \quad (10')$$

$$\begin{aligned} \langle p_1 r_1 \rangle = \sum_j [\Pr(Y_1 = 1 \text{ and } Y_{3j-1} = 1) + \Pr(Y_{3j-1} = 1 \text{ and } Y_{3n+2} = 1)] \\ + \sum_{k'} [\Pr(Y_1 = 1 \text{ and } Y_{3k-2} = 1) + \Pr(Y_{3k-2} = 1 \text{ and } Y_{3n+2} = 1)] \end{aligned} \quad (11')$$

Equally Probable Internal Rotations

One can see that $\forall \mu, \nu$, such that $1 \leq \mu, \nu \leq 3n+2$, $\Pr(Y_\mu = 1 \text{ and } Y_\nu = 1) = \Pr(X_\mu = a \text{ and } X_\nu = a) = \Pr(X_\mu = a) \cdot \Pr(X_\nu = a / X_\mu = a)$ and, by symmetry, $\Pr(Y_\mu = 1) = \Pr(X_\mu = a) = 1/4 \forall \mu$.

It is also evident that in the case in which there is equal probability of the three internal rotational positions $0, +120^\circ$, and -120° for all the

bonds of the molecule, only one matrix of transition probabilities is necessary to characterize the chain, viz.,

$$\mathbf{P} = \begin{vmatrix} P_{aa} & P_{ab} \\ P_{ba} & P_{bb} \end{vmatrix} = \begin{vmatrix} 0 & 1 \\ 1/3 & 2/3 \end{vmatrix} \quad (12)$$

It is known that $\text{Pr}(X_\nu = a/X_\mu = a) = [\mathbf{P}^{\nu-\mu}]_{11}$, where the subscripts identify the 1,1 element of the matrix product. Under these conditions, and by putting $\mathbf{P}^3 = \mathbf{R}$ the evaluation of the different sums according to similar calculations developed in Part I leads to:

$$\begin{aligned} \langle \gamma^2 \rangle = & \left\{ \frac{13n}{14} + \frac{27}{392} + \frac{8}{3} [\mathbf{R}^{n+1}\mathbf{Z}^2 - \mathbf{R}^*]_{11} \right\} \Gamma^2 \\ & + \left\{ \frac{10n}{7} + \frac{75}{98} + \frac{8}{3} [(\mathbf{P} + \mathbf{R})(\mathbf{I}_2 + \mathbf{P}^2)(\mathbf{R}^n\mathbf{Z}^2 - \mathbf{R}^*)]_{11} \right\} S_{\text{Co}^2} \\ & + \left\{ \frac{10}{3} + \frac{8}{3} [\mathbf{P}(\mathbf{R}^n - \mathbf{R}^*)]_{11} \right\} \gamma_{\text{OR}}^2 \\ & + \left\{ -\frac{6n}{7} - \frac{45}{98} + \frac{16}{3} [\mathbf{P}(\mathbf{P} + \mathbf{R})(\mathbf{R}^n\mathbf{Z}^2 - \mathbf{R}^*)]_{11} \right\} \Gamma S_{\text{Co}} \\ & + \left\{ \frac{3}{7} - \frac{16}{3} [\mathbf{P}^2(\mathbf{R}^n\mathbf{Z} - \mathbf{R}^*)]_{11} \right\} \Gamma \gamma_{\text{OR}} \\ & + \left\{ -\frac{10}{7} - \frac{16}{3} [(\mathbf{P} + \mathbf{R})(\mathbf{R}^n\mathbf{Z} - \mathbf{R}^*)]_{11} \right\} S_{\text{Co}} \gamma_{\text{OR}} \quad V_{n \geq 1} \quad (13) \end{aligned}$$

where \mathbf{I}_2 is the second-order unit matrix, $\mathbf{R}^* = \lim_{n \rightarrow \infty} \mathbf{R}^n$, and $\mathbf{Z} = [\mathbf{I}_2 - (\mathbf{R} - \mathbf{R}^*)]^{-1}$, these last matrices having the following forms:

$$\mathbf{R}^* = \begin{vmatrix} 1/4 & 3/4 \\ 1/4 & 3/4 \end{vmatrix}$$

and

$$\mathbf{Z} = \begin{vmatrix} 109 & 3 \\ 112 & 112 \\ 1 & 111 \\ 112 & 112 \end{vmatrix} \quad (14)$$

It is found that as n tends towards infinity, $\mathbf{R}^n\mathbf{Z}$, $\mathbf{R}^n\mathbf{Z}^2$, $\mathbf{R}^{n+1}\mathbf{Z}^2$, and \mathbf{R}^n all approach \mathbf{R}^* . Thus, the asymptotic behavior of $\langle \gamma^2 \rangle$ for large values of n , is easily obtained.

Independent Internal Rotations

Because of the different kinds of atoms that constitute the molecular skeleton of POE, the interactions between the atoms in the chain will also

be different. Later it will be necessary to distinguish several types of internal rotations relating to the different bonds in the chain. For further convenience we have chosen to "read" the molecule from left to right as given above and have adopted the plane of its first two bonds as the origin for the angles of internal rotation.

First, consider the case of POEM for which $R = \text{CH}_3$. Two types of internal rotations will be investigated,⁶ those of O-C or C-C bonds which are equivalent and those of C-O bonds. The statistical weight σ will be assigned to the conformations g and g' obtained by the rotation of bonds O-C or C-C in the three-bond units $\text{CH}_2\text{—CH}_2\text{—O—CH}_2$ or $\text{CH}_2\text{—O—CH}_2\text{—CH}_2$. This statistical weight takes into consideration the interactions between two CH_2 groups separated by three bonds of the molecular skeleton. Likewise, the statistical weight σ' will be associated with the conformations g and g' obtained by the rotations of the C-O bonds in the three-bond unit $\text{O—CH}_2\text{—CH}_2\text{—O}$. This statistical weight takes into account the interactions between two oxygen atoms separated by three bonds of the molecular skeleton. These weights can be expressed with the help of the Boltzmann factors

$$\begin{aligned}\sigma &= \exp \left\{ -\Delta E_{\sigma}/RT \right\} \\ \sigma' &= \exp \left\{ -\Delta E_{\sigma'}/RT \right\}\end{aligned}\tag{15}$$

where ΔE_{σ} and $\Delta E_{\sigma'}$ are the internal-rotation energy differences between the *gauche* isomers and the *trans* form, which is chosen as a reference state; R is the gas constant, and T is the absolute temperature. In the case of POEG, for which $R = \text{H}$, one must consider a supplementary internal rotation. It will be that of the C-C bond of the $\text{H—O—CH}_2\text{—CH}_2$ unit from the beginning of the chain or, what is equivalent, that of the O-H bond of the final $\text{CH}_2\text{—CH}_2\text{—O—H}$ unit. It will be supposed that the interactions due to the terminal hydrogens are weak³ and, consequently, equal statistical weights of unity will be assigned to each of the three internal rotation states of the C-C and O-H bonds in the units described above.

For a POEM chain the probabilities of having a *trans* state and then a *gauche* (or *gauche prime*) state for the O-C or C-C bonds in the chain are, respectively,

$$\text{Pr}(t) = 1/(1 + 2\sigma) = p$$

and

$$\text{Pr}(g) = \text{Pr}(g') = \sigma/(1 + 2\sigma) = q\tag{16}$$

Similarly, the probabilities of having a *trans* state and then a *gauche* (or *gauche prime*) state for the C-O bond in the chain are given by

$$\text{Pr}(t) = 1/(1 + 2\sigma') = p'$$

and

$$\text{Pr}(g) = \text{Pr}(g') = \sigma'/(1 + 2\sigma') = q'\tag{17}$$

In the case of a POEG chain it is necessary to consider the effect of the terminal hydrogen atoms on the internal rotations of certain bonds. An equal probability of $1/3$ is assigned (consistent with the choice of unit statistical weights) to each of the internal-rotation states of the first C—C bond in the chain and to that of the last O—H bond. For a chain of type $R-O-(CH_2-CH_2-O)_n-R$, it is necessary to define three transition probabilities matrices: $\mathbf{P}(C-O \rightarrow O-C \text{ or } O-C \rightarrow C-C)$, $\mathbf{P}'(C-C \rightarrow C-O)$, and $\mathbf{P}''(2 \rightarrow 3 \text{ or } 3n+1 \rightarrow 3n+2)$, where for each of these matrices the types of bonds between which the transition must be effected have been indicated in parentheses. Thus, the notation $C-O \rightarrow O-C$, for example, means passage from the C—O bond states to those of the O—C bond. In the case of a POEM chain these matrices have the forms

$$\mathbf{P} = \begin{vmatrix} 0 & 0 & 1 \\ q & p+q & 0 \\ p & 2q & 0 \end{vmatrix} \quad (18)$$

$$\mathbf{P}' = \begin{vmatrix} 0 & 0 & 1 \\ q' & p'+q' & 0 \\ p' & 2q' & 0 \end{vmatrix} \quad (19)$$

$$\mathbf{P}'' = \mathbf{P}$$

and, for POEG molecules, only the \mathbf{P}'' matrix changes; thus,

$$\mathbf{P}'' = \begin{vmatrix} 0 & 0 & 1 \\ 1/3 & 2/3 & 0 \\ 1/3 & 2/3 & 0 \end{vmatrix} \quad (20)$$

Now, consider the various average values defined by eqs. (6')–(11'). By noticing that for $2 \leq \mu \leq 3n+2$

$$\Pr(Y_\mu = 1) = \Pr(X_\mu = a) = 1/4$$

and

$$\Pr(Y_{\mu-1} = 1) = \Pr(X_\mu = c) = 1/4$$

and by putting $\mathbf{P}'\mathbf{P}^2 = \mathbf{R}$ (this last matrix is regular if both q and q' are non-null), one obtains after further developments, the average molecular optical anisotropy in the form:

$$\begin{aligned} \langle \gamma^2 \rangle = & \left\{ \left[\frac{8}{3} \mathbf{Z} - \frac{5}{3} \mathbf{I}_3 \right] n + \frac{8}{3} [\mathbf{Z} - \mathbf{Z}^2] + \frac{8}{3} [\mathbf{R}^{n+1} \mathbf{Z}^2 - \mathbf{R}^*] \right\}_{11} \Gamma^2 \\ & + \left\{ \left[\frac{8}{3} \mathbf{P}' (\mathbf{I}_3 + \mathbf{P}) \mathbf{Z} \mathbf{P}' (\mathbf{I}_3 + \mathbf{P}) - \frac{4}{3} \mathbf{I}_3 \right] n \right. \\ & + \left. \left[\frac{10}{3} \mathbf{I}_3 - \frac{8}{3} (\mathbf{P}' \mathbf{P} \mathbf{Z} \mathbf{P}' \mathbf{P} + \mathbf{P}' (\mathbf{I}_3 + \mathbf{P}) \mathbf{Z}^2 \mathbf{P}' (\mathbf{I}_3 + \mathbf{P}) - \mathbf{P}' \mathbf{Z} \mathbf{P}') \right] \right. \\ & \left. + \frac{8}{3} [(\mathbf{P}' \mathbf{P} + \mathbf{P}' \mathbf{R}) (\mathbf{R}^{n-1} \mathbf{Z}^2 - \mathbf{R}^*) (\mathbf{R} \mathbf{P}' + \mathbf{P}' \mathbf{P})]_{11} \right\} S_{co}^2 \end{aligned}$$

$$\begin{aligned}
& + \left\{ \frac{10}{3} \mathbf{I}_3 + \frac{8}{3} \mathbf{P}'\mathbf{P}''(\mathbf{R}^{n-1} - \mathbf{R}^*)\mathbf{P}'\mathbf{P}'' \right\}_{11} \gamma_{\text{OR}}^2 \\
& + \left\{ \frac{8}{3} [\mathbf{P}'(\mathbf{I}_3 + \mathbf{P})\mathbf{Z} + \mathbf{Z}\mathbf{P}'(\mathbf{I}_3 + \mathbf{P}) - \mathbf{I}_3]n \right. \\
& + \left. \left[\frac{4\mathbf{I}_3}{3} + \frac{8}{3} (\mathbf{P}'\mathbf{Z} + \mathbf{Z}\mathbf{P}' - \mathbf{P}'(\mathbf{I}_3 + \mathbf{P})\mathbf{Z}^2 - \mathbf{Z}^2\mathbf{P}'(\mathbf{I}_3 + \mathbf{P})) \right] \right. \\
& + \left. \frac{8}{3} [(\mathbf{P}'\mathbf{R} + \mathbf{P}'\mathbf{P})(\mathbf{R}^n\mathbf{Z}^2 - \mathbf{R}^*) + (\mathbf{R}^n\mathbf{Z}^2 - \mathbf{R}^*)(\mathbf{R}\mathbf{P}' + \mathbf{P}'\mathbf{P})] \right\}_{11} \Gamma S_{\text{CO}} \\
& + \left\{ \frac{8}{3} \left[\mathbf{P}'\mathbf{P}''\mathbf{Z} + \mathbf{Z}\mathbf{P}'\mathbf{P}'' - \frac{\mathbf{I}_3}{2} \right] \right. \\
& - \left. \frac{8}{3} [\mathbf{P}'\mathbf{P}''(\mathbf{R}^n\mathbf{Z} - \mathbf{R}^*) + (\mathbf{R}^n\mathbf{Z} - \mathbf{R}^*)\mathbf{P}'\mathbf{P}''] \right\}_{11} \Gamma \gamma_{\text{OR}} \\
& + \left\{ \frac{8}{3} \left[\mathbf{P}'\mathbf{P}''\mathbf{Z}\mathbf{P}'(\mathbf{I}_3 + \mathbf{P}) + \mathbf{P}'(\mathbf{I}_3 + \mathbf{P})\mathbf{Z}\mathbf{P}'\mathbf{P}'' - \frac{3}{2} \mathbf{I}_3 \right] \right. \\
& - \left. \frac{8}{3} [(\mathbf{P}'\mathbf{P} + \mathbf{P}'\mathbf{R})(\mathbf{R}^{n-1}\mathbf{Z} - \mathbf{R}^*)\mathbf{P}'\mathbf{P}'' \right. \\
& + \left. \mathbf{P}'\mathbf{P}''(\mathbf{R}^{n-1}\mathbf{Z} - \mathbf{R}^*)(\mathbf{R}\mathbf{P}' + \mathbf{P}'\mathbf{P})] \right\}_{11} S_{\text{CO}} \gamma_{\text{OR}} V_n \geq 1 \quad (21)
\end{aligned}$$

where \mathbf{I}_3 is a third-order unit matrix,

$$\mathbf{R}^* = \lim_{n \rightarrow \infty} \mathbf{R}^n$$

$$\mathbf{Z} = [\mathbf{I}_3 - (\mathbf{R} - \mathbf{R}^*)]^{-1}$$

The matrix \mathbf{R}^* having the following form

$$\mathbf{R}^* = \begin{vmatrix} 1/4 & 1/2 & 1/4 \\ 1/4 & 1/2 & 1/4 \\ 1/4 & 1/2 & 1/4 \end{vmatrix} \quad (22)$$

The matrix \mathbf{Z} is not given here because its form is not simple. However it can be easily calculated.

As n tends towards infinity, the limits of $\mathbf{R}^{n-1}\mathbf{Z}$, $\mathbf{R}^{n-1}\mathbf{Z}^2$, etc., all equal \mathbf{R}^* .

Interdependent Internal Rotations

Now consider the case of POEM, for which $\mathbf{R} = \text{CH}_3$. It is necessary to distinguish three types^{3,7} of internal rotations in the chain: those of bonds O-C, C-C, and C-O. The corresponding statistical weight matrices have been defined and can be written, respectively as

$$\mathbf{U}_{\text{OC}} = \begin{vmatrix} 1 & \sigma & \sigma \\ 1 & \sigma\xi & \sigma\omega \\ 1 & \sigma\omega & \sigma\xi \end{vmatrix} \quad (23)$$

$$\mathbf{U}_{\text{CC}} = \begin{vmatrix} 1 & \sigma & \sigma \\ 1 & \sigma\xi' & \sigma\omega' \\ 1 & \sigma\omega' & \sigma\xi' \end{vmatrix} \quad (24)$$

$$\mathbf{U}_{\text{CO}} = \begin{vmatrix} 1 & \sigma' & \sigma' \\ 1 & \sigma'\xi & \sigma'\omega \\ 1 & \sigma'\omega & \sigma'\xi \end{vmatrix} \quad (25)$$

where each statistical weight σ , ξ , ω , σ' , ξ' , and ω' is represented by a Boltzmann factor.

The total statistical weights for each of the nine possible conformations (see Part I¹) for the four-bond unit $\text{O}-\text{CH}_2-\text{CH}_2-\text{O}-\text{CH}_2$ are given by eq. (23). Furthermore, the statistical weights of the conformations corresponding to the units $\text{CH}_2-\text{CH}_2-\text{O}-\text{CH}_2-\text{CH}_2$ and $\text{CH}_2-\text{O}-\text{CH}_2-\text{CH}_2-\text{O}$ have been represented by eqs. (24) and (25).

In the case of POEG, for which $\text{R} = \text{H}$, one must distinguish two additional internal rotations: that of the $\text{C}-\text{O}$ bond in the unit $\text{H}-\text{O}-\text{CH}_2-\text{CH}_2-\text{O}$ at the beginning of the chain and that of the terminal $\text{O}-\text{H}$ bond in the final unit, $\text{O}-\text{CH}_2-\text{CH}_2-\text{O}-\text{H}$. If one assumes that all interactions due to the terminal hydrogen are weak,³ the corresponding statistical weights matrices have the forms

$$\mathbf{U}'_{\text{CO}} = \begin{vmatrix} 1 & \sigma' & \sigma' \\ 1 & \sigma' & \sigma' \\ 1 & \sigma' & \sigma' \end{vmatrix} \quad (26)$$

$$\mathbf{U}'_{\text{OH}} = \begin{vmatrix} 1 & 1 & 1 \\ 1 & 1 & 1 \\ 1 & 1 & 1 \end{vmatrix} \quad (27)$$

In general, for the POE chain these matrices will be designated \mathbf{U}_4 and \mathbf{U}_{3n+2} . Thus, if $\text{R} = \text{CH}_3$, $\mathbf{U}_4 = \mathbf{U}_{\text{CO}}$, and $\mathbf{U}_{3n+2} = \mathbf{U}_{\text{OC}}$. The significance of the statistical weights σ and σ' has already been specified in the preceding paragraph; it is now necessary to define ξ , ω , ξ' , and ω' . In the elementary sequences $\text{O}-\text{CH}_2-\text{CH}_2-\text{O}-\text{CH}_2$, as well as in $\text{CH}_2-\text{O}-\text{CH}_2-\text{CH}_2-\text{O}$, the statistical weight ξ is associated with the conformations gg and $g'g'$ which involve interactions between a CH_2 group and an oxygen atom separated by four skeletal bonds. In these same sequences the factor ω takes into account the interaction between a CH_2 group and an oxygen atom in the molecular conformations gg' and $g'g$. Finally, in the $\text{CH}_2-\text{CH}_2-\text{O}-\text{CH}_2-\text{CH}_2$ unit the weight ξ' is attributed to conformations gg and $g'g'$, and the weight ω' to conformations gg' and $g'g$. These factors represent interactions between two CH_2 groups separated by four skeletal bonds of the molecule and in the corresponding conformations. As in Part I,¹ the statistical weights $p_t^{\mu, 3n+2}$, $p_g^{\mu, 3n+2}$, $p_g^{\mu, 3n+2}$ can now be defined. In an analogous manner it is shown that

$$\begin{aligned}
[p_t^{4,3n+2}, p_o^{4,3n+2}, p_{o'}^{4,3n+2}]_T &= \mathbf{U}_4(\mathbf{U}_{oc}\mathbf{U}_{cc}\mathbf{U}_{co})^{n-1} \mathbf{U}_{3n+2}[1,1,1]_T \\
[p_t^{3j+1,3n+2}, p_o^{3j+1,3n+2}, p_{o'}^{3j+1,3n+2}]_T &= \mathbf{U}_{co}(\mathbf{U}_{oc}\mathbf{U}_{cc}\mathbf{U}_{co})^{n-j} \mathbf{U}_{3n+2}[1,1,1]_T \\
&\quad \text{For } 2 \leq j \leq n \\
[p_t^{3j+2,3n+2}, p_o^{3j+2,3n+2}, p_{o'}^{3j+2,3n+2}]_T &= (\mathbf{U}_{oc}\mathbf{U}_{cc}\mathbf{U}_{co})^{n-j} \mathbf{U}_{3n+2}[1,1,1]_T \\
&\quad \text{For } 1 \leq j \leq n \\
[p_t^{3j+3,3n+2}, p_o^{3j+3,3n+2}, p_{o'}^{3j+3,3n+2}]_T \\
&= \mathbf{U}_{cc}\mathbf{U}_{co}(\mathbf{U}_{oc}\mathbf{U}_{cc}\mathbf{U}_{co})^{n-j-1} \mathbf{U}_{3n+2}[1,1,1]_T \\
&\quad \text{For } 1 \leq j \leq n-1 \quad (28)
\end{aligned}$$

In these expressions the subscript T indicates the transpose. In order to evaluate the conditional probabilities for the POE chain it is necessary to define the ratio $\delta^{\mu,3n+2} = p_o^{\mu,3n+2}/p_t^{\mu,3n+2}$, which can be calculated analytically. However, the results are not simple; thus, it is preferable to obtain $\delta^{\mu,3n+2}$ directly by using eq. (28). The transition probabilities have the following form

$$\begin{aligned}
\Pr(X_{\mu+1} = t/X_{\mu} = t) &= \frac{1}{1 + 2u\delta^{\mu+2,3n+2}} = p_{\mu} \\
\Pr(X_{\mu+1} = g/X_{\mu} = t) &= \Pr(X_{\mu+1} = g'/X_{\mu} = t) = \frac{u\delta^{\mu+2,3n+2}}{1 + 2u\delta^{\mu+2,3n+2}} = q_{\mu} \\
\Pr(X_{\mu+1} = t/X_{\mu} = g) &= \Pr(X_{\mu+1} = t/X_{\mu} = g') \\
&= \frac{1}{1 + u(v + w)\delta^{\mu+2,3n+2}} = r_{\mu} \\
\Pr(X_{\mu+1} = g/X_{\mu} = g) &= \Pr(X_{\mu+1} = g'/X_{\mu} = g') \\
&= \frac{uw\delta^{\mu+2,3n+2}}{1 + u(v + w)\delta^{\mu+2,3n+2}} = s_{\mu} \\
\Pr(X_{\mu+1} = g'/X_{\mu} = g') &= \Pr(X_{\mu+1} = g'/X_{\mu} = g) \\
&= \frac{uw\delta^{\mu+2,3n+2}}{1 + u(v + w)\delta^{\mu+2,3n+2}} = t_{\mu} \quad (29)
\end{aligned}$$

with for

$$\begin{aligned}
\mu = 3 \text{ if R} = \text{CH}_3 &\begin{cases} u = \sigma' \\ v = \xi \\ w = \omega \end{cases} \\
\text{if R} = \text{H} &\begin{cases} u = \sigma' \\ v = 1 \\ w = 1 \end{cases}
\end{aligned}$$

$$\begin{aligned}
 \mu = 3j; (2 \leq j \leq n) & \begin{cases} u = \sigma' \\ v = \xi \\ w = \omega \end{cases} \\
 \mu = 3j + 1; (1 \leq j \leq n - 1) & \begin{cases} u = \sigma \\ v = \xi \\ w = \omega \end{cases} \\
 \mu = 3j + 2; (1 \leq j \leq n - 1) & \begin{cases} u = \sigma \\ v = \xi' \\ w = \omega' \end{cases} \\
 \mu = 3n + 1 \text{ if } R = \text{CH}_3 & \begin{cases} u = \sigma \\ v = \xi \\ w = \omega \end{cases} \\
 \text{if } R = \text{H} & \begin{cases} u = 1 \\ v = 1 \\ w = 1 \end{cases}
 \end{aligned} \tag{30}$$

Finally, one finds that

$$\begin{aligned}
 \text{Pr}(X_3 = t) &= \frac{1}{1 + 2u\delta^{4,3n+2}} = x_3 \\
 \text{Pr}(X_3 = g) = \text{Pr}(X_3 = g') &= \frac{u\delta^{4,3n+2}}{1 + 2u\delta^{4,3n+2}} = y_3
 \end{aligned} \tag{31}$$

with $u = \sigma$ for $R = \text{CH}_3$ and $u = 1$ for $R = \text{H}$.

If one denotes by \mathbf{P}_μ the matrix of transition probabilities from the states of bond μ to those of bond $\mu + 1$, V_μ such that $3 \leq \mu \leq 3n + 1$, one has:

$$\mathbf{P}_\mu = \begin{vmatrix} 0 & 0 & 0 & 0 & 0 & s_\mu + t_\mu & r_\mu \\ 0 & 0 & 0 & 0 & 0 & 2q_\mu & p_\mu \\ q_\mu & 0 & p_\mu & q_\mu & 0 & 0 & 0 \\ s_\mu & 0 & r_\mu & t_\mu & 0 & 0 & 0 \\ t_\mu & 0 & r_\mu & s_\mu & 0 & 0 & 0 \\ 0 & r_\mu & 0 & 0 & s_\mu + t_\mu & 0 & 0 \\ 0 & p_\mu & 0 & 0 & 2q_\mu & 0 & 0 \end{vmatrix} \tag{32}$$

In order to evaluate the average values corresponding to eqs. (6')–(11'), it is necessary to express these equations as a function of states a, b, \dots, h of the Markov process. With the transition matrices \mathbf{P}_μ , the average molecular optical anisotropy of the POE chain can be written:

$$\begin{aligned}
 \langle \gamma^2 \rangle &= \frac{16}{3} \left[\mathbf{W}_1' \prod_{j=1}^n (\mathbf{H}_1)_j \mathbf{W}_1 + \mathbf{W}_2' \prod_{j=1}^n (\mathbf{H}_2)_j \mathbf{W}_2 + \mathbf{W}_3' \prod_{j=1}^n (\mathbf{H}_3)_j \mathbf{W}_3 \right] \\
 &\quad - \frac{(n\Gamma + 2nS_{\text{CO}} + 2\gamma_{\text{OR}})^2}{3} \quad V_n \geq 1 \tag{33}
 \end{aligned}$$

in which

$$\begin{aligned} \mathbf{W}_1' &= [-\Gamma\mathbf{Q}_3 + 2S_{\text{CO}}(\mathbf{L}_3' - 2\mathbf{Q}_3\mathbf{M}) + 2\gamma_{\text{OR}}\mathbf{L}_3, 2\mathbf{Q}_3, \\ &\quad (2\gamma_{\text{OR}}^2 + \Gamma^2 + 4S_{\text{CO}}\Gamma)\mathbf{Q}_3 - 2\Gamma\gamma_{\text{OR}}\mathbf{L}_3] \\ \mathbf{W}_2' &= [2S_{\text{CO}}(\mathbf{L}_3' - \mathbf{Q}_3\mathbf{M}) + 2\gamma_{\text{OR}}\mathbf{L}_3, 2\mathbf{Q}_3, 2(S_{\text{CO}}^2\mathbf{Q}_3 - S_{\text{CO}}\gamma_{\text{OR}}\mathbf{L}_3)] \\ \mathbf{W}_3' &= [2S_{\text{CO}}(\mathbf{L}_3' - \mathbf{Q}_3) + 2\gamma_{\text{OR}}\mathbf{L}_3, 2\mathbf{Q}_3, 2(S_{\text{CO}}^2\mathbf{Q}_3 - S_{\text{CO}}\gamma_{\text{OR}}\mathbf{L}_3)] \quad (34) \end{aligned}$$

$$\begin{aligned} \mathbf{W}_1 &= \begin{vmatrix} \Gamma\mathbf{V} \\ \mathbf{O}_T \\ \mathbf{V} \end{vmatrix} \\ \mathbf{W}_2 &= \begin{vmatrix} S_{\text{CO}}\mathbf{V} \\ \mathbf{O}_T \\ \mathbf{V} \end{vmatrix} \\ \mathbf{W}_3 &= \begin{vmatrix} \gamma_{\text{OR}}\mathbf{V} \\ \mathbf{O}_T \\ \mathbf{V} \end{vmatrix} \end{aligned} \quad (35)$$

with

$$\begin{aligned} \mathbf{Q}_3 &= [y_3/2, x_3/4, x_3/2, y_3/2, y_3/2, y_3/2, x_3/4] \\ \mathbf{L}_3 &= [0, x_3/4, 0, 0, y_3/2, 0, 0] \\ \mathbf{L}_3' &= [0, 0, 0, 0, 0, y_3/2, x_3/4] \end{aligned} \quad (36)$$

the matrix \mathbf{M} and vector \mathbf{V} being defined by eq. (43) of Part I.¹ Then finally:

$$(\mathbf{H}_1)_j = \begin{vmatrix} \mathbf{P}_{3j-3}\mathbf{P}_{3j-2}\mathbf{P}_{3j-1} & \mathbf{O}_7 & \Gamma\mathbf{I}_7 \\ \Gamma\mathbf{P}_{3j-3}\mathbf{P}_{3j-2}\mathbf{P}_{3j-1}\mathbf{M} & & \\ + S_{\text{CO}}\mathbf{P}_{3j-3}\mathbf{M}\mathbf{P}_{3j-2}\mathbf{P}_{3j-1} & \mathbf{P}_{3j-3}\mathbf{P}_{3j-2}\mathbf{P}_{3j-1} & \mathbf{O}_7 \\ + S_{\text{CO}}\mathbf{P}_{3j-3}\mathbf{P}_{3j-2}\mathbf{M}\mathbf{P}_{3j-1} & & \\ \mathbf{O}_7 & \mathbf{O}_7 & \mathbf{I}_7 \end{vmatrix} \quad (37)$$

$$(\mathbf{H}_2)_j = \begin{vmatrix} \mathbf{P}_{3j-2}\mathbf{P}_{3j-1}\mathbf{P}_{3j} & \mathbf{O}_7 & S_{\text{CO}}\mathbf{I}_7 \\ \Gamma\mathbf{P}_{3j-2}\mathbf{P}_{3j-1}\mathbf{M}\mathbf{P}_{3j} & & \\ + S_{\text{CO}}\mathbf{P}_{3j-2}\mathbf{M}\mathbf{P}_{3j-1}\mathbf{P}_{3j} & \mathbf{P}_{3j-2}\mathbf{P}_{3j-1}\mathbf{P}_{3j} & \mathbf{O}_7 \\ + S_{\text{CO}}\mathbf{P}_{3j-2}\mathbf{P}_{3j-1}\mathbf{P}_{3j}\mathbf{M} & & \\ \mathbf{O}_7 & \mathbf{O}_7 & \mathbf{I}_7 \end{vmatrix} \quad (38)$$

$$(\mathbf{H}_3)_j = \begin{vmatrix} \mathbf{P}_{3j-1}\mathbf{P}_{3j}\mathbf{P}_{3j+1} & \mathbf{O}_7 & S_{\text{CO}}\mathbf{I}_7 \\ \Gamma\mathbf{P}_{3j-1}\mathbf{M}\mathbf{P}_{3j}\mathbf{P}_{3j+1} & & \\ + S_{\text{CO}}\mathbf{P}_{3j-1}\mathbf{P}_{3j}\mathbf{M}\mathbf{P}_{3j+1} & \mathbf{P}_{3j-1}\mathbf{P}_{3j}\mathbf{P}_{3j+1} & \mathbf{O}_7 \\ + S_{\text{CO}}\mathbf{P}_{3j-1}\mathbf{P}_{3j}\mathbf{P}_{3j+1}\mathbf{M} & & \\ \mathbf{O}_7 & \mathbf{O}_7 & \mathbf{I}_7 \end{vmatrix} \quad (39)$$

In the matrix products in eq. (33) the seventh-order unit matrices $\mathbf{P}_0 = \mathbf{P}_1 = \mathbf{P}_2 = \mathbf{I}_7$ occur. They have been introduced here for convenience.

Matrices \mathbf{H} are of order 21. The matrix \mathbf{O}_7 and the vector \mathbf{O}_7 which are used in the expressions above, are, respectively, a seventh-order, null, square matrix and a seventh-order, null, column vector.

Numerical Results and Discussion

The values $\Gamma = 0.87 \text{ \AA}^3$ and $S_{CO} = 1.00 \text{ \AA}^3$ have been chosen in agreement with previous determinations.^{6,8} Thus, taking into consideration the anisotropy⁹ $\gamma_{CH} = 0.22 \text{ \AA}^3$ of the C-H bond, it is seen that the optical anisotropies of the C-C and C-O bonds are, respectively, equal to 1.31 \AA^3 and 1.22 \AA^3 . Consequently, from the point of view of optical polarizability, the C-C and C-O bonds appear to be similar. In this case the approximation $\gamma_{OH} = \gamma_{CH}$ would seem to be reasonable, because of the weakness of the optical anisotropy of these bonds. In the course of recent work,^{6,7} the conformations in solution of several oligomers of ethylene oxide have been studied and the following internal-rotation energies have been chosen: $\Delta E_\sigma = 1100 \text{ cal/mole}$, $\Delta E_{\sigma'} = -250 \text{ cal/mole}$, $\Delta E_\omega = +250 \text{ cal/mole}$, $\Delta E_{\omega'} \equiv +\infty$, and $\Delta E_\xi = \Delta E_{\xi'} = 0$; or, at 25°C , $\sigma = 0.1562$, $\sigma' = 1.5249$, $\omega = 0.6557$, $\omega' = 0$, and $\xi = \xi' = 1$. Therefore, a comparison between theory and experiment will not be made here. However, some numerical values of $\langle \gamma^2 \rangle$ will be given in order to illustrate our results and to provide a basis for consideration of the validity of the chain models considered.

With the help of the above data values of $\langle \gamma^2 \rangle$ have been calculated up to $n = 50$ for both the independent and the interdependent internal-rotation models [eqs. (21) and (33)]. In the case in which there is an equal

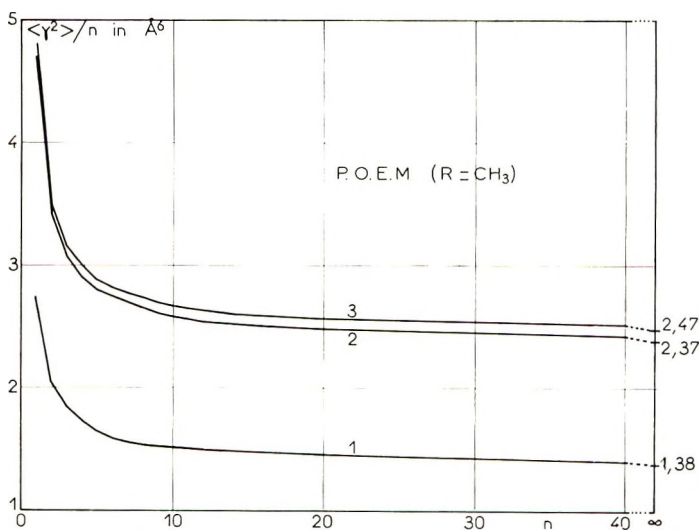


Fig. 1. Plots of $\langle \gamma^2 \rangle / n$ vs. n for POEM: (1) equiprobability; (2) independence; (3) interdependence.

TABLE I
 Values of $\langle \gamma^2 \rangle$ for POEM (R = CH₃) Calculated with the Aid
 of Markov Processes for the Various Models of Internal Rotation^{a,b}

n	$\langle \gamma^2 \rangle, \text{Å}^6$		
	Equiprobability ^c	Independence ^d	Interdependence ^e
1	2.7489	4.7041	4.8024
2	4.1335	6.8733	6.9906
3	5.5193	9.2634	9.5044
4	6.9050	11.6498	11.9725
5	8.2906	14.0255	14.4375
6	9.6763	16.4046	16.9067
7	11.0620	18.7833	19.3745
8	12.4477	21.1620	21.8425
9	13.8334	23.5406	24.3106
10	15.2191	25.9193	26.7786
11	16.6048	28.2980	29.2466
12	17.9905	30.6766	31.7147
13	19.3762	33.0553	34.1827
14	20.7619	35.4340	36.6507
15	22.1476	37.8127	39.1188
16	23.5333	40.1913	41.5868
17	24.9190	42.5700	44.0548
18	26.3047	44.9487	46.5229
19	27.6904	47.3273	48.9909
20	29.0760	49.7060	51.4589
.	.	.	.
.	.	.	.
30	42.9330	73.4927	76.1393
.	.	.	.
.	.	.	.
.	.	.	.
40	56.7899	97.2794	100.8196
.	.	.	.
.	.	.	.
.	.	.	.
50	70.6468	121.0661	125.4997

^a The degree of polymerization of the chain is n . Tetrahedral valence angles are assumed, the internal rotation angle is $\varphi = 0, \pm 120^\circ$; Γ and S_{CO} are equal to 0.87 Å^3 and 1.00 Å^3 , respectively.

^b The matrix method⁷ gives results in perfect agreement with the values in this table for the same choice of parameters.

^c By eq. (13).

^d By eq. (21) at 25°C , $\sigma = 0.1562$ and $\sigma' = 1.5249$, i.e., $p = 0.7619$, $q = 0.1190$, $p' = 0.2469$, and $q' = 0.3765$. Matrix \mathbf{P}'' is given by eq. (18).

^e By eq. (33) at 25°C , $\sigma = 0.1562$, $\sigma' = 1.5249$, $\omega = 0.6557$, $\omega' = 0$, and $\xi = \xi' = 1$ [to be substituted in relations (29), (30), and (31)]. In relations (28), \mathbf{U}_4 and \mathbf{U}_{3n+2} are equal to \mathbf{U}_{CO} and \mathbf{U}_{OC} , respectively.

probability of internal rotations, eq. (13) allows direct calculation, for each value of n , of the average molecular optical anisotropy of the chain.

These results are assembled in Tables I and II. It has been verified that

TABLE II
 Values $\langle \gamma^2 \rangle$ for POEG (R = H) Calculated with the Aid
 of Markov Processes for the Various Models of Internal Rotation^a

n	$\langle \gamma^2 \rangle, \text{\AA}^6$		
	Equiprobability ^b	Independence ^c	Interdependence ^d
1	1.6762	1.4783	1.4783
2	3.0535	3.6423	3.7020
3	4.4395	6.1404	6.3189
4	5.8252	8.4938	8.7435
5	7.2109	10.8739	11.2191
6	8.5966	13.2534	13.6869
7	9.9823	15.6318	16.1545
8	11.3680	18.0105	18.6227
9	12.7537	20.3892	21.0907
10	14.1394	22.7678	23.5588
11	15.5251	25.1465	26.0268
12	16.9108	27.5252	28.4948
13	18.2964	29.9038	30.9629
14	19.6821	32.2825	33.4309
15	21.0678	34.6612	35.8989
16	22.4535	37.0398	38.3670
17	23.8392	39.4185	40.8350
18	25.2249	41.7972	43.3030
19	26.6106	44.1759	45.7711
20	27.9963	46.5545	48.2391
.	.	.	.
.	.	.	.
.	.	.	.
30	41.8532	70.3412	72.9194
.	.	.	.
.	.	.	.
.	.	.	.
40	55.7102	94.1279	97.5998
.	.	.	.
.	.	.	.
.	.	.	.
50	69.5671	117.9146	122.2801

^a The degree of polymerization is n . Tetrahedral valence angles have been assumed, the internal rotation angle is $\varphi = 0, \pm 120^\circ$; Γ , S_{CO} , and γ_{OH} are 0.87\AA^3 , 1.00\AA^3 , and 0.22\AA^3 , respectively.

^b By eq. (13).

^c By eq. (21) at 25°C , $\sigma = 0.1562$, and $\sigma' = 1.5249$, i.e., $p = 0.7619$, $q = 0.1190$, $p' = 0.2469$, and $q' = 0.3765$. Matrix \mathbf{P}^n is given by eq. (20).

^d By eq. (33) at 25°C , $\sigma = 0.1562$, $\sigma' = 1.5249$, $\omega = 0.6557$, $\omega' = 0$, and $\xi = \xi' = 1$ [to be substituted in eqs. (29), (30), and (31)]. In eqs. (28), \mathbf{U}_1 and \mathbf{U}_{3n+2} are equal to \mathbf{U}'_{CO} and \mathbf{U}'_{OH} , respectively.

these numerical values are in excellent agreement with those obtained by using the matrix method⁷ for similar values of the parameters. The ratio $\langle \gamma^2 \rangle/n$ is plotted in Figures 1 and 2 as a function of n . In the case of POEM (Fig. 1), curves 1, 2, 3 show the same decrease as function of n . While the decrease in curve 1 is tied to the very nature of the model chosen

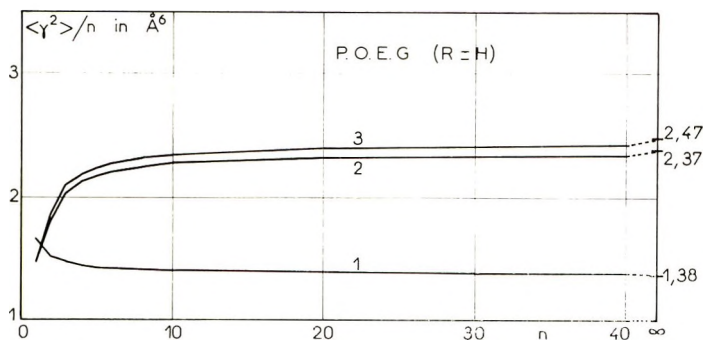


Fig. 2. Plots of $\langle \gamma^2 \rangle / n$ vs. n for POEG: (1) equiprobability; (2) independence; (3) interdependence.

(this decrease can be found in particular for POEG and PE), in the case of curves 2 and 3, it is due to the presence of terminal CH_3 groups. These groups have a strong stabilizing effect for the *trans* form ($\Delta E_\sigma = 1100$ cal/mole) of the terminal $\text{CH}_3\text{—O—CH}_2\text{—CH}_2$ and $\text{CH}_2\text{—CH}_2\text{—O—CH}_3$ units of the molecule. A strong molecular optical anisotropy must, therefore, be anticipated for the monomer molecule such that at the time of the addition of a new repeat unit to the chain, the corresponding increase of the optical anisotropy will be inferior to that of the monomer molecule, etc.

In the case of POEG (Fig. 2), on the contrary, curves 2 and 3 present an increase with n , and for the corresponding chain models, tend, respectively, to the same limits as in POEM. It is apparent that the presence of terminal hydrogen, i.e., O—H bonds of small optical anisotropy and their ability to turn freely around the adjacent bonds, results in a much weaker molecular optical anisotropy (see Tables I and II), all other things being equal.

It is essential to note that the general form of the curves for $\langle \gamma^2 \rangle / n$ as functions of n arises from the nature of the ends of the chain. However, the dependence of $\langle \gamma^2 \rangle / n$ on n is due to the internal correlations between the orientations of neighboring bonds in the molecule. It is well known that for a molecule in which the bonds are freely joined to one another without correlation between their directions, one has $\langle \gamma^2 \rangle / n = \text{constant}$ for all n . It is known¹¹⁻¹⁴ that, among the chain models that have been considered, only the hindered internal-rotation models corresponding to curves 2 and 3 of Figures 1 and 2 can lead to results in agreement with experiment. The model first studied, which corresponds to curve 1 of Figures 1 and 2, must be eliminated as unrealistic. The best agreement with the experimental results⁷ is obtained with the help of the model which explicitly takes into account the interdependence of the internal rotations (curve 3 of Figs. 1 and 2). The introduction of this condition of interdependence has the effect of augmenting the average molecular optical anisotropy of the chain by about 4% relative to the case of independence for large values of n . The difference is perceptible and must be taken into consideration. Meanwhile, it is clearly less important than that calculated under the same con-

ditions for polyethylene chains and which is of the order of 20% (see Part I¹). Because of the effect of interdependence, the internal rotations of each bond of a PE chain can lead to *gauche* conformations gg' and $g'g$ which are sterically impossible (such gg' and $g'g$ conformations are characterized by a very small molecular optical anisotropy). Consequently, a large number of molecular conformations containing such sequences are eliminated ($\omega \approx 0$ in eq. (28) of Part I], thus largely favoring the conformations with the largest molecular optical anisotropy.

In the case of polyoxyethylene chains the condition of interdependence, on the contrary, only leads to the elimination of the *gauche* conformations of the gg' and $g'g$ type for one internal rotation out of three, that of the C-C bonds [$\omega' = 0$ in eq. (24)].

The physical explication of this result can be found in the much smaller van der Waals radius of the oxygen atom (1.40 Å) compared to that of the methyl group (2.10 Å). Therefore because only a small number of molecular conformations is forbidden, the forms having the greatest molecular optical anisotropy are slightly favored. It is interesting to note here that the introduction of correlations between internal rotation angles of nearest-neighbor bonds in certain chain structures has a relatively small effect on $\langle \gamma^2 \rangle$.

Finally, it should be noted that in a general way the ratio $\langle \gamma^2 \rangle/n$ has already reached more than 90% of its limiting value for n greater than ≈ 20 . This observation shows that the part of the curve of $\langle \gamma^2 \rangle/n$ as a function of n which is the most interesting to study is that corresponding to the region where the molecular optical anisotropy per repeat unit varies most rapidly with n .

Helpful discussion with Professors P. Bothorel and G. Turrell are gratefully acknowledged.

References

1. B. Lemaire and G. Fourche, *J. Polym. Sci. A-2*, **9**, 961 (1971).
2. H. Tadokoro, Y. Chatani, T. Yoshihara, S. Tahara, and S. Murahashi, *Makromol. Chem.*, **74**, 109 (1964).
3. J. E. Mark and P. J. Flory, *J. Amer. Chem. Soc.*, **88**, 3702 (1966).
4. H. J. M. Bowen and L. E. Sutton, *Tables of Interatomic Distances and Configurations in Molecules and Ions*, The Chemical Society, London, 1958.
5. R. P. Smith and E. M. Mortensen, *J. Chem. Phys.*, **32**, 502 (1960).
6. G. Fourche, *J. Chim. Phys.*, **65**, 1500 (1968).
7. G. Fourche, *J. Chim. Phys.*, **66**, 320 (1969).
8. P. Bothorel, *J. Colloid. Sci.*, **27**, 529 (1968).
9. C. Clement and P. Bothorel, *J. Chim. Phys.*, **61**, 1262 (1964).
10. T. M. Birshtein and O. B. Ptitsyn, *Soviet Phys. Tech. Phys.*, **4**, 954 (1959).
11. S. Lifson, *J. Chem. Phys.*, **30**, 964 (1959).
12. K. Nagai, *J. Chem. Phys.*, **31**, 1169 (1958).
13. C. A. Hoeve, *J. Chem. Phys.*, **32**, 888 (1960).
14. P. J. Flory and R. L. Jernigan, *J. Chem. Phys.*, **42**, 3509 (1965).

Received July 14, 1970

Revised October 15, 1970

ESR Study of Radiation Damage in TPX Polymer (Poly-4-methylpentene-1)

D. T. GOODHEAD,* *Physics Department, St. Bartholomew's Hospital
Medical College, University of London, London, England*

Synopsis

Electron spin resonance spectroscopy has been used to study the effects of 15 MeV electrons, x-rays, and ultraviolet radiation on poly-4-methylpentene-1 (TPX) both at 77°K and at room temperature. At least seven identifiably different paramagnetic species are observable in unstabilized oxygen-free TPX after irradiation, and additional species exist in the stabilized grades. The species which predominates under most conditions is interpreted as being due to the loss of hydrogen from a main-chain tertiary carbon atom; interpretations of most of the other species are also given. Oxygen is found to diffuse rapidly into the polymer and to react with the free radicals to form peroxy species. In the absence of oxygen the radiation damage is expected to lead ultimately to crosslinking or double-bond formation, or with oxygen to degradation. The general nature of the free radicals produced by electron or x-ray irradiation is the same, but there are significant differences for ultraviolet irradiation. The observed spectra for irradiated TPX and their interpretations are in good agreement with the spectra and later interpretations for irradiated polypropylene, but are in less satisfactory agreement with the published papers on polybutene-1 and poly-3-methylbutene-1.

INTRODUCTION

Poly-4-methylpentene-1 is now commercially available as a clear or opaque polymer under the trade name of TPX (Imperial Chemical Industries, Ltd.). It has a combination of properties of commercial significance, including high optical transparency, high crystalline melting point and therefore good physical properties at high temperatures, very low density, and good electrical properties.¹

The radiation chemistry of related polymers has produced a considerable literature, much of it being the results of investigations by electron spin resonance spectrometry. Although many of the results and theories are contradictory and inconclusive, often because of minor differences in the samples used, controlled studies have now established many of the main features of the radiation chemistry of a number of well-known polymers such as polyethylene,²⁻⁴ poly(vinyl chloride),^{4,5} PTFE,^{4,6,7} and polyacrylates and polymethacrylates.^{4,8} Among the polymers more closely related to TPX are polypropylene,⁹⁻¹⁷ polybutene-1,¹⁸⁻²¹ and poly-3-methylbutene-

* Present address: Physics Department, University of Natal, Durban, South Africa.

1;²² of these, polypropylene has been the most fully studied. There is apparently at present no ESR literature on the radiation chemistry of TPX, and the understanding of the related polymers is not sufficiently precise to allow for a convincing extrapolation in the absence of experimental evidence. It will be seen that the results presented in this paper do, in general, reinforce the later interpretations of the predominant room-temperature ESR spectrum of polypropylene, for example as developed by Fischer and Hellwege,¹⁰ reinterpreted by Ayscough and Munari,¹⁶ and confirmed by Loy¹³ and Iwasaki et al.¹⁷ Our interpretations do not, however, agree with those published for polybutene-1¹⁸⁻²¹ or poly-3-methylbutene-1.²²

It has been suggested²³ that TPX may be suited for use as a convenient radiation dosimeter in the dose range ≥ 10 krad due to the radiation-induced changes in its optical density at selected ultraviolet wavelengths. Clear Perspex is now widely used in a similar manner²⁴⁻²⁷ but is only suitable for doses ≥ 500 krads. However, as with other polymers, this optical-density change in TPX undergoes "fading," in that the effect is a function of time and conditions of storage. In order to investigate this phenomenon further and to optimize the stabilizers and other contaminants in TPX, it is desirable to have an understanding of the radiation chemistry of TPX.

A knowledge of the pattern of damage due to ionizing radiation in TPX is also of commercial relevance to the mechanisms of degradation of this and other polymers, particularly in view of the potential use of TPX for radiation-sterilized products.

EXPERIMENTAL METHOD

TPX was supplied in 3 mm-thick sheets in three stabilized grades (coded R, M and K at the time of supply) and as the unstabilized polymer. The results which follow were obtained from samples of the unstabilized polymers, except where otherwise stated. For orientation studies some samples were warmed, stretched to approximately six times their original length, and cooled under tension.

Electron irradiations were carried out with a Mullard 15-MeV electron linear accelerator at an average dose rate of approximately 300 krad/min.* For irradiation with x-rays a Raymax 250 kV set was used at a dose-rate of about 500 rad/min. The ultraviolet irradiation used a focussed beam from a Phillips CS 1000-W super-high-pressure mercury lamp, with or without an ultraviolet filter (Schott UG 11) to remove wavelengths less than 2700 Å.†

For irradiation at 77°K the samples were pre-evacuated at room temperature overnight and then immersed directly into liquid nitrogen without a

* This is the dose averaged over the total irradiation time. Since the accelerator produced 1.3 μsec pulses of electrons at 400/sec, the average dose rate within the pulses is 5.8×10^6 krad/min.

† The peak transmission for a UG 11 filter is at 3300 Å and falls off to about 0.01% on either side at 3800 Å and 2700 Å, respectively. Transmission of the mercury line at 2536 Å is $\lesssim 10^{-5}$.

sample tube; this avoided background ESR spectra from irradiated sample tubes. Samples irradiated in vacuum at room temperature were irradiated in one end of an L-shaped sample tube and transferred to the other (shielded) end for ESR reading.

The electron spin resonance spectra were obtained on an X-band Hilger and Watts Microspin spectrometer operating at a microwave frequency of 9400 MHz and a magnetic field modulation frequency of 100 kHz. The first derivatives of the absorption spectra were recorded. The maximum microwave power in the cavity was not determined accurately but it was estimated to be of the order of 5 mW; nevertheless, this was sufficient to produce some power saturation in a number of the paramagnetic species observed. The most suitable general conditions for recording the spectra were found to be: microwave power level of -8 db, peak-to-peak modulation field amplitude of 3 oersted, total field sweep of 200 oersted in 10 min with a detector time constant of 0.15 sec. Most of the spectra illustrated in this paper were taken under these conditions. The magnetic field was calibrated against a proton resonance, and the number of paramagnetic unpaired spins in the samples was calculated by calibration against a freshly prepared solution of DPPH.

RESULTS

Electron or X-Ray Irradiation of TPX at 77°K

Irradiation of air-free unstretched TPX at 77°K and maintaining the sample at 77°K throughout produces a spectrum as shown in Figure 1, which we shall assume is due to a species radical I. (The particular sample shown had received an electron dose of 2 Mrad. The vertical arrow on this and subsequent figures shows the magnetic field position corresponding to a DPPH standard. The magnetic field increases from left to right.) It consists of eight approximately equidistant lines with a hyperfine splitting of $a = 23 \pm 1$ oersted, each line having a peak to peak width (on the first derivative trace) of approximately 16 oersted. The measured heights of the lines are in the approximate ratio $1.0 \pm 0.2:6.1 \pm 0.8:23 \pm 2:33$. The same spectrum is obtained from stretched irradiated TPX, and it shows no observable change with rotation of the magnetic field. The yield of unpaired spins produced by 15 MeV electrons is approximately 1.9/100 eV of deposited energy.

This paramagnetic species is stable against decay while stored in liquid nitrogen for an extended period of weeks. On warming the sample from 77°K to room temperature *in vacuo* the spectrum changes irreversibly to that of radical II described below. Maintaining the sample at room temperature for 4 min reduces the number of spins by no more than 50%, which eliminates the possibility that radical I has decayed away entirely to reveal a low-intensity radical II which had been there from the start.

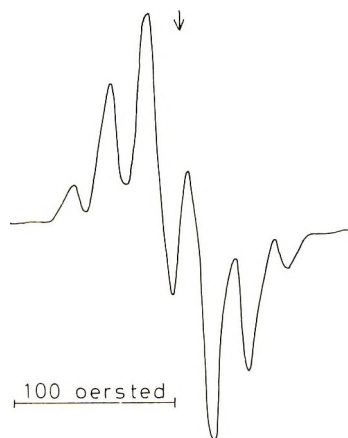


Fig. 1. Radical I. ESR spectrum (first derivative) of irradiated air-free TPX at 77°K.

Electron or X-Ray Irradiation of Unstretched TPX at Room Temperature in Vacuo

Irradiation of air-free samples at room temperature produces the spectrum shown in Figure 2, assigned to radical II. (It is shown later that this spectrum probably contains an equilibrium concentration of radical X with II.) The same spectrum is produced irreversibly on warming radical I to room temperature, and it therefore seems probable that I is the primary species even for irradiation at room temperature. The spectrum shown in Figure 2 consists of at least 17 lines with a complex intensity pattern and an overall width of 167 oersted between the centers of the outermost lines. It commences saturating strongly at a microwave power level of about -4 db.

Radical II decays slowly in vacuum at room temperature by approximately second-order kinetics with a half-life of about 5 hr when the concentration is ca. 10^{16} spins/g (corresponding to 1 day's decay after an initial radiation dose of 1 Mrad of electrons).

Attempts were made to separate the spectrum of Figure 2 into two or more identifiably different species, but all the experimental evidence pointed to its being due to one species only, or to two species with similar saturation properties over the range of microwave powers here available, identical relative production rates over a wide range of irradiation doses, identical decay rates in vacuum over extended periods of time, and similar reaction rates with oxygen. The most probable explanation including two or more species is that they are in thermal equilibrium (see Interpretation).

On cooling radical II to 77°K, the spectrum of Figure 3 (radical IIa) is obtained and is stable against decay at this temperature. This temperature change in the spectrum is reversible and shows quantitative equivalence in integrated intensities (after normalizing for spectrometer parameters including temperature). Therefore the spectra are probably due to the same

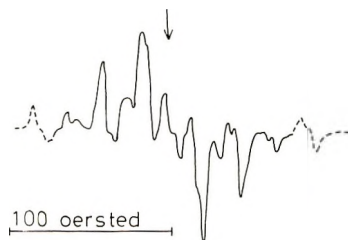


Fig. 2. Radical II in air-free TPX at room temperature (1 Mrad dose). The outermost extremes (shown in broken line) correspond to an increase in spectrometer gain by a factor 10.

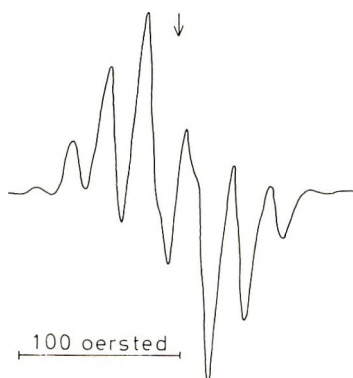


Fig. 3. Radical IIa. Spectrum obtained when a sample containing radical II is cooled to 77°K.

paramagnetic species, apart from any shift in the equilibrium on the above two-species hypothesis.

The spectrum of radical IIa is similar to that of radical I (Fig. 1), but line widths are smaller and more structure is visible. These differences are apparently independent of radical concentration or the nature of the incident ionizing radiation over the ranges studied; this does not, however, necessarily exclude the possibility that radical I is simply due to a dipole-dipole broadening of radical IIa, as will be discussed later. There is no noticeable difference in microwave power saturation properties of I and IIa over the limited power range available. The height ratios of the main lines of the spectrum of Figure 3 are $1.0 \pm 0.2:9.5 \pm 0.8:25 \pm 2:37$.

Residual Spectra

After radical II has been allowed to decay at room temperature in vacuum for a sufficient time, other small residual spectra become visible. At least three such spectra are observed in unstabilized TPX, and additional ones are present in the various stabilized grades. These residual spectra are now described, although no attempt is made to interpret those characteristic of the stabilized grades.

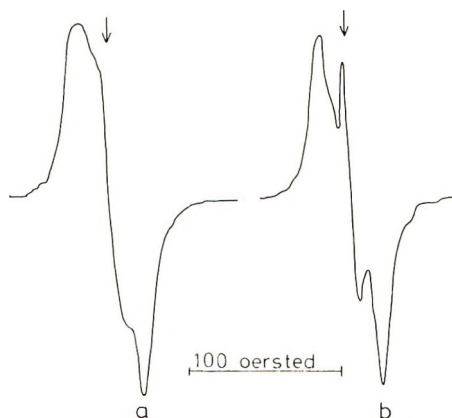


Fig. 4. Combinations of the high-dose residual radicals III (broad singlet) and IIIa (narrow singlet). These particular two spectra are from samples which were electron-irradiated at 77°K to 8 Mrad, raised to room temperature, and then (a) stored for 115 hr at room temperature, or (b) the sample tube inserted into boiling water for 30 min and the spectrum obtained at room temperature (the samples being *in vacuo* throughout).

At low doses ($\lesssim 500$ krad of electrons) unstabilized TPX shows little or no residual signal above the noise level of the spectrometer. However, at higher doses the spectrum shown in Figures 4a and 4b is observed (radicals III and IIIa). At doses of about 2 Mrad followed by room temperature decay in vacuum for 4 days, the integrated intensity of this spectrum is approximately one tenth of the initial integrated intensity of radical II. The relative intensity of the structure visible at the center of Figures 4a and 4b varies with dose, decay temperature, and microwave power level, and is therefore considered to be a separate species (termed radical IIIa). Radical III itself is therefore seen to consist of a broad singlet with no clearly resolved structure and a peak-to-peak width of 37 ± 2 oersted. It does not saturate significantly at full microwave power at room temperature. This species decays very slowly at room temperature in vacuum with a half-life of the order of weeks at the concentration studied.

Radical IIIa has been observed only in combination with other species, most notably the more slowly decaying radical III, and gives a narrow singlet of peak-to-peak width 9.5 ± 0.5 oersted. At power levels greater than about -12 db it shows strong saturation at room temperature.

A further interesting species was observed at high doses in unstabilized TPX which had 2 weeks previously received a dose of 2 Mrad and thereafter been stored in air. After giving a second irradiation of the same dose, and allowing radical II to decay in vacuum for 6 days, Figure 5 was obtained. The spectrum (radical IV) shows five well-resolved lines at a splitting of 10.4 ± 0.3 oersted; the smaller side lines are likely to be the remains of radical II, and there may well be some contribution due to radicals III and IIIa. The spectrum observed at 77°K is very similar, except that it power saturates heavily above about -10 db whereas at room temperature a slow

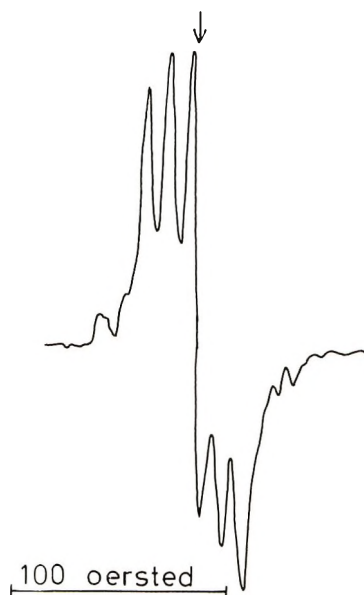


Fig. 5. Radical IV. Residual spectrum after split dose.

saturation commences only at about -4 db. Radical IV decays very slowly at room temperature with a half-life of the order of at least weeks at the above concentrations.

In stabilized K, M, and R grades of TPX three additional species (radicals V, VI, and VII) are formed even at low doses; and these may be initially dominant under certain conditions of low dose. Two of them may also dominate as more stable residuals after decay in air. The properties of these three species were studied in further detail, but they will not be discussed in this paper since the chemical natures of the stabilizers are not known to us. The radiation "scavenging" role of at least one of these stabilizers is clearly evident.

Electron or X-Ray Irradiation of Stretched TPX

It is found that the room temperature spectrum of radical II produced in irradiated stretched TPX is dependent on the angle θ between the external magnetic field and the axis of stretch of the sample, as shown in Figure 6. When $\theta = 0$, the spectrum shows less structure than does that of an unstretched sample (Fig. 2), and consists of 17 lines, eight of which are predominant. As the external magnetic field is rotated the spectrum changes progressively. This can be explained in terms of the inner six of the original main lines each splitting into two components with a maximum splitting of about 6 oersted for $\theta = 90^\circ$, at which stage the outermost lines have moved in slightly by about 2 oersted. The vertical lines drawn below spectra *a* and *c* show the positions of the individual hyperfine lines as calculated from the parameters deduced elsewhere in this paper.

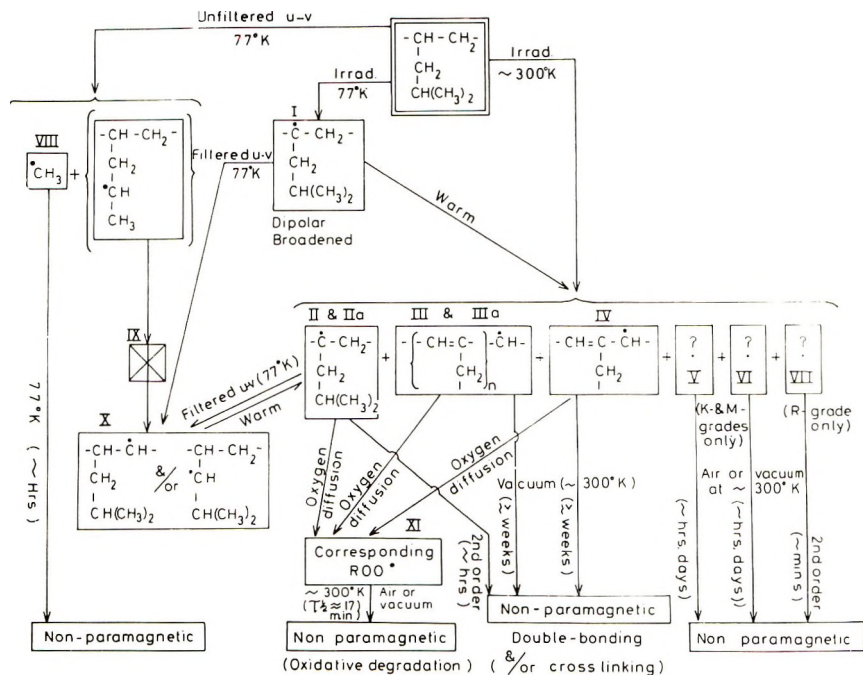


Fig. 6. Radical II in stretched TPX: (a) $\theta = 0^\circ$; (b) $\theta = 45^\circ$; (c) $\theta = 90^\circ$. The broken lines in (a) and (c) show the outermost lines with the spectrometer gain increased by a factor 6. Increases in gain by a factor 60 gave no indication of additional lines at higher or lower fields.

The corresponding 77°K spectrum of IIa does not show any significant dependence on the orientation of the sample and is in all cases as already shown in Figure 3.

Similarly the spectrum of the primary radical I, as in Figure 1, is independent of orientation.

Irradiation with Ultraviolet Light

Irradiation of TPX at 77°K with unfiltered ultraviolet light from the super-high-pressure mercury lamp, gives the spectra shown in Figure 7 which are assigned to radicals VIII and IX; the former is the very sharp quartet of approximately binomial intensity, hyperfine splitting constant $a = 22.6 \pm 0.2$ oersted and line width about 3.5 oersted, while IX is the less well resolved quartet just outside each of the lines of VIII. We make the assignment of two separate radical species on the basis of the following changes in the spectrum: (1) during the growth of the spectrum (the irradiation extending over a few hours with the sample in the cavity throughout), there are slight changes in the relative intensities of the peaks; (2) when the irradiation is terminated the peaks of VIII decay with a half-life of ca. 2 hr at these concentrations, while IX decays considerably more slowly; (3) the peaks of IX appear to saturate slightly at power levels above about -4 db while those of VIII are unaffected.

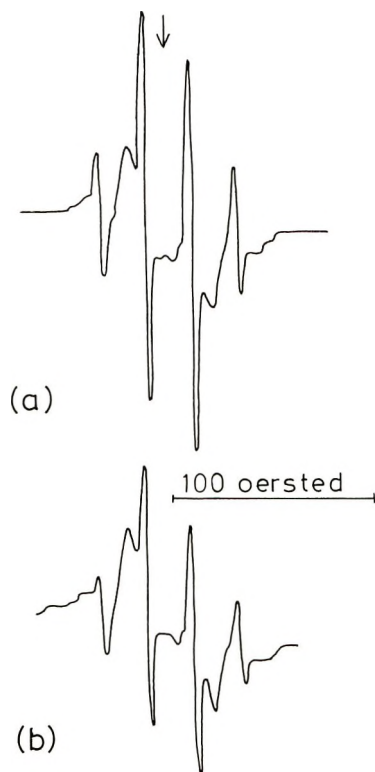


Fig. 7. Radicals VIII and IX from irradiation at 77°K with unfiltered ultraviolet radiation: (a) after 5 hr continuous irradiation, and (b) the same sample 100 min after the irradiation had ceased.

If dissolved air is present in TPX, irradiation at 77°K first produces an oxygen-dependent spectrum like XI, but this is soon surpassed by the growing spectra of VIII and IX. Irradiation at room temperature in air produces only the oxygen-dependent spectrum, while similar irradiation in vacuum produces no observable spectrum for the ultraviolet intensities available.

In K and M grades of TPX the additional spectra characteristic of these grades (V and VI) are produced at room temperature, or before the appearance of VIII and IX at 77°K. Spectra attributable to radicals V and VI are not observed in samples which have no access to oxygen during or after irradiation.

If the ultraviolet light is passed through a Schott UG11 filter to remove wavelengths of $\lesssim 2700 \text{ \AA}$, then irradiation of TPX gives no significant ESR spectrum at the doses used for the production of Figure 7.* It is therefore possible to use this filtered source to investigate the effect of soft ultra-

* Small effects are obtained, but over a much longer time scale than was used in the ultraviolet conversion experiments.

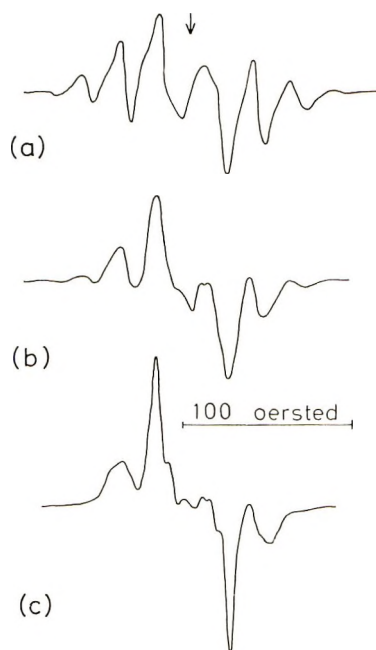


Fig. 8. Conversion of IIa into X at 77°K: (a) shows IIa as before, while (b) and (c) show the changed spectrum after irradiation with filtered ultraviolet for 15 min and a further 70 min, respectively.

violet light on the paramagnetic species produced by ionizing radiation. These results now follow.

Ultraviolet irradiation of radical IIa at 77°K converts the spectrum of Figure 3 progressively and quantitatively into a four-line spectrum (radical X) as shown in Figure 8. The two central lines are considerably narrower than the outer lines, and the latter do not appear to be exactly symmetric in shape about the center of the spectrum. The hyperfine splitting constant is approximately $a = 22$ oersted. The species begins to saturate slowly at a power level of about -8 db.

Warming the sample to room temperature reconverts radical X back to radical II (or IIa if recooled). The process



takes place without any detectable loss of radicals in either direction.

Ultraviolet irradiation of the primary radical I at 77°K converts it into a spectrum identical to that of Figure 8. On warming the sample, radical II (or IIa) is again produced.

Effects of Oxygen during or after Irradiation

When TPX is irradiated with electrons, x-rays, or ultraviolet light at room temperature in air, the asymmetric spectra shown in Figures 9a and

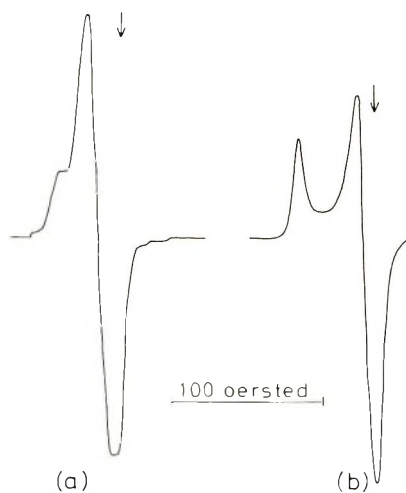


Fig. 9. The oxygen-dependent radical XI showing typical spectra at (a) 300°K and (b) 77°K, these particular spectra having been obtained after 100 krad electron irradiation in air at room temperature followed by (a) 5 min. storage or (b) immediate immersion in liquid nitrogen. [A slight background due to unoxidized II is visible in (a)].

9b are obtained (radical XI). Similar oxygen-dependent spectra have been obtained on irradiation of many other polymers^{12,20} and other substances²⁸ and have been ascribed to oxy or peroxy radicals. Assuming that the spectra of Figure 9 are due to axially symmetric g tensors, we obtain the approximate values of

$$\left. \begin{array}{l} g_{\parallel} = 2.028 \\ g_{\perp} = 2.014 \end{array} \right\} \text{at } 300^{\circ}\text{K}$$

$$\left. \begin{array}{l} g_{\parallel} = 2.034 \\ g_{\perp} = 2.008 \end{array} \right\} \text{at } 77^{\circ}\text{K}$$

This species does not saturate noticeably at full microwave power in either case. It shows no decay at 77°K and decays only slowly even at temperatures as high as 250°K. At room temperature, however, it decays rapidly in vacuum or in air with an approximately first-order decay and a half-life of about 17 min.

Irradiation in air at room temperature produces XI in conjunction with radical II (see Fig. 10), the relative proportions of the two species depending on the dose received and the thickness of the TPX sample. Admission of air to an evacuated sample containing II only, causes the almost immediate appearance of XI and the decay of II is now greatly accelerated, depending on the thickness of the TPX sample. Thus the reaction rate of species II with oxygen is seen to be controlled primarily by the rate of diffusion of oxygen into the polymer (see Discussion).



Fig. 10. Radicals II and XI in combination *in vacuo* at room temperature immediately after 1 Mrad electron irradiation in air, this dose being sufficiently high for all the dissolved oxygen to be exhausted.

The presence of the air normally dissolved in TPX is sufficient to produce XI even on irradiation in liquid nitrogen. It was therefore necessary to pre-evacuate all TPX samples before irradiation when the other species were to be studied alone.

Admission of air to radical III causes it to decay rapidly with the appearance of a spectrum of appearance similar to Figure 9; a similar effect is

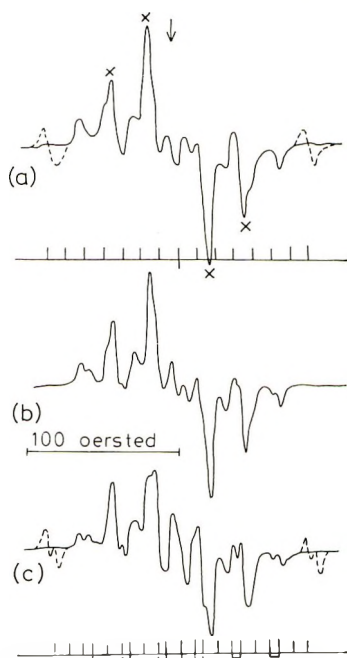


Fig. 11. Summary of experimentally observed paramagnetic species and their subsequent interpretations.

found with radical IV. The decay of the stabilizer-characteristic radicals V, VI, and VII does not appear to be affected by the presence of oxygen.

Summary of Experimental Observations

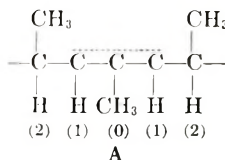
A summary of the modes of production of the various paramagnetic species observed in irradiated TPX is given in Figure 11.

INTERPRETATION OF SPECTRA

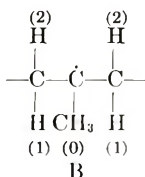
Dominant Species at Room Temperature (Radicals II and IIa)

Of the observed spectra, the one of most interest which is open to detailed interpretation is that of radical II due to its detailed structure and orientation dependence (Figs. 2, 6).

A similar spectrum of a few more lines has been observed in irradiated polypropylene by many workers.^{10,14,16,17,29,30} The complexity of the room-temperature spectrum in polypropylene has led to various interpretations, such as A



by Fischer and Hellwege¹⁰ and other workers^{29,30}, and later B,

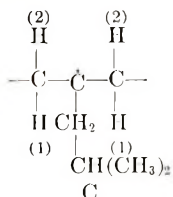


by Ayscough and Munari¹⁶ and others.^{13,17} The analysis of Fischer and Hellwege¹⁰ showed that the spectrum could be explained in terms of three equivalent protons with a hyperfine coupling constant $a_0 = 21$ gauss, two equivalent protons with $a_1 = 9$ gauss, and two equivalent protons with $a_2 = 43$ gauss. In addition, the one pair of protons have an asymmetric coupling component $b_1 = 0.75$ gauss which explains the orientation dependence of the spectrum. They assigned these protons to the allylic radical A shown above.

However Ayscough and Munari¹⁶ showed that these parameters are more consistent with an alkyl radical such as B. The main-chain β protons are not all equivalent due to an unsymmetric configuration about the C-CH₃ bond, as is observed with other alkyl hydrocarbon radicals in rigid matrices.³¹ Detailed reanalysis of the spectrum also gave an asymmetric component

$b_2 = -1.0 \pm 0.3$ gauss. This alkylic interpretation is supported by the spectra of deuterated polyethylene of Loy¹³ and the ultraviolet photolysis work of Iwasaki et al.¹⁷

It is proposed that the predominant component of radical II observed in TPX in the present study has the identity C:



The main difference from the polypropylene radical B above is that there are now only two side-chain β -protons, but their splittings will still be equivalent provided there is free rotation about this bond. The approximate resonance conditions for the individual hyperfine lines are^{10,32}

$$H_{\text{res}} = (h\nu/g\mu_{\beta}) - \sum [a_i + b_i(3 \cos^2 \theta - 1)]I_{H_i} \quad (1)$$

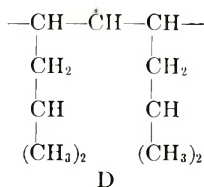
where h is Planck's constant; μ_{β} is the Bohr Magnetron; g is the g value of the electron; ν is the microwave frequency; I_{H_i} the magnetic spin quantum number of the i th proton ($\pm 1/2$); and a and b are the isotropic and anisotropic components, respectively, of the hyperfine splitting constants. A good fit is obtained with the observed TPX spectra on the assumption that there are three pairs of equivalent protons with the following parameters:

$$\begin{array}{l}
 a_0 = 24.6 \text{ oersted} \\
 b_0 = 0 \\
 a_1 = 10.2 \text{ oersted} \\
 b_1 = 0.74 \text{ oersted} \\
 a_2 = 48.1 \text{ oersted} \\
 b_2 = -0.19 \text{ oersted}
 \end{array} \quad (2)$$

These parameters are consistent with the above identity of radical II. The anisotropic components of the hyperfine splitting (b_1 and b_2) cause the spectrum of stretched TPX to alter as the magnetic field is rotated. On Figure 6a and 6c are shown the corresponding positions of the hyperfine lines as calculated by using the parameters (2). The fact that the magnified outer lines of Figure 6c are also slightly split is considered to be due to all the relevant molecules not being perfectly aligned, even in stretched TPX.

It is clear from the intensities of the observed spectra (Figs. 2 and 6) that a computed spectrum derived with the above parameters would not give good agreement in the intensities of some of the inner lines, even if the orientation dependence of the splitting parameters were taken fully into account. In particular the observed peaks marked "X" on Figure 6a are abnormally high. This is probably due to an underlying species consistent with the experimental spectrum of radical X (Fig. 8) which is later identified

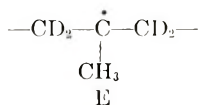
as an alkyl radical with the unpaired electron on a secondary carbon, most probably:



Since no difference could be observed in the relative intensities of II and X in the room temperature spectrum, irrespective of the dose of ionizing radiation or conditions or duration of decay, it seems that there exists a thermal equilibrium between these two species at room temperature. The implied mobility of the free electron along the main chain is relevant to the rate of decay of the radicals in vacuum, which is presumed to be by cross-linking or the formation of double bonds. At 77°K the equilibrium no longer exists, since radical II can be converted entirely into X by ultraviolet photolysis.

On cooling the irradiated TPX sample to 77°K much of the structure of the room temperature spectrum is lost (radical IIa as in Fig. 3) and there is no noticeable orientation dependence in the stretched sample. It seems reasonable that this eight-line spectrum can be computed by an adjustment of the parameters of eq. (2) and a slight broadening of the individual lines. However, minor adjustments are not in fact able to achieve this, and the observed spectrum does not contain sufficient detail to allow for a unique interpretation of the parameters. A good fit would probably require not only a nonequivalence of the two side-chain β protons, but also a major adjustment in the splittings of the main-chain β protons.

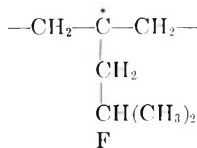
A similar low-temperature nine-line spectrum (but showing rather more structure) has been observed in polypropylene,^{10, 13, 14, 17, 29, 30} and this has been attributed to the same species as the room-temperature spectrum,^{10, 13, 17} i.e. the radical B, above. The corresponding spectrum in deuterated polypropylene¹³ has four lines and is consistent with



Detailed fits of the splitting parameters to the low-temperature polypropylene spectrum have not been achieved, but the change in the spectrum on cooling has been attributed to a restriction in the rotation of the side-chain β protons and a slightly distorted conformation from the original helical structure.¹⁷

One of the possible adjustments to the room temperature hyperfine parameters which would give the observed number of lines for both TPX and polypropylene at 77°K is $a_1 \rightarrow 0$, one of the side-chain β protons having $a_0 \rightarrow a_2$, and the other one (or two, for polypropylene) having $a_3' \rightarrow a_2/2$.

In view of the reversibility of the change of IIa to II with temperature, the overall similarity of the room-temperature and 77°K spectra apart from detailed structure, and the number of lines (8) as compared to that (9) for the low-temperature spectrum in polypropylene, it is concluded that radicals IIa and II are the same chemical species, viz.



(If X is in equilibrium with IIa at room temperature, it may still be present to some extent after cooling to 77°K.)

The *G* value for the production of II by electron-irradiation of TPX at 77°K and then warming to room temperature in the absence of oxygen is $\geq 0.8/100$ eV. This is of the same order as the alkylic free radicals produced in polyethylene² and in polypropylene¹⁰ by x-irradiation. It should also be noted that the stability of II in vacuum at room temperature is similar to that of the alkyl radicals in polypropylene¹⁶ and polyethylene which have half-lives of the order of days. These comparisons support our identification of II and IIa as alkyl radicals.

The observed second-order decay of II at room temperature in vacuum suggests that it decays by the formation of double bonds or by crosslinking due to the mobility of the unpaired electron along the main chain.

Primary Spectrum at 77°K (I)

The identification of radical I is now considered. The only two sites for the unpaired electron on the polymer molecule which could give a sufficiently large number of hyperfine lines of the observed splittings are the tertiary carbon atoms on the main or the side chains. The latter would be expected to give a nine-line spectrum for free rotation of all the appropriate C-C bonds, or probably more if the rotations are restricted; it is therefore difficult to reconcile such a species with the observed eight-line spectrum of I. The alternative suggestion is that I consists predominantly of radicals of the main-chain tertiary carbon which we have already identified above (radical IIa). The broader lines of I could be due to either underlying broad species or a poorly resolved low-intensity spectrum with an odd number of lines (e.g., perhaps 9).

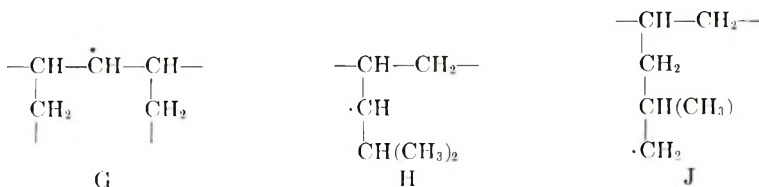
On the other hand, this broadening of II may be caused by a dipole-dipole effect due to the close proximity of the radicals. A sufficiently large dipole-dipole interaction to allow a $\Delta M = 2$ transition (at $g \approx 4$) has been observed in a number of irradiated polymers (including polypropylene) by Iwasaki and Ichikawa,³³ and they have attributed some of the primary broad species at *g ca.* 2 in polypropylene to such an interaction.¹⁷ Here in TPX, unpaired electrons on adjacent main-chain tertiary carbon atoms $\lesssim 3 \times 10^{-8}$ cm apart would have their $\Delta M = 1$ lines broadened by $\gtrsim 300$

oersted (in the absence of any exchange narrowing). The dipole field remains sufficient to cause significant broadening of the lines of radical IIa provided that the distances between the unpaired spins is $\lesssim 10 \times 10^{-8}$ cm. A uniform distribution of unpaired electrons 10×10^{-8} cm apart would require ca. 10^{21} spins/cm³, whereas at a typical dose of 2 Mrad of electron irradiation the observed spectrum corresponds to less than 10^{19} spins/cm³. Furthermore, the same broad-line spectrum of I is produced even at very much lower doses, including 5 krad of x-rays. The high concentrations required to produce the observed broadening must therefore be due to a very nonuniform distribution of free radicals, such as one would expect along the paths of charged particles of high linear energy transfer, such as slow electrons. This is consistent with the fact that most of the energy transferred from the incident radiation (be it high energy electrons, x-rays or γ -rays) to the polymer is ultimately via slow secondary electrons.

We therefore conclude that radical I is predominantly identical to IIa but with sufficient local concentration to cause dipolar broadening of the spectrum.* The change to the spectrum of IIa on warming and recooling the sample corresponds to the combination of those unpaired electrons which were close enough to one another to cause dipolar broadening.

Ultraviolet Photolysis of IIa and I to X

Photolysis of IIa at 77°K with filtered ultraviolet radiation converts it progressively and quantitatively into the four-line spectrum of X as described above (Fig. 8). Since the filtered ultraviolet radiation in use had been shown to be incapable of producing a significant proportion of paramagnetic species directly from TPX, Radical X is assumed to be a photolysis product of IIa. Assuming the correct identification of IIa above (which does not involve a rupture of the C-C main or side chains), there are only three possible species which could produce a four-line spectrum such as X, viz:



The spectra of G and H would be almost identical if there were no rotation about the appropriate side chain bonds. It is therefore not possible to make a definite choice between these two. Inspection of the observed spectrum favors a species with one α -hydrogen rather than two α -hydrogens. In particular, for one α -hydrogen there should be an asymmetry between the lowest and the highest field lines while for two α -hydrogens these two lines should have a characteristic doublet structure.³⁴ The former is observed

* Nevertheless, the existence of other additional underlying resonances in the primary spectrum cannot be ruled out.

on the spectrum of X while the latter is not; however, the spectral lines are broad and the overall resolution is low, so that these conclusions remain tentative.

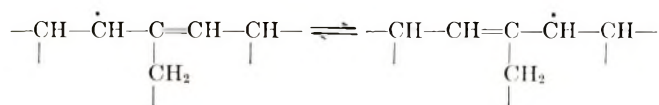
The most probable assignment of radical X is therefore considered to be G or H (or both).

It was shown above that I is most likely IIa at sufficiently high concentrations to cause dipolar broadening of the spectral lines. The ultraviolet photolysis of I is consistent with this conclusion, since it too converts into radical X.

On warming X to room temperature, it reverts immediately to the spectrum of II, although it was suggested that Figure 2 is in fact a thermal equilibrium of II and X. With the assumption of the above assignment G, this implies a high mobility of the unpaired electron along the main chain and hence a second-order decay with the formation of double bonds or cross links.

Residual Spectra (III-VII)

Radical IV (Fig. 5) has an overall line width and hyperfine splitting (ca. 10.4 oersted) comparable with allylic radicals in irradiated nonterminal olefins,³⁵ allylic alcohols,³⁵ liquid hydrocarbons,³⁶ and polyethylene.² Irradiated unsymmetric olefins show that in general the hydrogen is lost from the β -carbon atom in the longer chain.³⁵ Since radical IV was best produced after a split dose with a time interval of ca. 2 weeks between irradiations it seems that the appropriate double bonds were formed by the first irradiation. A likely assignment for IV is therefore



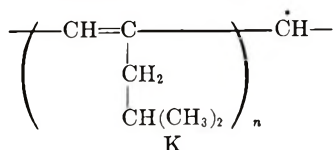
where the two α -protons and the two β -protons all have a similar hyperfine splitting of 10.4 ± 0.3 oersted. These values are consistent with theory^{37,38} and with the allylic radicals observed in other systems, as is the fact that the interaction with the protons on the side chain is unobservably small.³⁵ (Other assignments are possible if one includes crosslinking and chain ruptures due to the initial radiation.)

On the above model it would seem that IV may be observable after a single irradiation if this were undertaken at room temperature at a much lower dose rate (cf. 300 krad/min used here). A similar species has been observed in polypropylene under conditions of higher dose (ca. 20 Mrad), higher temperature, and unspecified (but presumably lower) dose rate.¹⁶ The lifetime of species IV, having a half-value of weeks at least, is similar to that of allylic radicals observed in irradiated polyethylene² and irradiated polypropylene.¹⁶

It is presumed that these allyl radicals ultimately decay by the formation of double bonds or crosslinks but they are clearly less mobile than the

alkyl radicals of II. A similar low mobility and long half-life should apply to the polyenyl radicals (III and IIIa) described below.

Radicals III and IIIa (Figs. 4) appear at high doses of irradiation and the spectrum of the former is of similar width to the allylic radical IV but with poorly resolved hyperfine structure. Similar spectra have been seen³⁹ after large dose irradiations ($>10^8$ rads) in polypropylene, polyethylene,^{2,40} poly(vinyl chloride),⁵ poly(methyl methacrylate), and poly(vinyl alcohol), and have been attributed to polyenyl radicals, being characteristic of electrons trapped in highly conjugated systems.³⁹ Consequently III and IIIa are attributed to polyenyl radicals of the type



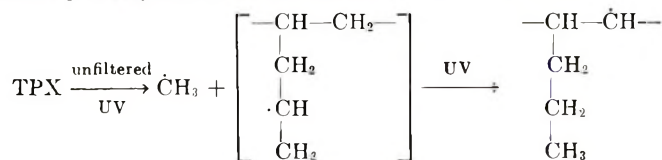
The fact that these polyenyl radicals are observed at much lower doses in TPX (ca. 10^6 rads) than has been reported in other systems may be due to the high dose-rates used in the present study and to the fact that these radicals are detectable above the other species (notably the alkyl radical II) only after many days of decay in vacuum.

Radicals V, VI, and VII are associated with the stabilizers in the various grades of commercial TPX; their observed spectra were all identifiably different (in shape, stability etc.) from any of the species found in unstabilized TPX. No attempt has been made to identify these species.

Unfiltered Ultraviolet Spectra (VIII and IX)

Hard ultraviolet irradiation of oxygen-free TPX at 77°K produces the spectrum shown in Figure 7. As stated, this spectrum is almost definitely due to two different species. The sharp quartet of narrow lines (radical VIII) is characteristic of the methyl free radical as has been observed in many different media.^{4,28,41} This methyl radical is observed to be sufficiently mobile in TPX at 77°K to decay by combination with identical or other species.

The quartet of broader lines (radical IX) is produced simultaneously with the methyl free radicals and in similar concentration; therefore it is probably the complementary species or a ultraviolet photolyzed derivative thereof. In this case the only site for the unpaired electron to produce a four-line spectrum (excluding chain breaks) is on the binary carbon of the main chain. This means that IX is the same as the most probable identification of X, which seems reasonable since they are both stable products of ultraviolet photolyzed rearrangements. Thus we have



This assignment of IX could be checked by warming an ultraviolet-irradiated sample to room temperature in vacuum when II should be obtained. However, the concentrations of free radicals produced by the ultraviolet source available were not sufficient to allow this test to be made with reliability.

Oxygen-Dependent Species (Radicals XI)

When oxygen is present during or after irradiation with ionizing radiation, the radicals XI are observed in TPX (Fig. 9). This spectrum with an axially symmetric g -tensor is typical of oxy or peroxy radicals, the latter being the more probable assignment, especially when molecular oxygen is admitted after irradiation. Similar peroxy species have been observed in a wide variety of substances including irradiated polymers like polypropylene,¹² PTFE,⁴² polyethylene;⁴³ in general, only polymers with extensive hydrogen bonding are resistant to reaction with oxygen during or after irradiation.⁴¹

In the present study it was found that the alkyl radicals (II), the allyl (IV) and the polyenyl (III and IIIa) all reacted with oxygen at 77°K (if oxygen was present within the polymer) and at room temperature, to give the corresponding peroxy radicals (ROO \cdot). The spectra from the different species are not detectably different, since the unpaired electron is isolated from the protons of the carbon chain.

These peroxy radicals were found to decay by approximately first-order kinetics, which suggests either a unimolecular rearrangement to a non-paramagnetic form or a chain mechanism of the type suggested by Fischer et al.¹² for the decay of the peroxy radicals in polypropylene. In either case, the peroxy radicals are thought to lead ultimately to the degradation of the polymer.

The rate of formation of peroxy radicals from the primary radicals is governed primarily by the diffusion rate of oxygen into the polymer (or for low doses by the concentration of dissolved oxygen). Owing to the rapid diffusion of oxygen into TPX at room temperature it is expected that most of the radiation damage in unstabilized TPX under normal conditions (room temperature, in air) will follow the path of peroxy radicals to oxidative degradation.

At the lower doses, the stabilized grade behaved significantly differently when irradiated in air by forming their characteristic spectra without the additional peroxy spectra. However, this was not studied in detail.

Summary

The above interpretations of the experimental evidence are summarized in Figure 11.

DISCUSSION

The observable radiation damage is apparently highly selective (even at 77°K, at which temperature the stability of the ultraviolet-photolyzed

radical X shows that the unpaired electron is not able to migrate freely). The predominant species at 77°K or at room temperature is due to loss of hydrogen from the main chain tertiary carbon (radicals I, II and IIa). It is somewhat surprising that no corresponding species is observed for the side-chain tertiary carbon, although it remains possible that this does in fact make some small contribution to the observed spectra of Figures 1, 2 and 3; alternatively it may be unstable even at 77°K.

The nature of the radiation damage in evacuated TPX is approximately independent of the nature of the ionizing radiation (electrons or x-rays), the dose (in unstabilized TPX from less than 10 krad up to more than 20 Mrad), the dose rate (from less than 300 rad/min with x-rays to more than 300 krad/min with electrons*), and the temperature of irradiation (77°K or room temperature) once the sample has attained room temperature. In all cases the overwhelmingly predominant free-radical species is that due to radical II (I,IIa). The initial yield of this species at 77°K is of the order of 1.5/100 eV. The additives in the three stabilized grades studied significantly alter the nature of the damage for the lower doses only (\lesssim 50 krad for V and VI, and ca. 300 krad for VII). It may be expected that differences of dose rate, linear energy transfer, and perhaps dose, would have a significant effect on the production rates of the allyl and polyenyl radicals (IV, III, and IIIa), but this was not investigated in detail.

A significantly different pattern of damage was found for irradiation with hard ultraviolet radiation in that the methyl free radical (VIII) was formed. Even under similar conditions of low dose-rate, and taking into account the decay of VIII at 77°K, no evidence was found of its production with 250 kV X-rays or with 15 MeV electrons. However, the complementary species produced by the hard ultraviolet radiation (IX) could well be identical to that produced by soft ultraviolet after ionizing radiation (X), and this is known to convert to radical II at room temperature. Hence the ultimate damage to the TPX main chain by ultraviolet radiation may well be the same as for ionizing radiation, although a methyl group will have been lost from the side chain.

The presence of oxygen during or after irradiation has a highly significant effect on the ultimate fate of the primary damage. In the absence of oxygen there is a relatively slow second-order decay of the primary species presumably by the formation of double bonds or crosslinks. Oxygen alters this by the rapid formation of peroxy radicals whose decay is highly temperature dependent and is supposedly followed by oxidative degradation. At low doses (\lesssim 100 krad) there is sufficient oxygen dissolved within the unevacuated polymer for most of the primary radicals to be immediately oxidized even at 77°K. At higher doses, the oxidation is limited by the oxygen diffusion rate in TPX which is greater than in most plastics. The data on the decay of radical II in air at room temperature show for example

* As stated before this is actually a true dose rate of 6×10^3 krad/min within the pulses.

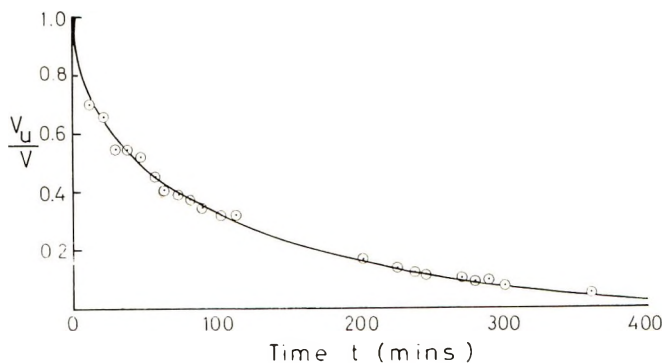


Fig. 12. Rate of oxygen diffusion into TPX at 300°K, showing experimental points and calculated curve for $k = 6.6 \times 10^{-3} \text{ cm/sec}^{1/2}$.

that oxygen has diffused completely throughout a 3 mm-thick sample within 500 min (see Fig. 12). If the diffusion data are fitted to an expression of the type

$$d = kt^{1/2}$$

where d is the depth to which the oxygen has diffused from the surface after time t , the value of k at atmospheric pressure and about 300°K is obtained as $6.6 \times 10^{-3} \text{ cm/sec}^{1/2}$.* Figure 12 shows this to be a remarkably accurate method of determining the diffusion rate of oxygen into such polymers.

It has been established that in general polymers with quaternary carbon atoms undergo radiation-induced degradation while those with secondary carbons undergo only crosslinking,⁴⁵ and those with tertiary carbons are expected to be intermediate in behavior (e.g., polypropylene⁴⁶). Consequently one might expect TPX to be intermediate in its behavior. The present study shows that the relative probability of degradation to crosslinking in TPX should be highly dependent on the access of oxygen to the sample. If it is irradiated and stored in vacuum a preponderance of crosslinking and unsaturation would be expected; but if it is in air during or shortly after irradiation, the damage should be largely by degradation. Even the thicker samples should undergo more degradation than polypropylene owing to the higher diffusion rate of oxygen in TPX. The dose rate would seem to play a part here, since at high dose rates there will be

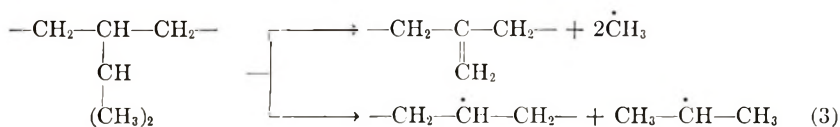
* In Figure 12, V is the total volume of the TPX sample used and V_u is that proportion which is still unoxygenated at time t . The experimental points are ratios of the height of a high-field peak of radical II (well clear of the peroxy spectrum) to its original height. Since the oxidation rate is much greater than the diffusion rate, this proportion of unoxidized II is considered to be an accurate measure of the unoxygenated volume. The calculated curve assumes diffusion from all sides of the sample of dimensions $(2.0 \times 0.30 \times 0.35) \text{ cm}^3$.

rapid cross linking and double-bond formation coupled with a temporary depletion of oxygen. Thus relatively low dose rates from natural radiation or smaller ^{60}Co γ -sources would be expected to give less crosslinking than the high dose-rate electron irradiations used in the present study.

It is seen from this paper that ESR irradiation studies of commercially supplied poly-4-methylpentene-1 may be expected to yield a variety of different results depending on the nature of the stabilizers and other additives, the ESR microwave power levels used (since many of the spectra saturate at relatively low power), and the presence of oxygen in even very low concentration. Differences in crystalline structure may also affect the spectra as has been observed in other polymers.^{18-20,21}

The general pattern of radiation damage in TPX as deduced from the present results is in good agreement with the observations and later interpretations of the damage in irradiated polypropylene,^{10,13,16,17} particularly in respect of the dominant room-temperature and 77°K spectra. Rather different interpretations have been put on the results of irradiated polybutene-1 by Hukuda, Kusumoto, Kawano and Takayanagi,¹⁸⁻²⁰ but as with most ESR data, their results are open to other interpretations, which may make them consistent with what one would expect from the polypropylene and TPX theories. Their results and those of Rubin and Huber²¹ do show conclusively, however, that the observed ESR spectra in polybutene-1 are dependent on the different crystalline modifications of the polymer, at least in respect of the decay rates of the different free radical species.

Also published are the results of one study of irradiation damage in poly-3-methylbutene-1.²² By infrared spectroscopy it was concluded that the probable effects of irradiation with 1 MeV electrons are as shown in eq. (3).



These effects are dissimilar to those seen in TPX. However, direct comparison of ESR data with those of infrared spectroscopy are difficult, since a large variety of different irradiation products are undoubtedly formed, as is seen below.

TPX samples tested by infrared were (1) unirradiated, (2) irradiated with 15-MeV electrons to about 2 Mrad in air at room temperature, (3) irradiated with 15-MeV electrons to about 2 Mrad in air at 77°K and then stored in air at room temperature, (4) an air-free sample irradiated at 77°K *in vacuo* and stored *in vacuo* at room temperature for two weeks. Infrared analysis showed that sample 1 contained some C=C bonds as detected by the absorption band near 6.1 μ ; the number of these appears to be reduced by irradiation and they are not detectable in samples 2-4. (There are no corresponding ESR observations since it was assumed that the initial

proportion of unsaturation in the polymer was negligible. The infrared data were not sufficiently sensitive to detect the small concentrations of radiation-induced C=C bonds which the TPX data suggest should be present in sample 4.) Small amounts of hydroperoxide groups (bands at 2.81μ) were seen in samples 2 and 3 but not in sample 4, which is consistent with the treatment of the samples. No carbonyl groups were detected. In addition, the volatiles produced by irradiation of TPX in an evacuated sealed tube were tested by mass spectrometry. The spectrum was not scanned low enough for hydrogen but it showed a mixture of low molecular weight hydrocarbons, including methane, ethane, propane, butanes, butenes, and longer chain hydrocarbons (up to at least C_7H_{16}). Although this run was not quantitative, there appeared to be present more methane and ethane than propane, and these three each outweighed the other hydrocarbons by more than an order of magnitude.

As mentioned before, TPX has been investigated with a view to its possible application in plastics dosimetry²³ in a dose range extending below that covered by clear Perspex dosimetry.²⁴⁻²⁷ However, as with most other plastics, the radiation-induced optical density change varies with time of storage after irradiation, and to have to take all readings at a fixed time partially defeats the simplicity and convenience of plastic dosimetry. This "fading" is relatively slight in Perspex,²⁵ hence the Perspex dosimetry is widely used in the range $\gtrsim 5 \times 10^5$ rads. Some of the grades of TPX studied²³ showed promise for extending this technique to lower doses (down to about 10 krad), apart from the problems due to fading. The present ESR study elucidates some of the transient phenomena in irradiated TPX, and it is seen that the kinetics of the decay of the free radicals can be partially correlated with some of the fading phenomena, particularly over the first few hours. This could be extended by studying the ultraviolet absorption by the free radicals (including conversions such as $II \rightarrow X$) as a function of wavelength. It also highlights the strong dependence of fading on such factors as the presence of oxygen and thickness of sample, temperature of storage, and nature and concentration of stabilizers used. The dosimetry work²³ has shown that unstabilized TPX is a less sensitive dosimeter than some of the stabilized grades and also fades more than most; the optimum grade contains a mixture of stabilizers. If the nature of the stabilizers is available, then an extension of the ESR studies to include these grades should assist in a better understanding of the dosimetry system and perhaps allow for more control of the sensitivity and fading. By comparison an optimum formulation of clear Perspex for dosimetry has been established,^{26,27} but mainly from the point of view of empirical studies of optical density.

The author wishes to thank Imperial Chemical Industries, and Dr. D. G. M. Wood in particular, for supplying the various grades of TPX, for helpful discussions, and for obtaining the infrared and mass spectrometry data. Thanks are also due to Dr. K. A. Hasan for his cooperation in the preliminary stages of this work.

References

1. "TPX" *Methylpentene Polymers*, I.C.I. Plastics Division, Bulletin T 101. Welwyn Garden City, England (1967).
2. S. Ohnishi, S. Sugimoto, and I. Nitta, *J. Chem. Phys.*, **37**, 1283 (1962).
3. A. Charlesby and M. G. Ormerod, paper presented at 5th International Symposium on Free Radicals, Uppsala, 1961.
4. P. B. Ayscough, *Electron Spin Resonance in Chemistry*, Methuen, London, 1967.
5. E. J. Lawton and J. S. Balwit, *J. Chem. Phys.*, **65**, 815 (1961).
6. H. N. Rexroad and W. Gordy, *J. Chem. Phys.*, **65**, 815 (1961).
7. N. Tamura, *J. Phys. Soc. Japan*, **16**, 3838 (1961).
8. M. G. Ormerod and A. Charlesby, *Polymer*, **5**, 67 (1964).
9. Yu. D. Tsetkov, Yu. N. Moline, and V. V. Voevodskii, *Vysokomol. Soedin.*, **1**, 1805 (1959).
10. H. Fischer and K.-H. Hellwege, *J. Polym. Sci.*, **56**, 33 (1962).
11. S. Ohnishi, *Bull. Chem. Soc. Japan*, **35**, 254 (1962).
12. H. Fischer, K.-H. Hellwege, and P. Neudöfl, *J. Polym. Sci. A*, **1**, 2109 (1963).
13. B. R. Loy, *J. Polym. Sci. A*, **1**, 2251 (1963).
14. V. K. Milinchuk and S. Ya. Pshezhetskii, *Vysokomol. Soedin.*, **6**, 666 (1964).
15. L. J. Forrestal and W. G. Hodgson, *J. Polym. Sci. A*, **2**, 1275 (1964).
16. P. B. Ayscough and S. Munari, *J. Polym. Sci. B*, **4**, 503 (1966).
17. M. Iwasaki, T. Ichikawa, and J. Toriyama, *J. Polym. Sci. B*, **5**, 423 (1967).
18. K. Hukuda, N. Kusumoto, I. Kawano, and M. Takayanagi, *Kogyo Kagaku Zasshi*, **67**, 2163 (1964).
19. N. Kusumoto, K. Hukuda, I. Kawano, and M. Takayanagi, *Kogyo Kagaku Zasshi*, **68**, 825 (1965).
20. K. Hukuda, N. Kusumoto, I. Kawano, and M. Takayanagi, *J. Polym. Sci. B*, **3**, 743 (1965).
21. I. D. Rubin and L. M. Huber, *J. Polym. Sci. B*, **4**, 337 (1966).
22. J. P. Luongo, *J. Polym. Sci. B*, **5**, 281 (1967).
23. K. A. Hasan, Ph.D. Thesis, St. Bartholomew's Medical College, University of London. London, 1968.
24. J. F. Fowler, *Phys. Med. Biol.*, **8**, 1 (1963).
25. J. W. Boag, G. W. Dolphin, and J. Rotblat, *Rad. Res.*, **9**, 589 (1958).
26. C. G. Orton, Ph.D. Thesis, St. Bartholomew's Medical College, University of London. London (1965).
27. R. J. Berry and C. H. Marshall, *Phys. Med. Biol.*, **14**, 585 (1969).
28. B. H. J. Bielski and J. M. Gebicki, *Atlas of Electron Spin Resonance Spectra*, Academic Press, New York, 1967.
29. V. K. Milinchuk and S. Ya. Pshezhetskii, *Dokl. Akad. Nauk SSSR*, **152**, 665 (1963).
29. V. K. Milinchuk and S. Ya. Pshezhetskii, *Dokl. Akad. Nauk SSSR*, **152**, 665 (1963).
30. H. Yoshida and B. Rånby, *Acta Chem. Scand.*, **19**, 72 (1965).
31. P. B. Ayscough and C. Thomson, *Trans. Faraday Soc.*, **58**, 1477 (1962).
32. D. J. E. Ingram, *Free Radicals as Studied by ESR*, Butterworths, London, 1958.
33. M. Iwasaki and T. Ichikawa, *J. Chem. Phys.*, **46**, 2851 (1967).
34. R. Lefebvre and J. Maruani, *J. Chem. Phys.*, **42**, 1480 (1965).
35. P. B. Ayscough and H. E. Evans, *Trans. Faraday Soc.*, **60**, 801 (1964).
36. R. W. Fessenden and R. H. Schuler, *J. Chem. Phys.*, **39**, 2147 (1963).
37. H. M. McConnell and D. B. Chestnut, *J. Chem. Phys.*, **28**, 107 (1958).
38. C. Heller and T. Cole, *J. Chem. Phys.*, **37**, 243 (1962).
39. S. Ohnishi, Y. Ikeda, S. Sugimoto, and I. Nitta, *J. Polym. Sci.*, **47**, 503 (1960).
40. E. J. Lawton, J. S. Balwit, and R. S. Powell, *J. Chem. Phys.*, **33**, 405 (1960).
41. P. J. Sullivan, and W. S. Koski, *J. Amer. Chem. Soc.*, **85**, 384 (1963).

42. T. Matsugashita and K. Shinohara, *J. Chem. Phys.*, **35**, 1652 (1961).
43. H. Fischer, K.-H. Hellwege, U. Johnsen, and P. Neudoerfl, *Kolloid Z.*, **196**, 129 (1964).
44. J. J. Hermans, *J. Colloid Sci.*, **2**, 387 (1947).
45. T. S. Nikitina, (Ed.) *Effects of Ionising Radiations on High Polymers*, Gordon & Breach, New York, 1963.
46. A. Charlesby, *Atomic Radiation and Polymers*, Pergamon Press, New York-London, 1960.

Received September 14, 1970

Revised December 14, 1970

Molecular Morphology of Cellulose

R. ST. JOHN MANLEY, *Department of Chemistry and Pulp and Paper Research Institute, McGill University, Montreal, Canada*

Synopsis

Native celluloses of various biological origins, as well as regenerated celluloses were examined by electron microscopy after suitable dispersion. In all cases the specimens were found to be composed of a common filamentary unit which is rectangular in cross section and has the approximate dimensions $35 \times 20 \text{ \AA}$. It is suggested that these are the basic morphological units of cellulose; they are therefore called protofibrils. For protofibrils of regenerated cellulose it is shown that: (1) the molecular contour length greatly exceeds the protofibril length, (2) the mass of the protofibril corresponds to that of a single molecule, and (3) the protofibril length increases with molecular weight. Additionally, high resolution electron micrographs of native and regenerated protofibrils show an apparent axial texture with a periodicity of about 40 \AA . From these observations and the knowledge that the molecular chain axis is aligned parallel to the protofibril axis, a model of the protofibril is deduced. The model consists of a ribbon which is pleated on itself so as to form a planar zigzag structure of rectangular cross section. This supersedes a previously proposed model of circular cross section. The structure is composed of a single folded chain, arranged so that the short extended segments between the folds are parallel to the protofibril axis. The protofibril is thus regarded as the morphological expression of the cellulose molecule. Microfibrils and protofibrils often exhibit kinks, the angle between the kinked portions being 120° . This phenomenon is satisfactorily explained by the protofibril model and in fact provides good support for it. Finally, various properties of cellulose are considered in relation to the model. By contrast with the earlier crystalline-amorphous concepts of cellulose fine structure, it is suggested that protofibrils are completely crystalline structures, and that the properties of cellulose may be understood by considering processes that occur at the level of the protofibril as a unit.

INTRODUCTION

The elucidation of the fine structure of cellulose is a complex problem which has received much attention but remains unresolved. This paper gives a comprehensive account of an investigation which has been carried out in this laboratory over a period of years. As a general frame of reference it may be well to begin with a recapitulation of the origins of the work.

Cellulose is a linear polymer composed of anhydroglucose units joined by 1-4 β -glycosidic bonds. It forms the principal constituent of plant cell walls where it occurs as thin threads of indefinite length called microfibrils. In width, microfibrils vary from 70 to 300 \AA , depending upon the source of the cellulose.¹⁻³ Cellulose can also be obtained in a regenerated form which in some cases has also been found to be fibrillar in structure.⁴⁻⁶ In the case of native cellulose the degree of polymerization is not known with certainty,

but recent research⁷ suggests that it may be at least as high as 15,000. For regenerated celluloses, the degree of polymerization is of the order of 500.

The existence of an ordered structure in celluloses is shown conclusively by x-ray and electron diffraction studies. The diffraction patterns exhibit many reasonably well-defined reflections which have been accounted for in terms of three spatial coordinates. There are four recognized crystalline modifications. Here we shall be concerned with two, namely, cellulose I and II, which occur normally in native and regenerated celluloses, respectively.

Although a considerable amount of work has been done on the crystal structure of cellulose, there is still no completely satisfactory answer. For cellulose I, the most favored structure is that proposed by Meyer and Misch.⁸ It is based upon a monoclinic unit cell with the dimensions $a = 8.35 \text{ \AA}$, $b = 10.3 \text{ \AA}$ (fiber axis), $c = 7.9 \text{ \AA}$, $\beta = 84^\circ$. The unit cell of cellulose II is similar, with the dimensions $a = 7.92 \text{ \AA}$, $b = 10.3 \text{ \AA}$ (fiber axis), $c = 9.08 \text{ \AA}$, $\beta = 63^\circ$.⁹ For both modifications the unit cell contains two cellobiose residues which belong to chain molecules passing through the center and corners of each cell; these chains are generally believed to be in an antiparallel arrangement.

In addition to the relatively sharp maxima, the diffraction patterns of cellulose also display more diffuse scattering. The latter has been interpreted to mean that the ordering process does not extend throughout the sample. In effect, therefore, the material is considered to be only partially crystalline, and the relative amounts of the total crystalline and amorphous regions determines the degree of crystallinity. There are several methods for the measurement of percentage crystallinity in cellulose. By the x-ray method as proposed by Hermans^{10,11} it has been found that native celluloses of different biological origin, vary in crystallinity over wide limits from 40% bacterial cellulose to 70% in *Valonia* cellulose. Regenerated celluloses have crystallinities in the region of 40%.

From the above, as well as other observations, the fine structure of cellulose came to be interpreted in terms of a two-phase crystalline-amorphous or "fringed micelle" model.¹² According to this concept cellulose microfibrils are regarded as assemblies of crystalline and amorphous regions, with each chain molecule extending through several crystalline and amorphous domains. This picture in various guises¹³⁻¹⁶ has dominated all discussions of the small-scale structure of cellulose and its relation to physicochemical properties. However, during the last decade, the study of polymer morphology has led to the realization that the fringed-micellar model is fundamentally incorrect for synthetic polymers. It is now recognized that the basic mode of polymer crystallization is the development of lamellar structures comprised of folded chain molecules.^{17,18} We were accordingly led to question the validity of the fringed-micellar model for cellulose, and the attempt to obtain further information followed two paths. On the one hand, a study was made of the growth and morphology of single crystals of cellulose derivatives and other carbohydrate polymers.^{19,20} The immediate

aim of this work was to ascertain whether chain folding, similar to that in crystals of the synthetic polymers, would occur, in spite of the generally supposed stiffness of the cellulose molecules. The crystals, obtained by precipitation from dilute solution, were found to have properties entirely analogous to those of the synthetic polymers. In particular, they are lamellar in structure and are composed of molecules folded perpendicular to the lamellae. While this observation did not necessarily imply that the cellulose molecule must also be folded in native cellulose, it did suggest a new possibility to be considered.

The second line of investigation was more direct and forms the subject matter of the present paper. The fine structure of a wide range of native and regenerated celluloses was investigated by high-resolution electron microscopy. These studies provide evidence that there is a fundamental morphological unit of structure common to all celluloses. We then examine the possible disposition of the cellulose molecules within this structural unit and arrive at a new proposal for the fine structure of cellulose. Preliminary accounts of this work have previously been published.^{21,22}

EXPERIMENTAL

Materials

The samples used are listed below.

Native Celluloses

Valonia ventricosa cellulose. This is a unicellular alga, the vesicles of which may reach a volume as large as 30 cc. The vesicles were obtained preserved in formalin solution from the General Biological Supply House, Chicago. Before use the cell walls were prepared as follows. Calcareous deposits were removed by soaking overnight in 0.1*N* HCl at room temperature. Noncellulosic amorphous material commonly present in the cell wall was removed by treatment with hot 0.5*N* ammonium oxalate and 6% NaOH.

Tunicate Cellulose. The specimen was supplied by Rayonier Inc., Shelton, Washington. It was obtained from a colonial tunicate of the genus *Botryllus*. The cellulose was isolated as follows. The specimens were homogenized, extracted with acetone, washed with water, and treated with solutions of chlorine dioxide at pH 7 and at room temperature. After five treatments with ClO₂ and one extraction with 4% sodium hydroxide solution at room temperature, the solids were further dispersed in an Osterizer for 45 sec. After two more treatments with ClO₂, the brei was thoroughly washed with water and freeze-dried. Nitrogen content was found to be 0.25%; the nitrate degree of polymerization was 3160, and paper chromatography of its hydrolyzate showed only traces of sugars other than glucose.

Bacterial Cellulose. This material was supplied by Dr. J. R. Colvin of the National Research Council, Ottawa. The cellulose was produced by

the bacterial species *Acetobacter xylinum* as thick pellicles on the surface of the culture medium. The pellicles were homogenized in a Waring Blender and the cellulose was purified by boiling under nitrogen for 4 hr with 1*N* NaOH. The cellulose was then washed repeatedly in distilled water.

Ramie Celluloses (*Bohemia nivea*). The fibers were subjected to an extraction first with hot ethanol and then with boiling water. The sample was then treated with hot 1% sodium hydroxide, and, after a thorough washing with distilled water, it was bleached with glacial acetic acid and sodium chlorite. The bleached material was then washed with water.

Cotton Linters. An acetate grade material supplied by the Hercules Powder Company. It was kier boiled and dewaxed by alcohol-benzene extraction.

Wood Cellulose. Softwood, acetate grade wood pulp, was used.

Regenerated Celluloses

Fortisan. This is a highly stretched commercial cellulose yarn supplied by the Celanese Corporation of America; it is prepared by steam-stretching cellulose acetate yarn and then saponifying with caustic soda and sodium acetate.

Cellulose Regenerated from Dilute Viscose Solution. Ripe viscose containing 7% cellulose and 6% sodium hydroxide was diluted to 1/10 of this concentration with water and stirred until the solution became homogeneous. Then 1% hydrochloric acid was added slowly with stirring until the deep orange color of the viscose impurities changed to yellow. The gelatinous precipitate which formed slowly was separated by centrifugation and washed with several changes of distilled water.

Cellulose Regenerated from Solution. The cellulose was dissolved in cadmium ethylenediamine as described by Henley,²³ the resulting solution was diluted with water and then dialyzed against water until all the cellulose had precipitated.

Films. Cellulose triacetate films were cast from chloroform solution (6%). The solution was spread on a mercury surface and the solvent was evaporated at a controlled rate. The films were saponified in 2% potassium hydroxide solution in aqueous methanol at room temperature. The resulting cellulose films were about 100 μ thick and were shown to be isotropic by x-ray measurements.

Methods

Swelling

Swelling treatments were carried out in 23*N* sulfuric acid at room temperature for 0.5–1 min. Specimens were then thoroughly washed with distilled water and prepared for electron microscopy.

Ultrasonics

Ultrasonic disintegration of the cellulose specimens was carried out under distilled water by using an MSE ultrasonic apparatus operating at 20 keps

with an output of 60 W. The suspensions so formed were diluted with water in order to obtain a suitable distribution of material on the specimen grids.

Specimen Preparation

Shadow Casting. In most cases the specimens were shadowed with platinum at an angle of 30°. A few preparations were, however, shadowed with platinum/carbon at an angle of 75°. The high angle of deposition was used to minimize the effects of background structure.²⁴ The procedure described by Bradley²⁴ was followed closely with the use of platinum/carbon pellets obtained from Ladd Industries Inc., Burlington, Vermont.

A drop of an aqueous suspension of the cellulose sample was placed on carbon-covered specimen grids and allowed to dry down. The grids were then shadowed at the appropriate angle.

Negative Staining. The bulk of the investigation was carried out with the aid of the negative contrast technique.²⁵⁻²⁷ The basic method was to apply a drop of the aqueous suspension under examination to carbon-coated specimen grids and allow this to dry down. A drop of staining agent was then applied to the grid, left for about 15 sec, and finally the excess liquid was removed by touching the grid with a piece of filter paper so that a thin film remained which dried at room temperature in a very short time.

The chief difficulty with these preparations arose from background "noise" due to surface structure in the supporting carbon film. In addition, the supporting film caused an appreciable decrease in the clarity and contrast of the specimen image. As Huxley and Zubay²⁷ pointed out, these difficulties can be obviated by viewing the stained specimen in the absence of the supporting carbon film. This is accomplished by using carbon films with holes. The staining material dries across the holes as a thin film in which the specimen is embedded.

Holey carbon films were prepared by a method due to Harris.²⁸ A Formvar film was cast on a glass slide from an emulsion containing 0.25% Formvar in dichloroethylene and glycerol in the ratio 32:1. The emulsion was formed just prior to use by sonication for about 5 min. After drying for about 10 min the slide was exposed to a jet of steam for 2 min. The film was then stripped on a trough of water and mounted on the supporting specimen grids. After drying, the grids were covered with a layer of evaporated carbon about 200 Å in thickness and the Formvar substrate was dissolved in dichloroethylene.

The preparation of the specimens with the holey carbon films was as follows: 1 cc of 1% staining agent was mixed with 2 cc of specimen suspension. A droplet of this mixture was applied to the grid and the excess blotted away to leave a thin film of liquid which dried rapidly by evaporation in the air.

Surface Replication. Fiber surfaces and the cell wall of *Valonia ventricosa* were replicated by a method described by Norberg.²⁹ The specimen supported on a glass slide, was shadowed with platinum at an angle of 30°,

and then coated with carbon evaporated at normal incidence. The coated specimen surface was then brought into contact with a sheet of polystyrene softened by heating to 150°C. On cooling, the polystyrene hardened and formed a protective backing on the replica. After removal of the cellulose by dissolution in copper ethylenediamine, the replica was mounted on specimen grids and the polystyrene was dissolved with toluene.

Electron Microscopy

Preparations were examined in a JEM 6A electron microscope by use of double condenser illumination, an accelerating voltage of 80 kV, a 300 μ condenser aperture, and a 50 μ objective aperture. Photographs were taken at instrumental magnifications of 20,000–80,000 \times .

The magnification was calibrated by directly imaging the lattice of indanthrene olive crystals in the microscope. Suitable thin crystals were obtained by cooling from solution in quinoline. The crystals are lathlike in habit and at high magnifications show a system of fringes running parallel to their length. The lattice translation corresponding to these fringes is 24.9 Å as determined by x-ray diffraction.³⁰

Molecular Weights

For some of the specimens it was necessary to know the contour length of the constituent cellulose molecules. This was generally calculated from the intrinsic viscosity in cadmium ethylenediamine (Cadoxen) at 25°C. Degrees of polymerization were approximated from the intrinsic viscosities by using the relation,²³

$$[\eta] = 1.7 \times 10^{-2} Z_w^{0.77}$$

Z_w denoting the weight average degree of polymerization. In a few cases the samples were converted into cellulose trinitrate by using a mixture of nitric acid and acetic anhydride;³¹ intrinsic viscosities were then measured in acetone at 25°C and degrees of polymerization were calculated from the equation,³²

$$[\eta] = 5.0 \times 10^{-3} Z_w$$

The viscosity measurements were made in an Ubbelohde dilution viscometer having a negligible kinetic energy correction, and the intrinsic viscosities were determined in the usual manner by plotting reduced viscosity against concentration and extrapolating linearly to zero concentration.

X-Ray Diffraction

The x-ray diffraction studies were made with a Seifert unit and the use of nickel-filtered $\text{CuK}\alpha$ radiation. Wide-angle patterns were obtained in a flat plate camera, while low-angle observations were made with a Kiessig vacuum camera³³ with a collimating system which permitted a resolution of about 300 Å.

OBSERVATIONS

Electron Microscopy

Native Celluloses: Identification of Fundamental Morphological Units

Preparations of *Valonia* cellulose obtained by ultrasonic dispersion of whole vesicles and examined by the negative staining method showed basically two types of structures. As illustrated in Figure 1 these comprise microfibrils (200–400 Å wide) which sometimes contain oval-shaped areas disposed along their length, and filaments about 35 Å in diameter.

Microfibrils showing the above mentioned oval-shaped areas are also seen in shadowed preparations at high magnification (Fig. 2). The oval-



Fig. 1. Typical preparation of separated filaments from *Valonia ventricosa* negatively stained with uranyl acetate. The preparation was obtained by ultrasonic dispersion of purified specimens. Most of the larger filaments show oval-shaped areas disposed along their length; as indicated in the text these are believed to be artifacts. Electron micrograph, magnification 218,000 \times .



Fig. 2. Microfibrils of *Valonia ventricosa* as seen at high magnification by the shadow-casting technique. Notice the oval-shaped discontinuities similar to those found in negatively stained preparations. Electron micrograph shadowed with platinum-carbon, magnification 110,000 \times .

shaped areas are then very clearly delineated. To our knowledge, such structures have not hitherto been observed in *Valonia* preparations. At first sight they give the impression of being holes in the microfibrils, but it is a little difficult to see how such an interpretation could be correct, especially since they occupy so large a proportion of the microfibril. The clue to what may be the correct interpretation, and what is in any case a plausible one, was found when negatively stained preparations were examined in the absence of a supporting carbon film (Fig. 3). The microfibrils were then embedded in a thin film of staining agent suspended over holes in the carbon film as described earlier. It was then found that the microfibrils no longer exhibited the oval-shaped areas. It therefore seems reasonable to suppose that the oval-shaped areas are not related to the struc-



Fig. 3. Preparation of *Valonia ventricosa* as visualized by the negative staining technique in the absence of a supporting carbon film. The specimen is supported in a thin film of uranyl acetate suspended over a hole in a carbon film. Electron micrograph, magnification 157,000 \times .

ture of the microfibril, but arise from the fact that the microfibril is not in contact with the substrate over its entire length. As a result the staining agent is able to creep between the fibril and the substrate in some areas, but is excluded from others. A similar effect would arise in shadowed specimens because back-scattered metal is only accessible to some portions of the microfibril-substrate interface.

In many cases the microfibrils were devoid of the oval-shaped areas, and it may be presumed, in accordance with the foregoing remarks, that in such cases the microfibrils are in contact with the substrate over their entire length (Fig. 1). On close inspection these microfibrils appeared to show a fine structure consisting of bands or threads, 30–40 Å wide, running parallel to the long axis. Further evidence for the presence of a fine structure in the microfibrils was found in cases where mechanical rupture had occurred, presumably during specimen preparation. Thin threads 30–40 Å wide were then seen extending between the fracture surfaces (Fig. 4). As already mentioned above, long isolated filaments of a similar width were frequently observed in all preparations (e.g., Fig. 1). The natural interpretation of these observations is that *Valonia* microfibrils are composed of finer structure elements consisting of filaments about 35 Å wide running parallel

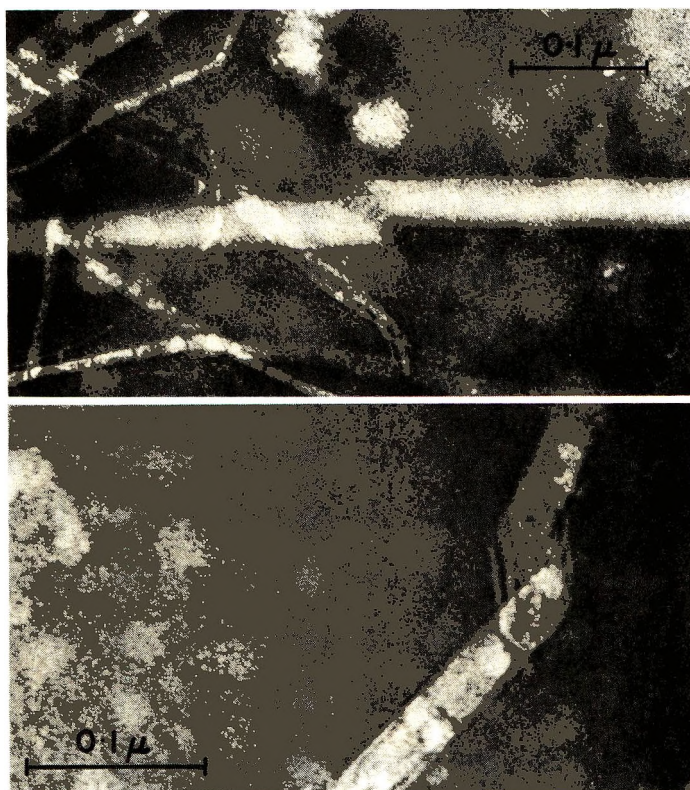


Fig. 4. Microfibrils of *Valonia ventricosa* fractured, presumably during specimen preparation. Thin filaments are pulled out between the fracture surfaces. Electron micrograph negatively stained with uranyl acetate; magnification (a) 180,000 \times , (b) 232,000 \times

to the length of the fibril. The isolated 35 Å filaments, to which attention has already been drawn, originate from the microfibrils from which they are torn during ultrasonic dispersion. In an attempt to verify this hypothesis the following experiment was performed. A *Valonia* vesicle was swollen in 23N sulfuric acid at room temperature for a few minutes. The vesicle was then neutralized in sodium hydroxide solution and washed thoroughly with water. When a piece of the vesicle was subjected to ultrasonic dispersion under water, it disintegrated completely and went into suspension. This is in contrast to the case of untreated material which is only partially dispersed by sonication. When a drop of the suspension was dried down and examined in the electron microscope with the negative staining method, only one structure element was found; i.e., filaments of varying length but having a uniform thickness of about 35 Å (Fig. 5). From this result it may be concluded that the 35 Å filaments are the structural constituents of *Valonia* microfibrils.

We now describe what appears to be a rather singular effect, observed principally in microfibrils of *Valonia* cellulose, but seen, though less frequently, in other kinds of cellulose. Figure 6 shows an example of a



Fig. 5. Filamentary structure elements of *Valonia microfibrils* isolated by swelling and subsequent sonication. Negatively stained with uranyl acetate, magnification 240,000 \times .

Valonia microfibril which is bent in a more or less regular geometrical manner. The kinking appears to occur without buckling and while the kink angles generally lie in the range of 100–150°, the most frequently observed value is 120°. In some preparations similar kinking was observed in the 35 Å constituent structure elements of the *Valonia* microfibrils. An example is shown in Figure 6. Here also the angle between the kinked portions is about 120°. It thus appears that the kinking occurs at the level of the individual 35 Å filaments. The frequency of occurrence of these deformed fibrils and the remarkable constancy of the kink angle suggest that the phenomenon is not a chance occurrence. We believe that these observations are intriguing enough on any count, but preeminently so in relation to the fine structure of the filamentary structure elements. This will be considered later.

Results with bacterial and tunicate cellulose were similar to those on *Valonia*. The microfibrils have dimensions of (300–700 Å) \times (60–80 Å) and (140–160 Å) \times (120–140 Å), respectively. On application of the swelling and sonication procedure described earlier, the microfibrils liberate regular filamentary units 35 Å in diameter, similar to those seen in *Valonia*. It may be concluded therefore that the microfibrils of these celluloses are,

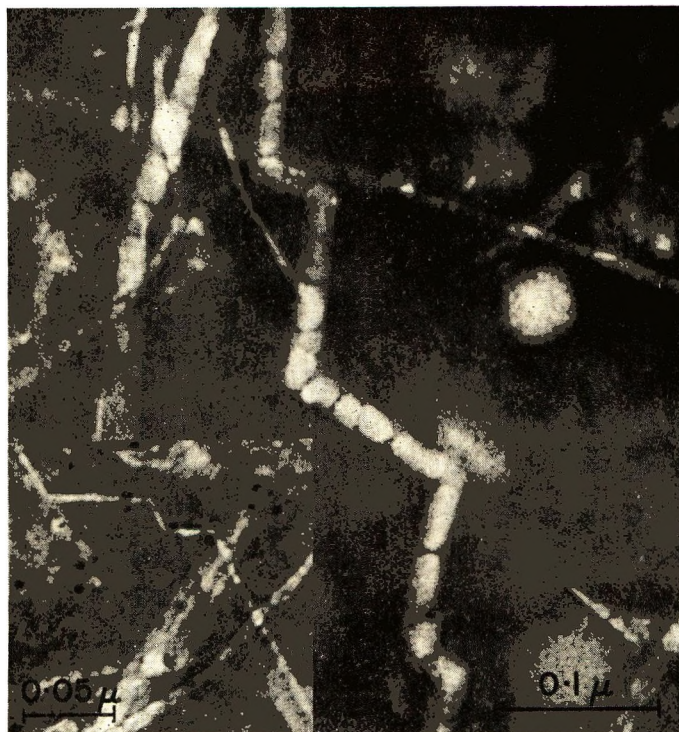


Fig. 6. A microfibril of *Valonia ventricosa* showing regular kinks. The kink angle is about 120° . The axially disposed oval shaped areas are an artifact (see text). Electron micrograph negatively stained with uranyl acetate, magnification $218,000\times$. (Inset) A 35 \AA filament isolated from *Valonia ventricosa*. The filament shows regular kinks similar to those observed in microfibrils. Electron micrograph negatively stained with uranyl acetate, magnification $230,000\times$.

like *Valonia*, composed of smaller filamentary structure elements which are aligned parallel to the microfibril axis.

It may be noted that in the celluloses considered so far, the microfibrils occur as coherent units of more or less uniform width and thickness. To judge from the electron micrographs it would appear that these microfibrils are ribbonlike structures, of rectangular cross section. Superficially, the main difference between them appears to be one of size. If the constituent filamentary structure elements are packed in the microfibrils in an ordered array, variations in microfibril size, from one species to another, can be accounted for in a simple manner as related to the total number of structure elements contained in the microfibril. By way of illustration, Figure 7 shows how microfibrils of *Valonia* and bacterial cellulose might be built up by close packing of the 35 \AA filaments.

To continue with our observations and deductions, we now consider some celluloses from higher plants. Preparations from ramie, cotton, and wood celluloses were examined. In all cases the specimens are found to consist of aggregates or bundles of filaments all having approximately the same

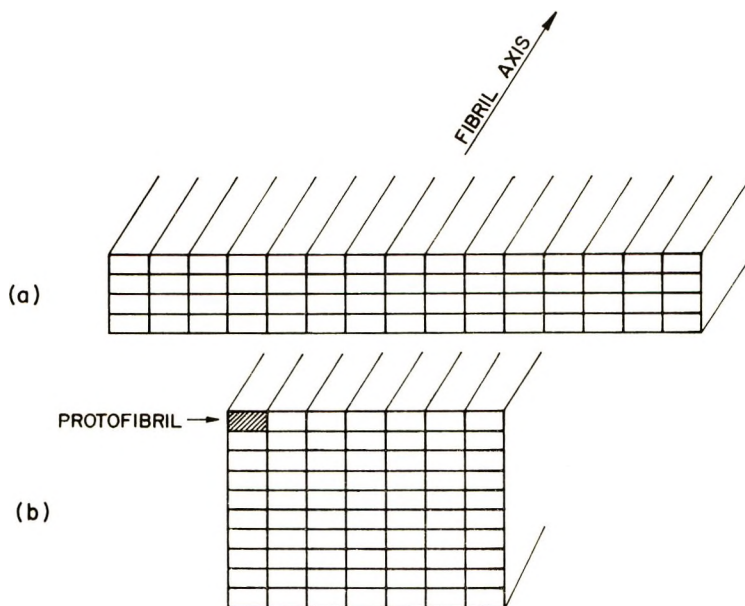


Fig. 7. Schematic drawing showing how cellulose microfibrils might be built up from protofibrils in close-packed arrays: (above) bacterial cellulose microfibril; (below) *Valonia* cellulose microfibril. The drawings have been made to scale taking into consideration the dimensions of the microfibrils and protofibrils as derived from electron micrographs. The protofibrils have been drawn with a rectangular cross section as suggested by experimental evidence to be presented later.

diameter and of indefinite length. The filaments are more loosely packed than in *Valonia*, tunicate, and bacterial cellulose and it is not necessary to resort to the acid swelling and sonication procedure to reveal their presence.

In the foregoing we have described observations on a variety of native celluloses. Invariably they have been found to consist of discrete filaments, about 35 Å wide and indistinguishable in appearance regardless of their biological source. The wide diversity of the specimens chosen, suggests that this finding is valid for all naturally occurring celluloses. We consider this to be a significant observation, and as no smaller structure elements were found, it seems justifiable to regard these filaments as the ultimate unit filaments or fundamental morphological units of natural celluloses in general. In accordance with accepted biological terminology we propose to designate them as cellulose protofibrils. For the same units Muhlethaler^{34,35} has used the term elementary fibril. As will be indicated later, these protofibrils are composed of cellulose molecules and accordingly are the carriers of the essential chemical and configurational characteristics of cellulose.

Regenerated Celluloses

When an oriented regenerated cellulose is disintegrated ultrasonically under water, pronounced fibrillation readily occurs. When the fragments

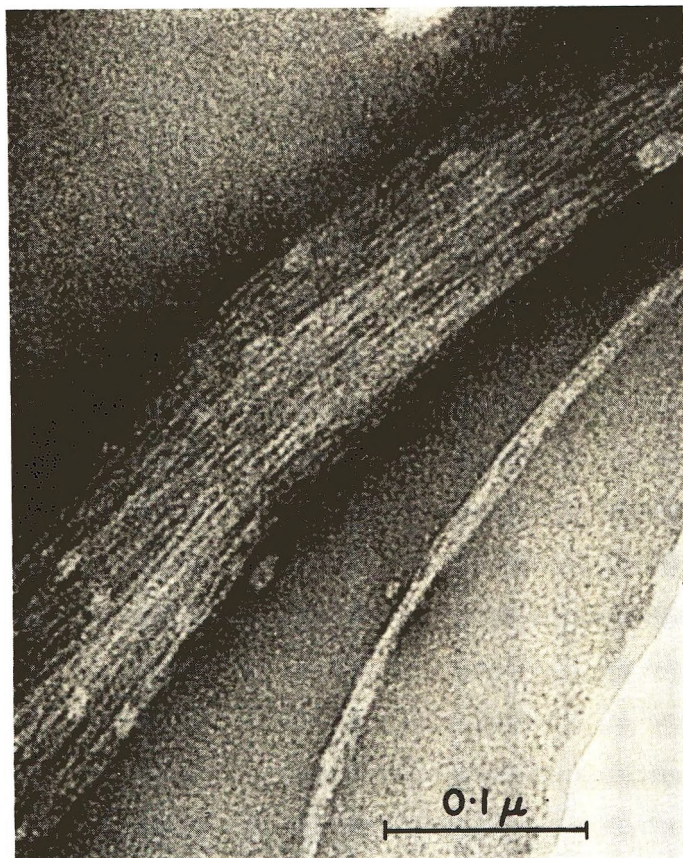


Fig. 8. Electron micrograph showing a fragment of a Fortisan fiber and its constituent protofibrillar structure elements. The specimen is supported in a thin film of uranyl acetate suspended over a hole in a carbon film, magnification 270,000 \times .

are examined by the negative-staining technique, they are observed to be composed of discrete structure elements. For the case of Fortisan this is illustrated in Figure 8. The structure elements are seen to be fine parallel filaments about 30 Å in width.

By swelling the Fortisan in sulfuric acid and then disintegrating by ultrasonic irradiation, it could be almost completely dispersed into the thread-like particles. In dimensions and appearance these particles are identical to the filaments in the unswollen preparations. Similar results were obtained with other types of oriented regenerated cellulose.

It was of interest to know whether the filaments observed in the oriented specimens originated in the molecular orientation process during fiber formation. Experiments similar to those described above were therefore carried out on unoriented films, and on specimens regenerated from dilute viscose (cellulose xanthate) and cadmium ethylenediamine (Cadoxen) solutions as described in the experimental section. For the films it was not found possible to achieve adequate dispersion purely by sonication in the water swollen

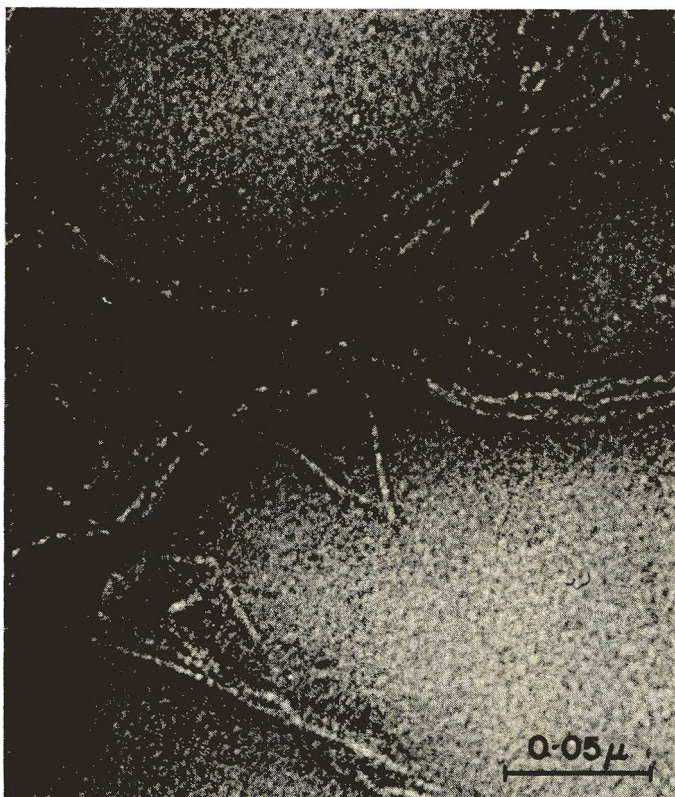


Fig. 9. Electron micrograph showing protofibrils of cellulose precipitated from cadmium ethylenediamine solution. Negatively stained with uranyl acetate, magnification $385,000\times$.

state. However, by swelling the film in sulfuric acid and then sonicating, excellent results were achieved. The visualization of all these preparations by the negative staining technique in the electron microscope (Fig. 9) again revealed the presence of filaments identical to those found in the oriented specimens.

The inference which then seems to emerge from these observations is that all regenerated celluloses are composed of filaments which are closely related to those found in native celluloses. This adds considerable weight to the earlier conclusion that the protofibrils are the basic morphological units of cellulose and, as will be shown later, suggests the synthesis of a model which unifies the morphology of native and regenerated celluloses at the molecular level.

Morphology of the Protofibrils

The examination of negatively stained preparations at high resolution reveals that the protofibrils appear to have a beaded texture along their length, the diameter of the beads being about 30 \AA . The clarity with which

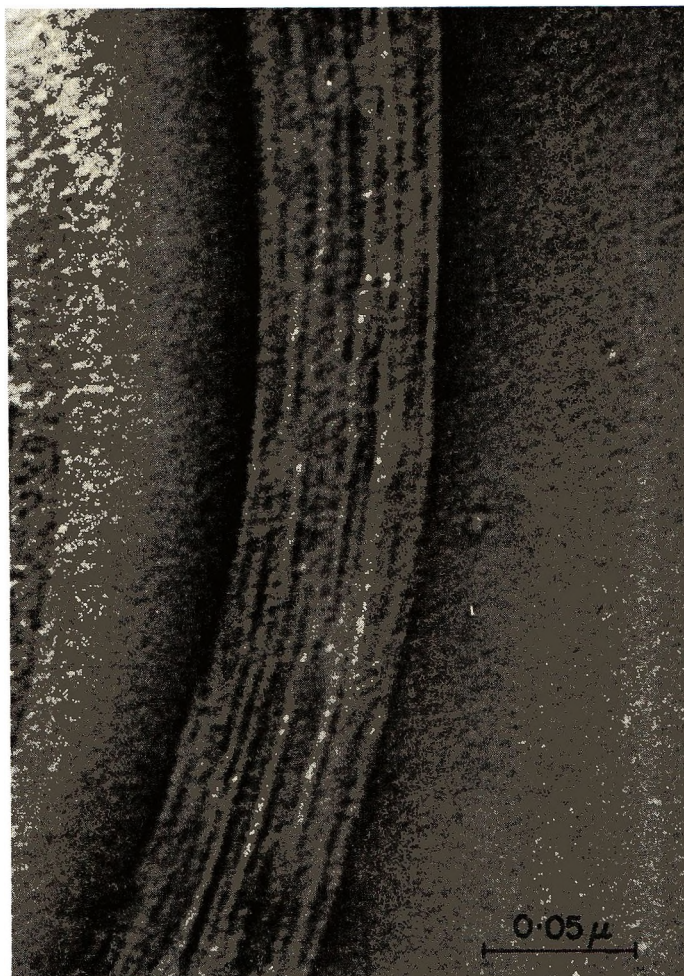


Fig. 10. Electron micrograph showing a bundle of protofibrils from ramie cellulose. The sample is suspended over a hole in a carbon film. Negatively stained with uranyl acetate; magnification 400,000 \times .

this structure is visible is somewhat variable, but the overall impression is unmistakable (Figs. 10 and 11). On close inspection one sometimes gets the impression that the beads are not structural singularities but are the expression of some kind of helical structure. The distance between the centers of successive beads is estimated to be about 40 Å.

In order to interpret the beaded appearance it is necessary to ascertain whether the beads are related to the morphology of the protofibrils, or are an artifact arising from the granularity of the substrate by a superposition effect. Artifacts of this kind can be produced by phase contrast when the objective lens is not perfectly focussed. Therefore, unless it is certain that the image is sufficiently free of astigmatism and appropriately focussed,



Fig. 11. Electron micrograph showing protofibrils in a microtomed section of *Valonia ventricosa*. Negatively stained with uranyl acetate; magnification 250,000 \times .

one must be reserved in deducing true specimen structure from the finest details that can be seen at high magnification.

At this point it should be emphasized that the beaded structure of the protofibrils is observed even in the absence of a carbon substrate, a condition which obtained when specimens were prepared by the "holey-film" method (see Experimental Section). The phenomenon is therefore not analogous to the oval-shaped areas in *Valonia* microfibrils to which reference has already been made, and which were concluded to be artifacts. It is also interesting to note that a similar beaded structure has recently been observed by Heyn³⁶ in protofibrils of cotton and ramie cellulose. His experiments carried out on thin sections which were stained *in situ* and mounted on bare grids.

The beaded appearance of the protofibrils is also apparent in replicas of cellulose fiber surfaces (Fig. 12). Paradoxically, the clarity of the effect is then somewhat greater than in the negatively stained preparations. The



Fig. 12. Electron micrograph (negative print) showing the surface of a spruce wood fiber. The finest filaments show an axial texture similar to that observed in negatively stained preparations. The fibers were freeze-dried and replicated as described by Norberg.²⁹ Platinum shadowed at 30° , magnification $60,000\times$.

observation of this texture with two totally different methods of specimen speaks for its authenticity. Nevertheless, it is very difficult to arrive at a decisive conclusion on this issue purely from electron microscopy, and at this stage the phenomenon must be regarded as suggestive but not conclusive. Later, however, the beaded texture will be used in conjunction with other observations in the derivation of a protofibril model.

To complete the picture of the morphology of the protofibril, it is necessary to make an estimate of its shape in cross section. Films of cellulose diffract x-rays in a manner which suggests that they have a uniplanar orientation. Thus when a piece of *Valonia* wall is irradiated at normal incidence, the 6.1 \AA (101) reflection is missing from the x-ray diffraction pat-

tern; it is observed, however, when the surface of the wall is arranged parallel to the x-ray beam.³⁷ Similar observations have been made on films of regenerated cellulose.³⁸ This indicates that the protofibrils cannot be circular in cross section; they must be anisotropic either with respect to transverse shape or structure. Ohad and Danon have measured the width of protofibrils in negatively stained preparations of corn and bacterial celluloses.³⁹ They obtained a distribution curve showing two peaks corresponding to widths of 30 and 20 Å, the 30 Å peak being dominant. Similar results have been obtained in this laboratory with preparations of ramie cellulose protofibrils. These observations suggest that the protofibrils are rectangular in cross section and lie for the most part on their broader faces.

X-Ray Diffraction

Wide-angle and low-angle x-ray diffraction studies were carried out on *Valonia* and ramie celluloses in an effort to obtain information on the texture of the protofibrils. The specimen of *Valonia* was a piece of cell wall, the plane of which was oriented parallel to the x-ray beam; in the experiments with ramie the beam was oriented perpendicular to the fiber direction. Examination of the diffraction patterns revealed the presence of equatorial maxima at spacings corresponding to 36, 20, 13, 10 and 6.7 Å in *Valonia* and 20, 13 and 10.5 Å in ramie. It may be noted that the reflections are in the ratio $1:\sqrt{3}:\sqrt{4}:\sqrt{7}$ characteristic of a hexagonal lattice. Additionally, in ramie a meridional reflection corresponding to a spacing of 8.4 Å was observed. All of these reflections are in addition to those corresponding to the simple unit cell structure.

Burge⁴⁰ has shown that for a system of cylindrical units packed in a hexagonal array of limited extent, the separation r between the centers of adjacent cylinders can be determined from the observed spacings d by plotting the line

$$d = 2\pi r [j_{i,2w}]^{-1}$$

where $j_{i,2w}$ represents the positions of the maxima of the zero-order Bessel function. When the extra equatorial reflections of cellulose are plotted against $[j_{i,2w}]^{-1}$, a straight line with zero intercept is obtained (Fig. 13). The value of r calculated from the slope of this line is 40 Å. The size of the protofibrils indicated by this analysis appears to be consistent with that determined from electron microscopy. It is then tempting to interpret the extra equatorial reflections as being related to the packing of the protofibrils. However, little reliance can be placed in such an interpretation, for as Sisson has shown, the reflections can also be explained as due to silver and bromine absorption edges on the x-ray negative, produced by diffracted general radiation from the (002) and (101) planes.⁴¹ In like manner, our calculations show that the 8.4 Å meridional reflection probably originates from absorption edges corresponding to the (020) and (040) reflections. The x-ray diffraction thus provides no information on the texture of the protofibrils.

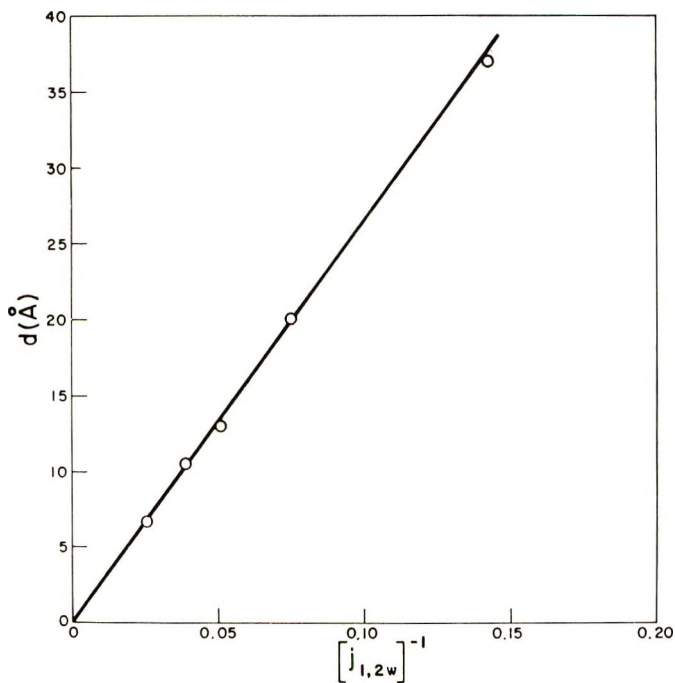


Fig. 13. Correlation of the extra equatorial x-ray spacings d with the maxima of the zero-order Bessel function.

Molecular Constitution of the Protofibrils

Evidence for Molecular Folding

The question now arises as to how the cellulose chains are disposed within the protofibrils. The discovery that regenerated celluloses consist of protofibrils provided a means of obtaining information on this point. Celluloses of various molecular weights were precipitated from solution in cadmium ethylenediamine. The molecular weight of the precipitated material was estimated from viscosity measurements, while the average protofibril length was determined from measurements on about 100 filaments on electron photomicrographs. From the molecular weights the molecular contour lengths could be calculated, the weight and length of each glucose residue being known. Molecular contour lengths L_m and protofibril lengths L_p were then compared. This comparison is most meaningful when the two quantities represent similar averages. The values of L_m closely approximate to a weight average since they are derived from viscosity measurements. Consequently, the values of L_p were also calculated as weight averages by using the expression $L_p = \Sigma N_i L_i^2 / \Sigma N_i L_i$, where N_i is the number of protofibrils of length L_i .

From x-ray diffraction studies it is known that the b axis, that is the molecular chain direction, is coincident with the protofibril axis. It then

follows that if the molecules are fully extended, L_m and L_p should be equal, while if the molecule is compacted or folded L_m should exceed L_p .

The results of these experiments are given in Table I. The first point of interest is that the length of the protofibrils increases with the molecular weight of the dissolved cellulose. From this it becomes attractive to suggest the hypothesis that the protofibril may be the morphological expression of a single cellulose molecule. Bittiger has made a similar suggestion for the amylose-iodine complex which crystallizes in the form of fibrils with a uniform diameter of 40 Å.⁴² If this idea has merit, then the cellulose protofibril is essentially a monomolecular crystal. Evidence bearing on this point will be presented later.

TABLE I
Comparison of Protofibril Length and Molecular Contour Length^a

Specimen ^b	DP	L_p , Å	L_m , Å	L_m/L_p
a	(470)	270	(2420)	(9.0)
	125	"	640	2.4
b	(710)	380	(3660)	(9.6)
	400	"	2060	5.4
c	1080	605	5500	9.1
d	1630	880	8300	8.5
e	2400	1150	12500	10.9

^a Data in parentheses are derived from viscosity measurements on acetone solutions of nitrate samples. The other DP values were obtained from viscosity measurements on cadoxene solutions.

^b Samples: a, obtained by saponifying a fraction of cellulose triacetate; b, Fortisan; c, sulfite pulp; d, bleached ramie; e, cotton.

For the higher molecular weight celluloses, L_m is about ten times L_p . The values of L_m/L_p are so far in excess of unity that the possibility of their being totally in error can be discounted. These results thus provide good evidence for molecular folding, for it is obvious that the molecules cannot be fully extended along the protofibril axis, and simultaneously exceed the protofibril in length by an order of magnitude. There is, however, an apparent enigma in the data to which attention is now directed. In the lower molecular weight range, the ratio L_m/L_p decreases in a systematic manner (Fig. 14). The lateral dimensions of the protofibrils are not affected by changes in molecular weight, and the x-ray diffraction pattern of the precipitated material shows no change over the range of molecular weights studied. Accordingly it would be expected that the molecular packing of the protofibril, and therefore L_m/L_p , would be independent of molecular weight. The means of reconciling the apparent inconsistency in the data probably lies in the molecular weight determinations. It is known that in cadmium ethylenediamine the cellulose molecule undergoes a change in configuration at lower molecular weights.⁴³⁻⁴⁵ Thus a single viscosity-molecular weight relation would not be applicable over the entire molecular weight range. The validity of this explanation was checked by nitrating

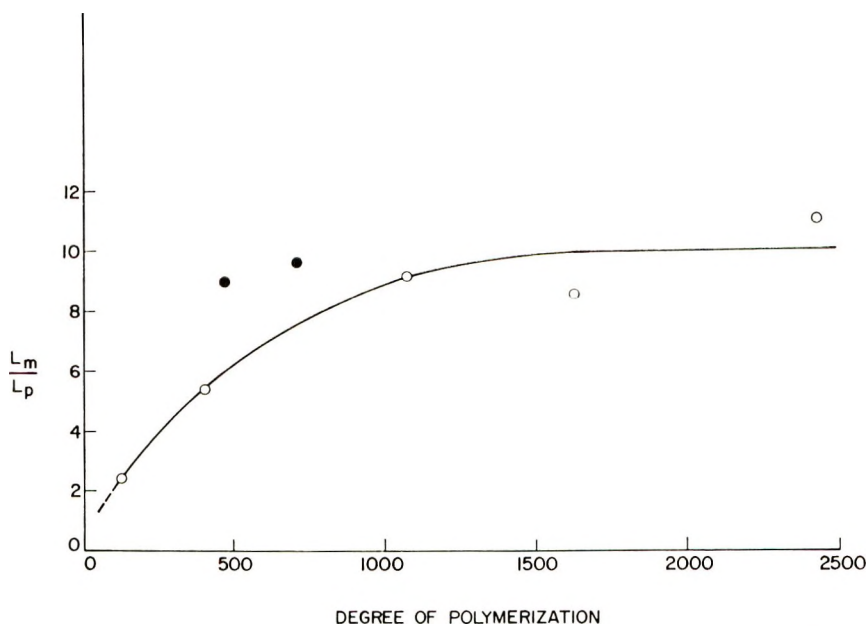


Fig. 14. Plot of the ratio of molecular contour length L_m to protofibril length L_p against the degree of polymerization: (●) data derived from viscosity measurements on nitrated samples; (○) data derived from viscosity measurements on cadoxen solutions.

the two samples of lowest molecular weight and measuring their intrinsic viscosities in acetone. For cellulose nitrate in acetone the viscosity-molecular weight relation is known to be valid over the range of molecular weights investigated here.³² Values of L_m/L_p based on these measurements are found to be in agreement with those of the higher molecular weight samples (see Table I).

Although the above results strongly suggest that molecular folding occurs in cellulose, it must be emphasized that, strictly speaking, they apply only to protofibrils of regenerated cellulose on which the measurements were actually made. Similar measurements have not been made on native celluloses because of the difficulty of obtaining protofibrils of a convenient length. However, the protofibrils of native and regenerated cellulose display an identical axial texture, suggesting that the chains are arranged in the same way in both cases. It thus seems reasonable to assume that these results are valid not only for protofibrils of regenerated cellulose but also for those of native cellulose.

We have considered the stereochemical feasibility of folding by studying a Stuart-Briegleb space-filling atomic model. It was found that the chain could be made to fold sharply on itself, provided that the glucose units are allowed to rotate around the glycosidic bonds. Furthermore, surprisingly enough, only two glucose units were required to negotiate the bend. There thus appear to be no inherent stereochemical restrictions in the molecule which would forbid folding.

Derivation of a Protofibril Model

The observations described in the preceding sections suggest that the cellulose protofibril is a structure of rectangular cross section, and that within this structure the chain molecules are folded in such a manner that the chain axis coincides with the axial direction of the protofibril. A way in which these basic conditions can be met is suggested by the apparent axial texture of the protofibrils as described earlier. This texture can be accounted for by postulating that the protofibril consists of a flat ribbon pleated on itself so as to form a planar zigzag structure which can best be likened to a helically wound ribbon distorted through total flattening (Fig. 15A). It then follows as a natural consequence of the planar zig-zag morphology that there is only one way in which the molecules can be arranged so as to be parallel to the protofibril axis. As illustrated in Figure 15B, the molecules form flat ribbons by folding regularly on themselves, in such a

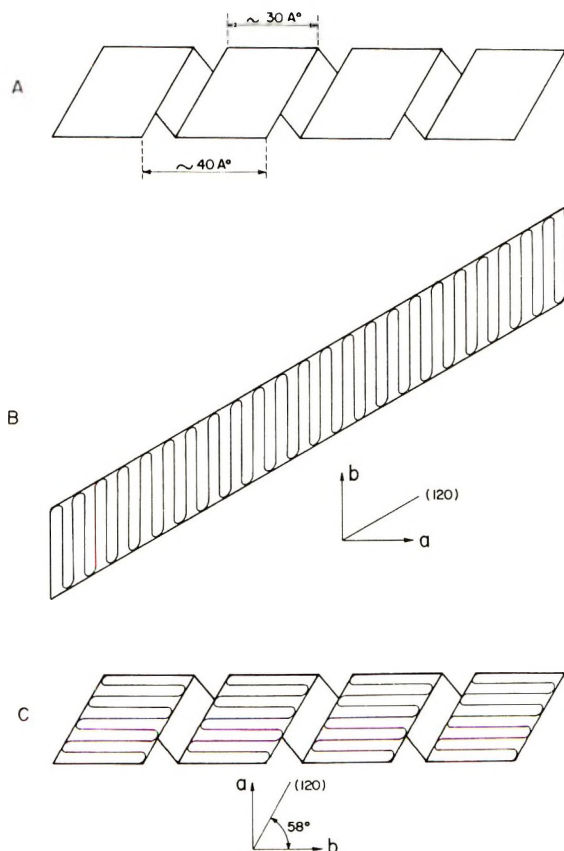


Fig. 15. Schematic drawing illustrating the proposed morphology of the cellulose protofibril; (A) the structure as a ribbon pleated on itself in a planar zigzag fashion; (B) the molecular disposition in the ribbon; (C) the molecular disposition in the pleated ribbon.

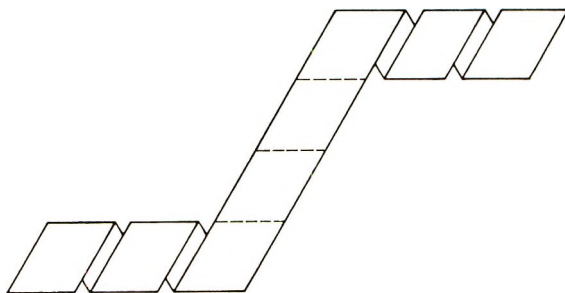


Fig. 16. Schematic drawing showing how kinking could occur in a protofibril through a partial "unwinding" of the planar zigzag structure.

manner that the short extended segments between the folds lie across the ribbon. With the ribbon wound in a planar zigzag manner, the extended chain segments become parallel to the protofibril axis (Figure 15C).

It is interesting to consider the previously described phenomenon of kinking (see Fig. 6) in the light of the above model. Assume that the angle between the direction of the pleat and the axis of the protofibril is 60° . If one or more turns of the planar zigzag structure are pulled out by unwinding, then a kink would be formed with an angle of 120° . The resultant structure, shown in Figure 16, bears a striking resemblance to the kinked fibrils shown in Figure 6. When we come to consider the mechanism of kinking, there is no difficulty in visualizing that in a single protofibril an unwinding could be induced by stresses developed by sonication during specimen preparation. However, such a mechanism seems highly improbable for a microfibril which, as suggested earlier, is a close-packed array of protofibrils. It thus seems more reasonable to suppose that the effect is not due to the unwinding of a preformed structure, but that the kinks develop directly during the formation of the protofibrils. Support for the correctness of this deduction is provided by the observation of kinked microfibrils in *Valonia* cell walls (Fig. 17). On this basis one is led to suppose that the kinking effect must ultimately be crystallographic in origin. The relation between the unit cell and the protofibril will be discussed later. Here, however, it may be noted that in the unit cell of cellulose I (Meyer-Misch) the (120) planes lie at an angle of 58° to the b axis or chain direction (see Fig. 18). Let us assume then that the ab plane of the unit cell lies parallel to the broad face to the protofibril. Then if the folds are located in the (120) planes, and the protofibril is a regularly pleated structure as proposed, it can readily be seen that a protofibril segment in the unpleated state must make an angle of about 120° with a pleated segment.

On the face of it then, the phenomenon of kinking seems to provide good support for the folded chain planar zigzag protofibril model. Last, it is apparent that kinking in microfibrils implies that the constituent protofibrils must be packed in crystallographic registry. For all essential purposes such microfibrils can thus be regarded as single crystals. The mecha-



Fig. 17. Electron micrograph of the wall of *Valonia ventricosa*. Notice the bundles of kinked microfibrils. Shadowed with Pt at 30° , magnification $56,000\times$ (negative print).

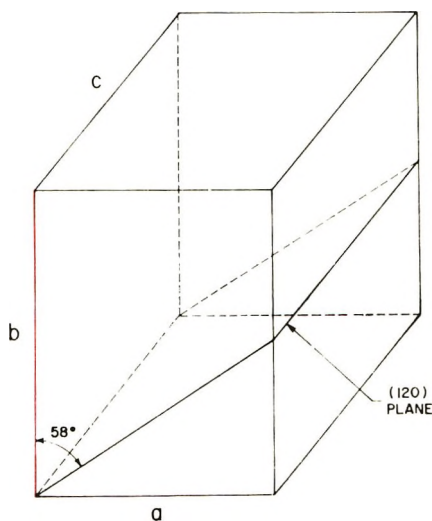


Fig. 18. Schematic representation of the unit cell of cellulose I showing the disposition of the (120) plane.

nism by which this astonishing effect is achieved is part of the unsolved problem of cellulose biosynthesis.

It is now of interest to estimate the mass of a protofibril in order to determine the number of cellulose chains contained in the structure. This will test the validity of the supposition made earlier, that a protofibril may be a monomolecular crystal. For purposes of calculation it is convenient to idealize the planar zigzag structure as a rod of rectangular cross section with dimensions $30 \times 16 \text{ \AA}$. Geometrically this approximates sufficiently closely to the proposed model that one should not depart too far from

reasonable conclusions. The molecular weight M_p of the protofibril can then be estimated from the relation

$$M_p = L_p A N \rho$$

where L_p is the length of the protofibril, A is the cross-sectional area, ρ is the density of cellulose, and N is Avogadro's number.

From experiments described earlier, in which cellulose was precipitated from solution as protofibrils, we know L_p the length of a protofibril corresponding to cellulose of a given molecular weight \bar{M}_v . With the density of cellulose as derived from x-ray data (1.59 g/cm³), values of M_p can readily be calculated for comparison with \bar{M}_v . The results are given in Table II.

TABLE II
Comparison of Protofibril Mass and Molecular Weight^a

DP	L_p (Å)	$\bar{M}_v \times 10^{-3}$	$M_p \times 10^{-3}$	M_p/\bar{M}_v
125	270	20	125	6.1
(470)		(76)		(1.6)
400	380	65	170	2.7
(710)		(116)		(1.5)
1080	605	175	277	1.6
1630	880	265	400	1.5
2400	1150	390	526	1.3

^a Values in parentheses correspond to molecular weights derived from viscosity measurements on nitrated samples. All other molecular weights were obtained from viscosity measurements on cadoxen solutions (see Experimental section).

In assessing the data it should be noted that values of M_p as calculated here are somewhat overestimated, since they correspond to a solid rod which would obviously have a higher mass per unit length than the envisaged planar zigzag structure of corresponding dimensions. This probably accounts for the fact that the values of M_p are systematically greater than those of \bar{M}_v . Bearing this overestimation in mind we may now compare the values of M_p and \bar{M}_v . When \bar{M}_v is obtained from viscosity measurements on cadoxen solutions, the ratio M_p/\bar{M}_v approximates to unity for the higher molecular weight samples but shows a tendency to increase at degrees of polymerization lower than 500. On the other hand, the ratio also approximates to unity for the lower molecular weight samples when \bar{M}_v is derived from viscosity measurements on nitrated material. As was pointed out earlier, the abnormal behavior of the lower molecular weight samples in cadoxen solution is probably related to a deviation from random coiling.

From these results it appears that there is essentially a one-to-one correspondence between protofibril mass and molecular weight. It is thus difficult to escape the conclusion that the protofibril contains a single folded cellulose molecule. We may now proceed to consider in greater detail how the molecule is packed in the protofibril. For this purpose the relation between the unit cell and the protofibril must be known. It is first necessary to establish the crystallographic directions in the protofibril. Figure

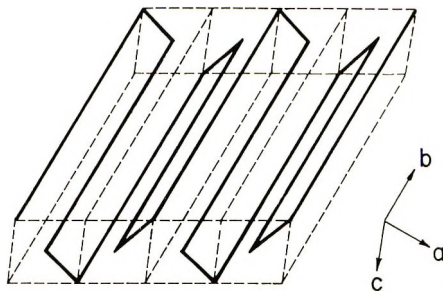


Fig. 19. Drawing showing a portion of the protofibril "unwound" as a flat ribbon. The drawing illustrates the relation between the cellulose molecule (heavy lines), the protofibril and the unit cell. There are three lattice translations along the b axis, one along the c axis, and an indefinite number along the a axis.

19 shows a section of a protofibril unwound as a flat ribbon. We already know that the extended chain segments (i.e., the b axis) must lie across the ribbon. The c axis must coincide with the thickness of the ribbon in order to place the (120) plane in the appropriate orientation to account for the phenomenon of kinking; the a axis will then lie in the plane of the ribbon and perpendicular to the b axis. To satisfy the geometrical requirements of the proposed planar zigzag structure we would expect about three unit cell translations along the b axis, one translation along c and an indefinite number along a . Granted that the molecule is folded within the ribbon, and subject to the condition that it must be disposed within the structure in such a way as to satisfy the Meyer-Misch relations between the straight chain segments, three basic schemes of packing can be envisaged. These are illustrated in Figure 20, which shows the projection of the ribbon along the chain direction onto the (120) fold plane. The chain axis is normal to the plane of the figure, and its direction is indicated by plus and minus signs corresponding respectively to movement into and out of the plane. The folds are not all identical since their width (i.e., the distance between segments joined by the fold) depends upon the plane in which it is located. In the (10 $\bar{1}$) plane the width is 6.1 Å, while in the (101) plane it is 5.4 Å.

In the first scheme (A), the folds lie alternately in the (101) and (10 $\bar{1}$) planes in each cell, and lattice sites on the front surface of the ribbon are vacant. In the second scheme (B), the folds lie in the (101) and 10 $\bar{1}$) planes in successive cells. Alternate lattice sites on the front and rear surfaces of the ribbon are thus vacant. The third scheme (C) is a combination of the others. The folds are located in the same planes as before, but their disposition is random throughout the structure and there is consequently no regularity in the positions of the vacant lattice sites. In relation to the unpleated ribbon which has been considered here, none of the proposed schemes of chain packing could account for the basic translations of the structure as defined by the Meyer-Misch model. Scheme A does not provide for the 7.9 Å translation, while B implies a c axis repeat of 16.6 Å and

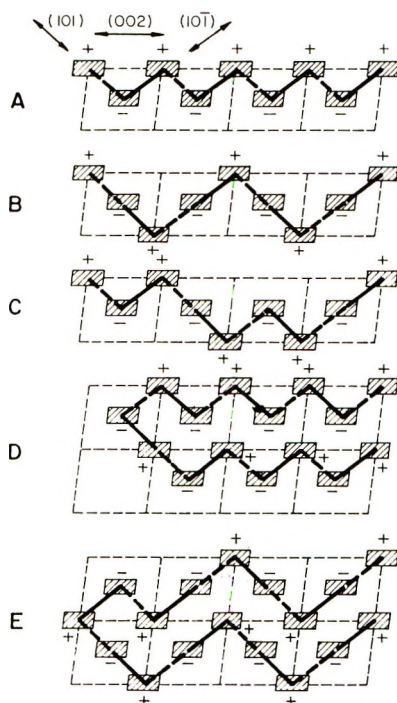


Fig. 20. Projection of the cellulose lattice along the b axis onto the (120) plane, to illustrate various schemes of chain packing in the protofibril. Each of the smaller parallelograms represents one unit cell. The small hatched rectangles represent the straight chain segments which are normal to the plane of the figure; the plus and minus signs denote directions into and out of the plane of the paper. The solid and dotted lines represent folds in the cellulose chain. A, B, and C show the packing in the protofibril "unwound" as a ribbon. D and E show chain packing similar to A and B, respectively, in the pleated ribbon.

forbids the 8.3 \AA translation. The third scheme (C) is characterized by order deficiency in the stacking of the straight chain segments. However, when the pleated morphology of the protofibril is taken into consideration it becomes clear that lattice registry must exist between the turns of the planar zigzag structure. As indicated in Figure 6 (D and E) for a pleated structure, alternatives A and B would appear to be equally likely since they would both account for the density of cellulose and the basic lattice translations. The third alternative (scheme C) is considered to be unlikely because of its inherent deficiency in order.

Present knowledge of hydrogen bonding in the cellulose I lattice suggests that within the protofibril the straight chain segments are linked by hydrogen bonds in the (101) , $(10\bar{1})$ and (002) planes. Thus the proposed pleated structure would be securely "locked together" by the hydrogen bonds and would be expected to display considerable rigidity in the axial direction.

In order to build up the type of micelle envisaged here there must be a staggering of the folds, so that each extended-chain segment is translated

stepwise along the molecular chain direction, relative to the neighboring extended-chain segment (Fig. 15). The effect is analogous to that occurring in hollow pyramidal crystals of polyethylene^{46,47} and presumably occurs in order to fulfill the requirements for efficient packing of the folds. Meyer and Misch have deduced that in the unit cell of cellulose I the center and corner chains are displaced by about 3 Å in the chain direction. This result is understandable in terms of the staggering of the folds enunciated here, and follows directly from the earlier suggestion that the folds are located in the (120) planes which lie at an angle of about 60° to the *b* axis.

The molecular packing has been discussed above in relation to the protofibrils of native celluloses. For the case of regenerated celluloses, the same basic schemes of packing can be envisaged. The difference between the protofibrils of these two modifications would then reside chiefly in the mutual disposition of the straight chain segments as defined by their respective crystal structures.

In concluding this section, the question may be raised whether the model proposed would not lead one to expect off-meridional low-angle x-ray reflections corresponding to the fold period. As indicated earlier, such reflections are in fact not observed. Inspection of the model suggests that there is no discrete discontinuity in electron density in the axial direction such as exists in single crystals of synthetic polymers. This would seem to preclude the observation of low-angle diffraction effects.

DISCUSSION

It has been proposed that cellulose is composed of protofibrils, which consist of a single cellulose molecule folded in an antiparallel manner to form a micellar ribbon that is regularly pleated on itself giving a planar zigzag structure. Presumably this structure is stabilized chiefly by intramolecular hydrogen bonds comprising those linking contiguous glucose units in the straight chain segments, and those linking glucose units in adjacent straight chain segments.^{48,49}

Three observations argue to the correctness of the conclusion that the protofibrils are the morphological expression of the cellulose molecule; first the ubiquity of the unit in various types of cellulose; secondly, the lateral dimensions of the unit remain constant while the length increase with molecular weight, and thirdly there is an apparent equality between protofibril mass and molecular weight. If the unit were an extended chain crystallite it would contain many molecules and it would be difficult to understand what determines its size. A folded chain structure, as opposed to one with extended chains, also provides a natural explanation for the widely held view that adjacent chains in the unit cell of cellulose are packed in an antiparallel manner; it is obvious that adjacent straight chain segments must be antiparallel if the chains are folded.

The concept that protofibrils of cellulose are chain-folded monomolecular crystals, bold though it may perhaps seem, evokes no new principles of molecular conformation. In fact there is an obviously close analogy between the present observations and the recognition of chain folding in polymer single-crystals.^{17,18} Furthermore, the tendency of a chain molecule to aggregate with itself has been established in other biopolymers that have many functional groups capable of forming hydrogen bonds. The best known example of this phenomenon is the so-called cross-beta conformation of the polypeptide chain as found in bacterial flagella^{50,51} and the egg stalk of the green lace-wing fly *Chrysopa*, where the fold period is 25 Å.^{52,53}

In seeking to understand the genesis of the structure of the protofibril, as it is here pictured, one is faced with two formidable questions. The first is, what determines the observed fold-period. No answer can be given to this question at present. However, at least this much can be said; the fact that the protofibrils can be reconstituted from solution, implies that the chain can unfold, lose its specific conformation and regain it of its own accord. This leads to the suggestion that the protofibril must represent the state of lowest free energy or highest stability of the cellulose chain. Presumably the explanation for the folding is to be found in the theory of the crystal growth kinetics. This has been treated by Lauritzen and Hoffman,⁵⁴ Frank and Tosi,⁵⁵ Lauritzen and Passaglia,⁵⁶ and Price.⁵⁷ The second question relates to the origin of the pleat in the folded-chain ribbon. Two possibilities can be suggested: first, the pleating occurs in order to minimize the surface area of the protofibril, and thus its total free energy; and second, by pleating, a surface is provided on which molecular segments can be attached through hydrogen bonding. Possibly the most reasonable way of visualizing the formation of the protofibril, is to suppose that chain folding and crystal pleating occur simultaneously by a process of continuous growth as the chain molecule is transformed into an ordered structure; the less likely, if not altogether improbable alternative, is that the growth of the protofibril occurs by a two-step process, in which the chain folds on itself to form a ribbon, which then pleats in a regular manner.

The underlying cause of the deviation from regular pleating in protofibrils, leading to the formation of a kink, is obscure. It may be emphasized in passing, however, that kinking provides a mechanism whereby microfibrils can undergo an abrupt change in their direction of growth. This may bear on the problem of fibril orientation in plant cell walls.³⁷

We now wish to consider some of the characteristics of cellulose in relation to the model. It is not the intention to give a comprehensive explanation of properties, but rather to indicate the lines of thought suggested by the model. In the first place there is the question of the heterogeneous hydrolysis of cellulose. The glycosidic linkages in cellulose are susceptible to attack by mineral acids.⁵⁸⁻⁶¹ The reaction proceeds rapidly in its initial stages, but becomes extremely slow after a small fraction of the bonds has been broken. The major part of the reduction in chain length occurs before there has been any significant loss in weight. In the later stages of the

reaction, especially under drastic conditions of hydrolysis, there can be considerable loss in weight although the chain length decreases slowly.⁶¹

In order to explain these observations, it may be supposed that hydrolysis occurs simultaneously on the lateral and end surfaces of the protofibrils. Scission of the covalent bonds on the lateral surfaces would generally be expected to cause an appreciable decrease in average chain length. However, the extent to which the lateral attack proceeds will depend on the accessibility of the surfaces to the acid, and this in turn is determined by the lateral aggregation or packing of the protofibrils. The initial rapid decrease in chain length is thus caused principally by lateral attack and the leveling off degree of polymerization will depend on the packing of the protofibrils, which will vary with the origin of the cellulose (ramie, wood, cotton, etc.) and its pretreatment (e.g., mode of drying, swelling, etc.). In the later stage of hydrolysis, the average chain length decreases only slowly, since the protofibrils are attacked at the ends with the removal of low molecular weight oligomers. Evidence for such a mechanism has been given by Sharples.⁶²

It is well known that various chemical processes occur with greater facility in some celluloses than in others. If, as in the traditional picture, cellulose is regarded as a crystalline-amorphous system, then it is natural to suppose that the crystalline regions are not penetrated by reagents; the extent to which a given process occurs under given conditions is then taken as a measure of the accessible cellulose present. On this view crystallinity and accessibility are related properties. In the model proposed here, the crystallinity is thought to arise from the packing of the molecule within the protofibril; no amorphous regions are present in the structure. Accessibility would depend on the availability of the protofibril "matter" to chemical reagents and is thus a function of the state of aggregation of the protofibrils.

The definition of the reflections in x-ray diffraction patterns of cellulose depends on the biological origin of the material studied (Fig. 21). In order to account for this effect it is suggested that the protofibrils must associate in sufficiently ordered arrays for in-phase scattering to occur. This suggestion is in accord with the earlier deduction that protofibrils can be packed in crystallographic registry, at least in microfibrils of certain celluloses. The larger the size of the bundle of protofibrils over which coherent scattering extends, the lower is the accessibility and the greater is the resolution of the diffraction maxima. The dimensions of the coherently scattering regions (i.e. the crystallites) is given by x-ray line-broadening measurements. These indicate that the protofibrils must be packed longitudinally so that the (040) planes are in registry over a distance of at least 600 Å.⁶³ The lateral dimensions of the crystallites are considerably lower; they vary with the origin of the cellulose but lie in the range 50-170 Å.⁶⁴

Finally, we must relate the model to swelling and mercerization. When native cellulose fibers are placed in an aqueous solution of sodium hy-

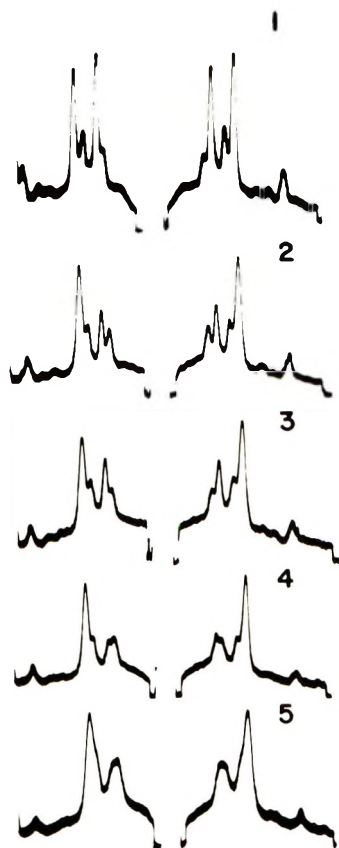


Fig. 21. The x-ray diffraction patterns of several native celluloses: (1) *Valonia ventricosa*, (2) tunicate, (3) bacterial, (4) cotton, (5) wood. There are wide variations in the resolution (i.e., sharpness) of the maxima.

dioxide, there is an absorption of alkali and water, and swelling occurs. In the process, the structural elements of the fiber (i.e., the protofibrils) are forced apart. At low alkali concentrations the internal arrangement of the protofibril is not altered and the x-ray diagram undergoes no modification. At higher alkali concentrations, the alkali molecules interact strongly with the protofibril, causing the disruption of the system of hydrogen bonds that stabilizes the structure and giving rise to alkali celluloses. When the alkali is washed out, a so-called mercerized or regenerated cellulose is formed with a new system of hydrogen bonds. The formation of the new polymorph may be regarded as a genuine intramolecular transformation that takes place in such a manner that the essential morphological identity of the protofibril is reconstituted.

The discussion of properties in relation to the proposed model, as outlined above, serves to emphasize the difference between the conception of

cellulose derived from the present work and the crystalline-amorphous concept embodied in earlier theories. The thrust of the concept emerging from the present work is that there is no amorphous phase in cellulose; it is the packing of the protofibrils that determines the crystallinity and accessibility of cellulose.

In conclusion it seems only fair to mention that the hypothesis developed in the present work is at variance with the conceptions of several other authors. Muggli^{65,66} has measured the molecular weight in microtomed sections of a native (ramie) cellulose and concludes that the chains are in the extended conformation. Thus the point at issue is whether the protofibril is composed of many extended chains or a single folded chain as suggested here. It is clear that the reasons for the difference between the results of this experiment, and the predictions of the model proposed here, must ultimately be resolved. It is difficult, however, to see how a protofibril composed of extended chains can be consistent with the phenomena of kinking or the apparent axial texture.

Mark et al.⁶⁷ have recently shown that the experimentally observed elastic modulus of cellulose is several orders of magnitude higher than that calculated on the basis of a model formally similar to that developed here. On the strength of this discrepancy the authors claim to refute the idea of chain folding in cellulose and support the concept of extended chain protofibrils. It should be noted, however, that the protofibril model used in their calculations consists of a tightly wound helical spring with a circular cross section. This corresponds to the working hypothesis formed at the outset of the present investigation. That model differs in important points of detail from the one proposed here; in the present model the hypothesis of a protofibril with circular cross section has been abandoned in favor of one with a rectangular cross section.

In summary, the model proposed in the present work explains a variety of experimental observations in a rational manner and appears to be consistent with the known facts of cellulose structure. Its principal attractions are: (1) it accounts for the occurrence of a common morphological unit (the protofibril) in native and regenerated cellulose; (2) it accounts for the size and morphology of the protofibrils in terms of well-established principles of macromolecular crystal growth; (3) it explains the phenomenon of kinking in microfibrils and protofibrils; (4) it explains why the chains in the unit cell of cellulose are antiparallel; (5) it suggests new ways of interpreting "order-disorder" effects in cellulose.

The author is indebted to Dr. P. H. Norberg of Mo och Domsjö AB, Örnsköldsvik Sweden for making available an unpublished photograph which gave the original stimulus for replicating cellulose fiber surfaces as a means of revealing the axial texture of the protofibrils.

The work was assisted under the Pioneering Research Program administered by the Institute of Paper Chemistry, Appleton, Wisconsin.

References

1. M. C. Probine and R. D. Preston, *J. Expt. Bot.*, **12**, 261 (1961).
2. A. J. Hodge and A. B. Wardrop, *Austral. J. Sci. Res.*, **3B**, 265 (1950).
3. R. D. Preston and A. B. Wardrop, *Discussions Faraday Soc.*, **11**, 165 (1951).
4. K. Mühlethaler, *Experimentia*, **6**, 226 (1950).
5. E. Ribí, *Arkiv Kemi*, **2**, 551 (1960).
6. J. Dlugosz and R. I. C. Michie, *Polymer*, **1**, 41 (1960).
7. D. A. I. Goring and T. E. Timell, *Tappi*, **45**, 454 (1962).
8. K. H. Meyer and L. Misch, *Helv. Chim. Acta*, **20**, 232 (1937).
9. K. R. Andress, *Z. Physik. Chem.*, **B4**, 190 (1929).
10. P. H. Hermans, *J. Chem. Phys.*, **44**, 135 (1947).
11. P. H. Hermans and A. Weidinger, *J. Appl. Phys.*, **19**, 491 (1948).
12. K. Hermans, O. Gerngross, and W. Abitz, *Z. Physik. Chem.*, **B10**, 371 (1930).
13. A. Frey-Wyssling, *Protoplasma*, **25**, 261 (1935).
14. A. Frey-Wyssling, *Die Pflanzliche Zellwand*, Springer, Berlin, 1959, pp. 367.
15. R. D. Preston and J. Cronshaw, *Nature*, **181**, 248 (1958).
16. K. Hess, H. Mahl, and E. Gutter, *Kolloid-Z.*, **155**, 1 (1957).
17. A. Keller, *Discussions Faraday Soc.*, **25**, 114 (1958).
18. P. H. Geil, *Polymer Single Crystals*, Interscience, New York-London, 1963.
19. R. St. J. Manley, *J. Polym. Sci. A*, **1**, 1875 (1964).
20. R. St. J. Manley, *J. Polym. Sci. A*, **2**, 4503 (1964).
21. R. St. J. Manley, *Nature*, **204**, 1155 (1964).
22. R. St. J. Manley and S. Inoue, *J. Polym. Sci. B*, **3**, 691 (1965).
23. D. Henley, *Arkiv Kemi*, **18**, 327 (1961).
24. D. E. Bradley, in *Techniques for Electron Microscopy*, D. Kay, Ed., Blackwell, Oxford, 1961, pp. 129-134.
25. C. F. Hall, *J. Biochem. Biophys. Cytol.*, **1**, 1 (1955).
26. S. Brenner and R. W. Horne, *Biochem. Biophys. Acta*, **34**, 103 (1959).
27. H. E. Huxley and G. Zubay, *J. Mol. Biol.*, **2**, 10 (1960).
28. W. J. Harris, *Nature*, **196**, 499 (1962).
29. P. H. Norberg, *Svensk Paperstidn.*, **71**, 869 (1968).
30. L. W. Labaw, paper presented at EMSA Conference, Detroit, Oct. 1964.
31. J. W. Green, in *Methods of Carbohydrate Chemistry*, Vol. 3, R. L. Whistler, Ed., Academic Press, New York, 1963, p. 224.
32. A. M. Holtzer, H. Benoit, and P. Doty, *J. Phys. Chem.*, **58**, 624 (1954).
33. H. Kiessig, *Kolloid-Z.*, **152**, 62 (1957).
34. K. Mühlethaler, *Z. Schweiz Forstw.*, **30**, 55 (1960).
35. K. Mühlethaler, *Papier*, **17**, 10a, 546 (1963).
36. A. N. J. Heyn, *J. Cell. Biol.*, **29**, 181 (1966).
37. R. D. Preston, *The Molecular Architecture of Plant Cell Walls*, Chapman and Hall, London, 1952.
38. W. A. Sisson, *J. Phys. Chem.*, **44**, 513 (1940).
39. I. Ohad and D. Danon, *J. Cell. Biol.*, **22**, 302 (1964).
40. R. E. Burge, *Proc. Roy. Soc. (London)*, **A260**, 558 (1961).
41. W. A. Sisson, *J. Amer. Chem. Soc.*, **58**, 1635 (1936).
42. H. Bittiger, E. Husemann, and A. Kuppel, *Proceedings of the Sixth Cellulose Conference (J. Polym. Sci. C, 28)*, R. H. Marchessault, Ed., Interscience, New York, 1969, p. 45.
43. W. Brown and R. Wikstrom, *Europ. Polym. J.*, **1**, 1 (1965).
44. L. S. Bolotnikova and T. I. Samsonova, *Vysokomol. Soedin.*, **6**, 533 (1964); *Abstr. Inst. Paper Chem.*, **35**, 6963.
45. W. Brown, *Svensk Paperstidn.*, **70**, 458 (1967).
46. W. D. Niegisch and P. R. Swan, *J. Appl. Phys.*, **31**, 1906 (1960).
47. A. Keller, *Rept. Progr. Phys.*, **31**, Part 2, 652 (1968).

48. C. Y. Liang and R. H. Marchessault, *J. Polym. Sci.*, **37**, 385 (1959).
49. R. H. Marchessault and C. Y. Liang, *J. Polym. Sci.*, **43**, 71 (1960).
50. W. T. Astbury and C. Weibull, *Nature*, **163**, 280 (1949).
51. W. T. Astbury, E. Beighton, and C. Weibull, *Symp. Soc. Exptl. Biol.*, **9**, 282 (1955).
52. K. D. Parker and K. M. Rudall, *Nature*, **179**, 905 (1957).
53. A. J. Geddes, K. D. Parker, E. D. T. Atkins, and E. Beighton, *J. Mol. Biol.*, **32**, 343 (1968).
54. J. I. Lauritzen and J. D. Hoffman, *J. Res. Nat. Bur. Stand.*, **A64**, 73 (1960).
55. F. C. Frank and M. Tosi, *Proc. Roy. Soc. (London)*, **A263**, 323 (1961).
56. J. I. Lauritzen and E. Passaglia, *J. Res. Nat. Bur. Stand.*, **A71**, 261 (1967).
57. F. P. Price, *J. Chem. Phys.*, **31**, 1679 (1969); *J. Polym. Sci.*, **42**, 49 (1969); *J. Chem. Phys.*, **35**, 1884 (1961).
58. R. F. Nickerson and J. A. Harble, *Ind. Eng. Chem.*, **37**, 1115 (1945); *ibid.*, **38**, 299 (1946).
59. G. F. Davidson, *J. Text. Inst.*, **34**, T87 (1943).
60. O. A. Battista, *Ind. Eng. Chem.*, **42**, 502 (1950).
61. M. A. Millett, W. E. Moore, and J. F. Saeman, *Ind. Eng. Chem.*, **46**, 1493 (1954).
62. A. Sharples, *Trans. Faraday Soc.*, **53**, 1003 (1957); *ibid.*, **54**, 913 (1958).
63. J. Hengstenberg and H. Mark, *Z. Kristallog.*, **69**, 271 (1928).
64. I. Nieduszynski and R. D. Preston, *Nature*, **225**, 273 (1970).
65. R. Muggli, H-G. Elias, and K. Mühlethaler, *Makromol. Chem.*, **121**, 290 (1969).
66. R. Muggli, *Cellulose Chem. Technol.*, **2**, 549 (1968).
67. R. E. Mark, P. N. Kaloni, R.-C. Tang, and P. P. Gillis, *Science*, **164**, 72 (1969).

Received October 1, 1970

Structural Phenomena in Polymers Arising at Low Temperatures and by the Action of High Forces*

V. A. KARGIN,† G. P. ANDRIANOVA, and I. YU. TSAREVSKAYA,
*Institute of Petrochemical Synthesis, Academy of Sciences of the U.S.S.R.,
 Moscow, U.S.S.R.*, and V. I. GOLDANSKII, and P. A. YAMPOLSKII,
*Institute of Chemical Physics, Academy of Sciences of the U.S.S.R.,
 Moscow, U.S.S.R.*

Synopsis

New structural phenomena which can be produced in polymers at low temperatures or by the action of high forces are described and discussed. Experimental evidence supports the argument that the deformation of polymers can develop not only as a result of conformational changes of the macromolecules proper but also by transformation of more complex structural formations. The consequence of this phenomenon is the possibility of large deformations far below the glass-transition temperature in a crystalline polymer with well-developed supermolecular structure. This type of deformation takes place without molecular orientation. Another phenomenon discussed is the sharp change of supermolecular structure in crystalline polymers caused by the action of a shock wave. These effects ought to be connected with an energetic rather than entropic deformation mechanism because the transformations occur at a supermolecular level. Thus, there can be two extreme types of deformation processes: the well-known conformation changes that occur at a molecular level, and the deformation of supermolecular structures. Examples of the pure form of the latter type of mechanism obtained under extreme conditions are given.

The statistical theory of elasticity, in which high elastic deformation of polymers is regarded to be the result of conformation changes in chain molecules, has guided the development of our concepts on the nature of mechanical properties of polymers. The behavior of natural rubber at elevated temperatures, where essentially the entire change of free energy in deformation is determined by a change of entropy, the change in internal energy being very small, may serve as a typical example of application of these concepts.

However, the entropic nature of elasticity reveals itself in its pure form only in extreme cases. Numerous data indicate that an increase of intermolecular interaction and the possibility of structure formation in rubbers results in a change of the internal energy which then plays an appreciable role in deformation processes. This may be illustrated by referring to data

* Paper presented as a Section Lecture at the 22nd International Congress of Pure First and Applied Chemistry, Sydney, Australia, 1969.

† Deceased.

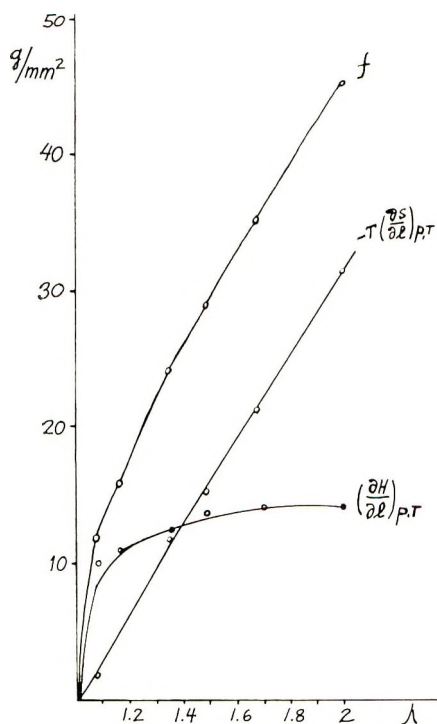


Fig. 1. Change of total stress f and its entropy $-T(\partial S/\partial l)_{p,T}$ and energy $(\partial H/\partial l)_{p,T}$ components with the extension of chlorinated natural rubber (3% chlorine) at 20°C.

on the deformation of natural rubber which had been chlorinated to the extent of 3% chlorine.

Figure 1 depicts the change of total stress on stretching of chlorinated rubber as well as the entropy and energy contributions to the stress. It is evident that the energy changes are already quite significant in this case.¹

The statistical theory of elasticity regards the deformation of a polymer as a result of deformation of disordered uncorrelated chain molecules. However, in recent years structures have been found in practically all polymer systems, not only in crystalline polymers but in amorphous ones as well. Data concerned with the existence of structures in glasslike polymers, elastomers, solutions, and polymer melts were reported recently.²

It has been shown in numerous investigations that the deformation of crystalline polymers is not always connected primarily with the conformational changes of macromolecules but involves concurrent different structural and phase transformations.² Finally, it is of interest to recall the properties of some inorganic gels, particularly those of vanadium pentoxide, which are composed of very long, fine crystals. The only source of elastic behavior is the flexibility of the crystals, which is sufficient to allow completely reversible deformations up to several hundred per cent.

Thus, we can have confidence that the deformation of polymers develops not only as a result of conformational changes of individual macromolecules

but by transformations of more complex structural formations as well. Such processes ought to be purely energetic in nature.

The first type of process is widely known and is manifested almost in pure form in rubbers at elevated temperatures. Thus, the necessity arises to single out the second mechanism in its purest form. This paper deals with these efforts.

The most simple method for excluding conformation changes in macromolecules is to decrease the temperature. High-elastic deformation practically disappears at the glass-transition temperature T_g . However, since an increase of force leads to a shift in T_g , a complete disappearance of all high-elastic phenomena occurs only at the brittle temperature.³ Nevertheless, the molecular mobility does become very low at T_g ; the polymer molecules cease to move relative to one another and, hence, to change their form, though they maintain the potential ability to change their conformation down to the brittle temperature. It ought to be added that, as a rule, intramolecular and intermolecular interactions are very much alike and, therefore, amorphous and poorly ordered polymers are always transformed into a brittle glass at temperatures below T_g . In this case it appears to be impossible to realize the particular conditions under which high deformation can arise without conformational changes.

The genesis of supermolecular structures changes the entire picture, as more or less large structural elements can change their positions even though molecular chains within these elements tend to preserve their form and mutual spacing. Thus, ordered polymer bodies may behave as microcrystalline solid bodies and not as glasslike liquids; deformation may be possible even at temperatures much below T_g and even below the brittle temperature.

Evidently one could expect large deformations to take place at temperatures below T_g in polymers with well developed supermolecular structures. On this basis, a few years ago two of us in collaboration with G. G. Kardash examined the deformation of polypropylene over a wide range of temperatures, including very low ones.^{4,5} It appeared that at low rates of strain, very high deformations can occur down to liquid nitrogen temperature (-196°C). This ability to deform at low temperatures occurs solely in crystalline specimens with pronounced large-scale supermolecular formations. One can trace a definite relation between the ability to undergo low temperature deformation and the size of polypropylene spherulites. Amorphous atactic polypropylene and specimens containing minute spherulites break at temperatures below T_g before appreciable deformations are observed. Specimens with spherulites ranging in size from 80 to 150 μ can be extended as much as 140% down to liquid nitrogen temperatures. With larger spherulites, the maximum deformations decrease once again owing to small cracks developing along the structural boundary lines. Figure 2 shows the dependence of ultimate deformations in polypropylene on spherulite size at temperatures of 20°C (above T_g) and -40°C (below T_g). Figure 3 depicts the relation between ultimate extension and tem-

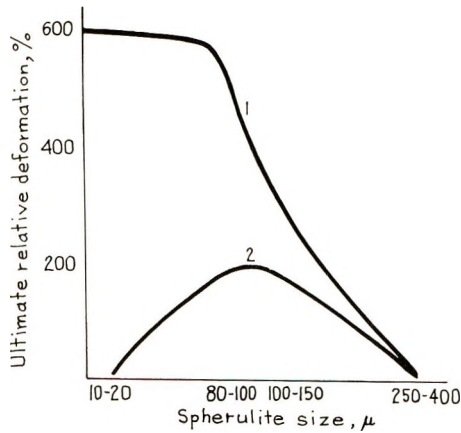


Fig. 2. Dependence of ultimate deformation upon spherulite size for stretching of polypropylene: (1) at 20°C; (b) at -40°C.

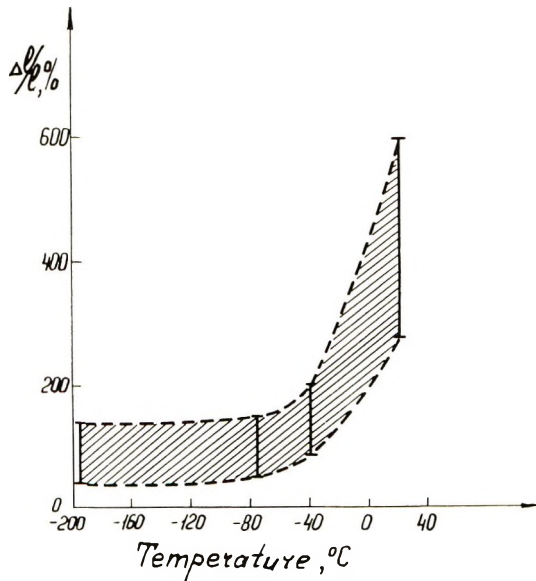


Fig. 3. Dependence of ultimate deformation upon temperature for polypropylene with spherulites of optimum size (80-150 μ). The band width reproduces the scatter of data.

perature for spherulites of optimum size. It is evident that slow application of stresses to specimens with well-developed supermolecular structure allows large-scale deformation which may develop even at temperatures where the elasticity of chain molecules cannot be exhibited. Naturally, at this point the problem of structural phenomena intimately connected with these processes arises.

The most typical phenomenon developing during a uniaxial stretching of polymers is the orientation of macromolecules which occurs either as a result

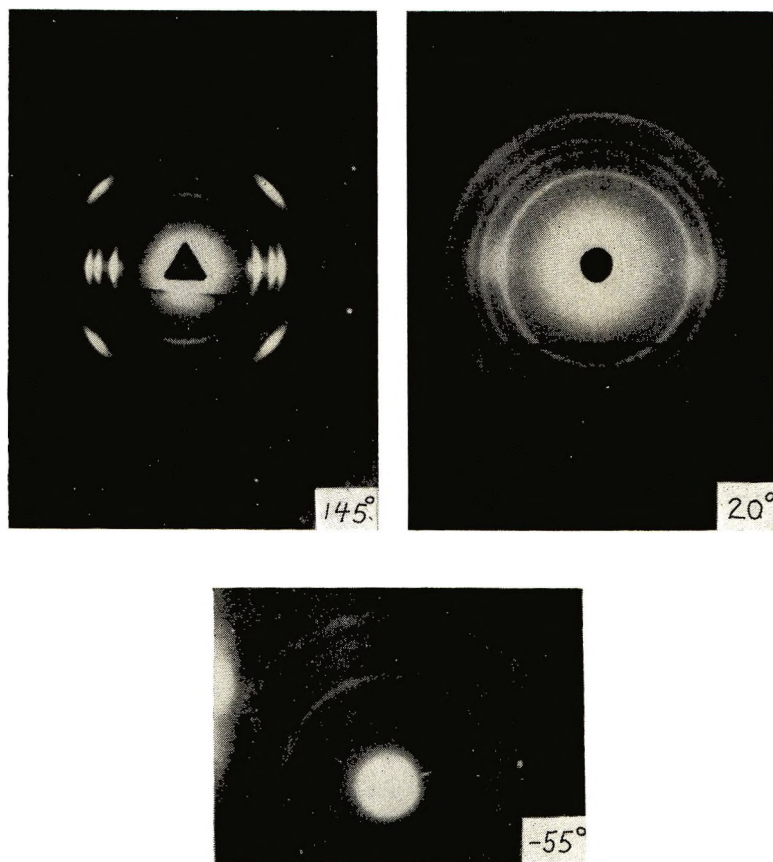
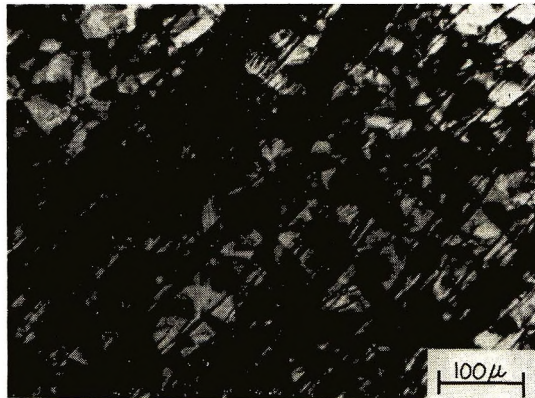


Fig. 4. X-Ray diagrams for polypropylene stretched up to 120% at (a) 145°C (b) 20°C, and (c) -55°C.

of an immediate arrangement in the direction of extension or as a result of recrystallization. The degree of orientation is estimated from the texture in x-ray diagrams and the development of birefringence. Figure 4 shows x-ray diagrams of polypropylene extended to 120% at temperatures of 145, 20, and -55°C. At high temperature the texture is revealed most distinctly, at room temperature it is less distinct, and at -55°C (i.e., much below the glass transition temperature) there are no traces of texture. An x-ray examination shows that the extended specimen is isotropic. Figure 5 is a series of micrographs taken by polarized light at different stages of extension at low temperature (-55°C).

Thus, the investigator is confronted with a rather strange phenomenon, i.e., lack of anisotropy despite a considerable uniaxial extension of the solid polymer. It is most implausible that there could be a flow which would lead to the disappearance of the original anisotropy. Even in rubbery or molten states, the anisotropy arising in the course of deformation disappears rather slowly. At temperatures below the glass transition similar processes,



(a)



(b)



(c)

Fig. 5. Polypropylene films stretched at -55°C to various elongations: (a) 20%; (b) 50%; (c) 100%.

providing ordinary forces are involved, are in fact nonexistent. However, special experiments have shown that low-temperature deformations in polypropylene are entirely reversible. Deformed specimens, when heated to 10–20°C return fully to initial size. Microscopic investigations have also revealed a complete return to initial supermolecular structures. These studies may be supplemented by the results on the temperature dependence of stress-strain behavior. A considerable change of free energy develops in the course of deformation, depending on the change of internal energy. It is characteristic that entropy does not decrease for low-temperature deformation but, on the contrary, increases. Possibly, this is due to the rearrangement of crystalline areas along the boundary in large structural formations. Unlike the case of deformation of a rubber, the entropic contribution to the change of free energy is negative.

Thus, the study of polypropylene deformed at temperatures much below the glass transition temperature conclusively shows the existence of large-scale reversible deformation processes in polymers, which differ radically from the processes of elastic deformation in rubbers. We arrive at the conclusion that in this case the deformation is accomplished by displacements of large-scale supermolecular formations, which are so large that, on the average the body cannot be regarded as isotropic and the displacements of the structure elements cannot lead to microanisotropy.

The higher the temperature, the greater is the mobility of macromolecules. At temperatures above both the glass transition and the melting point, the mobility of molecules is high enough for deformation to be accomplished by molecular conformational changes and mutual displacements. In the temperature interval between the glass transition and melting point, the molecular mobility is already highly restricted; but it is still sufficient for some manifestations of conformation transformations and for the disintegration of large-scale supermolecular formations into smaller structural components.

Evidently, throughout this temperature interval deformation is accomplished according to a mixed mechanism. However, the basic role gradually passes over from separate macromolecules to large-scale supramolecular formations. In Figures 6 and 7 are shown micrographs representing the extension of large polypropylene spherulites at 20°. The changes in shape of spherulites and their disintegration into a system of closely adjacent fibrils, which in this particular case appear as independent structural units, are most explicit. Separate molecules have already almost lost their mobility, and large structural formations may still disintegrate into simple structural elements, in our particular case, into fibrils. Within this temperature range the deformation process is almost reversible and is associated with the development of a texture, whereas the fibrils individually are rather asymmetric. And, finally at lower temperatures molecular mobility ceases entirely, and large structural formations begin to move as a whole if they are adequately formed and their boundaries are not the sources of cracks. Thus, we gradually depart from the picture of deformation and

displacement of separate chains to phenomena involved with the change of positions of larger and larger aggregates of symmetric structural blocks.

What factors cause the low-temperature deformation to be reversible? Under these circumstances of deformation, large blocks remain unchanged.

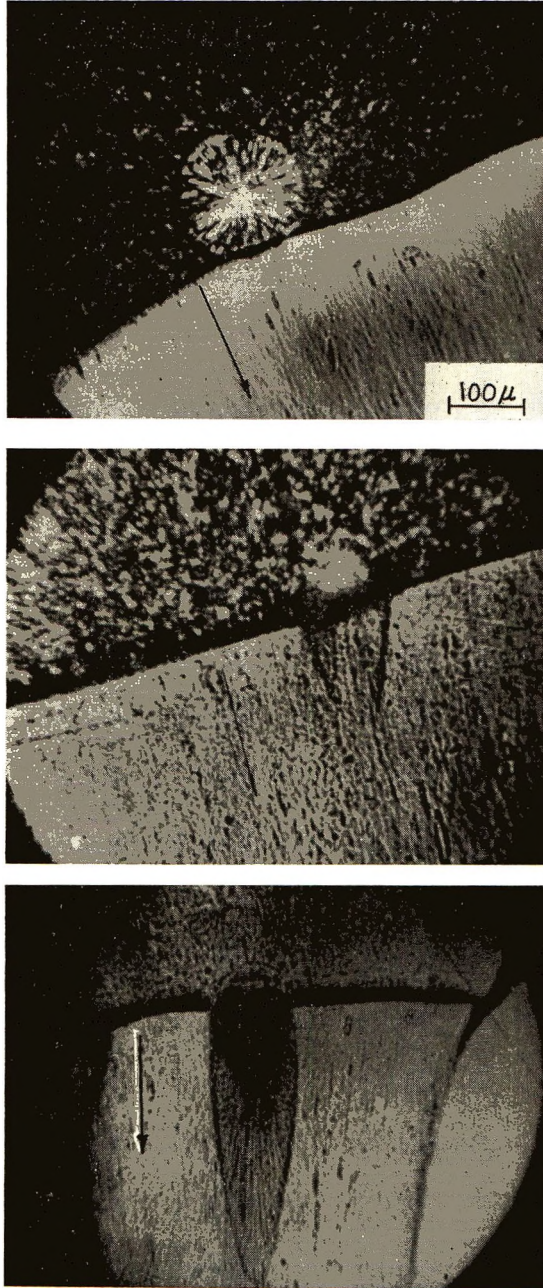


Fig. 6. Deformation of large polypropylene spherulites at 20°C.

Hence, the relevant factors ought to be sought in phenomena developing along the boundary lines. As a rule, deformations developing in solid polymers lead to their loosening; and as a result of a breakup of larger formations into smaller ones, new boundary surfaces are established.

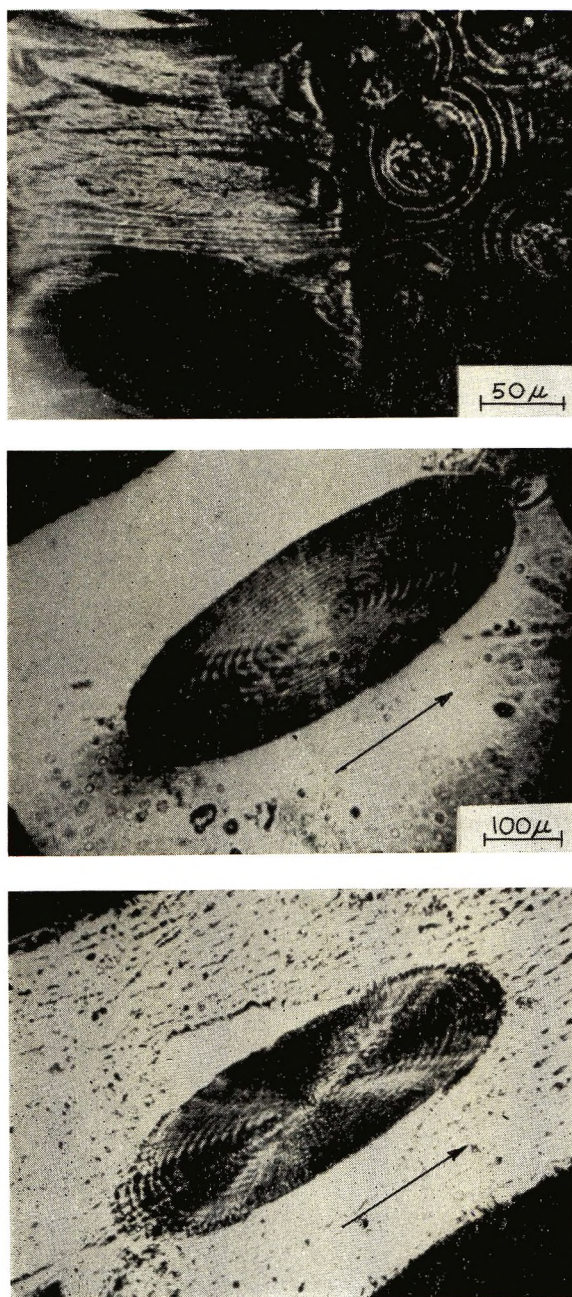


Fig. 7. Deformation of ringed polypropylene spherulites at 20°C.

These events are associated with an increase of the surface free energy of the system. A semiquantitative evaluation indicates the possibility of such processes.^{4,5}

Naturally, observations of such unusual phenomena as large deformation at very low temperatures without the development of orientation suggest the desirability of approaching this category of phenomena from another angle and with other experimental means. On the one hand, a decrease of

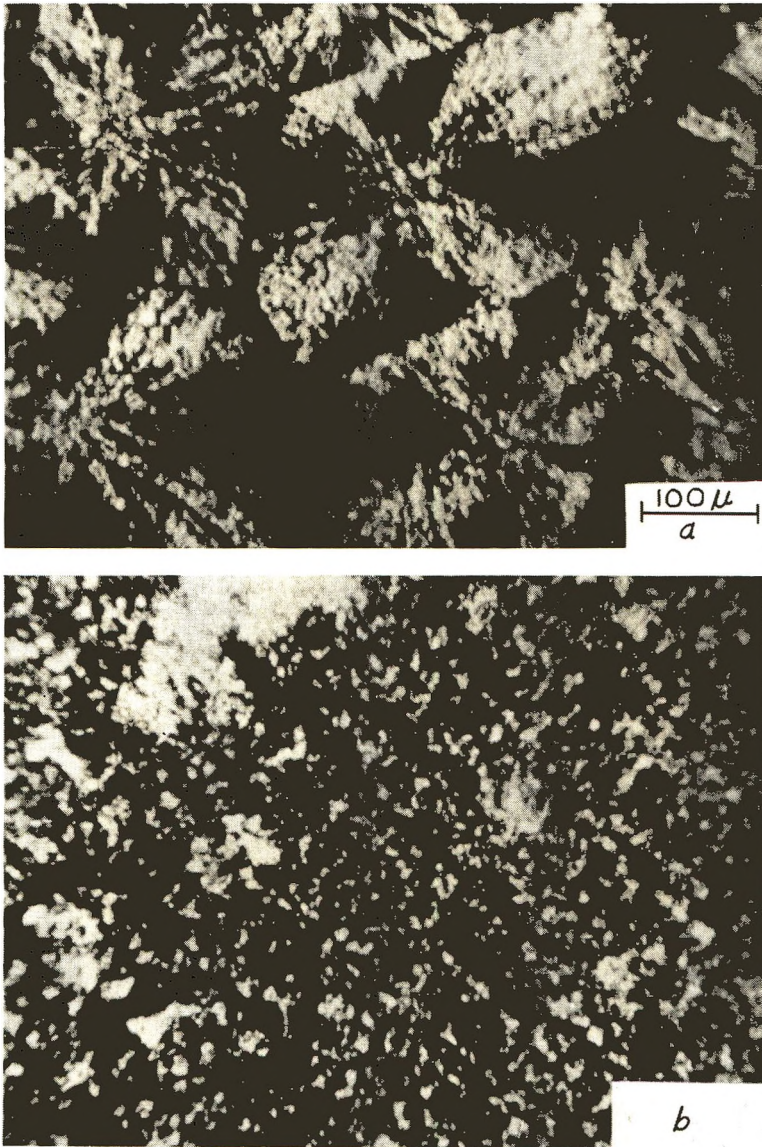


Fig. 8. Polypropylene films with large spherulite structure (*a*) before and (*b*) after action of a 200 kbar shock wave.

temperature and an increase in the rate of an impact lead to equivalent results. On the other hand, transient effects require higher forces. Both of these conditions are produced by a shock wave. The results of a study of structural phenomena occurring when shock waves pass through polymers

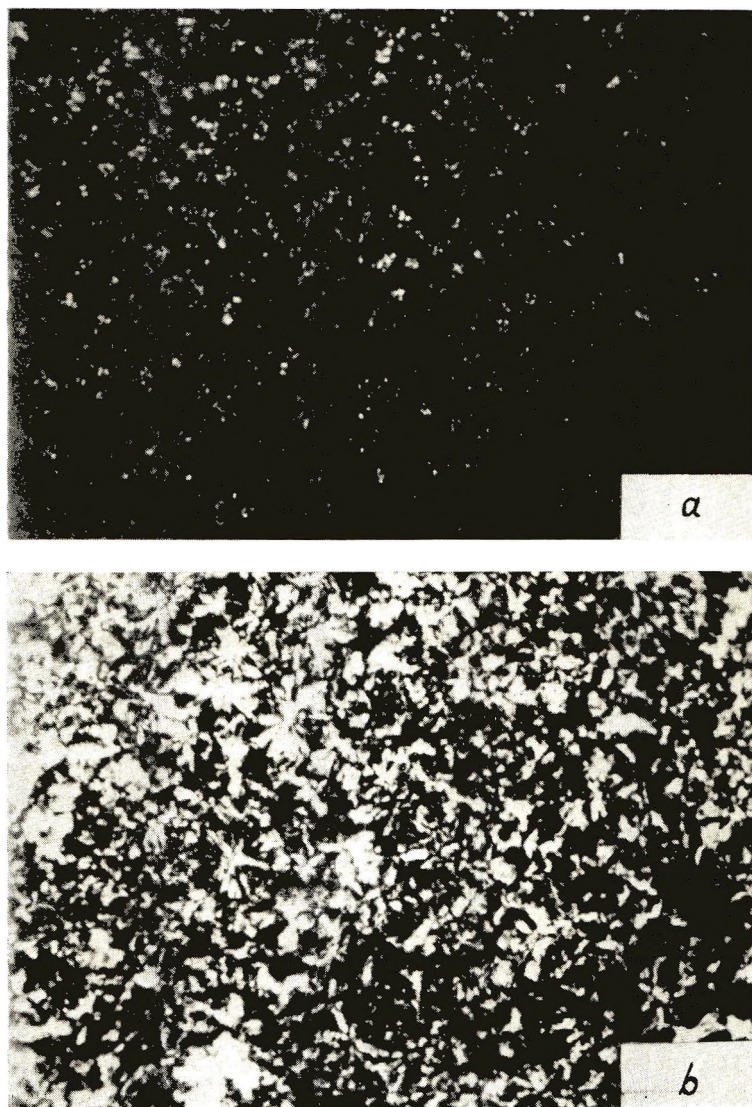


Fig. 9. Films of quenched polypropylene (*a*) before and (*b*) after action of a 200 kbar shock wave.

appeared to be of most striking interest; moreover, they are in agreement with the observations made during the deformation at low temperature.⁶

Experiments were carried out on films 0.05–1 mm thick. The time of passage of the wave was 5–8 μ sec, and pressures arising in the wave varied

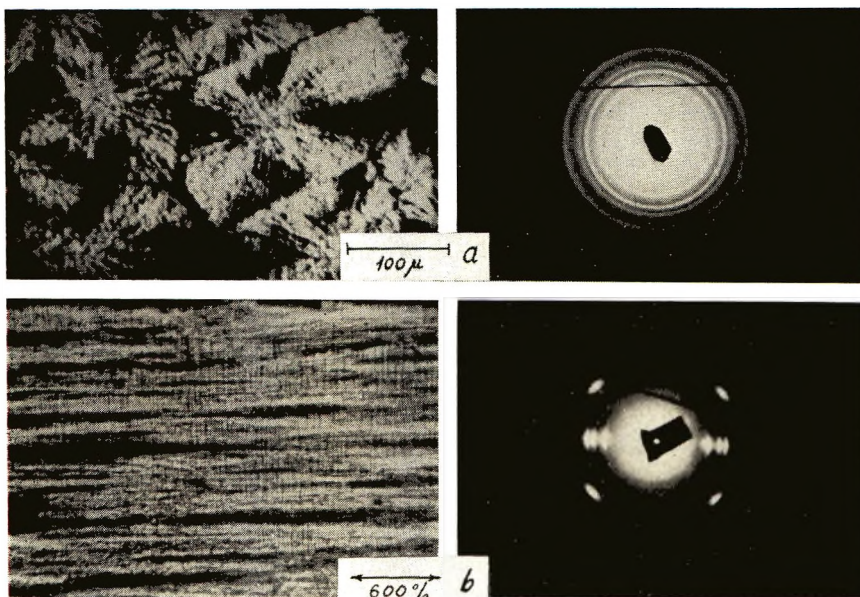


Fig. 10. Micrographs and x-ray diagrams of polypropylene: (a) unstretched; (b) stretched 600%.

from 10 to 500 kbar. The shock wave was produced by detonating 1 kg of explosive.

Despite the very short period of its action, the shock wave sharply changes the supermolecular structures in crystalline polymers. Figure 8 shows the structural changes in large polypropylene spherulites under a shock wave with an intensity of 200 kbar. One can observe a transition of large spherulites into a fine spherulite structure. Figure 9 reveals the action produced by a similar wave upon a specimen of quenched unordered polypropylene. In this case, as in the previous ones, the development of the same fine spherulitic structure can be seen. Thus, by the action of a shock wave it appeared to be possible to obtain very similar structures from two specimens initially exhibiting quite different supermolecular structures. Though the period of action is very short, a state close to equilibrium is achieved under the conditions of the wave action.

However, the most spectacular results have been obtained when a shock wave acts on an oriented film. The formation of a "neck" associated with a sharp transition of an isotropic polymer into an oriented state, is a widely observed effect. Figure 10 includes micrographs and x-ray diffraction patterns of a large-spherulite polypropylene film, both unstretched and stretched 600%. Figure 11 displays microphotographs and x-ray diagrams for the same specimens subjected to shock waves of 200 and 500 kbar amplitude. These two figures reveal that a fibrous structure established after stretching disappears following the passage of a shock wave. As a result there arises a fine spherulite structure very similar to the one ob-

served as a result of the action of shock waves on an isotropic polypropylene. The texture disappears almost entirely at 200 kbars and totally after 500 kbars. However, the most remarkable feature is that, having lost its orientation, the specimen does not change in any of its dimensions. Besides measuring its thickness, we succeeded in inscribing a grating on the film. Our specimens revealed no longitudinal or transverse shrinkage due to the shock wave. Furthermore, there was no dimensional change during subsequent heating to a temperature close to the melting point of polypropylene. If orientation disappears on raising the temperature, one always observes an abrupt change in shape of the specimen.

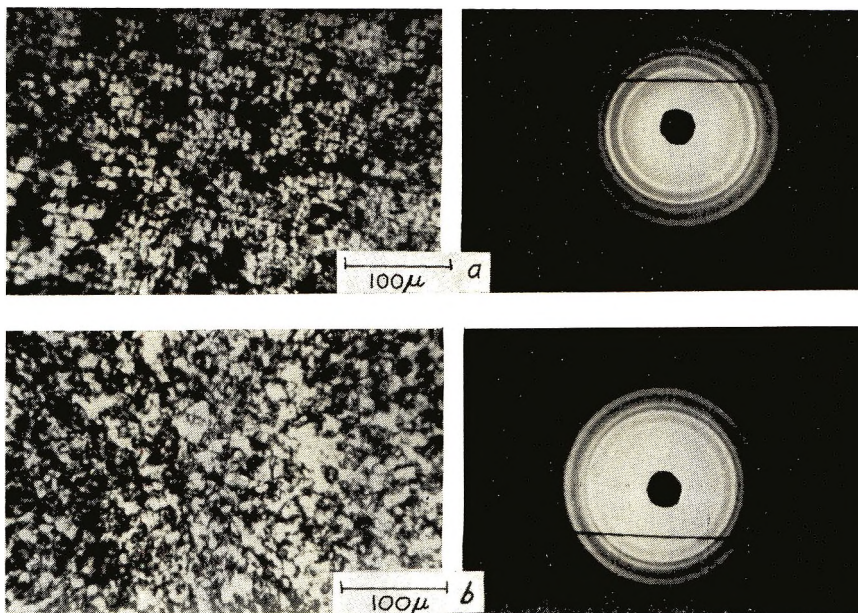


Fig. 11. Microphotographs and x-ray diagrams of polypropylene stretched 600% (see Fig. 10) after action of shock waves: (a) 200 kbar; (b) 500 kbar.

The first presumption is that the polymer may melt during the passage of a shock wave, no matter how short the time of passage happens to be. To establish whether there is any melting of polymer, a dye which crystallizes into needles with a melting point below that of polypropylene (165°C) was introduced into the polymer. Experiments with 500 kbar shock waves showed that regardless of any changes experienced by the polypropylene, the dye crystals remained unmelted, and scratches marked on specimen surface failed to change. Finally, experiments were carried out with an unmelted polymer, polyethylenepiperazine. Figure 12 reveals changes in this polymer following the passage of a shock wave of 200 kbars. Once again a typical fragmentation of the sperulite structure was observed. Thus, it may be concluded that structural changes are not connected with polymer melting.

There is another possibility, namely, a degradation of the polymer due to flow and structural transformations. However, viscosity measurements of polypropylene prior to and after the passage of 500 kbar shock waves showed that no degradation occurred. For example, intrinsic viscosity values for an initial specimen and specimens after the passage of 200, 350 and 500 kbar waves were 1.82, 1.84, 1.80, and 1.86, respectively. Thus, the molecular weight remained unchanged.

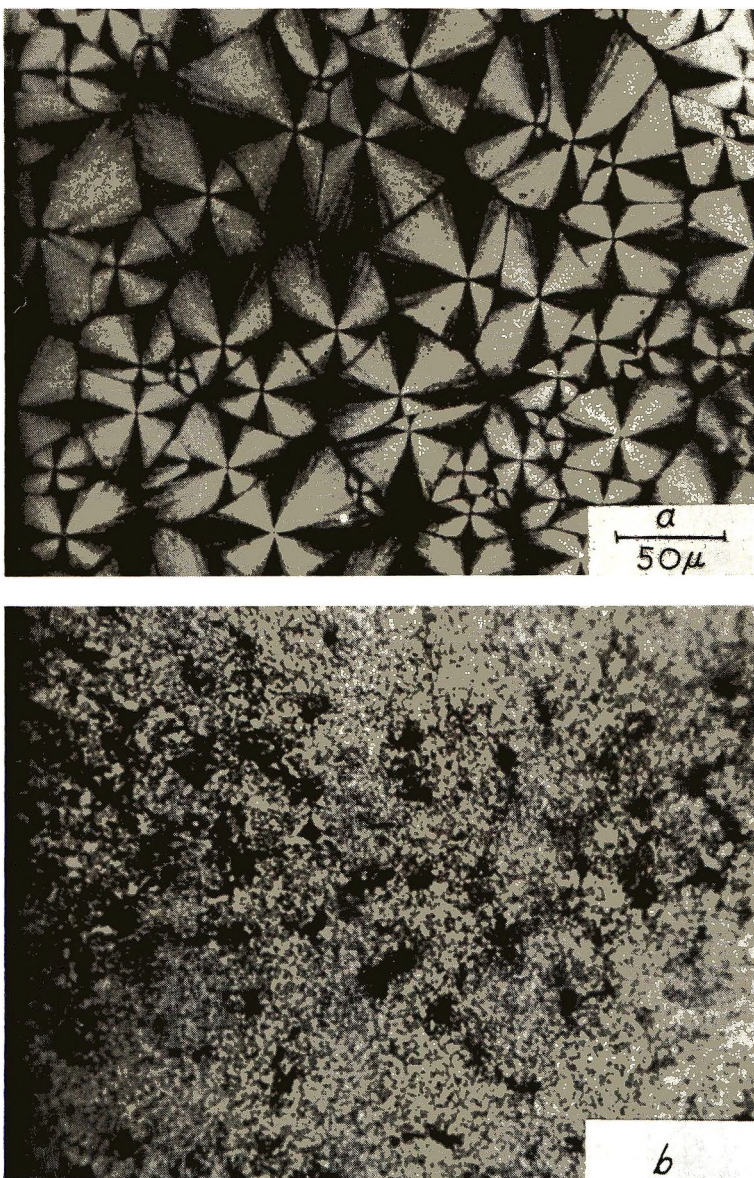


Fig. 12. Polyethylene piperazine (a) before and (b) after passage of a 200-kbar shock wave.

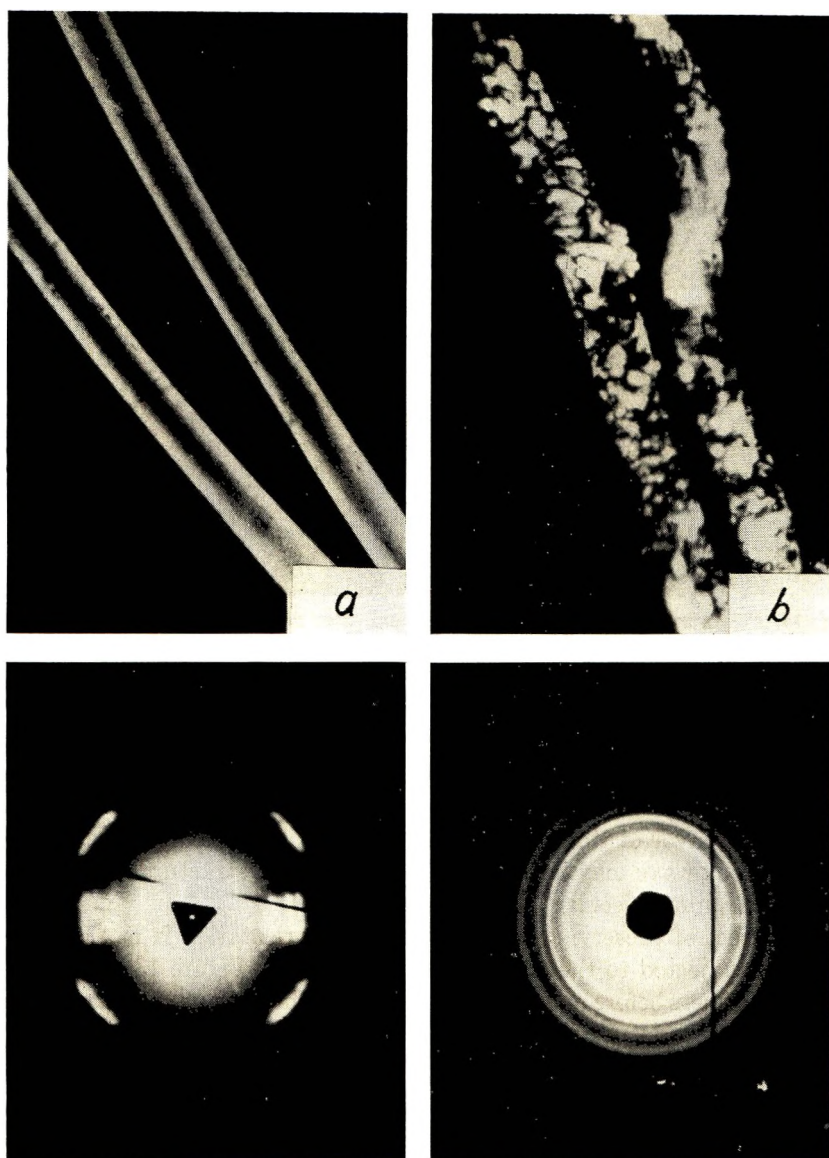


Fig. 13. Polypropylene fibers (*a*) before and (*b*) after passage of a 200-kbar shock wave.

Remaining doubts are connected with possible degradation resulting from a shock wave and subsequent restoration of molecular weight due to recombination of macroradicals produced in the initial degradation. In this case the introduction of inhibitor ought to produce a decrease of molecular weight. It was shown experimentally that an introduction of inhibitor fails to produce such an effect.

Thus, we arrive at the conclusion that a change of position of large structural units similar to the picture observed in low-temperature de-

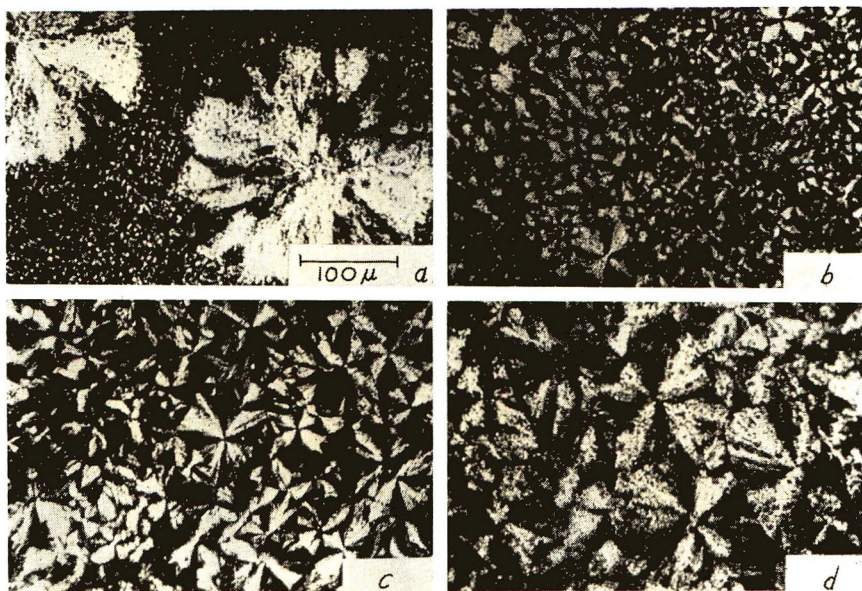


Fig. 14. Polybutene-1: (a) original sample and after action of (b) 120 kbar, (c) 200 kbar, and (d) 400 kbar.

formations, is the basic effect from the passage of a shock wave. Fragmentation of large-scale structures and mainly the transformation of anisotropic structures into isotropic ones with no changes of shape of the sample and molecular weight of the polymer ought to be regarded as the chief evidence in favor of this assumption. All changes in the polymer caused by the shock wave may be regarded as nothing but structural transformations at a supramolecular level.

The effect of preserving shape while losing orientation is most evident in fibers subjected to the action of a shock wave. Figure 13 shows polypropylene fibers before and after the action of a shock wave. The retention of the fiber size despite the transformation of oriented structure into a fine spherulitic type can be seen distinctly. Very similar phenomena have also been observed in polyester fibers.

It is strikingly curious that structural transformations begin only above a threshold value of the shock wave amplitude. For instance, in polypropylene, both in isotropic and oriented form, changes are noted at 120–200 kbar. In the case of poly(ethylene terephthalate) the critical range is 350–500 kbar, and in rubbers and polybutene it drops below 100 kbar. Structural changes occur only after an initial shear which depends on the interaction of structural elements is exceeded. A maximum breakup of large structures ensues immediately after the initial shear. An increase of wave amplitude leads to a formation of progressively larger structures as a result of the degradation of the original units. Just as an increase of molecular mobility occurs with increasing temperature, the mobility of the structural blocks is increased following the passage of a shock wave. The arrangement of

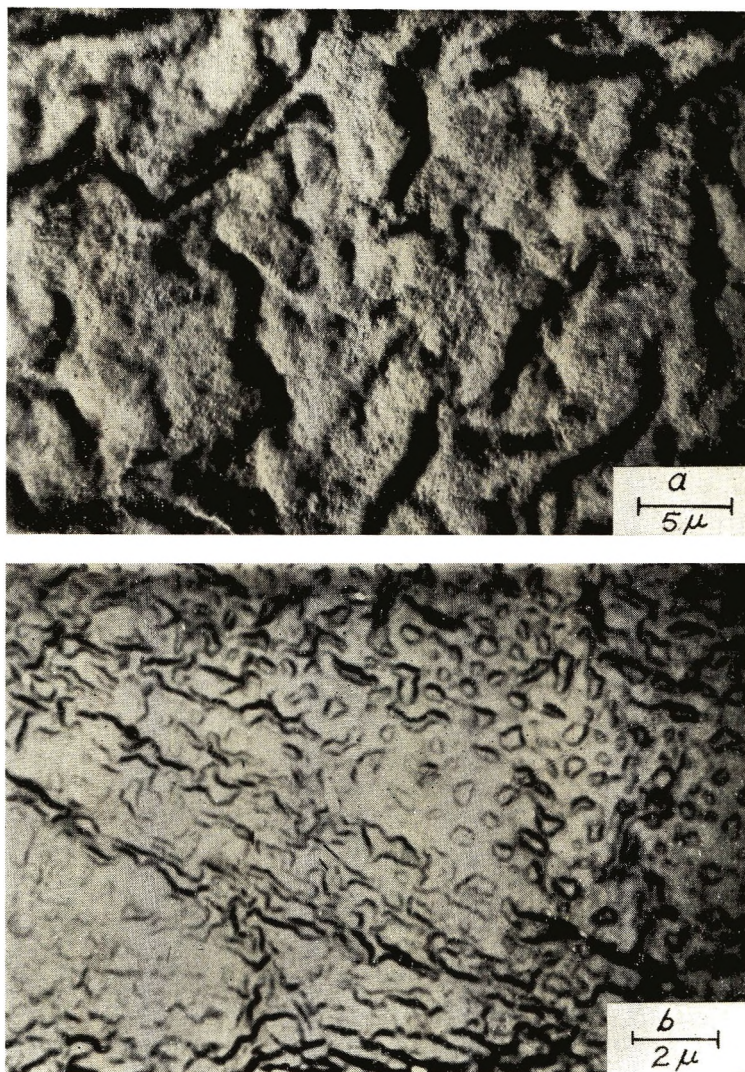


Fig. 15. Electron micrographs of replicas of butadiene rubber: (a) original sample; (b) after action of a 100-kbar shock wave.

these blocks may lead to degradation of initially large-scale structures and to the genesis of new and even more perfect structures. This type of transformation in polybutene is seen in Figure 14. At this state, the degradation of large spherulites with the formation of the fine spherulite structure is observed. The size of spherulites increases with increasing wave amplitude.

The processes of structural rearrangements in amorphous polymers (rubbers) prove to be most significant. Figure 15 depicts structural changes in amorphous polybutadiene rubber caused by a 100-kbar shock wave. One can see the fragmentation of the much smaller bandlike struc-

tures, characteristic of polymers in the elastic state. In rubber the structural units that move under the influence of the shock wave reach sizes of hundreds or thousands of Angstroms.

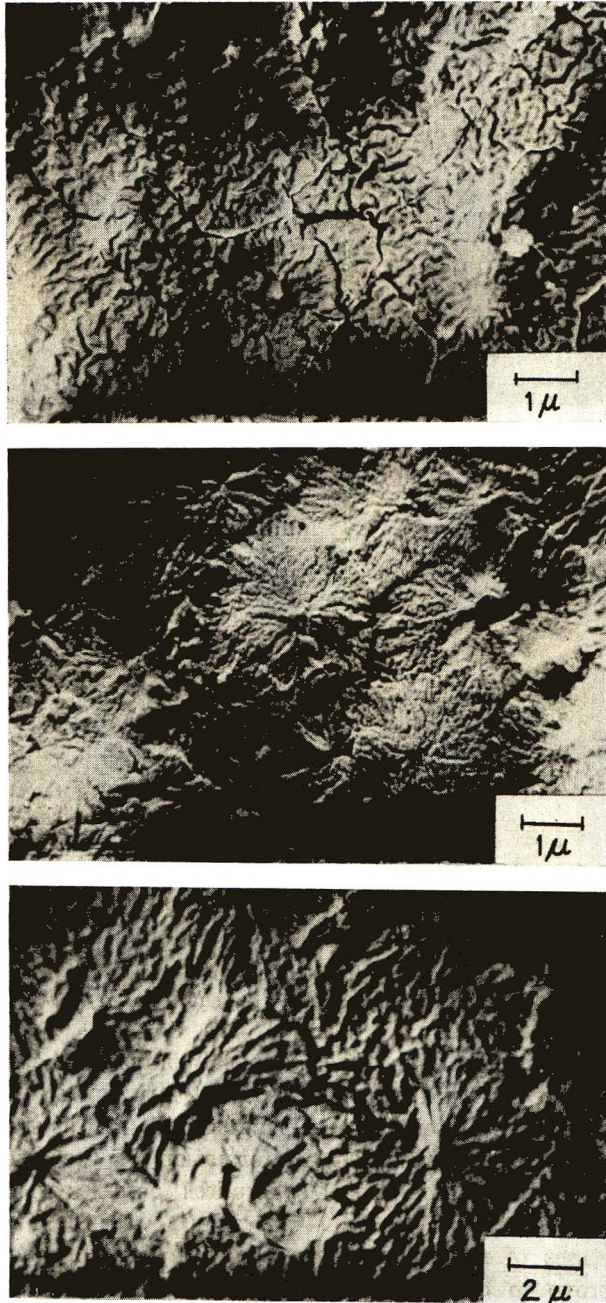


Fig. 16. Electron micrographs of replica of butadiene rubber containing phenyl- β -naphthylamine after the action of an 80-kbar wave

This sequence of events is observed in rubbers from which low-molecular additives have been removed. Had we introduced such additives, which serve as interstructural plasticizers, the situation would be somewhat different. Figure 16 displays electron micrographs of the same rubber following the introduction of small amounts of phenyl- β -naphthylamine.



Fig. 17. Electron micrograph of poly(methyl methacrylate) after exposure to a laser beam with energy density of 10 joule/cm².

At this point one observes the buildup of more complex structures, the breakup of the rubber into relatively large domains with distinct boundaries, very much like those noted in spherulites. The origin of complex supermolecular formations and a subsequent buildup of spherulitic formations in rubber is a well established fact and has been described elsewhere.⁷ The curious point is that these formations have developed under the action of a shock wave, which, unlike heating, increases the mobility of large structural formations that are the constituent elements of spherulites.

How can one estimate the transfer of structural blocks during the period of action of a wave? We made a rough evaluation by studying polypropylene in which a dye was distributed more or less uniformly within the polymer mass. Thus, we had an opportunity to follow the change of the dye distribution after the passage of a shock wave. After the action of the wave, a distinct separation of the dye and polymer within large domains was found.

Hence, despite the short duration of the wave action, structural motions occur over relatively large distances (100–300 μ) and involve large domains.

Thus, we arrive at the conclusion that at low temperature and upon application of very high force, there occur large-scale deformations and profound structural transformations at a supermolecular level, even though deformation of individual polymer molecules is excluded. Thus, we are in a position to acknowledge the existence of two types of processes developing at a molecular and supermolecular levels. Each may be singled out in its pure form under extreme conditions. In ordinary circumstances they are superimposed. The study of a polymer in a real situation is aimed at revealing the contribution of each of the above mentioned mechanisms to deformation and structural transformations.

What do we know of the sequence of events occurring along the boundaries of structural formations, when motions occur at low temperatures or under the high forces? What factors cause the difference between these two processes, namely, the reversibility of low temperature deformations and a total irreversibility of deformation caused by the shock wave? Some conclusions have been formulated by Novikov and co-workers,^{8,9} who observed supermolecular transformations in poly(methyl methacrylate) irradiated by a laser beam. Supermolecular structures may also be revealed in amorphous polymer glasses in which pigments¹⁰ have been introduced or by the use of laser radiation which leads to breaking up of an organic glass into discrete formations of spherulitic type. No chemical changes occur in the polymer. Figure 17 is an electron micrograph of poly(methyl methacrylate) subjected to laser radiation with an energy density of 10 joule/cm². This energy density corresponds to that of separation of domains held together by van der Waals forces but not by primary chemical bonds.

It must be understood that all these estimates are of a highly approximate nature, for only minute amounts of polymer are involved in processes developing along boundaries of relatively large structural blocks. We must, therefore, avoid speculations concerned with all these processes. It may be hoped that the recent studies of polymers containing long side chains successfully carried out by Platé et al.¹¹ will cast light on these phenomena and advance knowledge in this field. In polymers of this type the structural boundary lines run within the molecules proper, and the behavior of such systems is closely determined by use of a complex optical method and structural analysis.

References

1. N. A. Platé, *Vysokomol. Soedin. A*, **10**, 2650 (1968).
2. V. A. Kargin, paper presented at the 21st IUPAC Congress, Toronto, Canada, 1968.
3. V. A. Kargin and G. L. Slonimskii, in *Encyclopedia of Polymer Science and Technology*, Vol. 8, Interscience, New York, 1969, p. 445.
4. G. G. Kardash, G. P. Andrianova, N. F. Bakeev, V. A. Kargin, *Vysokomol. Soed.*, **7**, 1670 (1965).
5. V. A. Kargin, G. P. Andrianova, and G. G. Kardash, *Vysokomol. Soedin. A*, **9**, 267 (1967).
6. V. A. Kargin, I. Y. Tsarevskaya, V. N. Zubarev, V. I. Goldanskii, and P. A. Yampolskii, *Vysokomol. Soedin. A*, **10**, 2600 (1968).
7. V. A. Kargin, Z. Ya. Berestneva, V. G. Kalashnikova, *Uspekhi Khim.*, **36**, 203 (1967).
8. N. P. Novikov, S. S. Saluenya, M. M. Tribbel, *Dokl. Akad. Nauk SSSR*, **182**, 604 (1968).
9. N. P. Novikov, A. A. Kholodilov, F. N. Chernyavskii, and V. A. Kargin, *Dokl. Akad. Nauk SSSR*, **183**, 1375 (1968).
10. M. I. Karyakina, V. A. Kargin, Z. Ya. Berestneva, and N. V. Maiorova, *Vysokomol. Soedin. B*, **9**, 346 (1967).
11. V. P. Shibaev, B. S. Petrukhin, Yu. A. Zubov, N. A. Platé, and V. A. Kargin, *Vysokomol. Soedin. A*, **10**, 216 (1968).

Received April 15, 1970

Revised November 4, 1970

Redrawing of Oriented Polyethylene Film

MITSUO YAMADA, KEIZO MIYASAKA, and KINZO ISHIKAWA,
*Laboratory of Textile Physics, Tokyo Institute of Technology,
Ookayama, Meguro-ku, Tokyo, Japan*

Synopsis

Drawn and subsequently annealed polyethylene film was restretched along the original draw axis at various temperatures. The internal deformation was analyzed in terms of the structural parameters of a simplified model. The elementary deformations are the rotation of crystals around the b axis and shear at the crystal interface. The rigidity of the crystal plays an important role during extension; and as a result, disorientation of chains in the crystal occurs at high strain. At the same time, crystals deform in such a way that the crystalline chains tilt about the b axis along the ($h00$) plane. This deformation of the crystal is affected by temperature. The increase in long spacing with extension can be interpreted roughly by the changes in structural parameters. The strain in amorphous region is also discussed in relation to these parameters.

INTRODUCTION

In the previous paper,¹ the effects of compression along the fiber axis on uniaxially drawn materials were investigated by wide-angle (WAXS) and small-angle (SAXS) x-ray scattering. The results showed that the mechanism of internal deformation is intimately related to structure. However, the complexity of structures including the unit cell order, superstructure, and the sample shape makes it difficult to discuss the deformation mechanism in a unified way. In this paper, the deformation mechanism and its dependence on temperature are investigated for drawn polyethylene film, the structure of which may be regarded as especially simple.

Specimens were obtained by drawing a polyethylene film and subsequent annealing and the x-ray diffraction photographs of a specimen so treated obtained. The structure proposed by Seto² and shown schematically in Figure 1A was supported by our previous work.¹ The crystalline and amorphous layers are stacked periodically along the draw direction, and the normal to the crystalline interface inclines toward the draw direction at an angle δ in the Y - Z plane. There is another habit characterized by mirror symmetry with respect to a plane XY parallel to the film plane. In each of the crystalline lamellae, the molecules tilt away from the draw direction by an angle φ . Thus, in this case, the internal structure of the specimen can be defined by parameters shown in Figure 1A, i.e., φ , δ , α , L , and so on, where α is the tilt angle of chains in the crystalline lamella and L is the long spacing.

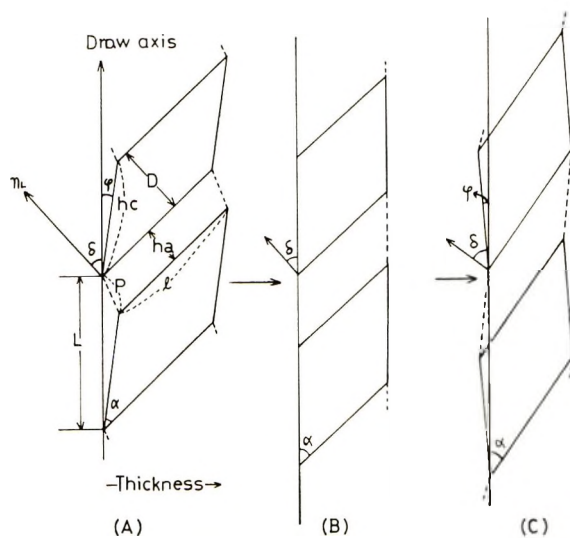


Fig. 1. Schematic representation of structural changes in YZ plane during extension: (A) before stretching; (B) low extension, uniaxial orientation of chains in crystals; (C) high extension, disorientation of chains in crystals. The structural parameters are defined as follows: φ , angle between chains in crystals and the draw direction; δ , angle between the normal of the crystal interface and the draw direction; α , angle between chains in crystal and the crystal interface (tilt angle); L , long spacing; l , width of a crystal lamella (assumed equal to that of an amorphous region); D , thickness of a crystal lamella; h_c , length of a chain in the crystal; h_a , thickness of an amorphous region.

Then, the deformation mechanism can be investigated by discussing the changes in these parameters during deformation. This kind of approach has been tried by several authors.³⁻⁷ However, there are many unsolved problems about the deformation mechanism itself and the state of strain of the internal structural units.

PRELIMINARY CONSIDERATIONS

In our simple model, the volumes of the adjacent crystalline and amorphous regions are represented, respectively, by

$$V_c = DKl \quad (1)$$

$$V_a = h_a Kl \quad (2)$$

where K is the length of an edge of crystal in the X direction and l is the length of an edge in the YZ plane, as in Figure 1A. The thicknesses of the crystalline and amorphous regions are denoted by D and h_a . If h_c denotes the length of a chain traversing a crystal, as shown in Figure 1A, D is obtained from

$$D = h_c \sin \alpha = h_c \cos (\varphi + \delta) \quad (3)$$

where φ , δ , and α are defined above. From eqs. (1), (2), and (3), we obtain

$$h_a = (V_a/V_c)h_c \cos (\varphi + \delta) \quad (4)$$

The long spacing L is expressed by

$$\begin{aligned} L &= (h_a + D)/\cos \delta \\ &= h_c[\cos(\varphi + \delta)/\cos \delta][1 + (V_a/V_c)] \\ &= h_c[\cos(\varphi + \delta)/\cos \delta](1/X_v) \end{aligned} \quad (5)$$

where X_v is the volume-fraction crystallinity of the sample under strain. As the volume of the specimen changes upon stretching, the crystallinity also changes according to

$$X_v = X_v^0/(1 + \epsilon_v) \quad (6)$$

where X_v^0 denotes the crystallinity before stretching and ϵ_v is the relative change in volume of the specimen. The change in volume of the unit cell caused by stretching is small enough to be neglected.⁸⁻¹¹ Thus the increase in total volume can be attributed to the change in the amorphous region, when h_c is kept constant during extension. Then, the long spacing at any stage of stretching is expressed by

$$L = h_c[\cos(\varphi + \delta)/\cos \delta][(1 + \epsilon_v)/X_v^0] \quad (7)$$

The fractional increase of the long spacing is calculated from the relation:

$$\begin{aligned} \epsilon_{L,\text{calc}} &= (L - L_0)/L_0 \\ &= \frac{\cos(\varphi + \delta)}{\cos \delta} \cdot \frac{\cos \delta_0}{\cos(\varphi_0 + \delta_0)} (1 + \epsilon_v) - 1 \end{aligned} \quad (8)$$

The subscript zero indicates values in the unstretched state. Our concern is with changes of parameters φ , δ , and L during extension of the sample and with their temperature dependence. It should be noted that these parameters are all measurable, and therefore one can discuss the deformation in terms of these observed quantities.

EXPERIMENTAL

Preparation and Characterization of the Samples

Linear polyethylene (Hizex 5000S) was melt-pressed at 180°C and then quenched in water at room temperature to obtain a film about 1 mm thick. Strips 10 mm in width were cut from the isotropic sheets and then drawn uniaxially eightfold at room temperature. The unconstrained samples were then heat-treated at 126°C in a silicon oil bath for 15 hr. The resulting samples were characterized by WAXS and SAXS with the incident beam in the two principal directions, X and Z , perpendicular to the stretching axis, as shown in Figure 2.

X-Ray Measurements

In WAXS and SAXS measurements, the temperature in the heating bath was controlled to within $\pm 1.5^\circ\text{C}$. WAXS measurements were made with a Rigaku-Denki D-3F apparatus equipped with a copper target, nickel filter,

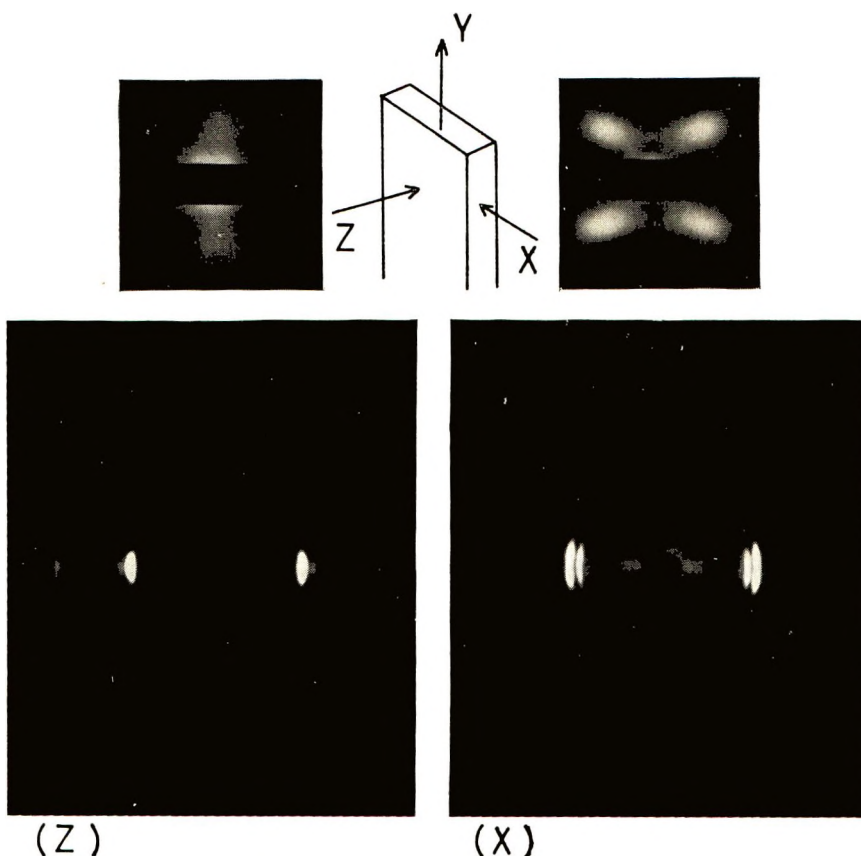


Fig. 2. X-Ray diffraction photographs of original polyethylene sample: *Y*, draw direction; *Z*, thickness direction; *X*, perpendicular to *Y* and *Z*.

and GM-counter detector system. The angle φ was obtained in terms of the azimuthal angle of maximum intensity of the (200) reflection from the equator with the incident beam in the *X* direction. In the procedure, the counter was fixed at the scattering angle of the (200) reflection ($2\theta = 24^\circ$), and the sample was rotated around the *X*-axis. The 0.3 mm and 0.5 mm slits were used for the incident and scattering beams, respectively. SAXS measurements were made with the Rigaku-Denki Rota-unit 3. A nickel-filtered $\text{CuK}\alpha$ beam was used. Conditions for collimation were as follows: (1) the first slit aperture was 0.3 mm, and the second, 0.2 mm; (2) the distance between the first and the second slits was 300 mm; the distance between the sample and the x-ray film was 400 mm. The specimen was set 50 mm behind the second slit. The angle δ was obtained directly from the SAXS patterns with an enlarger. The appearance of the second order scattering maximum in the SAXS diagram was effective for the precise evaluation of the angle δ . The experimental error is probably within $\pm 1.5^\circ$. The long spacing was directly obtained by GM-counter method.

From these x-ray measurements, the internal structure of the unstretched sample was characterized as follows. The angles φ and δ at 25°C are 7° and 42°, respectively. Long spacings are 350, 355, and 375 Å at 25, 70, and 110°C, respectively. Equation (5) results in h_c of about 295 Å, with 350 Å and 0.72 used for L and X_v , respectively. The crystallinity X_v was calculated by the relation

$$X_v = (\rho_s - \rho_a)/(\rho_c - \rho_a) \quad (9)$$

where ρ_s , ρ_c , and ρ_a are the densities of the sample, and of crystalline and amorphous regions, respectively. In this case, ρ_c is 1.0 g/cm³ and ρ_a is 0.856 g/cm³; ρ_s is 0.960 g/cm³ (measured in a gradient of methanol and water at 30°C). The width l of the crystal lamellae was estimated roughly as about 400–500 Å from the data of Seto.¹³

RESULTS

WAXS and SAXS diagrams under extension along Y direction at 110°C with the incident beam in the Z direction are shown in Figure 3. Similar features were observed at other temperatures. These photographs showed no detectable change in the molecular and textural orientation. That is, in

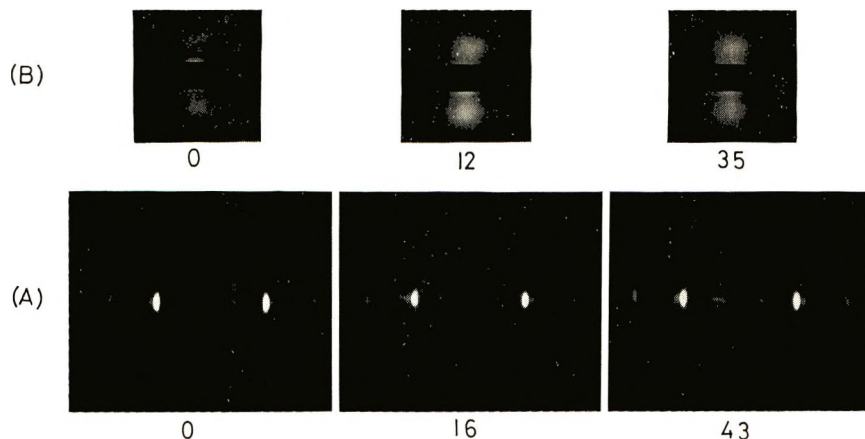


Fig. 3. X-Ray diffraction photographs during extension at 110°C: (A) wide-angle pattern; (B) small-angle pattern. The incident beam is along the Z axis. The strain (%) is indicated beneath each photograph.

the WAXS diagrams the (200) and the (020) reflections remain on the equator under extension; and in the SAXS patterns, two spots remain on the meridian. In SAXS, only broadening of the spots and a decrease of the scattering angle at the intensity maximum were observed. But, this says nothing concerning textural orientation. Thus, x-ray diagrams imply that no change in orientation of crystals occurs in the XY plane, the plane of the film.

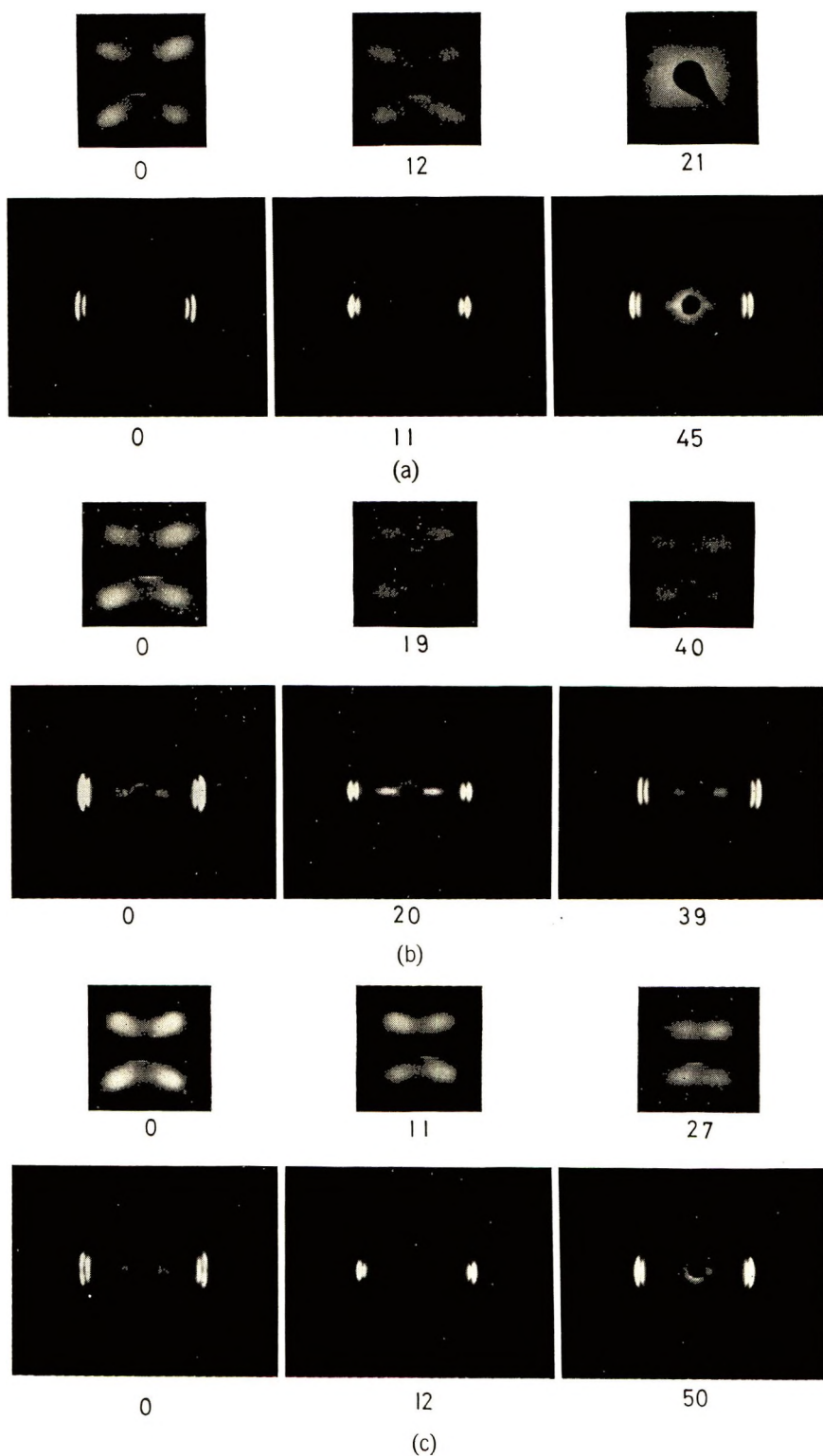


Fig. 4. X-Ray diffraction photographs during extension at (a) 25°C, (b) 70°C, and (c) 110°C. The incident beam is along the X axis. Numbers indicate strain.

On the other hand, x-ray diagrams with the incident beam in the X direction indicate characteristic changes in the molecular and textural orientation. In WAXS diagrams, as in Figure 4, the (200) reflection, which originally was several degrees away from the equator, moves to the equator with extension of the sample. On further stretching, it separates again from the equator. When the load is removed, the (200) reflection comes back to the equator.

Changes in SAXS diagrams were characterized by: (1) a decrease of scattering angle at the intensity maximum due to the increases in long spacing, (2) a change of the angle δ of the four-point pattern showing the change in textural orientation, (3) a change of the sharpness of the spots.¹⁴ The

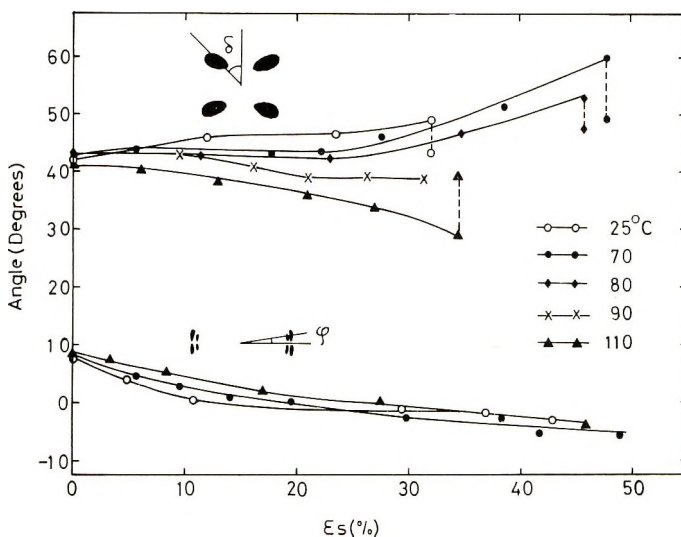


Fig. 5. Changes of angles of φ and δ with the strain.

third point may be related to the disordering of the long spacing, the irregular change of textural orientation, and the change of the shape function of the coherent region.¹⁵ This is not discussed here, for our interest is in the mean changes in textural orientation and long spacing. In Figure 5, the angles φ and δ are plotted against the macroscopic strain ϵ_s of the sample. The negative values of φ at high extension are related to the fact that the (200) reflection peaks again are away from the equator. This means that chain axes in crystals orient in the YZ plane away from the draw direction. In contrast to the angle φ , the angle δ shows considerable dependence on temperature. The change of δ seems to be affected by the so-called α_c dispersion of polyethylene. Below the dispersion temperature (80°C) the angle δ is nearly constant or increases slightly; above 80°C it tends to decrease. When the sample is allowed to relax, the angle φ recovers only to zero in all cases, whereas the points given by dotted lines in Figure 5 show high recovery of the angle δ .

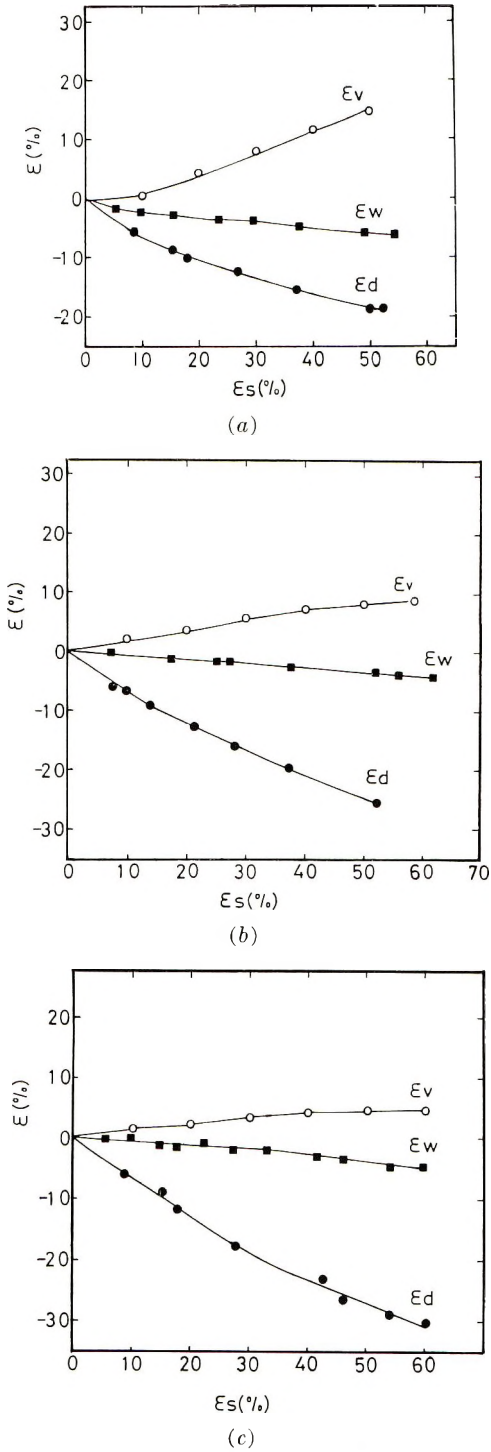


Fig. 6. Changes of thickness ϵ_d , width ϵ_w , and volume ϵ_v of specimen in stretching at (a) 25°C, (b) 70°C, (c) 110°C.

In Figure 6, the fractional changes in thickness (ϵ_d), width (ϵ_w), and volume (ϵ_v) are plotted against the macroscopic strain of the sample. The fractional volume change was estimated by the relation

$$\epsilon_v = (1 + \epsilon_s)(1 + \epsilon_d)(1 + \epsilon_w) - 1 \quad (10)$$

DISCUSSION

Deformation of the Crystalline Region

Figure 1 shows schematic diagrams of deformation deduced from the data on φ and δ for stretching at 70°C, where the constancy of h_c and V_c is assumed. Stage A represents the state before stretching. Stage B corresponds to chains in crystals uniaxially oriented along the stretching axis. Stage C corresponds to 30–50% stretching, where chains in the crystal again tilt away from the stretching direction in the YZ plane. Bending of crystalline lamellae may be also effective in changing the orientation of chains in crystals. The change of orientation caused by crystal bending is expected to be continuous along the azimuthal angle. However, the observed patterns of WAXS have a discrete intensity peak, suggesting that the effect of crystal bending on orientation is not substantial. Thus the main elementary changes of internal structure in stretching are concluded to be (1) rotation of crystals around the b axis, (2) shearing along the crystal interfaces, and (3) deformation of the crystals. The first two mechanisms are due to the rigidity of the crystal and the last to the viscoelastic behavior of the crystal.

Now, we turn to the change within the crystal lamella. According to the simplified structure in Figure 1, the tilt angle α is given by

$$\alpha = 90^\circ - (\varphi + \delta) \quad (11)$$

TABLE I
Observed Values of Tilt Angle α and Corresponding Values of Integer N

Temp, °C	ϵ_s , %	$\alpha(0)$	N
25	0	39.5	3–4
	10	43.5	3
	20	43.5	3
	30	41.5	3–4
70	0	39.5	3–4
	10	44.0	3
	20	46.5	3
	30	45.0	3
	40	40.0	3–4
110	0	39.5	3–4
	10	45.0	3
	20	51.5	2–3
	30	57.0	2

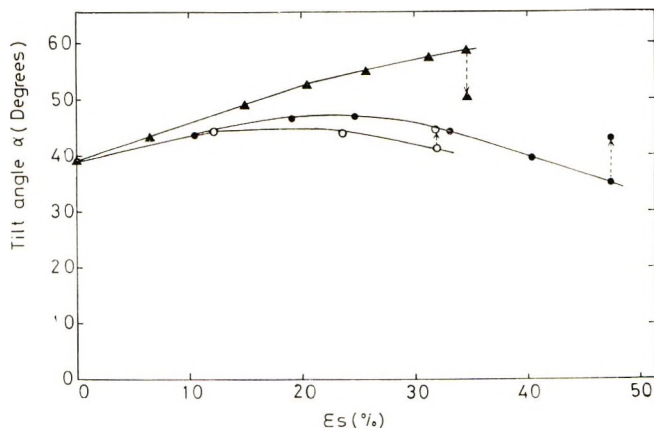


Fig. 7. Relation between tilt angle and macroscopic strain: (○) 25°C; (●) 70°C; (▲) 110°C.

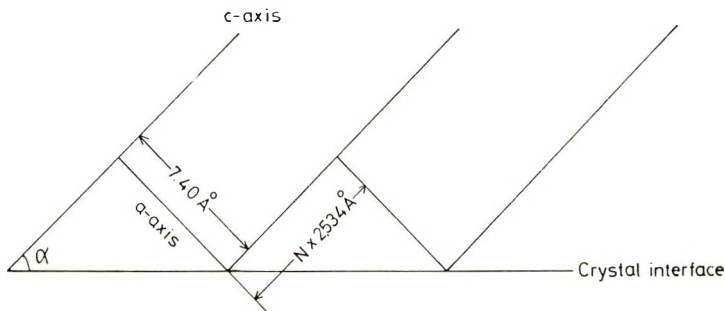


Fig. 8. Schematic model of slippage along the (100) plane: N is an integer; the length of c axis is 2.534 Å.¹⁷

If the small elastic deformation of crystals is ignored,⁸⁻¹¹ the most favorable mode of deformation of a crystal is by slippage along the ($h00$) plane. In Figure 1, the ($h00$) plane of polyethylene is parallel to h_c and perpendicular to the plane of the paper. This slippage causes a change in the tilt angle α . Figure 7 shows the dependence of α on the strain of the sample. Up to strains of about 20%, the angle increases gradually at all temperatures. On further extension, however, the direction of the change depends on temperature, i.e., at low temperature, it decreases, but at 110°C it continues to increase. Thus, it appears that the tilt angle changes in different ways above and below the so called α_c dispersion temperature. On the assumption of slippage in the (100) plane,¹⁶ stable tilting can occur stepwise, as is shown in Figure 8. Thus, a continuous change of the tilt angle α , as in Figure 7, is not reasonable. The experimental behavior may be attributed to irregularity of the changes throughout a sample and to errors in measurement of the angles φ and δ from WAXS and SAXS diagrams.

The integers N corresponding to the observed α are tabulated in Table I. At 110°C, N changes from 4 to 2 when the sample is stretched 30%. On

relaxation of the sample, the tilt angle α showed high recoverability, especially at high temperature. This high recoverability is noteworthy, for the change of tilt angle is usually irreversible. This suggests that the energy stored in the amorphous region is high enough to cause recovery of the deformation of the crystal. On the other hand, this seems to emphasize the existence of "tie chains" in the amorphous region.¹⁸ The deformation of the amorphous region will be discussed later. Last, it should be noted that the fact that the crystalline regions are more rigid than the amorphous regions plays an important role, even though the crystals themselves deform.

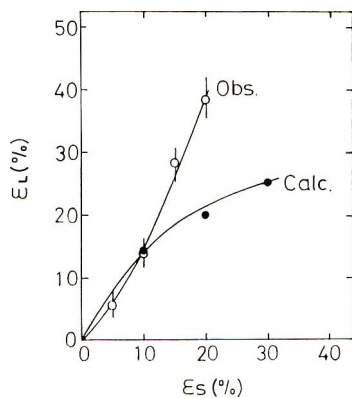
Change of Long Spacing

The fractional increase in long spacing is calculated from eq. (8), and the results shown in Figures 5 and 6. In Figure 9, $\epsilon_{L, \text{calc}}$ and the observed values $\epsilon_{L, \text{obs}}$ are plotted against the strain ϵ_s of the sample. Up to 10% strain, the calculated values agree rather well with observations at each temperature. On further extension, $\epsilon_{L, \text{obs}}$ becomes much larger than $\epsilon_{L, \text{calc}}$ at 25°C. This discrepancy is mainly due to the observed long spacing. This means that the measured long spacing is larger than the real value. This conclusion is supported by the fact that $\epsilon_{L, \text{obs}}$ is much larger than the macroscopic strain ϵ_s . With the exception of the result at 25°C, $\epsilon_{L, \text{calc}}$ is larger than $\epsilon_{L, \text{obs}}$ by about $25 \pm 5\%$. This means that $\epsilon_{L, \text{obs}} \propto \epsilon_{L, \text{calc}}$, approximately. One of the reasons for the discrepancy of $\epsilon_{L, \text{calc}}$ from $\epsilon_{L, \text{obs}}$ may be due to the evaluation of ϵ_v , for the increase in total volume caused by stretching may not necessarily be attributable only to the increase in the amorphous region. However, such a problem is beyond our simple treatment in terms of the series model of crystalline and amorphous regions.

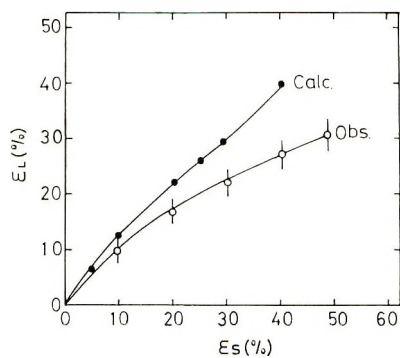
When the assumption of constant h_c fails, i.e., when h_c decreases during extension because of partial melting,^{19,20} the discrepancy between $\epsilon_{L, \text{obs}}$ and $\epsilon_{L, \text{calc}}$ becomes larger than in Figure 9. Further, the thicknesses of crystalline and amorphous layers are not constant throughout the sample, with a consequent distribution of long spacing. As pointed out by Reinhold et al.,²¹ the diffraction peak angle is affected by an asymmetric distribution of long spacing. Further the irregularity on the crystalline lamellae surface also shifts the diffraction peak angle.^{22,23} These inhomogeneities of structure may be emphasized in stretching. Thus the discrepancy observed above may be due, some extent, to the $\epsilon_{L, \text{obs}}$.

Deformation of the Amorphous Region

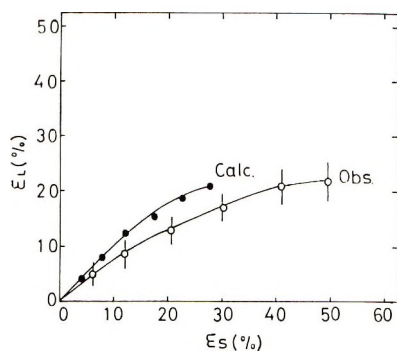
According to Figure 1, the amorphous region, which is sandwiched between the crystalline lamellae, must undergo a large deformation. It may consist of tie chains, cilia and loose loops and molecules of low molecular weight. The orientation of the amorphous halo under compression along the fiber axis and the high recoverability of internal structure¹ are considered as the evidence that tie molecules are an important component of the amorphous region.¹⁸ Now, let us assume that the ends of tie chains are situated at the corresponding coordinates on the interface of adjacent crys-



(a)



(b)



(c)

Fig. 9. Fractional increase of long spacing $\epsilon_{L,calc}$ and $\epsilon_{L,obs}$ as function of strain ϵ_S : (a) 25°C; (b) 70°C; (c) 110°C.

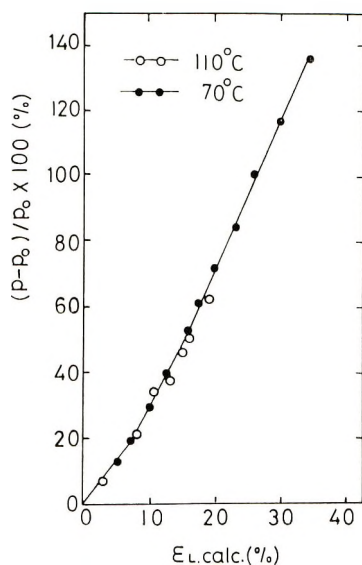


Fig. 10. Relation between fractional increase of P and $\epsilon_{L,calc.}$

tals, though the assumption may be a bit too extreme. Then, the end-to-end distance is equal to the length P in Figure 1. Then P is given by

$$\begin{aligned}
 P^2 &= L^2 + h_c^2 - 2Lh_c \cos \varphi \\
 &= h_c^2 \left\{ \left[\frac{\cos(\varphi + \delta)}{\cos \delta} \frac{1 + \epsilon_v}{X_v^0} \right]^2 - 2 \left[\frac{\cos(\varphi + \delta)}{\cos \delta} \frac{1 + \epsilon_v}{X_v^0} \right] \cos \varphi + 1 \right\}
 \end{aligned} \quad (13)$$

If constancy of h_c is assumed during extension, the relative increase in P can be calculated from φ , δ , ϵ_v , and X_v^0 . In Figure 10, changes in P so obtained are plotted against the calculated strain of long spacing $\epsilon_{L,calc.}$, as given in Figure 9. It is noted $(P - P_0)/P_0$ is about three times $\epsilon_{L,calc.}$. As can be seen from Figure 9, at high extension, $\epsilon_{L,calc.}$ is larger than $\epsilon_{L,obs.}$ at 70°C and 110°C. Therefore, the strain of tie chains may be larger than that indicated by Figure 10.

References

1. K. Ishikawa, K. Miyasaka, M. Maeda, and M. Yamada, *J. Polym. Sci. A-2*, **7**, 1259 (1969).
2. K. Tanaka, T. Seto, T. Hara, and Y. Tajima, *Repts. Progr. Polym. Phys. Japan*, **7**, 63 (1964).
3. Y. Tajima and T. Seto, *Repts. Progr. Polym. Phys. Japan*, **10**, 205 (1967).
4. A. I. Slutsker, T. P. Sanphirova, A. A. Yastrebinskii, and V. S. Kuksenko, in *Macromolecular Chemistry Prague 1965 (J. Polym. Sci. C, 16)*, O. Wichterle and B. Sedláček, Eds., Interscience, New York, 1968, p. 4093.
5. D. R. Beresford and H. Bovan, *Polymer*, **5**, 247 (1964).
6. I. L. Hay and A. Keller, *J. Mat. Sci.*, **2**, 538 (1967).
7. A. Cowking, J. G. Rider, I. L. Hay, and A. Keller, *J. Mat. Sci.*, **3**, 646 (1967).

8. W. J. Dulmage and L. E. Contois, *J. Polym. Sci.*, **28**, 275 (1958).
9. S. Newman and R. L. Miller, *J. Polym. Sci.*, **60**, 14 (1962).
10. I. Sakurada, Y. Nukushina, and T. Ito, *J. Polym. Sci.*, **57**, 651 (1962).
11. K. Miyasaka and K. Makishima, *Kobunshi Kagaku*, **23**, 785 (1966).
12. E. W. Fischer, H. Goddar, and G. F. Schmidt, *Makromol. Chem.*, **118**, 144 (1968).
13. T. Seto and T. Hara, *Repts. Progr. Polym. Phys. Japan*, **9**, 207 (1966).
14. G. W. Groves and P. B. Hirsch, *J. Mat. Sci.*, **4**, 929 (1969).
15. R. Hosemann and S. N. Bagchi, *Direct Analysis of Diffraction by Matter*, North Holland, Amsterdam, 1962.
16. P. Ingram and A. Peterlin, *J. Polym. Sci. B*, **2**, 739 (1964).
17. C. W. Bunn, *Trans. Faraday Soc.*, **35**, 482 (1939).
18. A. Peterlin and G. Meinel, *J. Appl. Phys.*, **36**, 3028 (1965).
19. H. C. Zachman, *Z. Naturforsch.*, **19a**, 1397 (1964).
20. E. W. Fischer, *Kolloid-Z.*, **218**, 97 (1967).
21. Chr. Reinhold, E. W. Fischer, and A. Peterlin, *J. Appl. Phys.*, **71**, 35 (1964).
22. D. Ya. Tsvankin, *Vysokomol. Soedin.*, **6**, 2078 (1964).
23. D. Ya. Tsvankin, *Vysokomol. Soedin.*, **6**, 2083 (1964).

Received February 26, 1970

Revised December 28, 1970

Low-Temperature Mechanical Relaxations in Polymers Containing Aromatic Groups

C. I. CHUNG* and J. A. SAUER, *Rutgers University, New Brunswick,
New Jersey 08903*

Synopsis

Studies have been made of the secondary relaxation processes in the solid state of a number of polymers containing aromatic groups in the polymer chain. The polymers investigated include one, polystyrene, with the aromatic group in side-chain positions, and six high polymers in which phenylene rings lie in the main backbone chain. In polystyrene, wagging and torsional motions of the side chain phenyl rings give rise to a low-temperature δ -relaxation which is centered at 33°K (1.7 Hz) and which has an activation energy of about 2.3 kcal/mole. Most of the polymers with phenylene rings in the main chain exhibit a low-temperature relaxation in the temperature region from 100°–200°K. This relaxation process is centered at 159°K (0.54 Hz) in poly-*p*-xylylene, at 162°K (0.67 Hz) in polysulfone, and at 165°K (1.24 Hz) in poly(dian-carbonate). In poly(2,6-dimethyl-*p*-phenylene oxide), two overlapping low-temperature relaxations are found, one in the range 125–140°K and the other near 277°K (ca. 1 Hz). The low-temperature secondary relaxation process in all of these polymers is believed to be associated with local reorientational motion of the phenylene, or substituted phenylene, rings or with combined motion of the phenylene ring and nearby chain units. For these low temperature relaxation processes, the activation energy is about 10 kcal/mole. The temperature location of the relaxation appears to depend on the specific units to which the phenylene rings are attached and on steric and polar effects caused by substituents on the ring. In the poly-*p*-xylylenes the relaxation is shifted to much higher temperatures by a single Cl substitution on the ring but remains at essentially the same temperature position when dichlorosubstitution is made. The effects of water on the magnitude and temperature location of the observed low temperature relaxations, as well as the implications of the study for other polymers containing aromatic groups in their backbone chains, are discussed.

INTRODUCTION

Low-temperature relaxation processes have been frequently observed in linear high polymers in the vicinity of 150°K at a measuring frequency of about 1 Hz. These relaxations, usually referred to as γ -processes, have been found in both low-density and high-density polyethylenes, in various polyamides, and in a wide variety of polyesters. The γ -relaxation is generally considered to arise from local twisting or reorientational motions in the amorphous or disordered phase of a small number of CH₂ type sequences.^{1–3}

It has also been observed that polystyrene (PS), with a pendant phenyl

* Present address: Esso Research and Engineering Co., Linden, N. J.

group attached to every other C atom, shows a mechanical relaxation at an even lower temperature. This relaxation process, termed a δ -relaxation, has been attributed to a coupled oscillational and wagging motion of the pendant phenyl side chains.^{4,5} In view of this behavior, the question arises as to whether motion of phenyl rings in the backbone chain, rather than the side branch, can also give rise to low-temperature mechanical relaxation. If so, it might be expected that this relaxation would be found at higher temperatures than for polystyrene, just as the γ -processes arising from reorientations of CH₂ sequences in the main chain are approximately 50° higher in temperature position than the corresponding processes arising from side-chain motion.^{1,4,6}

The present investigation was undertaken to explore the possibility of a low-temperature relaxation process arising from motion of ring structures located in the main backbone chain. The polymers selected for this study were three types of poly-*p*-xylylene (PPX), poly(4,4'-isopropylidene-diphenylene-*co*-4,4'-sulfonyldiphenylene dioxide) (PSF), poly(dian carbonate) (PDC), and poly(2,6-dimethyl-*p*-phenylene oxide) (PDMPO). The three types of poly-*p*-xylylene included an unsubstituted polymer, (PPX) a monochloro-substituted polymer, (PCPX), and a dichloro-substituted sample, (PDCPX). In addition, tests were also made on polystyrene samples both to serve as a calibration of the apparatus and to confirm the presence of a low temperature relaxation process arising from motion of phenyl rings.

Some mechanical and dielectric relaxation data on these materials are already available.^{1,6,7-16} For example, Reding et al.⁹ observed a low temperature relaxation in polycarbonate at 163°K (1.2 Hz) and attributed it to motion of the OCOO group lying between phenyl rings. A loss peak at the same temperature position at 1 Hz has been reported by Kurz et al.¹⁶ in PSF and associated with processes involving SO₂ group motion. Also for the polymer PDMPO, de Petris et al.¹¹ show a low-temperature shoulder near 150°K in their mechanical data taken at acoustical frequencies (7×10^3 Hz) and Karasz et al.¹⁷ report a low-temperature peak in their dielectric data near 175°K (10³Hz). NMR studies on this same polymer show that the methyl groups rotate at liquid nitrogen temperatures and that there is a gradual decrease of line width with temperature between 80°K and room temperature.¹⁸ A brief account of the low-temperature data taken below 280°K on poly-*p*-xylylene has been given.¹⁹ Acoustic data taken at 5-10 kHz have also been reported for some substituted polystyrenes, polyvinyl benzoates, polyvinylpyridines, and polyphenylene oxides.^{13,20} Data from these various investigations will be compared and contrasted with data from the present investigation wherever applicable.

EXPERIMENTAL

All measurements of the real and imaginary parts G' , G'' , of the shear modulus, or of log decrement Δ , that are reported herein, were made by

means of an inverted torsional pendulum apparatus. The specimen in the form of a thin film, is supported between a fixed lower clamp and an upper clamp that is connected to the moment arm. This, in turn, is supported by a constantan wire connected to an adjustable counterbalancing weight. The torsional oscillations of the system are detected by means of a rotary variable differential transformer and are recorded on chart paper. The specimen can be cooled to liquid nitrogen temperatures and, if necessary, down to about 20–25°K by use of a liquid-helium Dewar. The system can be evacuated but, for the tests reported herein, this provision was not necessary.

Because of the thinness of some of the test samples (ca. 2 mils), it is necessary to make appropriate corrections for the response of the supporting wire and for the effect of any tensile load on the specimen. A small axial tensile stress was found desirable to avoid excessive wagging of the specimen. A computer program was established so that G' , G'' , and Δ could be calculated for each temperature at which measurements were made, from the observed periods and amplitudes of the free decaying oscillations. Readings were taken at close temperature intervals, every 2–3°K, and the heating rate was maintained, by means of a resistance heater wrapped around the specimen can, at about 1°K/min. Details of the testing apparatus, the test procedures, and the method of calculations are given elsewhere.²¹

The polysulfone was supplied in sheet form by Union Carbide. Its number-average molecular weight was reported as 26,000. The poly-(bisphenol A carbonate) or poly(dian carbonate) was supplied as extruded sheets by General Electric. Its weight-average molecular weight was reported as 30,000. The poly(dimethylphenylene oxide) was supplied by the same company in the form of compression molded sheets. The poly-*p*-xylylene samples were supplied in the form of thin films by Union Carbide. They were prepared by vapor-phase pyrolysis and subsequent vapor-phase

TABLE I
Test Sample Characteristics

Polymer	Designation	Thickness, cm	Density, g/cm ³	Crystallinity, % (est.)	Glass Tempera- ture, °C
Polysulfone	PSF	0.062	1.24	Amorphous	190
Poly(dian carbonate)	PDC	0.025	1.20	Amorphous	145
Poly(2,6-dimethyl- <i>p</i> -phenylene oxide)	PDMPPO	0.0285	1.05	Amorphous	210
Poly- <i>p</i> -xylylene	PPX	0.0053	1.11	50–70	60–70
Polymonochloro- <i>p</i> -xylylene	PCPX	0.0075	1.289	50–70	80–100
Polydichloro- <i>p</i> -xylylene	PDPCPX	0.0038	1.41	50–70	110
Polystyrene	PS	0.029	1.05	Amorphous	105

deposition of di-*p*-xylylene according to the method outlined by Gorham.²² The resulting polymers are linear, of high molecular weight, and free of impurities and byproducts.

Test specimens were cut to the desired size from the available sheet of film. The test specimen length between clamps was 6 cm and the width of the specimens was 0.60 cm. In Table I other characteristics of the test samples are given. The densities were determined by a density-gradient column, and the estimated crystallinities and glass transition temperatures are those reported by the manufacturer.

RESULTS AND DISCUSSION

Polystyrene (PS)

The test results, which for this sample were recorded down to about 20°K, are shown as a function of temperature in Figure 1. A low-temperature relaxation process is clearly evident both in the G' and G'' data. The modulus and loss data are in general accord with those of Sinnott.²³ The δ -loss peak appears to be located at approximately 33°K (1.7 Hz) in this study as compared to 38°K (5.6 Hz) in Sinnott's investigation, and 48°K (6.3 kHz) in the studies of Crissmann et al.,^{24,25} who used longitudinal vibrations. The low-temperature δ -relaxation in PS has also been studied by dielectric techniques;^{4,5} if one uses the available mechanical and dielectric data^{4,5,23-26} together with the present data, a reasonably good fit to the experimental observations is obtained for an activation energy of 2.3 kcal/mole.

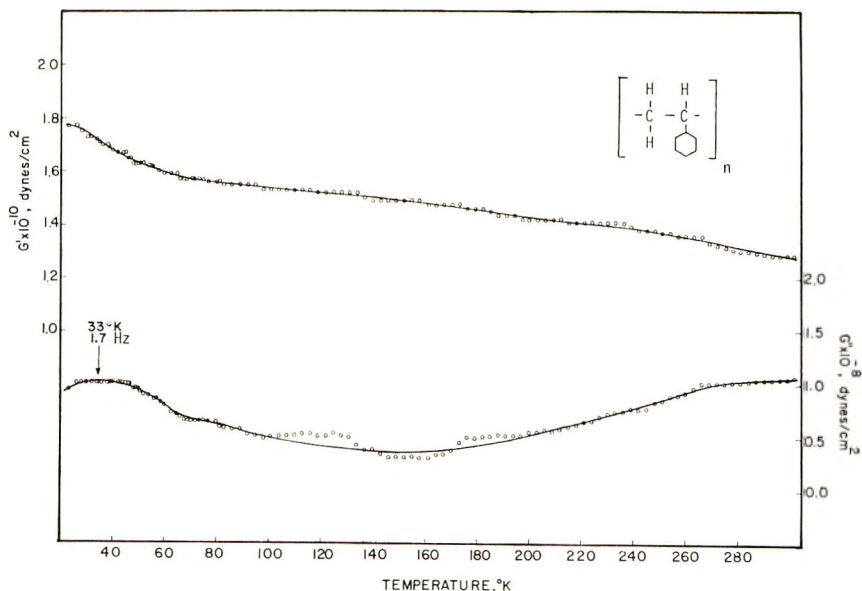


Fig. 1. Temperature dependence of shear modulus G' and loss modulus G'' for polystyrene.

Figure 1 indicates that no other significant modulus dispersions or loss peaks occur in PS in the temperature range up to 300°K. Small relaxations have sometimes been reported in the temperature range 100°–200°K,^{1,6} and there is some scatter in this region in the loss data of Figure 1. However, it is known that the relaxation spectrum in this region is sensitive to the presence of small amounts of impurities.^{4,5} Hence the slight variations of loss about the general trend of Figure 1 may arise from this source or from experimental error. The modulus data show only a steady decline over the region from about 70°K to 300°K, and this is to be expected as a result of thermal expansion. The thermal expansion of polystyrene has been measured by Saba²⁷ over the temperature range from 4°K to room temperature. His data show a fairly large change in expansion coefficient in the 4–40°K region, probably indicative of the onset of the δ -relaxation process and a fairly constant expansion coefficient over the range 80–200°K.

It has been suggested, on the basis of combined results of the mechanical and dielectric studies, that the δ -relaxation in polystyrene is a result of, or is accompanied by, a combined torsional and wagging motion of the phenyl ring. The conclusion that wagging, as well as rotational oscillation about the C–C bond joining the phenyl ring to the main chain, is involved stems from the fact that poly-*p*-chlorostyrene, with a much larger dipole moment, shows a loss maximum at the same temperature location as polystyrene, although the intensity of the dissipation is some four times higher. Torsional oscillations alone would not be dielectrically active in either of these two polymers and hence a coupled rotational wagging motion appears at present as the most likely interpretation.

Poly-*p*-xylylene (PPX) and Polychloro-*p*-xylylene (PCPX)

The temperature dependence of the loss modulus G'' for the unsubstituted polymer PPX and for the chloro-substituted polymer PCPX is shown in Figure 2. In the unsubstituted polymer there is a large damping peak centered at about 154°K (0.54 Hz). This relaxation is absent in the substituted polymer PCPX in which one of the hydrogen atoms on the ring has been replaced by a chlorine atom.

The low-temperature relaxation in PPX—which we refer to as a γ -relaxation because it occurs in approximately the same temperature range as the γ -relaxation observed in other linear polymers such as polyethylene and the polyesters—cannot be attributed to local reorientational motion of three or more flexible CH₂ sequences as it has been for other polymers.^{1,2} In PPX, the phenylene rings in the main chain are separated by only two adjacent CH₂ groups, and observations on Fischer-Hirshfelder models show that conformational changes of the CH₂ units are impossible without large-scale motion of the adjacent phenylene units. However, the phenylene units can undergo reorientational motions with little or no cooperation from the adjacent methylene units. Hence the γ -relaxation in PPX is considered to arise primarily from reorientational motions of the phenylene rings situated in amorphous regions of the polymer.

The situation in PPX may be somewhat similar to that discussed by McCammon et al. for polystyrene⁵ or that discussed by Tanabe et al.²⁸ for polymers containing side-chain methyl groups, except that the group involved is now a phenylene unit rather than a phenyl or methyl unit. These authors have suggested that in thermal equilibrium a certain distribution of angular displacements of the phenyl or methyl units exists, and that when stress is applied to the polymer, as in a mechanical relaxation experiment, thermal equilibrium is upset and a new distribution is realized. This requires a finite relaxation time, and when the experimental frequency is comparable to this time, maximum absorption of energy occurs. In PPX, this situation appears to take place at 1 Hz at about 160°K, while

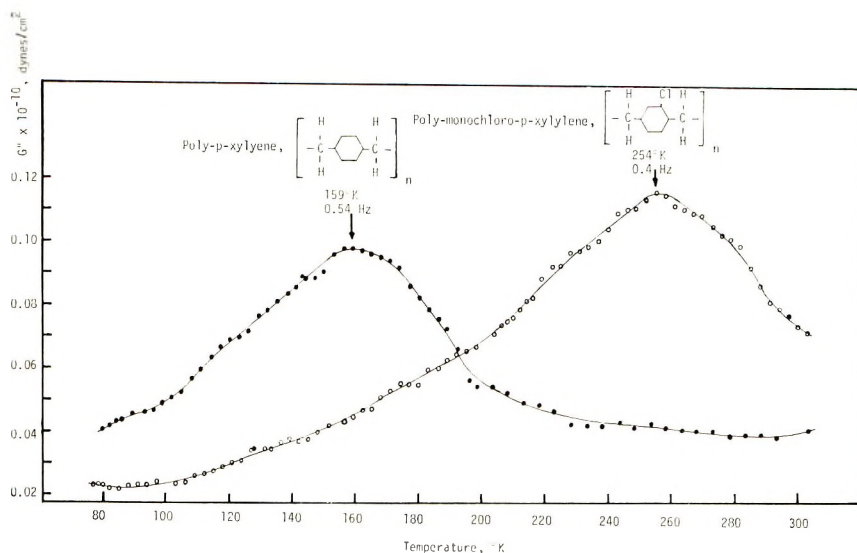


Fig. 2. Temperature dependence of the loss modulus for poly-*p*-xylylene and poly-monochloro-*p*-xylylene.

in PS, where only a side-chain phenyl group is involved, it appears to occur at about 40°K. The strength of the relaxation is also much greater when the moving unit is in the main chain, as one can see from comparison of the loss-peak heights of Figures 1 and 2.

Further evidence for the assignment of the 160°K relaxation primarily to local motion of the phenylene groups comes from the data on the monochloro-substituted sample of poly-*p*-xylylene. As Figure 2 shows, there is now no damping maximum in the vicinity of 160°K. The effect of the Cl substitution has been to shift the relaxation to much higher temperatures and the damping peak is now located at 254°K (0.4 Hz). A similar shift has been observed in the modulus dispersion.¹⁹ Clearly, there are now much greater constraints on the molecular motions involved. As a result of the asymmetric nature of a single Cl substitution, one would expect both greater steric hindrance and also increased dipolar forces.

The effect of these factors is to raise the barrier to reorientational motions and thus shift the relaxation process to higher temperatures, as has been observed.

Polydichloro-*p*-xylylene (PDCPX)

Figure 3 shows the temperature dependence of the shear modulus G' and the loss modulus G'' for the dichloro-substituted polymer PDCPX. The measurements in this case were taken from 80°K up to 420°K. Over this temperature range, PDCPX exhibits at least two, and possibly three, relaxation processes. There is a high-temperature relaxation, designated the α -process, marked by a large modulus drop and a loss peak in the region of 350–400°K. Since T_g of this polymer (see Table I) is about 380°K, the α -relaxation is attributed to large-scale micro-Brownian motions of the

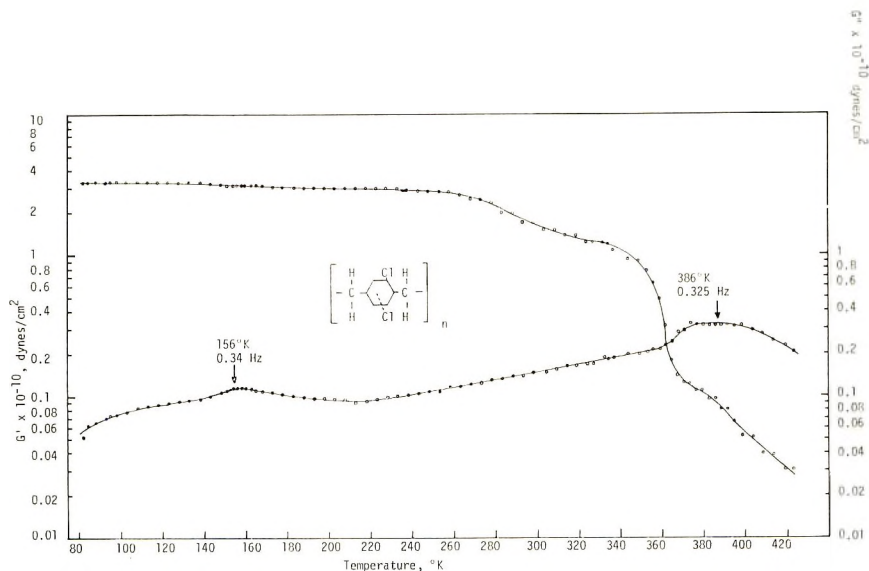


Fig. 3. Temperature dependence of the shear modulus and the loss modulus for polydichloro-*p*-xylylene.

polymer backbone chain. The T_g for this polymer is higher than that for PPX (see Table I) because of the stiffening effects on main-chain mobility of the bulky Cl substituents. Similar increases in T_g have been observed in some linear epoxy resins upon methyl and chlorine substitutions on phenylene rings.²⁹

There is also a definite low-temperature relaxation in the vicinity of 156°K (0.34 Hz), or at approximately the same temperature as that for the unsubstituted polymer, PPX, and of approximately the same magnitude. Thus the effect of the double Cl substitution on the ring has been effectively to shift the secondary relaxation that occurred near 254°K

in the singly substituted polymer back to the 160°K region, where its relaxation occurred in the unsubstituted PPX.

The precise location of the second chlorine atom on the phenylene group in PDCPX is not known.³⁰ However, the present data shed some light on this question. If the Cl atoms were in the 2,3 or 5,6-positions on the ring, there would be a large dipole moment present, and motions of the ring would be hindered by both dipolar effects as well as by increased asymmetric geometry. However, if the Cl atoms are in the 2,5 positions, the dipolar effects would cancel out. Similarly, if they were in the 2,6-positions, the transverse components of the dipole moment cancel. Hence, the location of the γ -relaxation at approximately the same temperature position for both the PPX and the doubly substituted PDCPX would favor one of the latter two assignments. The data suggest that dipolar and steric effects are important in shifting the secondary loss process to higher temperatures, as occurs in the singly substituted polymer, PCPX, but that steric hindrances are apparently not much different for the disubstituted ring than for the unsubstituted one. Another possibility is that intramolecular interactions may be higher for the disubstituted polymer but intermolecular interactions are reduced because of the greater average distance between chains.

There is evidence in Figure 3 of an additional small relaxation process occurring between the low-temperature γ -process and the high-temperature α -process. This is shown, for example, by the drop in modulus that occurs between 240 and 340°K. Although there is no definite damping peak in this temperature region, the loss modulus G'' rises steadily from a minimum at about 220°K as the temperature is increased. This behavior is in contrast with that observed in the unsubstituted PPX, where the damping is still falling up to 300°K and the shear modulus is fairly independent of temperature, at a value of about 1.8×10^{11} dyne/cm², over the temperature range from about 200 to 300°K.

The reason for the observed differences in these two materials is not clear. If the gradual drop in modulus and rise in loss from 240 to 340°K in PDCPX is attributed to the beginning of the glass transition, then one might expect a similar process to occur at even lower temperatures in PPX, as its T_g is even lower than that of PDCPX (see Table I). One possible explanation of the observed effects in PDCPX has been given.¹⁹ It is that the modulus fall and increase in loss in the intermediate temperature range may reflect a small secondary relaxation arising from motion of asymmetric phenylene units having more or less than two Cl atoms. From the results shown in Figure 2 for the singly substituted polymer, PCPX, it is expected that rings with a single asymmetric Cl substitution will give rise to an increased loss and a modulus dispersion in the 220–320°K temperature region. Another point in favor of the proposed explanation is that it is believed that a considerable number, possibly up to 15%, of the phenylene groups in the disubstituted polymer, PDCPX, do not have two Cl atoms.

Polysulfone (PSF)

The temperature dependence of the shear and loss modulus of polysulfone is shown in Figure 4. Two different samples were tested and they both gave essentially the same results. A large low-temperature γ -relaxation is present, and the maximum in loss occurs at about 162°K (0.67 Hz). Baccaredda et al.¹² have also observed in PSF a low temperature maximum, which they termed a β -relaxation. At their test frequency of 6000 Hz, this relaxation was centered at about 230°K. It is considered that their so-called β -relaxation is identical with our γ -relaxation, the shift in temperature being purely a result of differences in test frequency. Our data are also in excellent agreement with those recently reported by Heijboer¹⁵ and Kurz et al.¹⁶

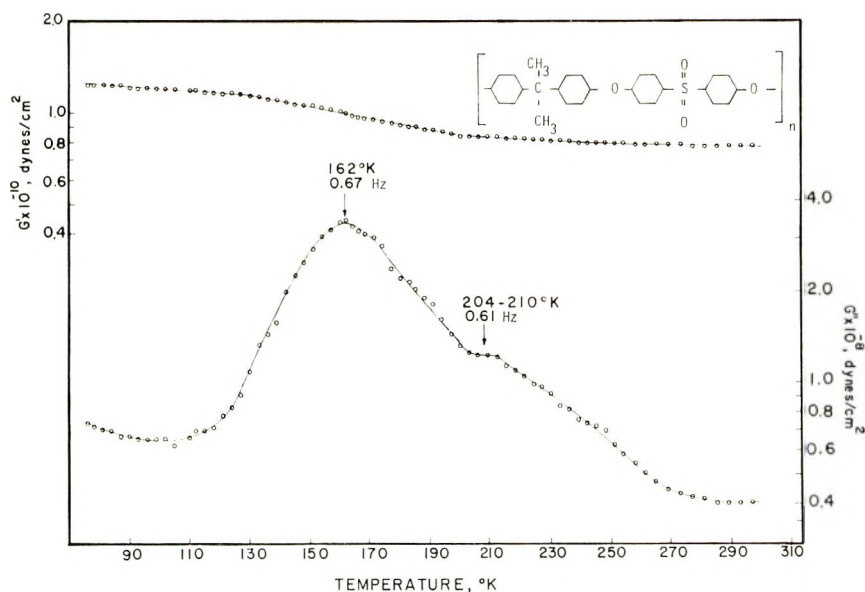


Fig. 4. Temperature dependence of shear modulus and loss modulus for polysulfone

The large loss peak in the vicinity of 160°K in polysulfone, like that in PPX, cannot be due to any flexible CH₂ or equivalent sequences in the chain. In PSF the basic backbone structural unit contains four phenylene groups linked respectively by an isopropylidene unit $\text{-(C(CH}_3\text{)}_2\text{-)}$, an ether unit -(O-) , a sulfone group $\text{-(SO}_2\text{-)}$, and another ether unit. In view of this structure, it appears that low-temperature mobility could arise only from onset of motion of the methyl groups, which, as discussed below, should occur at much lower temperatures, or from local reorientational motions of the phenylene units. By analogy of the results on PSF with those on PPX, the observed γ -relaxation near 160°K is considered

to arise from motion of the phenylene units, probably coupled with oscillational motion of the nearby polar units. Molecular models of polysulfone show that such motions are possible.

With regard to the shoulder in the test data near 205°K (0.61 Hz), at least two hypotheses can be made. If we assume it arises from a second overlapping relaxation, then one relaxation may involve motions of the two phenylene units situated between the isopropylidene and the ether groups, while the second relaxation reflects similar motions of the two phenylene units situated between the sulfone and the ether units. From the test results on PDC, discussed below, it appears that the 160°K relaxation, which occurs in both polymers, is associated with the first set of phenylene units. A second hypothesis is that the high-temperature shoulder near 205°K may result from motion of absorbed water molecules, as it is well known that a loss peak arises in this region for many polymers, such as the polyamides, when water is added.^{1,6} In fact, Heijboer¹⁵ has noted that this high temperature shoulder tends to disappear and the loss peak to shift to somewhat lower temperatures when the sample is annealed.

With regard to the onset of methyl group motion, it is pertinent to examine the results of nuclear magnetic resonance studies that have been made on polymers containing methyl groups.^{6, 18, 28, 31, 32} From these studies it is known that methyl group rotation at a frequency of 10⁴–10⁵Hz occurs well below 150°K in polymers such as polypropylene, poly-4-methylpentene-1, and poly(2,6-dimethylphenylene oxide). In fact, mechanical loss peaks (1–10⁴ Hz) attributed to methyl group motion have been detected in the 4–25°K range.^{4, 23, 33} Hence methyl rotation is not a reasonable cause for the γ -relaxation near 160°K in PSF. Also, no methyl groups are present in PPX, yet it has a low-temperature relaxation comparable to that of PSF, as comparison of Figures 2 and 4 shows.

It is, however, considered likely that a loss peak due to methyl rotation would have been encountered if our measurements had been carried out to temperatures below that of liquid nitrogen. For example, it may be noted from Figure 4 that there is a minimum in the loss data at 110°K and a gradual but steady rise in loss magnitude as the temperature is lowered to 80°K. We also consider methyl group motion to be a likely explanation of a secondary relaxation that appears near 125°K in the data of Baccaredda et al.¹² taken at 6000 Hz. Since the activation energy for methyl group motions is low,^{4, 28} it would be expected that the 125°K loss maximum (6000 Hz) would fall well below 80°K at 1 Hz. Hence the low-frequency data of this investigation appear to be in good agreement with the high-frequency acoustical data.

It is also possible to utilize both sets of data, as well as those of Kurz et al.¹⁶ and Heijboer,¹⁵ to obtain a more accurate value of the activation energy of the γ -relaxation. Baccaredda et al., on the basis of measurements taken over a limited frequency range (6–45 kHz), gave a value of 12 kcal/mole, while we find, taking all available data into account, a value of ΔH of 10.5 kcal/mole.

Another explanation that has been given¹² for the γ -relaxation in PSF is that it is due to rotational movements of adsorbed water molecules bound to polar groups along the polymer chain. This interpretation was suggested by the fact that the height of the loss peak was found to increase with added water content of the sample. However, the interpretation cannot be correct, as three different sets of investigators^{12,16,34} have shown that a significant relaxation is still present in carefully dried samples. In fact, in the studies of Kurz et al.¹⁶ not only were the samples vacuum-dried, but they were maintained in a dry nitrogen atmosphere during the test run. Nevertheless, the findings of Baccaredda et al. from mechanical measurements in PSF that the strength of the relaxation increases with water content have been corroborated by recent dielectric studies of Allen et al.³⁴

The most reasonable interpretation of the low-temperature 160°K relaxation in PSF, taking into account the occurrence of a comparable relaxation in PPX (as well as in PC) and also that both mechanical and dielectric data show a rise in peak height with added water, is that it is a combined motion of the phenylene rings and the nearby polar units as well. As such it will occur in a dry sample, but one would expect it to be considerably enhanced, as has been found, in wet samples in which water is hydrogen-bonded to the polar oxygen groups along the chain.

Poly(dian carbonate) (PDC)

The test results on the polycarbonate prepared from bisphenol-A are shown in Figure 5. It is seen that a large modulus drop (from $>1.4 \times 10^{10}$

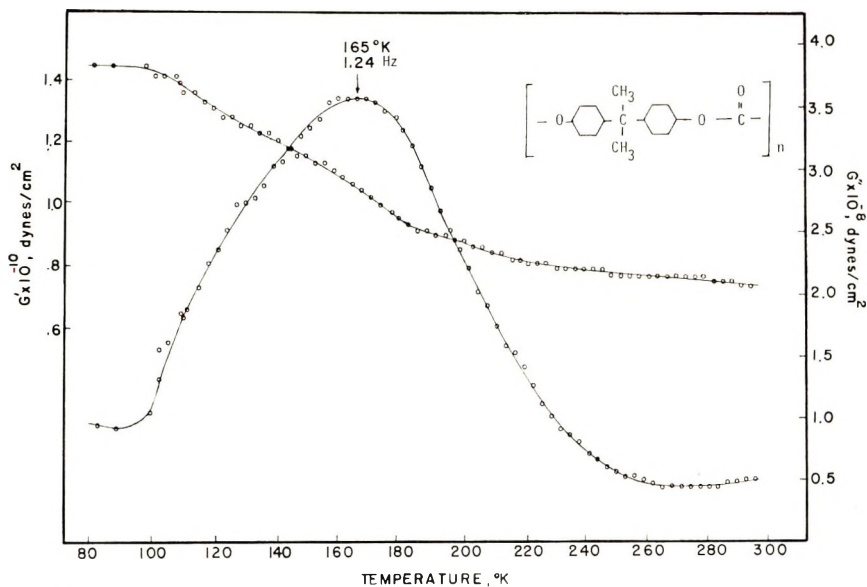


Fig. 5. Temperature dependence of shear modulus and loss modulus for poly(dian carbonate).

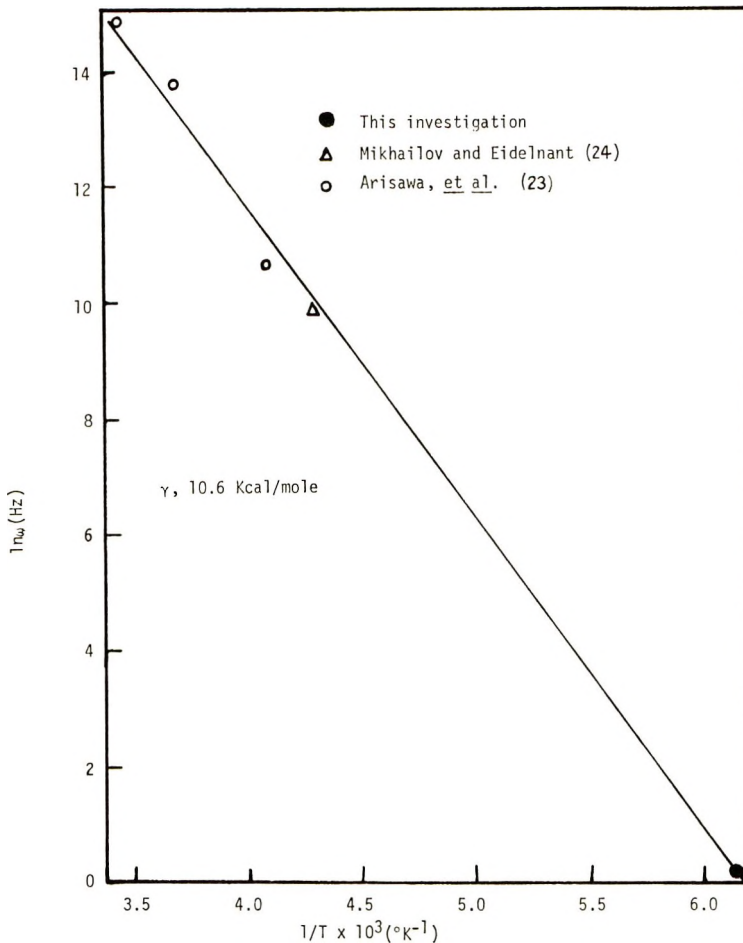


Fig. 6. Plot of \ln frequency vs. $1/T$ for poly(diancarbonate).

dyne/cm² to $<0.9 \times 10^{10}$ dyne/cm²) occurs in the temperature range between 100 and 200°K; associated with this drop there is also a large maximum in G'' . The maximum occurs in about the same place as for polysulfone and poly-*p*-xylylene, being situated for the polycarbonate at 165°K (1.24 Hz).

The data of Figure 5 are in general agreement with previously reported data on this polymer.^{1,7-9} For example, Reding et al.⁹ noted that PDC, when examined over a broad temperature range, revealed two relaxation processes. One, which we term α , was located at 423°K (0.5 Hz). They attributed the high-temperature α -process to large-scale backbone motions of the main chain (note the proximity of the dilatometric T_g transition in Table I) and the low-temperature γ -process to local motions of the carbonate group.

In view of the similarity of the data on PDC with data on PSF and PPX, as well as from studies of molecular models, it is our opinion that the

interpretation of Reding et al.⁹ must be modified. It seems likely that local reorientational motions of the phenylene units are involved in all three polymers, probably coupled with motions of the carbonate group in the case of PDC. In support of this interpretation, the molecular model of PDC shows that the carbonate group cannot move without considerable motion of the adjacent phenylene units, but the reverse is not true. The polar carbonate groups must, however, be involved in the molecular motion that is responsible for the broad γ -relaxation, as the loss peak is revealed in dielectric^{7,34,35} as well as mechanical data. As for PSF, it is also present in PC, even in dry samples, but is enhanced in samples containing water.³⁴

An approximate value of the activation energy for this γ -process can be obtained by using the mechanical data of this investigation and of Arisawa et al.¹⁰ and also the dielectric data of Mikhailov and Eidelnant.⁷ Figure 6 shows a plot of the logarithm of frequency versus $1/T$. The data can be approximately fitted with a straight line. The apparent activation energy for this process is estimated to be 10.6 kcal/mole.

Illers and Breuer⁸ observed structure on both the high- and low-temperature side of the loss which they found at about -100°C at 1 Hz. There is no evidence of such structure on the high-temperature side of the damping maximum shown in Figure 5. In fact, our low value of G'' at 260°K of about 0.5×10^8 dyne/cm² is much less than theirs. Hence it is possible that water was present in their samples and contributed to the breadth of the peak. Allen et al.³⁴ have observed that added water slightly shifts the loss peak to higher temperatures. On the low-temperature side of the loss peak, there is some symmetry, as Figure 5 shows, and our data are akin to those of Illers and Breuer. Our data for PC, like those for PSF, also show a low-temperature minimum, in this case at about 90°K , and a rise in loss values as one proceeds to lower temperatures. As for the PSF polymer, this rise with decreasing temperatures is probably indicative of a lower temperature δ -type relaxation process associated with motions of the groups attached to the isopropylidene unit.

Poly(2,6-dimethyl-*p*-phenylene Oxide) (PDMPO)

Figure 7 shows the shear modulus and logarithmic decrement Δ as a function of temperature for the PDMPO. Because of the presence of a relaxation in the room-temperature region, the experimental data were recorded from liquid nitrogen temperatures to 400°K . The log decrement has been plotted in Figure 7 instead of G'' , as it reveals the separate relaxation processes more clearly. There are at least two overlapping low-temperature processes in this polymer, and the damping is at a high level over the whole range from about 120°K to 300°K . A very broad loss peak, which we term β , is centered at 277°K (1.32 Hz). This process is also present in the high-frequency data (7 kHz) of de Petris et al.,^{11,13} but it was not observed in the dielectric studies of Karasz et al.¹⁷

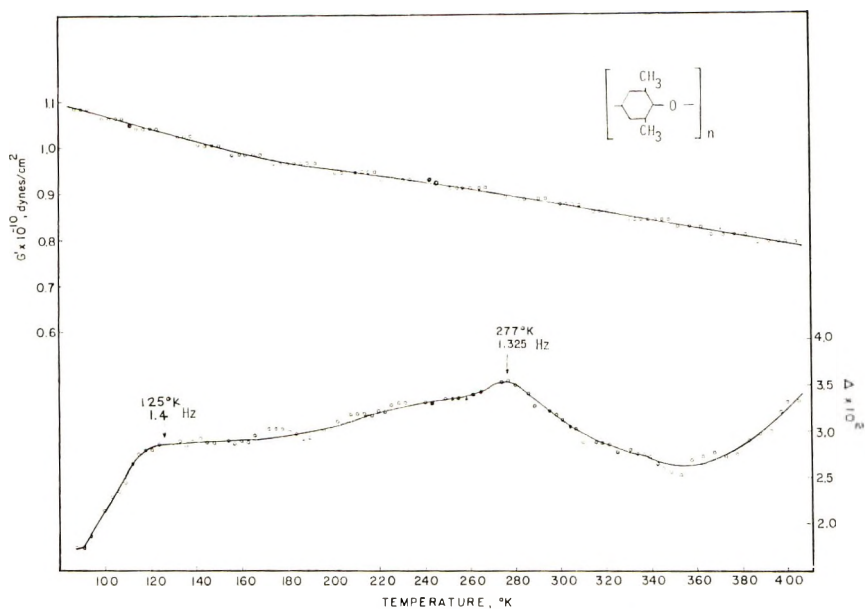


Fig. 7. Temperature dependence of shear modulus, and log decrement Δ for poly(2,6-dimethyl-*p*-phenylene oxide).

A broad, lower-temperature relaxation, which we term γ , seems to be present in the 120–140°K range. An approximate location of this loss maximum is 125°K (1.4 Hz). The shear modulus seems to decrease with increasing temperature in two stages, a more rapid stage between 80 and 160°K and a slower rate from 160 to 400°K. The glass transition temperature of PDMPO is about 480°K, and the rise in loss with increasing temperature that occurs from 350°K on is an indication of this transition.

Our data on PDMPO will now be compared with those obtained by other investigators. Heijboer's damping curve, measured at about 1 Hz,¹⁴ shows three distinct relaxation processes in PDMPO: an α -transition above 460°K, a β -relaxation peak near 275°K, and a γ -relaxation peak near 155°K. Measurements of de Petris et al.,¹¹ made at acoustic frequencies, show an α -transition, marked by a large drop in modulus, occurring above 480°K, and a β -relaxation characterized by a damping peak at 373°K (7.04 kHz). They report no other transitions or relaxations down to liquid-nitrogen temperatures, but their test data show a marked rise in damping in the 100–160°K range which we interpret as a manifestation of the same γ -type process that we observe at about 125°K at our test frequency. It is difficult to give a precise temperature location for their "peak" or shoulder, but it appears to be at about 160°K (7.04 kHz). Our data are in good agreement with theirs, with the shift of all relaxations to lower temperatures being a result of a shift in frequency of measurement.

Baccaredda et al.¹³ have also presented test data for several other poly(*p*-phenylene oxides), including poly(2-monomethyl-*p*-phenylene oxide),

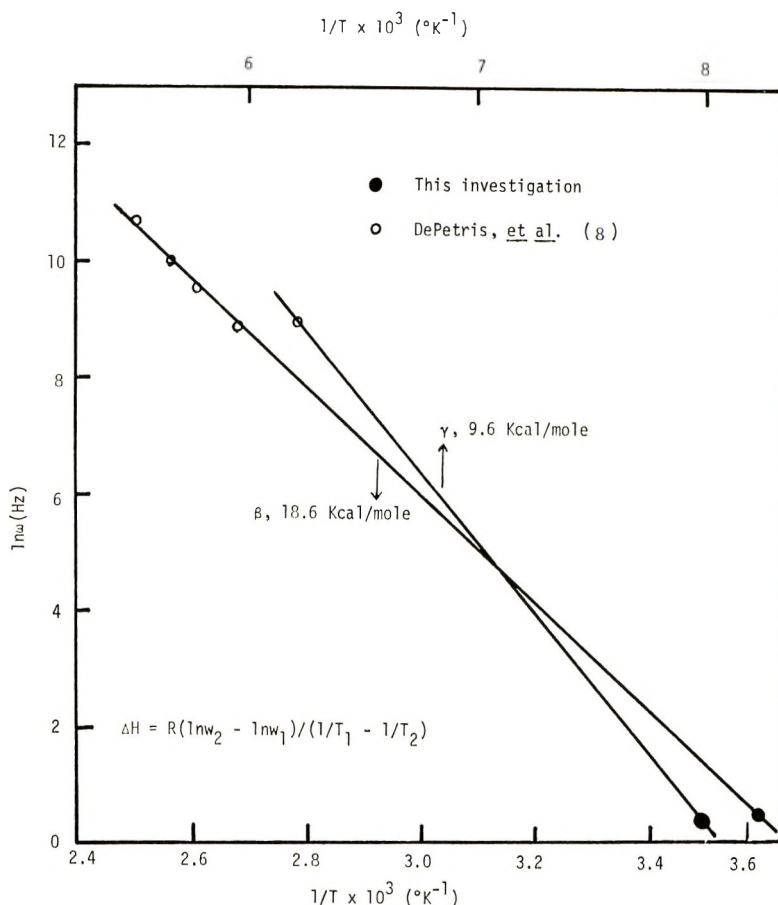


Fig. 8. Plots of \ln frequency vs. $1/T$ for poly(2,6-dimethyl-*p*-phenylene oxide).

poly(2,6-dimethyl-*p*-phenylene oxide), and the unsubstituted polymer. It is interesting that all of these exhibit the β -relaxation near 370°K and a γ -relaxation shoulder in the region 140 – 170°K for test frequencies of about 7 kHz. Thus, it is clear that the methyl groups themselves cannot be the cause of the relaxations, and nuclear magnetic experiments and calculations confirm this. From comparison of observed second moments with values calculated on the basis of a rigid lattice, Mattes and Rochow¹⁸ conclude that both methyls rapidly reorient at a temperature of 80°K . Also, they find a gradual reduction in linewidth from 80°K to room temperature.

One possible interpretation of our data is that the γ -relaxation observed in the 125 – 140°K range at about 1 Hz is, like that for the other polymers already mentioned, a result of reorientations of the phenylene group about C–O bonds. If so, it would appear that the steric hindrance is somewhat less for PDMPO where the oscillation can occur about colinear C–O bonds than for the other polymers that we have studied, such as

PSF, PDC and PPX, where at least one of the colinear bonds is a C-C bond or a C-S bond. Some evidence that the steric factor for the C-O bond is much lower than the usual values found for the simple C-C bond has been given by Barrales-Rienda and Pepper³⁶ from calculations of the unperturbed dimensions and gyration radius of PDMPO in solution. The continued high level of mechanical loss, as well as the gradual NMR drop, over the temperature range from 120 to 300°K, may indicate an increasing amplitude of phenyl group oscillation.

Although sufficient data are not available to determine activation energies of the β and γ relaxations in PDMPO, approximate values can be obtained from a plot of log frequency versus $1/T$ by using present data and those of de Petris et al.¹¹ Plots of this type are shown in Figure 8. From the straight lines drawn to fit the data, we estimate the activation energies to be about 9.6 kcal/mole for the low-temperature γ -process and about 18.6 kcal/mole for the higher-temperature β -process. The value obtained for the γ -process in PDMPO is thus comparable to that for PDC or PSF, as might be expected if they both involve phenylene, or substituted phenylene, group motion. The ΔH value for the β -relaxation is in good agreement with 20 kcal/mole given by Baccaredda et al. from high-frequency measurements. In view of its higher activation energy, the β -relaxation may arise from local cooperative motions of several monomer units.

CONCLUSIONS

Data have been presented above which clearly show that many polymers that do not possess three or more adjacent CH₂ or equivalent groups in their structure may nevertheless show a significant low-temperature relaxation. The common structural features of these polymers are the aromatic groups in the polymer backbone chain.

In view of the experimental results obtained to date by both mechanical and dielectric studies, a reasonable interpretation is that the low-temperature relaxation arises from reorientational motion of the phenylene rings, probably coupled with torsional or rotational motions of nearby chain units. The temperature location of the relaxation is a function of the nature of the units adjacent to the phenylene ring as well as of the nature of substituents on the ring.

The ring motion seems to occur more readily when oxygen atoms are adjacent to the phenylene group and hence PDMPO shows a secondary relaxation at a somewhat lower temperature than does PC or PSF, where the phenylene rings lie between an O atom and a C atom with a double methyl substituent, or between an O and a sulfone group. The ring motion is also severely hindered when an asymmetric polar group is present, as in PCPX, where the loss peak is observed to shift up in temperature some 90°. However, it does not appear to be much affected by a more symmetrical substitution as occurs, for example, in PDMPO with two methyl groups on the ring or for PDCPX, with two Cl groups on the ring.

In water-containing samples, the low-temperature peak is enhanced, presumably because the water molecules are hydrogen-bonded to the polar oxygen atoms along the chain, and these participate in the motion giving rise to the relaxation. It is difficult to say, in most cases, whether two separate relaxations are present, one arising from reorientational motions of the phenylene rings themselves and another from motion of the hydrogen-bonded water molecules. It is clear that the loss peaks are rather diffuse and that the peak position can be altered by the presence of water. In the case of the polyamides, it is well known^{1,6} that as water is added to the sample the usual γ peak near 150°K (ca. 1 Hz) decreases in magnitude, while a new β peak near 200°K (ca. 1 Hz) arises and increases in strength. A somewhat similar situation appears to arise in the case of branched methacrylates containing OH groups. For example, Janacek et al.³⁷ have shown that poly(methoxyethyl methacrylate) will give a γ peak near 150°K but that this peak reduces in magnitude and a new peak appears at 196°K in a water-swollen sample. They also observed similar behavior in poly(diethylene glycol monomethacrylate) upon addition of water, only in this case the temperatures involved were some 30° higher.

The question naturally arises: if phenylene ring motions occur at low temperatures in polymers containing aromatic groups in the main chain, such as PPX, PSF and PC, should they not also be present in other polymers such as polyimide (PI) and poly(ethylene terephthalate) (PET)? Although these materials have been quite widely studied, it does not appear that low-temperature relaxations in these polymers have been heretofore assigned to reorientational motion of phenylene groups. Nevertheless examination of the pertinent literature does show that this possibility exists.

First, with regard to PET, it is well known^{1,38} that the low-temperature loss peak in the polymer is extremely broad, with a large low-temperature tail. Illers and Breuer³⁸ indicated that it might well arise from three overlapping relaxations. We think it quite likely that the breadth of this peak on the low temperature side, or the resolved peak which Illers placed at 168°K (1 Hz), arises from reorientational motions of the phenylene units themselves. These motions are probably soon coupled to motions of adjacent polar units, as in PSF and PC, and hence this peak is also seen in dielectric studies and also increases in intensity with water. The 203°K resolved peak mentioned by Illers probably involves motion of water molecules as well as of $-\text{CH}_2-\text{CH}_2-\text{O}-$ sequences. In this connection, it may be noted that Janacek³⁷ has shown that the substitution of a polar O atom in place of a CH_2 unit, as in poly(methoxyethyl methacrylate) as compared to poly(propyl methacrylate), causes the side-branch γ -relaxation to shift up in temperature some 30°. It is also well known¹ that as the number of methylene sequences is increased in the poly(methylene terephthalates), the position of the loss peak goes to lower temperatures.

With regard to polyimide, two recent publications show that there is some evidence of a low temperature loss peak in this polymer which is not

due merely to the presence of water. For example, Bernier and Kline³⁹ report an internal-friction peak in a dry sample at about 130°K (ca. 700 Hz). Also Butta et al.,⁴⁰ who made a thorough study at about 15 kHz test frequency of the effects of water, show an asymmetric broad low-temperature tail for a sample dried under vacuum at 200°C. Both of these investigators have also noted that as water is added a new "water" peak arises which is situated at about 230°K (ca. 700 Hz). More extensive studies of the effects of water on polyimide have been carried out in our own laboratory by Lim.^{41,42} These studies, carried out at a frequency of about 10³ Hz, show clearly that as a "water" peak near 240°K builds up in magnitude, a very broad lower-temperature loss peak near 140–150°K is reduced in magnitude. While no interpretation has heretofore been given to this low-temperature shoulder or broad loss maximum, it is reasonable, by analogy with the results already presented in this paper, to associate it with reorientational motions of the phenylene ring. This ring, in polyimide, is unsubstituted and is situated between the N atom and O atom and hence the barrier to its reorientation would not be expected to be much different from that for PDMPO. The close similarity of the relaxation behavior of PDMPO and a dried sample of PI has, in fact, been noted.⁴⁰

Our thanks are extended to the Textile Research Foundation for the award of a Fellowship (to C.I.C.), to the Rutgers Research Council for the award of a faculty fellowship to carry on research at Oxford University (to J.A.S.), to the industrial companies already mentioned for supplying us with samples and data, and to various colleagues, R. W. Gray, N. G. McCrum, G. M. Jeffs, D. E. Kline, and W. D. Niegisch, for consultation and discussion.

References

1. N. G. McCrum, B. E. Read, and G. Williams, *Anelastic and Dielectric Effects in Polymeric Solids*, Wiley, New York, 1967.
2. A. H. Willbourn, *Trans. Faraday Soc.*, **54**, 717 (1958).
3. K. D. Lawson, J. A. Sauer, and A. E. Woodward, *J. Appl. Phys.*, **34**, 2492 (1963).
4. J. A. Sauer and R. G. Saba, *J. Macromol. Sci.-Chem.*, **A3**, 1217 (1969).
5. R. D. McCammon, R. G. Saba, and R. N. Work, *J. Polym. Sci. A-2*, **7**, 1721 (1969).
6. A. E. Woodward and J. A. Sauer, in *Physics and Chemistry of the Organic Solid State*, Vol. II, Interscience, New York, 1965, p. 637.
7. G. P. Mikhailov and M. P. Eidelnant, *Vysokomolekul. Soedin.*, **2**, 287 (1960).
8. K. H. Illers and H. Brener, *Kolloid-Z.*, **176**, 110 (1961).
9. F. P. Reding, J. A. Faucher, and R. D. Whitman, *J. Polym. Sci.*, **54**, 556 (1961).
10. K. Arisawa, H. Hirose, M. Ishikawa, T. Harada, and Y. Wada, *J. Appl. Phys. Japan*, **2**, 695 (1963).
11. S. de Petris, V. Frosini, E. Butta, and M. Baccaredda, *Makromol. Chem.*, **109**, 54 (1967).
12. M. Baccaredda, E. Butta, V. Frosini, and S. de Petris, *J. Polym. Sci. A-2*, **5**, 1296 (1967).
13. M. Baccaredda, E. Butta, V. Frosini, and S. de Petris, *Mater. Sci. Eng.*, **3**, 157 (1968/69).

14. J. Heijboer, in *Macromolecular Chemistry, Prague 1965* (*J. Polym. Sci. C*, **16**) O. Wichterle and B. Selbáček, Eds., Interscience, New York, 1968, p. 3755.
15. J. Heijboer, *Brit. Polym. J.*, **1**, 3 (1969).
16. J. E. Kürz, J. C. Woodbrey, and M. Ohta, *J. Polym. Sci. A-2*, **8**, 1169 (1970).
17. F. E. Karasz, W. J. MacKnight, and J. Stoelting, *J. Appl. Phys.*, **41**, 4357 (1970).
18. R. Mattes and E. G. Rochow, *J. Polym. Sci. A-2*, **4**, 375 (1966).
19. C. I. Chung and J. A. Sauer, *Polymer*, **11**, 454 (1970).
20. M. Baccaredda, E. Butta, V. Frosini, and P. L. Magagnini, *J. Polym. Sci. A-2*, **4**, 789 (1966).
21. C. I. Chung, Ph. D. Dissertation, Rutgers University, 1969.
22. W. F. Gorham, *J. Polym. Sci. A-1*, **4**, 3027 (1966).
23. K. M. Sinnott, *SPE Trans.*, **2**, 65 (1962).
24. J. M. Crissman and R. D. McCammon, *J. Acoust. Soc. Am.*, **34**, 1703 (1962).
25. J. M. Crissman, A. E. Woodward, and J. A. Sauer, *J. Polym. Sci. A*, **3**, 2693 (1965).
26. V. Frosini and A. E. Woodward, *J. Polym. Sci. A-2*, **7**, 525 (1969).
27. R. Saba, Ph. D. Dissertation, Pennsylvania State University, 1967.
28. Y. Tanabe, J. Hirose, K. Okano, and Y. Wada, *Polym. J.*, **1**, 107 (1969).
29. H. Van Hoorn, *J. Appl. Polym. Sci.*, **12**, 871 (1968).
30. W. F. Gorman and W. D. Niegisch, in *Encyclopedia of Polymer Science and Technology*, Interscience, to be published.
31. A. Odajima, A. E. Woodward, and J. A. Sauer, *J. Polym. Sci.*, **55**, 181 (1961).
32. A. E. Woodward, A. Odajima, and J. A. Sauer, *J. Phys. Chem.*, **65**, 1384 (1961).
33. J. M. Crissman, J. A. Sauer, and A. E. Woodward, *J. Polym. Sci. A*, **2**, 5075 (1964).
34. G. Allen, J. McAinsh, and G. M. Jeffs, *Polymer* **12**, 85 (1971).
35. S. Matsuoka and Y. Ishida, in *Transitions and Relaxations in Polymers* (*J. Polym. Sci. C*, **14**), R. F. Boyer Ed., Interscience, New York, 1966, p. 247.
36. J. M. Barrales-Rienda and D. C. Pepper, *J. Polym. Sci. B*, **4**, 939 (1966).
37. J. Janacek and A. Zahradnikona, *J. Polym. Sci. A-2*, **6**, 1810 (1968).
38. K. H. Illers and H. Breuer, *J. Colloid Sci.*, **18**, 1 (1963).
39. G. A. Bernier and D. E. Kline, *J. Appl. Polym. Sci.*, **12**, 593 (1968).
40. E. Butta, S. de Petris, and M. Pasquini, *J. Appl. Polym. Sci.*, **13**, 1073 (1969).
41. T. Lim, Ph. D. Dissertation, Rutgers University, 1967.
42. J. A. Sauer, paper presented at Battelle Seminar on Molecular Order, Seattle, October 1970.

Received May 25, 1970

Revised November 30, 1970

Diffusive and Hydraulic Permeabilities of Water in Water-Swollen Polymer Membranes

H. YASUDA, C. E. LAMAZIE and A. PETERLIN,
*Camille Dreyfus Laboratory, Research Triangle Institute,
Research Triangle Park, North Carolina 27709*

Synopsis

The diffusive permeability of water P , which relates to diffusive flux of water under a concentration gradient of water (measured by diffusion of tritiated water), and the hydraulic permeability of water K , which relates to the water flux under a hydraulic pressure gradient are defined. For the case of diffusive transport one has $P = KRT/v_1$, where v_1 is the molar volume of water. The relationship between P and K was investigated as a function of hydration H , i.e., the volume fraction of water in swollen polymer membranes. The following characteristic features of water permeability are revealed. (a) In the low-hydration region ($H < 0.2$), water permeates by diffusion even under an applied hydraulic pressure gradient and $KRT/v_1 = P$. (b) In the higher hydration region KRT/v_1 is greater than P , and the ratio $\omega = KRT/v_1P$ increases nearly exponentially with decrease of $(1-H)/H$. Water in this region moves partly by bulk flow under an applied hydraulic pressure gradient but moves only by diffusion in the absence of a pressure gradient. (c) The dependence of $\log P$ on $(1-H)/H$ is nearly linear in regions of both high and low hydration but the slopes are different. The transition occurs in about the same H range where the discrepancy between P and KRT/v_1 becomes significant. Excellent agreement was found between the experimental data for P as a function of H and the theoretical prediction based on the free-volume concept of diffusive transport in hydrated homogeneous membranes.

INTRODUCTION

The nature of water transport through hydrophilic polymer membranes is vitally important to proper understanding of transport phenomena of aqueous solutes through the membranes, particularly with respect to permselectivity of solutes and semipermeability of membranes. The investigations of water transport through such membranes as a function of their water content seems to be a promising approach in this direction.

It has been observed for highly hydrated polymer membranes¹⁻³ that the water flux under a pressure gradient exceeds the value calculated from the self-diffusion constant of water, suggesting either that the equation used to calculate the diffusion does not apply to the highly swollen polymer membranes or that bulk flow of water occurs in these membranes and transport of water is no longer determined by diffusion only. In this study, therefore, two permeabilities relating to concentration and pressure gradients are de-

finned to express the water flux quantitatively. The change in the relationship between them is examined as a function of membrane hydration

DIFFUSIVE AND HYDRAULIC PERMEABILITIES OF WATER

The diffusive permeability, P , is defined by

$$J_d \equiv P(\Delta C/\Delta X) \quad (1)$$

where J_d is the diffusive flux of a permeant ($\Delta p = 0$) per unit membrane area, ΔX is the thickness of the membrane, and ΔC is the external concentration difference of the permeant across the membrane. The diffusive permeability can be obtained by the use of radioactive water to measure the diffusive flux of water under zero hydraulic pressure gradient. The hydraulic permeability, K , is defined by

$$J_f \equiv K\Delta p/\Delta X \quad (2)$$

where J_f is the flux of the water per unit membrane area under the hydraulic pressure gradient $\Delta p/\Delta X$. Both P and K are material constants for a homogeneous membrane with a constant concentration or pressure gradient throughout the membrane.

One usually expresses the flux J_d in $\text{g}/\text{cm}^2\text{-sec}$ and J_f in $\text{cm}^3/\text{cm}^2 \text{ sec} = \text{cm}/\text{sec}$, the concentration in g/cm^3 , and the pressure in $\text{g}/\text{cm}\text{-sec}^2$. Hence, one obtains P in cm^2/sec and K in $\text{cm}^3\text{-sec}/\text{g}$.

In terms of the chemical potential in an ideal solution

$$\mu_i = \mu_i^\circ + p\bar{v}_i + RT \ln (c_i/M_i) \quad (3)$$

the flux of i th component through the membrane can be generally written (without suffix i) as

$$J = c^*u = -\frac{c^*}{f} \frac{\Delta\mu}{\Delta x} = -\frac{sc}{f} \left(\frac{\partial\mu}{\partial c} \frac{\Delta c}{\Delta x} + \frac{\partial\mu}{\partial p} \frac{\Delta p}{\Delta x} \right) \quad (4)$$

where $c^* = sc$ is the concentration of the diffusing component in the membrane, s is the partition coefficient, u is the velocity, and f is the molar friction coefficient of the component in the membrane. With the partial derivatives

$$\partial\mu/\partial c = RT/c \quad (5)$$

$$\partial\mu/\partial p = \bar{v} \quad (6)$$

one obtains the diffusive flux (in $\text{g}/\text{cm}^2\text{-sec}$) of the tritium-labeled molecules

$$\begin{aligned} J_d &= -\frac{sc}{f} \left(\frac{\partial\mu}{\partial c} \right) \frac{\Delta c}{\Delta x} \\ &= -(sRT/f)(\Delta c/\Delta x) \\ &= -P(\Delta c/\Delta x) \end{aligned} \quad (7)$$

and the hydraulic flux of water (in $\text{cm}^3/\text{cm}^2 \text{ sec}$)

$$\begin{aligned} J_f &= - \frac{sc}{f\rho} \left(\frac{\partial \mu}{\partial p} \right) \frac{\Delta p}{\Delta x} \\ &= - (scV/f\rho)(\Delta p/\Delta x) \\ &= - K(\Delta p/\Delta x) \end{aligned} \quad (8)$$

where ρ is the density of water.

From eqs. (7) and (8), one derives

$$\begin{aligned} P &= sRT/f \\ &= sD \end{aligned} \quad (9)$$

and

$$\begin{aligned} K &= scv_1/f\rho \\ &= sv_1/f \\ &= Pv_1/RT \end{aligned} \quad (10)$$

Equation (10) describes the relation between K and P of an ideal membrane in which no viscous flow occurs under a hydraulic pressure gradient. It also describes the amount of water which moves in the general membrane because of the chemical potential gradient resulting from the increase in pressure. The total water flux through a general membrane may exceed the K given by the equation; however, since the chemical potential of water is increased by the additional pressure, the diffusive flux of water given by the equation should occur. When K exceeds the value predicted by eq. (10), the ratio

$$\omega = KRT/Pv_1 \quad (11)$$

becomes larger than unity. The difference $\omega - 1$ is used in this study as a parameter to describe the extent of transport by flow relative to that by diffusion. The lower limit, $\omega = 1$, as given by eq. (3) characterizes transport by diffusion only.

Thau, Bloch, and Kedem⁴ have presented a similar parameter (the ratio of hydraulic to diffusive permeabilities) derived from application of an irreversible thermodynamics approach to the porous model of membranes, and reported that this ratio for cellulose film was approximately 80. Since the membrane model used in this study is considerably different from the pore-model of membranes on which most of the derivation of equations are based (e.g., by Ticknor¹ for the diffusion constant, and Thau et al.⁴ for ω), it becomes necessary to explain briefly the homogeneous membrane model for which details can be found in the literature.^{5,6}

In the homogeneous polymer membrane model, no fixed pores or channels are assumed in which the transport of water can be expressed by a flow equation such as Poiseuille's. The membrane phase in the dry state is packed uniformly with randomly coiled macromolecules leaving some unoc-

occupied space per unit volume of the phase as free volume $V_{f,3}^{\circ}$. In a water-swollen membrane the polymer occupies the fraction $(1 - H)$, and the water, the fraction H of the membrane volume. Pure water has a free volume $V_{f,1}^{\circ}$. In the membrane the actual free volume is determined by the amount of water and polymer which are supposed to be interdispersed completely at random. In the first approximation, one may assume additivity of free volume contributions of both components

$$V_f^{\circ} = HV_{f,1}^{\circ} + (1 - H)V_{f,3}^{\circ}. \quad (12)$$

This value has to be used as free volume of the hydrated membrane in the expressions for the diffusional constant and permeability in the case of purely diffusional transport. It turns out, indeed, that this concept excellently reproduces the experimental data of P in the whole range of H between zero (dry membrane) and unity (pure water).

In the homogeneous membrane model, the water-filled space through which transport of permeants can occur may be conceived as fluctuating pores or channels of the polymer matrix which are not fixed either in size or in location. As a consequence of the plasticizing effect of water in the case of swollen membranes, the macromolecules in the water-swollen polymer membrane exhibit a fair degree of mobility so that the size and shape of the pores or channels may continuously change. The geometry of the polymer network sets the upper limit for the size of such pores and hence also for the size of permeant molecules which can be accommodated and can pass through that section of the membrane. The transport, therefore, is dependent upon the probability that the permeant molecule finds at its location such a hole.

The diffusion coefficient can be generally written as⁷

$$\begin{aligned} D &= \nu \exp \{ -F/kT \} \\ &= \nu \exp \{ S/k \} \exp \{ -E/kT \} \end{aligned} \quad (13)$$

where ν is the translational oscillation frequency of the diffusing molecule⁷ it is related to the diffusional jump distance l and Boltzman's and Planck's constants by $\nu \approx d^2 (kT/h)$, and has the units cm^2/sec . The quantities F , S , and E are the free energy, entropy, and energy of activation for diffusion, respectively.

According to statistical thermodynamics, the entropy term in eq. (13) can be related to the conformational probability W , for formation of a hole (intersegmental space) sufficiently large for the passage of the diffusing molecules. According to the concept developed by Cohen and Turnbull⁸ and DiBenedetto and Paul,⁹ the probability W is given by

$$W = \exp \{ -V^*/V_f^{\circ} \} \quad (14)$$

where V^* is a characteristic volume parameter describing the diffusion of a permeant molecule in the medium (i.e., a critical volume proportional to the cross section of the diffusing entity multiplied by the diffusional jump distance) and V_f° is the total free volume per unit volume of membrane.

Hence, we have

$$S/k = \ln W = -V^*/V_f^\circ \quad (15)$$

The diffusion constant D of water in the membrane is given by

$$D = \nu \exp \{-E/kT\} \exp \{-V^*/V_f^\circ\} \quad (16)$$

The empirical energy of activation includes E and the temperature dependence of the free volume.

The self-diffusion constant D_0 of water can be expressed in these terms as

$$D_0 = \nu \exp(-E/kT) \exp(-V^*/V_{f,1}^\circ) \quad (17)$$

where $V_{f,1}^\circ$ is the free volume in unit volume of pure water.

In the first approximation, one may assume that $\nu \exp \{-E/kT\}$ for water in water-swollen polymer systems at a given temperature is a constant. This assumption seems to be reasonable at least for the high H region, where most water may move through preexisting water. Keeping in mind that E is only a part of the empirical activation energy, one may extend this assumption to the lower H region (e.g., to $H = 0.1$) where water still has a considerable plasticizing effect on the polymer. With this assumption, the term $\nu \exp \{-E/kT\}$ can be considered as characteristic of water (describing the thermal translational movement) and the term $\exp \{-V^*/V_f^\circ\}$ as characteristic of the membrane. Then from eqs. (16) and (17), the diffusion constant of water in a water-swollen polymer membrane at a given temperature can be expressed as a function of the self-diffusion constant of water and the free volume:

$$D = D_0 \exp \{-V^*(1/V_f^\circ - 1/V_{f,1}^\circ)\} \quad (18)$$

The combination of eqs. (18) and (12) leads to

$$\ln (D/D_0) = -\beta x(1 - \alpha)/(1 + x\alpha) \quad (19)$$

where

$$x = (1 - H)/H$$

$$\alpha = V_{f,3}^\circ/V_{f,1}^\circ$$

$$\beta = V^*/V_{f,1}^\circ$$

Equation (19) indicates that $\ln D$ versus x approaches a straight line in the region of high H ($x \rightarrow 0$), starting from the self-diffusion constant of water and with a negative slope $\beta(1 - \alpha)$. It also indicates that with decreasing H ($x \rightarrow \infty$) the logarithm of the ratio of diffusion constants approaches asymptotically the values of $\beta(1 - \alpha)/\alpha = \beta(1/\alpha - 1)$.

The diffusive permeability P is generally given by eq. (9) as

$$P = sD$$

The partition coefficient s is the ratio of concentration of permeant in the membrane to that of the permeant in solution outside the membrane. Since the partition coefficient for water in water-swollen membranes is H , P turns out to be

$$P = HD \quad (20)$$

Combination of eqs. (19) and (20) leads to an expression for P as a function of x :

$$\ln (P/D_0) = -\beta[x(1-\alpha)/(1+\alpha x)] - \ln(1+x) \quad (21)$$

Since the preexponential term plays much less a role than the exponential term, P for high H (small x) can be approximated by

$$P = D_0 e^{-\Phi(1-H)/H} = D_0 e^{-\Phi x} \quad (22)$$

where Φ is a constant.

Equation (22) is similar to the expression for the diffusive permeability of solutes.^{5,10,11} It yields a straight line for a plot of $\log P/D_0$ versus x ; but one must not forget that this expression is limited to highly swollen membranes. According to eq. (21), the permeability for less hydrated membrane will deviate considerably from this expression.

Without speculating about the mechanism of water transport under an applied pressure gradient, one might be able to express the dependence of hydraulic permeability on hydration to a first approximation in the same form as for transport by diffusion. Experimental results suggest that in the range $\omega \gg 1$, one can describe K by

$$K = K_0 \exp \{-\Phi_K x\} \quad (23)$$

where K_0 and Φ_K are constants. The constant K_0 may be interpreted as the hypothetical hydraulic permeability of a pure water membrane ($H = 1$, $x = 0$), although K at $H = 1$ has no physical meaning (free flow) and can be obtained only by extrapolation of experimental data to $x \rightarrow 0$. Consequently, the parameter ω in the region of high H (low x) also follows the similar approximate relation (see Fig. 2)

$$\omega = \omega_0 \exp \{-\Phi_\omega x\} \quad (24)$$

where

$$\omega_0 = K_0 RT/D_0 v_1$$

and Φ_ω is a constant.

EXPERIMENTAL

Materials

The films used in this study are described in Table I. Films 1-6 are termed hydrogels. They were formed by simultaneous polymerization and crosslinking of the monomers, glycerol methacrylate (GMA) and hydroxy-

TABLE I
Description of Films Studied

Film	Polymer composition (monomer mole-%)	Preparation composition (wt.-%)	H^a	Wet thickness ΔX , cm $\times 10^3$
1	GMA, 100 (no cross-linker)	GMA-H ₂ O, 36:64	0.86	54
2	GMA, 100 (TEI)GMA - 0.47)	GMA-HCOOH-H ₂ O, 34:36:30	0.78	52
3	GMA/TEGDMA, 90:10	GMA-HCOOH-H ₂ O-TEGDMA, 31:33:30:6	0.60	44
4	GMA/TEGDMA, 88:12	GMA-HCOOH-H ₂ O-TEGDMA, 31:33:28:8	0.58	38
5	HEMA, 100 (no crosslinker)	HEMA-ethylene glycol-H ₂ O, 44:30:26	0.40	24
6	HEMA, 100 (no crosslinker)	HEMA-ethylene glycol-H ₂ O 55:24:21	0.38	22
7	Avisco	Commercial	0.58	6.4
8	Cuprophane	Commercial	0.47	2.2
9	HPPA-MMA, 95:5	HPMA-MMA-(dioxane-acetone), 14:40:46	0.21	3.7
10	MMA-GMA, 79:30	MMA-GMA-(dioxane-acetone), 14:40:46	0.15	5.1
11	MMA-GMA, 85:15	MMA-GMA-(dioxane-acetone), 14:40:46	0.01	3.0
12	Cellulose acetate (31-33% acetyl)	Cellulose Ac-acetone-ethyl cellosolve-H ₂ O, 14:57:19:10	0.24	1.9
13	Cellulose acetate (30-31% acetyl)	Cellulose Ac-acetone-ethyl cellosolve-H ₂ O, 14:57:19:10	0.20	2.0
14	Cellulose acetate (39.8% acetyl)	Cellulose Ac-acetone, 20:80	0.12	3.5
15	Cellulose acetate (43.8% acetyl)	Cellulose Ac-1,1,2,2-tetrachloroethane, 6:94	0.10	0.6

^a Type of Membrane: No. 1-6 Hydrogel. No. 7-15 Cast Film.

ethyl methacrylate (HEMA), in an appropriate solvent system (water or water/formic acid for the GMA, and water/ethylene glycol for the HEMA). In three cases, the crosslinking agent tetraethylene glycol dimethacrylate (TEGDMA) was added in relatively low concentration in order to obtain a wide range of membrane hydration for the same monomer. The mixtures were initiated with an aqueous redox system (solutions containing 1% $K_2S_2O_8$ and 2% $Na_2S_2O_5$ by weight) by adding each solution to the extent of 1–2% of the total mixture volume. The monomer mixtures were then poured onto a glass plate and covered with a second plate, care being taken to avoid air pocket formation. Spacers were used to give a film of the desired thickness. After polymerization and crosslinking, the membranes were removed from the plates and equilibrated in water.

Films 7 and 8 were cellulose regenerated from viscose and cuprammonium solution, respectively. They were commercial products.

Films 9–15, were cast films, prepared by casting solutions of various polymers onto glass plates with an adjustable casting blade and then allowing the films to air-dry slowly to obtain clear, homogeneous films, which were then equilibrated in water.

The hydroxypropyl methacrylate/methyl methacrylate copolymers used to prepare films 9–11 (HPMA/MMA: 95/5 monomer mole ratio; MMA/GMA: 70/30; and MMA/GMA: 85/15) were prepared in this laboratory. The general method was polymerization of the monomers at room temperature in nonaqueous solvent with 2,2'-azobis(2-methylpropionitrile) as the initiator. The polymers were then precipitated in a nonsolvent, washed, and dried. The preparation of these copolymers was described in full detail previously.¹⁰ Cellulose acetate polymers of various degrees of substitution (used to prepare films 12–15) were commercial Eastman products. The polymers were dissolved in appropriate solvent systems (listed in Table I) and cast.

Measurements

Diffusive Permeability. The measurement of the diffusive permeability was effected in a modified Leonard-Bluemle cell constructed of Lucite^{12,13} by using tritiated water (specific activity = 1.0 mCi/g). The membrane was clamped between the two halves of the cell with no membrane support. The compartments of equal volume (76.4 cm³) were then filled with deionized water and the liquid on both sides of the membrane was stirred by stirrers driven from a common shaft at a monitored speed. The exposed membrane area was 23.25 cm² and all runs were made at 23–24°C at a stirring speed of 240 rpm. At time zero, one side of the cell was "dosed" with 50 μ l of tritiated water. At subsequent time intervals small samples were withdrawn from both sides of the cells simultaneously, in 50- μ l syringes to assure negligible volume changes during the experiment. Taking samples from both sides of the cells allows one (a) to calculate P on the basis of the change in the concentration difference of tritiated water across the membrane and (b) to follow the sum of the concentrations of tritiated water on the two

sides in order to detect sampling errors, cell leaks, or significant "exchange" of tritiated water in the membrane.

Analysis of the samples was effected by diluting each 50- μ l sample with 1.0 ml H₂O and 15 ml scintillation mix (4 g Omnifluor in 1 liter of 2:1 toluene:Triton-X solution). Both tritiated water and Omnifluor were obtained from Nuclear-Chicago Corporation. The samples were then counted by a Packard Tri-Carb Unilux II, spectrometer.

Permeability was calculated from the slope of the plot of $\log \Delta C$ versus time t according to the equation

$$P/\Delta X = - \frac{V \Delta \ln \Delta C}{2A \Delta t} = - \frac{2.3V \Delta \log (\Delta C)}{2A \Delta t} \quad (25)$$

where A is the membrane area, V is the volume of each cell compartment, ΔX is the membrane thickness, and ΔC is the difference in concentration (counts) between the two compartments at time t . Most experiments lasted 1 $\frac{1}{2}$ -2 hr with the taking of five or six samples. Data points for which the sum of counts on both sides were more than a few per cent from the average of all values were discarded.

Hydraulic Permeability. The measurement of the hydraulic permeability of the hydrogels was carried out by using low-pressure Amicon ultrafiltration cells (Model 50). For most films, the plot of flux versus pressure was linear as expected, and K was calculated from the slope. Whenever this plot was not linear, the initial slope was used for the calculation.

With films of lower hydration and hence much lower flux, measurement of K at very low pressures became impractical. For the cast films, K measurements were made in Amicon Model 420 cells at 550 psi. For several films of moderate hydration measurements of K could be made in both cells because the film had a relatively high flux and was fairly strong. This was done in order to assure that the data were not dependent on the cell or pressure used. All measurements were made at 23-24°C.

RESULTS AND DISCUSSION

The results for K , P , and Pv_1/RT are summarized in Table II. The approximate dependence of K and ω on $x = (1 - H)/H$ is shown in Figure 1 and 2, respectively. The dependence of K and P on x is shown in Figure 3. The validity of eq. (19) is examined in Figure 4.

From these results, it is possible to point out the following important characteristics of water transport in water-swollen polymer membranes.

In the region of low hydration, K and Pv_1/RT are nearly identical functions of x . Consequently, water permeates through these membranes only by diffusion, even under a hydraulic pressure gradient.

In the region of high hydration, K and Pv_1/RT are not identical and the ratio between the two permeabilities, expressed by ω , increases exponentially with decrease of x , i.e., with increasing hydration H (see Fig. 2). Hence, K and P are represented by two different functions of x .

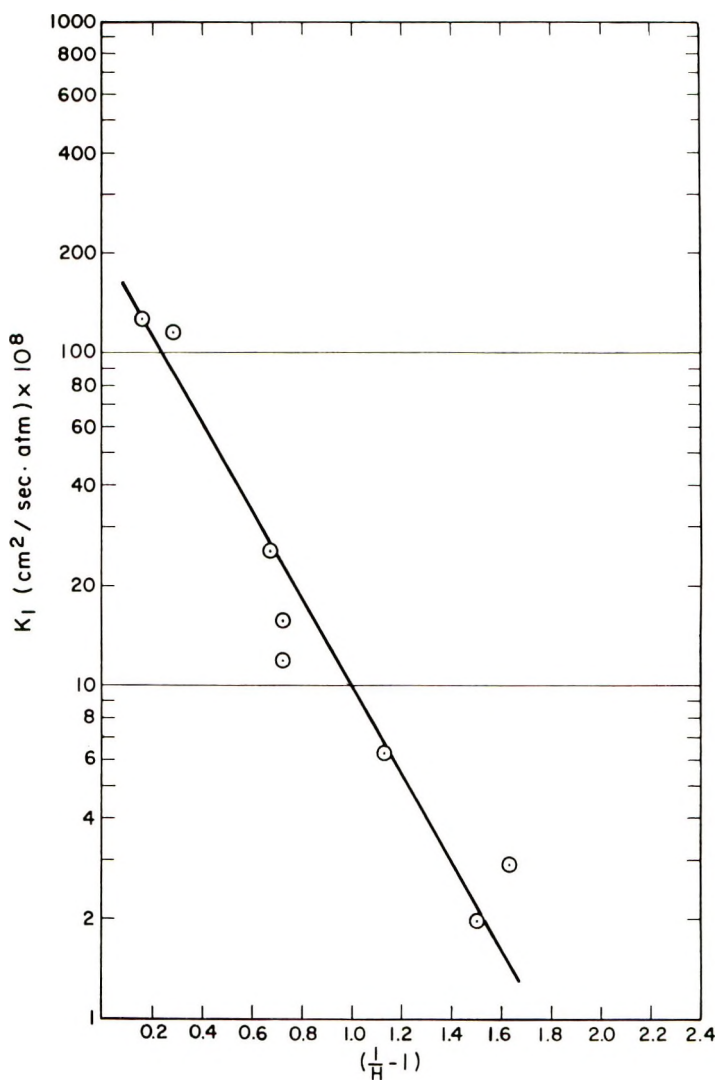


Fig. 1. Dependence of the hydraulic permeability of water K on the parameter $(1-H)/H$ as approximated by eq. (23) for high H .

The diffusive permeability P in the whole range of x can be expressed by eq. (21).

From these observations, it is possible to postulate that in polymer membranes which have H values less than 0.2, i.e. $x > 4$, water permeates predominantly by diffusion. This applies equally when a concentration gradient or a pressure gradient is the driving force.

Since $P = HD$ and D can be described in a satisfactory manner by the free volume concept over the whole range of hydration, it may be worthwhile to examine the experimental data on P and $D = P/H$ in more detail.

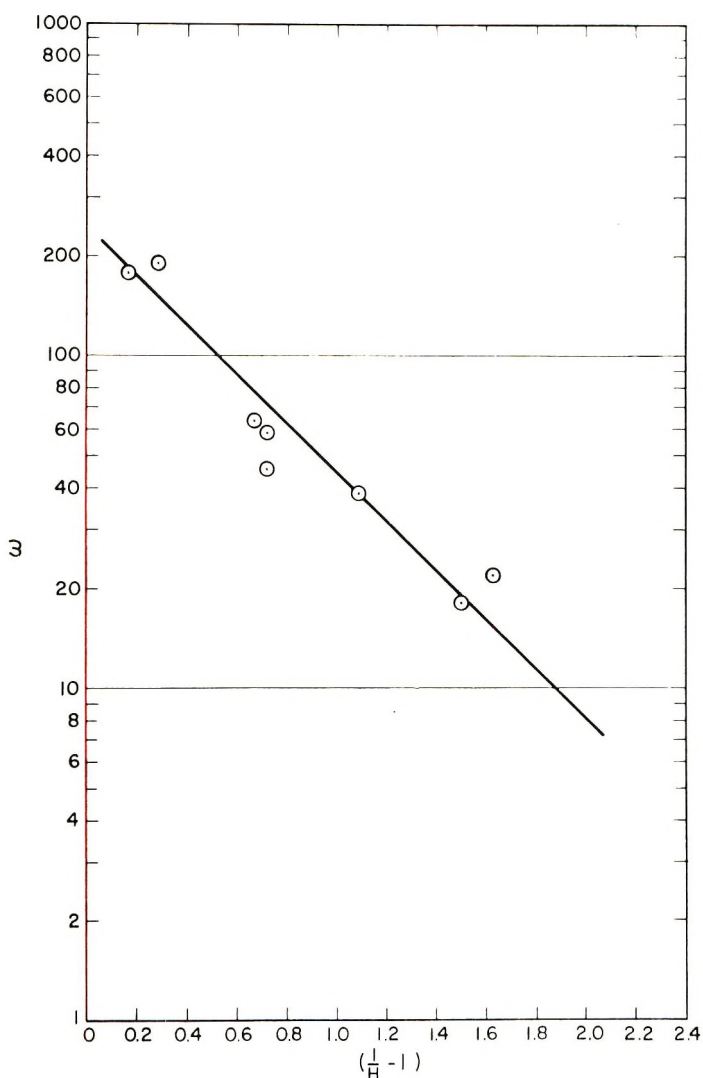


Fig. 2. Dependence of ω at high H on $(1 - H)/H$ as approximated by eq. (24).

On the basis of eq. (19), the parameters α and β can be obtained from the initial slope, a_1 , of a plot of $\ln D/D_0$ versus x and from the asymptotic value, a_2 , of $\ln D/D_0$ at $x = \infty$, which can be best derived from a plot of $\ln D/D_0$ versus H (Fig. 5), i.e.,

$$\alpha = a_1/a_2 \quad (26)$$

$$\beta = a_1 a_2 / (a_2 - a_1) \quad (27)$$

With $D_0 = 2.44 \times 10^{-5}$ cm²/sec at 25°C,¹⁴ $\ln D/D_0$ is plotted against x in Figure 4. From data points for small x , a_1 is estimated as 2.25. From the plot of $\ln D/D_0$ versus H (Fig. 5), the value of a_2 is estimated as 4.5. By

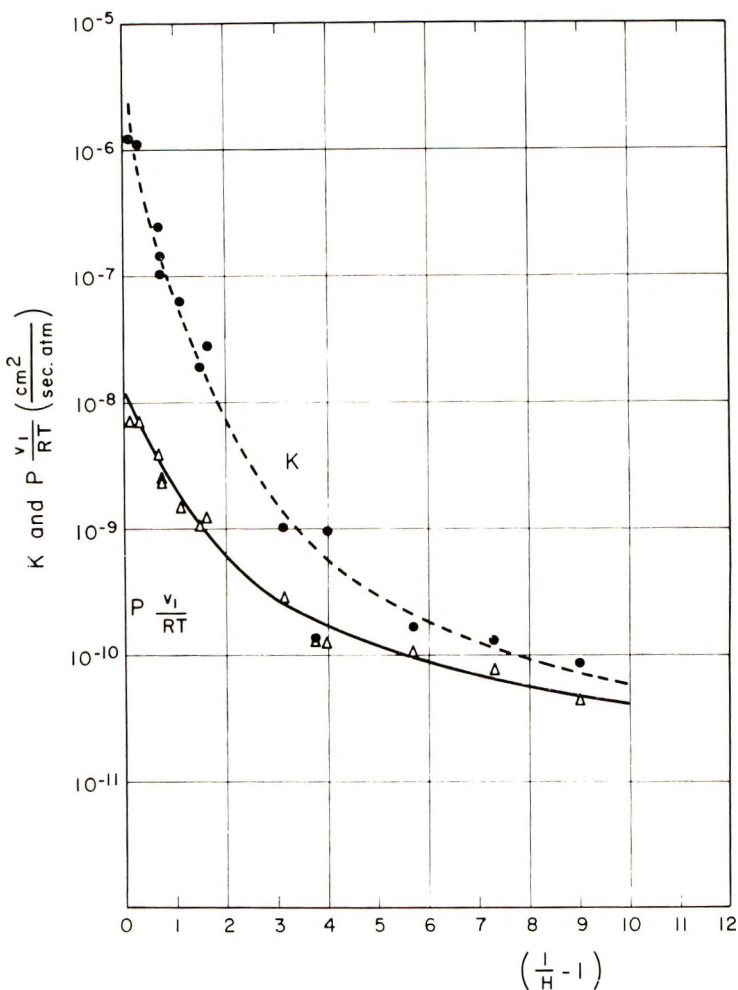


Fig. 3. Dependence of K and Pv_1/RT on $(1 - H)/H$.

using these values, i.e., $\alpha = 0.5 = V_{f,3}^\circ/V_{f,1}^\circ$ and $\beta = 4.5 = V^*/V_{f,1}^\circ$ it is possible for this special case to construct the theoretical curve given by eq. (19) (solid lines in Fig. 4). Within limits of error, it fits the experimental data. It is also possible to construct from this curve the theoretical curve for the diffusive permeability constant $P = HD$ [eq. (21)], which is shown as the solid line in Figure 3.

From Figures 3 and 4, it is quite evident that the diffusion constant and diffusive permeability of water of a membrane in the whole range of hydration from $H = 1$ to $H = 0$ can be indeed described by the equation derived on the basis of the free volume concept of diffusion in membranes [eq. (18)] and on the assumption of additivity of free volume of membrane polymer and hydration water [eq. (12)].

The value of a_2 represents the hypothetical situation of polymer at $H = 0$, i.e., of dry membrane. Since in contact with water every membrane ex-

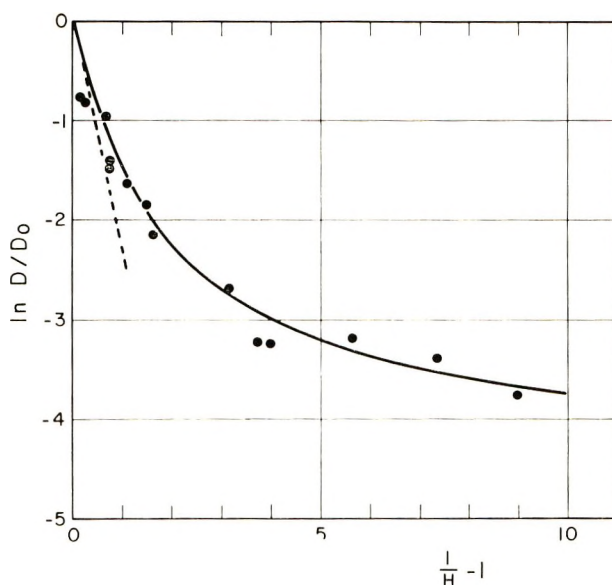


Fig. 4. Plot of $\ln(D/D_0)$ vs. $(1 - H)/H$, where D is the diffusion constant of water through swollen polymer membranes calculated by P/H ; D_0 is the self-diffusion constant of water. The solid line represents calculated values from $\ln D/D_0 = -\beta x(1 - \alpha)/(1 + x\alpha)$ for $\alpha = 0.5$ and $\beta = 4.5$.

hibits finite hydration, the permeability of the dry membrane corresponds better to the case of water vapor permeability at zero activity. It is interesting to note that $a_2 = 4.5$ yields a diffusion constant for dry polymer approximately $1/100$ of D_0 , i.e., in the vicinity of 2×10^{-7} cm^2/sec . Values

TABLE II
Water Permeabilities of Films Studied

Film	K_1 $\text{cm}^2/\text{sec-atm}$	P_1 cm^2/sec $\times 10^7$	$P_1 v_1 / RT$ $\text{cm}^2/\text{sec-atm}$ $\times 10^{10}$	$\omega =$ $K_1 v_1 / P_1 RT$	$(1 - H)/H$
1	1.27×10^{-6}	96.1	70.8	179	0.16
2	1.17×10^{-6}	83.7	61.9	189	0.28
3	2.56×10^{-7}	54.3	39.8	64.3	0.67
4	1.53×10^{-7}	34.7	25.8	59.3	0.72
5	1.96×10^{-8}	15.3	11.0	17.8	1.50
6	2.92×10^{-8}	17.7	13.1	22.3	1.63
7	10.2×10^{-8}	32.3	23.8	42.8	0.72
8	6.26×10^{-8}	22.2	16.2	38.6	1.13
9	1.45×10^{-10}	2.01	1.47	0.99	3.76
10	1.70×10^{-10}	1.49	1.10	1.55	5.66
11	1.43×10^{-11}	0.523	0.386	0.370	99.0
12	10.5×10^{-10}	3.96	2.87	3.32	3.17
13	9.7×10^{-10}	1.89	1.39	6.97	4.00
14	1.48×10^{-10}	0.956	0.705	2.01	7.33
15	0.873×10^{-10}	0.558	0.413	2.11	9.00

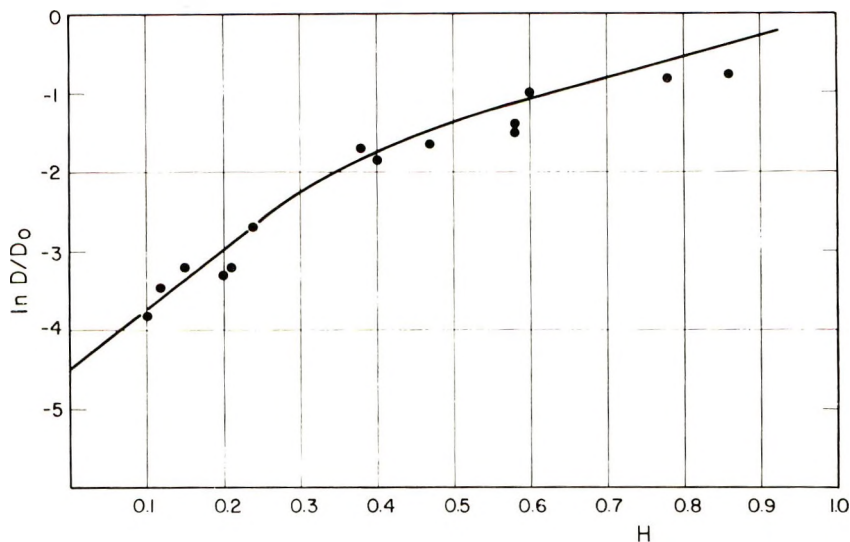


Fig. 5. Plot of $\ln (D/D_0)$ vs. H .

of the diffusion constant in methacrylate polymers and cellulose derivatives at zero water activity are in fact of this order of magnitude.¹⁵

The experimental values of ω show considerable scatter, particularly at high x . This may in part be due to the fact that ω is the ratio of two independent measurements, and also to the ambiguity (due to some possible asymmetry of the membranes) and accuracy of the membrane thickness, ΔX , under the various condition of the measurements. For this reason, the values of ω should not be interpreted too literally within an order of magnitude.

The fact that the ratio ω also follows a dependence on x similar to that of P (see Fig. 4) has the following important implications: (1) the permeability K can be expressed, to a good approximation, by the empirical eq. (23); (2) it is a critical evaluation of appropriateness of the membrane model in interpretation of permeability data. This aspect may be worth further discussion in connection with comparisons of membrane models. In the widely used two-component pore model, an impermeable polymer matrix with a large number of fixed channels or pores traversing the membrane is assumed. Transport, either by diffusion or by flow under a pressure gradient, occurs only in the pores. According to the pore model, the diffusive permeability P depends only on the porosity ϵ , while the hydraulic permeability K depends on ϵr^2 where r is the average radius of the pores, an ill-defined and nonexplicit parameter described as the tortuosity factor being neglected. Therefore, according to the pore model, the ratio K/P is proportional to r^2 . Indeed, the ratio K/P has been used to estimate the pore radius r from this relationship in the literature. If the pore model is correct, ω should show no correlation with ϵ or H , since r and ϵ (or H) cannot be uniquely related. The fact that ω is nearly unity for low H requires a

constant pore radius for all membranes of low hydration, according to the pore model. The dependence of P on H (or ϵ) is in apparent contradiction with the observations. Therefore, additional and not self-evident assumptions are needed for a satisfactory description of experimental data. It is obvious that the pore model of a membrane is a purely mathematical model which can be used only in a qualitative manner to characterize the transport property of a membrane by such terms as pore-size and porosity; and neither the physical picture of the model nor the results (such as pore size) should be interpreted in the physical sense. In this respect, the homogeneous polymer membrane model based on the free volume concept offers a more realistic model for the polymer membranes, and correctly explains without additional assumptions the diffusive permeability in the whole range of P , the identity of K with PV_1/RT at low hydration, and the more rapid increase of the hydraulic permeability at high hydration.

In conclusion, the homogeneous membrane model with the free volume concept of diffusive transport thus excellently explains: the diffusive water permeability P of hydrated membranes over the whole hydration range, the hydraulic permeability K at low hydration, and also gives a qualitatively satisfactory description of the higher values of flow permeability K at high hydration. From the slope of $\log D$ versus x at small x and the limiting value D_∞/D_0 at $x \rightarrow \infty$, one derives the ratios $V^*/V_{f,1}^\circ$, $V_{f,3}^\circ/V_{f,1}^\circ$ and hence $V^*/V_{f,3}^\circ$.

The authors gratefully acknowledge the support of Camille and Henry Dreyfus Foundation and the assistance of Dr. L. D. Ikenberry in the measurement of diffusive permeability of water.

References

1. L. B. Ticknor, *J. Phys. Chem.*, **62**, 1483 (1958).
2. M. L. White, *J. Phys. Chem.*, **64**, 1563 (1960).
3. M. F. Refojo, *J. Appl. Polym. Sci.*, **9**, 3417 (1965).
4. G. Thau, R. Bloch, and O. Kedem, *Desalination*, **1**, 129 (1966).
5. H. Yasuda, A. Peterlin, C. K. Colton, K. A. Smith, and E. W. Merrill, *Makromol. Chem.*, **126**, 177 (1969).
6. H. Yasuda and C. E. Lamaze, *J. Macromol. Sci. (Phys.)* **B5**(1), 111 (1971).
7. W. Jost, *Diffusion*, Academic Press, New York, 1969.
8. M. H. Cohen and D. Turnbull, *J. Chem. Phys.*, **31**, 1164 (1959).
9. A. T. DiBenedetto and D. R. Paul, *J. Polym. Sci. A*, **2**, 1001 (1964).
10. H. Yasuda, C. E. Lamaze, and L. D. Ikenberry, *Makromol. Chem.*, **118**, 19 (1968).
11. H. Yasuda, L. D. Ikenberry, and C. E. Lamaze, *Makromol. Chem.*, **125**, 108 (1969).
12. E. F. Leonard and L. W. Bluemle, *Trans. Amer. Soc. Artificial Internal Organs*, **8**, 182 (1962).
13. H. Yasuda and L. D. Ikenberry, final report to National Institute of Arthritis and Metabolic Diseases—NIH—USDHEW, Contract PII-43-66-547, (1969).
14. J. H. Wang, C. V. Robinson, and I. S. Edelman, *J. Amer. Chem. Soc.*, **75**, 466 (1953).
15. J. A. Barrie, in *Diffusion in Polymers*, J. Crank and G. S. Parks, Eds., Academic Press, New York, 1968, p. 274.

Received June 17, 1970

Revised October 5, 1970

Glass Transition Temperatures of some Linear Polymers Containing Phenyl Side Groups

GIOVANNA PIZZIRANI, PIERLUIGI MAGAGNINI, and PAOLO GIUSTI, *Istituto di Chimica delle Macromolecole del C.N.R., Istituto di Chimica Industriale e Applicata, Facoltà di Ingegneria, Università di Pisa, 56100 Pisa, Italy*

Synopsis

The glass transition temperatures of a number of poly(vinyl phenyl ketones), poly(vinyl benzoates), and poly(phenyl acrylates) have been measured by a refractometric method. The effects exerted on T_g by the nature and position of the ring substituents and by the different groups binding the pendant phenyl rings to the polyvinyl chain are discussed. The importance of knowledge of the side-group motions in the glassy state for the interpretation of glass temperature data is emphasized.

INTRODUCTION

During the past few years a number of attempts have been made to correlate the glass transition temperature T_g of a polymer with its chemical structure. The experimental confirmation of most of these rationalizations is never simple and is often hampered by the lack of sufficient experimental data. An additional difficulty comes from the variety of the experimental methods used to measure T_g . Thus, the data are not easily comparable. From the latter point of view only results obtained by dilatometry or by refractive index-temperature measurements are usually considered satisfactory.

Recently some noteworthy efforts have been made by different authors to provide consistent experimental data on series of homologous polymers. In particular, for polymers containing phenyl side groups, extensive dilatometric and refractometric data are now available. These refer to poly(phenyl acrylates)^{1,2} poly(phenyl methacrylates),¹ poly(vinyl benzoates),³ and polystyrenes.⁴ In addition to the potential usefulness of these data as tools for testing the validity of any theoretical approach to T_g , they lead to definite, if qualitative, conclusions about the influence of different structural features on T_g .

In the present note we discuss results obtained in our laboratory over the last three years on the glass transition of poly(vinyl phenyl ketones), poly(phenyl acrylates), poly(vinyl benzoates), and some related polymers. For the discussion of the results reference is made, in some cases, to the dynamic mechanical behavior of the polymers in the glassy state.

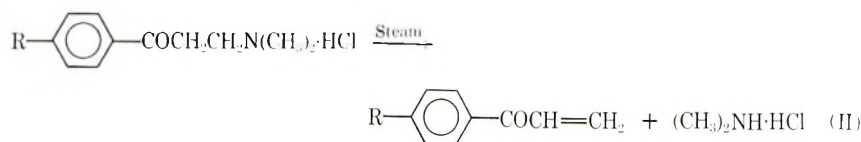
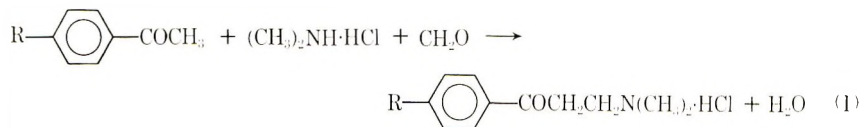
EXPERIMENTAL

Monomers

Vinyl benzoates⁵ and phenyl acrylates⁶ were prepared as described elsewhere.

Vinylphenylketones were obtained by dehydrochlorination of the corresponding β -chloropropiophenones or by decomposition of the Mannich bases, depending on the availability of the starting materials. Thus vinyl phenyl ketone and its *p*-Cl, *p*-*n*-Pr and *p*-*i*-Pr derivatives were obtained by the first route. Benzene (Carlo Erba), chlorobenzene (Carlo Erba), *n*-propylbenzene (Schuchardt), and cumene (Schuchardt) were purified by fractionation and reacted with freshly distilled β -chloropropionyl chloride (Schuchardt) following the procedure of Marvel and Casey.⁷ The resulting β -chloropropiophenones were purified by repeated crystallizations from *n*-hexane and finally dehydrochlorinated to vinyl ketones with potassium acetate in boiling ethanol.

A second amount of vinyl phenyl ketone together with its *p*-Me, *p*-Et, *p*-*tert*-Bu and *p*-Br derivatives was prepared by the second route according to eqs. (1) and (2).



Reaction (1) was accomplished by following the procedure described in the literature.⁸ The products of reaction (1) were purified by crystallization from acetone or diethyl ether and steam-decomposed [eq. (2)].

Phenyl vinyl ketones polymerize very easily even if impure, especially when heated. They were therefore isolated and purified by fractionation under reduced pressure in the presence of inhibitors such as hydroquinone. However, the yields of pure monomers were usually low because of extensive polymerization during fractionation. For this reason we could not isolate an appreciable amount of pure *p*-bromophenyl vinyl ketone.

Vinyl benzoates and phenyl acrylates were also purified by repeated fractionations under reduced pressure.

Solid monomers were further purified by repeated crystallizations from appropriate solvents (usually *n*-hexane) up to constant melting point.

In Table I are given some of the physical properties of the monomers used in the present work. All the monomers but *p*-bromophenyl vinyl ketone were identified through the iodine number and in some cases by elemental analysis, infrared spectroscopy, and molecular weight deter-

mination. The purity of the monomers was checked, just before polymerization, by gas-liquid chromatography (see Table I).

Polymers

All the monomers listed in Table I but *p*-bromophenyl vinyl ketone were polymerized in bulk or in benzene solution either with benzoyl peroxide or thermally (see Table II). In the polymerizations in bulk the monomers were introduced into Pyrex ampoules containing 0.02 mole-% initiator (in some cases no initiator was used). The ampoules were connected through a liquid nitrogen trap to an oil pump. The monomers were thoroughly degassed by repeated freeze-thawing cycles. The ampoules were sealed off and placed in a water bath at the appropriate temperature.

The polymerizations in solution were carried out in stirred flasks immersed in a thermostatic bath, by addition of initiator (0.002 mole/l.) to a solution of the monomer in benzene under dry nitrogen.

Both bulk and solution polymerizations were stopped at 40–60% conversion in order to prevent crosslinking.

The polymers were isolated by repeated precipitation in an excess of methanol or petroleum ether (bp 35–50°C) and dried under vacuum to constant weight.

The sample of poly(*p*-bromophenyl vinylketone) used for T_g determination was obtained by careful purification of the polymer formed during fractionation of the monomer.

Poly(vinyl *m*-nitrobenzoate), poly(vinyl *p*-nitrobenzoate), poly(vinyl nicotinate), and poly(vinyl isonicotinate) were prepared by esterification of commercial poly(vinyl alcohol) (Elvanol 71–30) as previously described.^{9,10}

The molecular weights of the polymers were determined with a high-speed membrane osmometer (Hewlett Packard 501).

Procedure

The glass transition temperatures of the polymers were determined by the refractometric method developed by Wiley¹¹ as already described.³



The determination of the dynamic mechanical properties was carried out by means of a resonance electrostatic method at acoustic frequencies¹² in the temperature range between 80 and 300°K, under high vacuum.

The samples were compression-molded circular plates (36 mm diameter, 3 mm thickness). Measurements were performed on the first flexural mode of vibration.

RESULTS AND DISCUSSION

Table II lists the glass transition temperatures of the polymers and their molecular weights together with the polymerization conditions. Most of the polymers have number-average molecular weights above 40,000. This is the commonly accepted limit above which T_g becomes independent of molecular weight.

TABLE I
Physical Properties of Monomers

Series	R	Bp, °C/mm Hg	n_D^{20}	d_4^{20}	Iodine number		GLC purity, %
					Calcd	Found	
Vinyl phenyl ketones, 	H	53-54/0.6	1.5503	1.044	192.0	189.3	98.7
	<i>p</i> -CH ₃	73/0.6	1.5582	1.017	173.6	172.5	99.2
	<i>p</i> -CH ₂ CH ₃	120/7.0	1.5349	0.976	158.4	157.8	98.5
	<i>p</i> -CH ₂ CH ₂ CH ₃	95-96/0.6	1.5340	—	145.8	146.1	99.4
	<i>p</i> -C(CH ₃) ₂	106/2.6	1.5321	0.985	145.8	143.7	99.2
	<i>p</i> -C(CH ₃) ₃	110/2.6	1.5727	—	135.5	136.2	98.9
	<i>p</i> -Cl	94/1.5	1.5756	1.190	152.2	151.3	99.8
	<i>p</i> -Br	—	—	—	—	—	—
	H	59.5/1.4	1.5215	1.077	171.4	169.7	99.8
	Phenyl acrylates, 	<i>o</i> -CH ₃	60-61/1.0	1.5176	1.049	156.2	154.7
<i>m</i> -CH ₃		70-71/1.5	1.5189	1.049	156.2	159.3	98.1
<i>p</i> -CH ₃		83.5/3.0	1.5187	1.041	156.2	155.1	99.1
<i>o</i> -C(CH ₃) ₃		106-107/3.5	1.4982	1.041	124.1	123.7	97.9
<i>p</i> -C(CH ₃) ₃		97-98/1.3	1.5108	1.006	124.1	124.3	99.8
<i>p</i> -OCH ₃		91-92/1.0	1.5358	1.138	142.6	156.2	98.5

<i>o</i> -Cl	100-101/2.5	1.5312	1.210	139.4	134.7	97.6
<i>p</i> -Cl	101-102/3.5	1.5357	1.215	139.4	137.6	99.2
H	68/2.0	1.5282	1.068	171.3	170.8	99.8
<i>o</i> -CH ₃	67.5/1.1	—	—	156.3	157.1	98.7
<i>m</i> -CH ₃	88/0.6	1.5282	—	156.3	155.8	99.2
<i>p</i> -CH ₃	73/0.8	1.5269	—	153.3	156.2	99.9
<i>p</i> -CH ₂ CH ₃	104-105/0.9	1.5260	1.026	144.0	142.7	99.3
<i>p</i> -CH(CH ₃) ₂	74-75/0.5	1.5205	1.001	132.4	133.1	99.3
<i>p</i> -C(CH ₃) ₃	110-111/2.0	1.5188	1.002	124.2	123.3	99.1
<i>o</i> -OCH ₃	117/8.0	1.5390	1.145	142.4	140.7	98.6
<i>m</i> -OCH ₃	83/0.2	1.5366	1.117	142.4	141.3	99.2
<i>p</i> -OCH ₃	127-128/7.5	58.5 ^a	—	142.4	141.7	99.7
<i>p</i> -OCH ₂ CH ₃	95-96/1.5	1.5409	1.0913	132.0	134.2	99.4
<i>o</i> -OCOCH ₃	117/8	—	—	123.0	119.5	98.2
<i>p</i> -OCOCH ₃	120/1.3	45 ^a	—	123.0	121.2	99.4
<i>p</i> -OCOCH ₂ CH ₃	142-143/3.9	1.5204	1.134	115.2	112.3	98.4
<i>p</i> -OCOCH ₂ CH ₂ CH ₃	152-153/2.1	1.5167	1.109	108.3	112.2	98.7
<i>p</i> -C ₆ H ₅	166/0.3	50.5 ^a	—	113.1	110.6	99.8
<i>o</i> -Cl	74-75/0.6	1.5448	—	138.9	134.7	99.5
<i>m</i> -Cl	84/1.8	—	—	138.9	139.8	99.4
<i>p</i> -Cl	93/4.5	48-49 ^a	—	138.9	137.9	99.6
<i>m</i> -Br	105-106/2.9	1.5651	1.4515	111.8	114.2	98.2
<i>p</i> -Br	100/1.0	58.5 ^a	—	111.8	113.1	99.6

^a Melting point, °C.

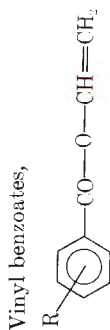
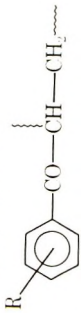
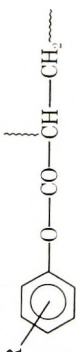



TABLE II
 Glass Temperature Data and Polymerization Conditions

Series	R	T_g , °C	$\bar{M}_n \times 10^{-3}$	Polymerization conditions					
				Solvent	Initiator	Temperature, °C	Time, hr	Conversion, %	
Poly(vinyl ketones), 	H	73.5	83	None	Bz ₂ O ₂	65	2	55	
	<i>p</i> -CH ₃	71	73	None	Bz ₂ O ₂	70	3	45	
	<i>p</i> -CH ₂ CH ₃	51.5	47	None	Bz ₂ O ₂	75	4.5	47	
	<i>p</i> -CH ₂ CH ₂ CH ₃	44	59	None	Bz ₂ O ₂	75	4.5	51	
	<i>p</i> -CH(CH ₃) ₂	62.5	31	None	Bz ₂ O ₂	75	2.5	52	
	<i>p</i> -C(CH ₃) ₃	103.5	46	None	Bz ₂ O ₂	75	2.5	55	
	<i>p</i> -Cl	89	69	None	Bz ₂ O ₂	65	1.5	54	
	<i>p</i> -Br	101.5	75	—	—	—	—	—	
	H	56.5(55) ^a	97	Benzene	Bz ₂ O ₂	60	2	47	
	Poly(phenyl acrylates), 	<i>o</i> -CH ₃	51.5	49	Benzene	Bz ₂ O ₂	60	3.5	55
		<i>m</i> -CH ₃	24.5	38	Benzene	Bz ₂ O ₂	60	3.5	62
		<i>p</i> -CH ₃	42.5	51	Benzene	Bz ₂ O ₂	60	3	42
		<i>o</i> -C(CH ₃) ₃	72	46	Benzene	Bz ₂ O ₂	70	7.5	45
<i>p</i> -C(CH ₃) ₃		71	87	Benzene	Bz ₂ O ₂	60	6	38	
<i>p</i> -OCH ₃		50.5(48) ^a	48	Benzene	Bz ₂ O ₂	60	8	52	
<i>o</i> -Cl		60.5(53) ^a	52	Benzene	Bz ₂ O ₂	75	10	61	
<i>p</i> -Cl	58	83	Benzene	Bz ₂ O ₂	60	7	48		

Poly(vinyl benzoates), R	H	70.5	127	None	80	18	35
							
<i>o</i> -CH ₃		48	118	None	Bz ₂ O ₂	4	52
<i>m</i> -CH ₃		51	87	None	Bz ₂ O ₂	3.5	47
<i>p</i> -CH ₃		70	92	None	Bz ₂ O ₂	3	41
<i>p</i> -CH ₂ CH ₃		52.5	45	None	Bz ₂ O ₂	4.5	55
<i>p</i> -CH(CH ₃) ₂		68.5	41	None	Bz ₂ O ₂	5.5	45
<i>p</i> -C(CH ₃) ₃		101	92	None	Bz ₂ O ₂	4.5	47
<i>o</i> -OCH ₃		65	37	None	Bz ₂ O ₂	7	51
<i>m</i> -OCH ₃		44	27	None	Bz ₂ O ₂	6	49
<i>p</i> -OCH ₃		86.5	108	Benzene	Bz ₂ O ₂	10.5	62
<i>p</i> -OCH ₂ CH ₃		70	47	None	Bz ₂ O ₂	4.5	51
<i>o</i> -OCOCH ₃		59.5	61	None	Bz ₂ O ₂	7.5	41
<i>p</i> -OCOCH ₃		76	36	Benzene	Bz ₂ O ₂	11.5	42
<i>p</i> -OCOCH ₂ CH ₃		71.5	41	None	Bz ₂ O ₂	4.5	37
<i>p</i> -OCOCH ₂ CH ₂ CH ₃		61	143	None	Bz ₂ O ₂	6	35
<i>p</i> -C ₆ H ₅		84.5	32	Benzene	Bz ₂ O ₂	3.5	52
<i>o</i> -Cl		61.5	86	None	Bz ₂ O ₂	2.5	27
<i>m</i> -Cl		64.5	81	None	Bz ₂ O ₂	4	42
<i>p</i> -Cl		83.5	136	Benzene	Bz ₂ O ₂	6.5	55
<i>m</i> -Br		57.5	69	None	Bz ₂ O ₂	7	46
<i>p</i> -Br		92	147	Benzene	Bz ₂ O ₂	8	50
<i>m</i> -NO ₂		93	—	—	—	—	—
<i>p</i> -NO ₂		122	—	—	—	—	—

a Data of Krause et al.¹

For only a few of the polymers listed in Table II were we able to find previously published glass transition temperature data. When available, the values obtained by others by dilatometry have been included in Table II. The discrepancies between our data and those from the literature are fairly small.

The results of Table II allow some qualitative conclusions to be drawn about the dependence of T_g on different structural parameters. These are discussed in the following paragraphs.

Effect of the Nature of the Substituents

It is largely accepted by now that the glass transition temperature of a polymer is strongly influenced by the flexibility, bulkiness, and polarity of the side groups, T_g being the higher the more bulky and polar and the less flexible the side groups are. If we apply this general rule to the substituent groups bonded to the phenyl rings in polymer series such as those of Table II, then our data serve to confirm some of the general statements already set forth by different authors.

Thus an increase of the *para*-substituent flexibility, while accompanied by an increase of its bulk, makes T_g decrease. This pattern is observed in several polymer series picked up from Table II, i.e., poly(vinyl phenyl ketones): *p*-Me (71°C), *p*-Et (51.5°C), *p*-*n*-Pr (44°C); poly(vinyl benzoates): *p*-Me (70°C), *p*-Et (52.5°C); *p*-OMe (86.5°C), *p*-OEt (70°C); *p*-OCOMe (76°C), *p*-OCOEt (71.5°C), *p*-OCOnPr (61°C).

These examples show that this general rule applies not only to alkyl substituents, as already demonstrated for example for polystyrenes,⁴ but also for ether or ester groups.

The effect of flexibility usually exceeds that of bulkiness. This is clearly illustrated also by the following series: poly(vinyl phenyl ketones)

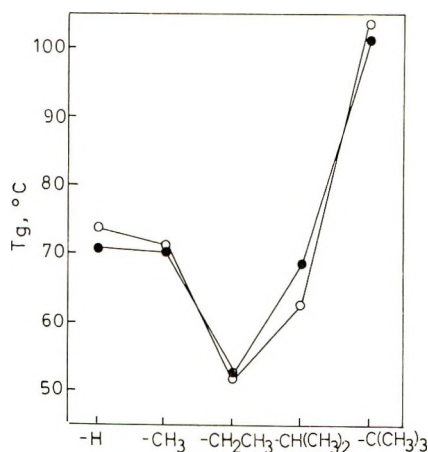


Fig. 1. Glass transition temperature of *para*-substituted poly(vinyl phenyl ketones) (○) and poly(vinyl benzoates) (●).

and poly(vinyl benzoates) substituted with *p*-Me, *p*-Et, *p*-*i*-Pr and *p*-*tert*-Bu groups. Although the bulk of the substituent groups steadily increases throughout the series, in both cases T_g reaches a minimum value for the polymer with the most flexible *para* group (see Fig. 1). When the intrinsic stiffness of the substituent increases (*i*-Pr and *tert*-Bu groups) T_g is strongly enhanced, the effects of bulk and stiffness being now concordant.

Also the effect of the polarity of substituent groups or atoms bonded to the side phenyl rings is clearly illustrated by the data of Table II. Thus Cl-substituted polymers have a higher T_g than Me-substituted ones, whatever the substituent location in the ring. The effect of polarity is also clearly demonstrated by the high T_g of nitrosubstituted poly(vinyl benzoates). The high glass transition temperatures of poly(vinyl nicotinate) (86.5°C) and poly(vinyl isonicotinate) (98.5°C),¹⁰ as compared with that of poly(vinyl benzoate), are also easily explained by the polarity of the pyridine rings.

The above discussion shows that the generally accepted statements concerning the influence of flexibility, bulk, and polarity of side groups on the glass transition temperature of a polymer can be easily applied to the substituents bonded to phenyl rings in the polymer series considered in the present work. Far more complicated is the extension of the same concepts to entire side groups of the same polymers, since this involves understanding of effects of the location of substituents in the phenyl ring and of the nature of the groups binding the phenyl ring to the poly vinyl backbone chain.

Effect of Position of Ring Substituents

As for the effect of the position occupied by ring substituents, it is well known, for example, that for polystyrenes the highest transition temperatures are found in *ortho*-substituted isomers. This has been explained by assuming that the *ortho* substituent raises the intrinsic stiffness of the backbone as does the α -methyl group in poly- α -methylstyrene. However this interpretation has been challenged,¹³ by considering that, for example, *o*-methyl styrene has a normal heat of polymerization whereas α -methyl styrene presents a heat of polymerization which is about half of that for styrene. A more convincing explanation of the high T_g of poly-*o*-methyl styrene is based on the assumption that in this polymer the *o*-Me groups prevent the benzene rings from rotating in the glassy state (see below).

The results of Table II clearly show that the pattern observed for polystyrenes is actually reversed for poly(vinyl benzoates). In the latter class of polymers, in fact, the highest transition temperatures are those of *para*-substituted isomers. A tentative explanation of this discrepancy may be possible through knowledge of the molecular motions of the different polymers below T_g . As already noted, *ortho*-substituted polystyrenes, contrary to *para*-substituted ones, do not show, in the glassy state, relaxation phenomena ascribable to movements of the benzene rings.^{14,15} Contrary to this, Crissman *et al.*¹⁶ found a relaxation effect in poly-*o*-methyl-

styrene with a loss maximum at a somewhat lower temperature than for unsubstituted polystyrene. This result, however, needs confirmation before being accepted since it is difficult to understand why the presence of the *o*-Me group should decrease, rather than increase, the steric hindrance to phenyl motion. Also for *meta*-substituted polystyrenes the dynamic mechanical methods fail to show any sign of movement of the benzene rings (δ relaxation) below T_g .^{14,15}

However the dielectric data of Curtis,¹⁷ who found a low temperature relaxation effect in poly-*m*-chlorostyrene, indicate that in *meta*-substituted polystyrenes the δ relaxation is probably present also but shifted toward higher temperatures. The relevant mechanical damping peak might be therefore completely masked by the exponential part of the loss curve in the vicinity of the glass transition.

Also for poly(vinyl benzoates) a detailed study of dynamic mechanical behavior in the glassy state^{14,18} has shown that a secondary relaxation effect ascribable to motions of the benzene rings is shown by all *para*-substituted derivatives, whereas for *ortho* and *meta* isomers no such phenomenon is observed. However all these polymers show another secondary relaxation in the glassy state (β relaxation) which has been attributed to motions of the carboxyl groups. It seems reasonable to envisage this relaxation effect as being due to a complex motion involving the benzene rings too. If this were so, for poly(vinyl benzoates), the pendant phenyl groups would be allowed to rotate before the glass transition temperature is reached. This might explain why for these polymers *ortho* substitution does not involve enhancement of T_g such as happens for polystyrenes. The higher T_g of *para*-substituted poly(vinyl benzoates) might therefore be explained simply by assuming that the *para* substituents are in the best position for steric and/or polar interference with other macromolecules.

The latter argument was adopted, on the other hand, also by Krause and collaborators¹ in order to explain similar results obtained in studying the glass transition temperatures of *ortho*-, *meta*-, and *para*-substituted carbo-methoxyphenyl and carboethoxyphenyl acrylate polymers.

These facts are however complicated by some of the results obtained by us for substituted poly(phenyl acrylates): the *o*-Me-, *o*-*tert*-Bu-, and *o*-Cl-phenyl acrylate polymers have, in fact, glass transition temperatures which are higher than (or at least of the same order of magnitude as) those of the corresponding *para* isomers (see Table II). This is not easily explicable at present. Our feeling is that schematization of the effect of the position of the substituent groups in the benzene rings upon T_g is never simple, unless we know for any polymer the exact nature and intensity of movements of the side groups below T_g .

Effect of the Groups Binding the Phenyl Rings to the Polyvinyl Chain

Some interesting observations about the effect exerted on T_g by the nature of the groups binding the phenyl rings to the polyvinyl chain can

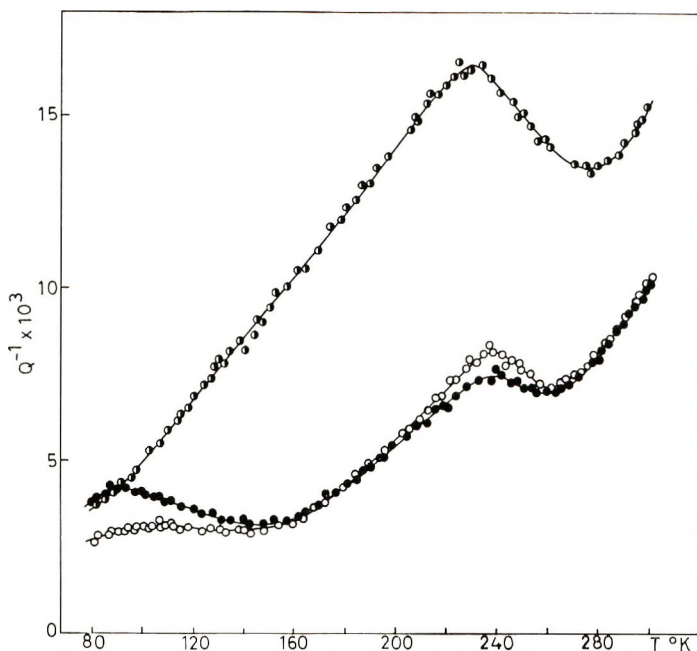


Fig. 2. Damping factor Q^{-1} as a function of absolute temperature for (O) poly(vinyl phenyl ketone), (●) poly(vinyl benzoate), and (◐) poly(phenyl acrylate).

be made by comparing the glass transition temperatures of analogously substituted polymers belonging to different classes.

First of all it must be noted that all the unsubstituted polymers reported in Table II have glass transition temperatures considerably lower than that of unsubstituted polystyrene (ca. 100°C). Krause and collaborators¹ had already shown that a decrease in glass temperature occurs whenever a bulky group, in particular a phenyl group, is moved farther away from the polymer backbone. Thus the introduction of a carbonyl group, as in poly(vinyl phenyl ketone), or of a carboxyl group, as in poly(vinyl benzoate) and poly(phenyl acrylate), between the polyvinyl chain and the benzene rings of polystyrene causes a marked decrease of T_g . This effect can be interpreted as due to a flexibilization of the side groups and to a reduction of the steric hindrance which opposes the segmental cooperative motions of the backbone chain.

It is not, however, immediately obvious why the magnitude of the reduction of T_g is almost equal for poly(vinyl benzoate) and poly(vinyl phenyl ketone) and considerably greater for poly(phenyl acrylate).

Poly(vinyl phenyl ketone) resembles poly(phenyl acrylate) in that both polymers have the carbonyl groups directly bonded to the polyvinyl chain, whereas poly(vinyl phenyl ketone) and poly(vinyl benzoate) are similar in that they both have the carbonyl groups directly bonded to the phenyl rings. Since the latter two polymers have in fact about the same T_g we must conclude that the presence of an oxygen atom between the polyvinyl

chain and carbonyl groups does not play an important role in determining T_g . On the contrary, if the oxygen atom is located between the carbonyl groups and the benzene rings, a noticeable reduction of T_g is observed.

These simple observations lead to the conclusion that the experimental results cannot be interpreted on the basis of the intrinsic stiffness of the backbone chain but are most probably to be connected with the mobility of the side groups in the glassy state. It is in this respect of much help to compare the dynamic mechanical behavior of these three polymers at low temperatures. In Figure 2 the curves of the damping factor Q^{-1} against temperature for poly(vinyl phenyl ketone), poly(vinyl benzoate), and poly(phenyl acrylate) are shown. As already reported,^{14,18} the damping curve of poly(vinyl benzoate) is characterized by the presence of two loss peaks (δ relaxation at 90°K and β relaxation at 230°K) which have been connected with motions of the phenyl groups and of the carboxyl groups, respectively. At higher temperatures, another increase of Q^{-1} is observed which is connected with the onset of the relaxation phenomenon due to the glass transition. The corresponding curve of poly(vinyl phenyl ketone) is indeed very similar. The loss peak at low temperature is not well resolved, but the curve shows with certainty the presence of a weak secondary relaxation, at about 100°K, which can be ascribed to the motion of the phenyl rings (δ relaxation). For this polymer, another damping peak is found at about 235°K and can be associated with motions of the carbonyl groups.

The mechanical behavior of poly(phenyl acrylate) is quite different. For this polymer, in fact, only a very broad peak is observed with a high damping maximum at about 230°K. Most probably this region of high loss is associated with a complex motion of the side chains in which the subgroups (phenyl ring, oxygen, carbonyl) are progressively involved.

Whatever the exact molecular processes connected with the different damping peaks may be, it is important to note here that for poly(phenyl acrylate), in the low-temperature region, the energy dissipated by these processes is much higher than for the other two polymers. This fact may well account for the lower T_g of poly(phenyl acrylate). It is also interesting that the almost exact coincidence of the glass transition temperatures of poly(vinyl benzoate) and poly(vinyl phenyl ketone) matches the very close similarity of the mechanical behavior of these two polymers below T_g .

It is also noteworthy that, as shown in Table II and Figure 1, whatever the nature and the location of the substituents, all the poly(vinyl phenyl ketones) have glass temperatures which are almost identical with those of the corresponding poly(vinyl benzoates).

CONCLUSIONS

The results obtained in the present work confirm some of the general statements already made by others about the dependence of T_g on bulk, stiffness, and polarity of side groups and/or of substituents bonded to side groups. They also show that the glass transition temperature of poly-

styrene (ca. 100°C) is actually reduced considerably when a carbonyl or a carboxyl group is introduced between the backbone chain and the pendant benzene rings. The T_g data of poly(vinyl phenyl ketones) and poly(vinyl benzoates) largely prove that an oxygen atom placed between carbonyl groups and the main chain, has no effect on T_g , nor does it alter appreciably the dynamic mechanical behavior of the polymer in the glassy state. Both a reduction of T_g and an increase of the mechanical energy dissipated by group motions in the glassy state are observed, on the contrary, for poly-(phenyl acrylate) in which the oxygen atom bonds the benzene rings to the carbonyl groups of the macromolecule.

From the above discussion it is also evident that knowledge of the secondary relaxation phenomena occurring in the low temperature region is of great help in the interpretation of T_g data, especially as related to the chemical structure of polymers.

References

1. S. Krause, J. J. Gormley, N. Roman, J. A. Shetter, and W. H. Watanabe, *J. Polym. Sci. A*, **3**, 3573 (1965).
2. G. Pizzirani and P. L. Magagnini, *Chim. Ind. (Milan)*, **50**, 1218 (1968).
3. P. L. Magagnini, *Chim. Ind. (Milan)*, **49**, 1041 (1967).
4. C. G. Overberger, C. Frazier, J. Mandelman, and H. F. Smith, *J. Amer. Chem. Soc.*, **75**, 3326 (1953).
5. G. Pizzirani, *Chim. Ind. (Milan)*, **49**, 1068 (1967).
6. P. L. Magagnini and G. Pizzirani, *Gazz. Chim. Ital.*, **96**, 1035 (1966).
7. C. S. Marvel and D. J. Casey, *J. Org. Chem.*, **24**, 957 (1959).
8. R. Adams, *Organic Reactions*, Wiley, New York, 1947, p. 302.
9. P. L. Magagnini, G. Pizzirani, and S. de Petris, *Chim. Ind. (Milan)*, **49**, 34 (1967).
10. G. Pizzirani and P. L. Magagnini, *J. Appl. Polym. Sci.*, **11**, 1173 (1967).
11. R. H. Wiley, *J. Polym. Sci.*, **2**, 10 (1947).
12. P. G. Bordoni, *Acustica*, **4**, 184 (1954).
13. R. F. Boyer, *Rubber Chem. Technol.*, **36**, 1303 (1963).
14. M. Baccaredda, E. Butta, V. Frosini, and P. L. Magagnini, *J. Polym. Sci. A-2*, **4**, 789 (1966).
15. V. Frosini and P. L. Magagnini, *Europ. Polym. J.*, **2**, 129 (1966).
16. J. M. Crissman, A. E. Woodward, and J. A. Sauer, *J. Polym. Sci. A*, **3**, 2693 (1965).
17. A. J. Curtis, *SPE Trans.*, **2**, 82 (1962).
18. P. L. Magagnini and V. Frosini, *Europ. Polym. J.*, **2**, 139 (1966).

Received October 15, 1970

NOTES

Low-Angle Light-Scattering Equations for Polymer Spherulites

Equations have previously been developed for the intensity of polarized light scattered at low angles by models of two-dimensional and three-dimensional anisotropic polymer spherulites.¹⁻³ Two different derivations have been presented for the three-dimensional case.^{1,2} It has been pointed out⁴ that a sign difference exists in the results of the two methods for the V_v (polarizer and analyzer vertical) equations. We have investigated this matter.

An error in sign was discovered in the original calculations.¹ The sign of the third term in brackets of eqs. (10) and (15) of ref. 1 should be negative. We also have re-derived the equation following the method of van Aartsen² and found no error in his results. The sign was correctly stated in eq. (A-5) of ref. 3, and in ref. 5. The sign discrepancy is thus resolved.

Now, the equations for two-dimensional and three-dimensional spherulites can be cast into similar forms, for the case where β , the angle between the optic axis and the spherulite radius, equals zero:

Two-dimensional

$$E_{V_v} = KA(2/w^2) \cos \rho_1 [(\alpha_r - \alpha_t)J^I + \alpha_t J^{II} - (\alpha_r - \alpha_t) \cos^2 \mu (2J^I - J^{II})] \quad (1)$$

Three-dimensional

$$E_{V_v} = KV(3/U^3) \cos \rho_1 [(\alpha_r - \alpha_t)S^I + \alpha_t S^{II} - (\alpha_r - \alpha_t) \cos^2 \mu (\cos^2 (\theta/2)/\cos \theta)(3S^I - S^{II})] \quad (2)$$

where

$$S^I = SiU - \sin U \quad (3)$$

$$S^{II} = \sin U - U \cos U \quad (4)$$

$$J^I = 1 - J_0(w) \quad (5)$$

$$J^{II} = wJ_1(w) \quad (6)$$

and the other symbols are defined in ref. 3. These equations are approximations valid at small scattering angles. Keijzers, et al.⁵ have presented more complete equations valid for larger angles as well. For the small angles where scattering from spherulites predominates, $\cos^2(\theta/2)/\cos \theta$ is nearly equal to unity and eq. (2) becomes

$$E_{V_v} = KV(3/U^3) \cos \rho_1 [(\alpha_r - \alpha_t)S^I + \alpha_t S^{II} - (\alpha_r - \alpha_t) \cos^2 \mu (3S^I - S^{II})] \quad (7)$$

The similarity in form of eqs. (2) and (7) indicates that, in general, one cannot distinguish between two-dimensional and three-dimensional spherulites by inspection of the light-scattering pattern, if the former lie in a plane normal to the incident beam. However, if one tilted the sample with respect to the incident beam, the pattern would change for two-dimensional spherulites, while remaining unchanged for the three-dimensional case. Further, for randomly oriented two-dimensional spherulites, the (average) pattern would appear different than for three-dimensional ones.

References

1. R. S. Stein and M. B. Rhodes, *J. Appl. Phys.*, **31**, 1873 (1960).
2. J. J. van Aartsen, ONR Technical Report No. 83, Polymer Research Institute, University of Massachusetts (1966).
3. S. Clough, J. J., van Aartsen, and R. S. Stein, *J. Appl. Phys.*, **36**, 3072 (1965).
4. R. Samuels, Amherst Forum on Light Scattering by Solid Polymers, Amherst, Mass., July (1969).
5. A. E. M. Keijzers, J. J. van Aartsen and W. Prins, *J. Amer. Chem. Soc.*, **90**, 3107 (1968).

Department of Chemistry
Lowell Technological Institute
Lowell, Massachusetts 01854

S. B. CLOUGH

Polymer Research Institute
University of Massachusetts
Amherst, Massachusetts 01002

R. S. STEIN
C. PICOT

Received September 11, 1970

Revised November 9, 1970

Configurational Statistics of Polysaccharides. V. Free Rotational Dimensions of (1 \longrightarrow 2')-, (1 \longrightarrow 3')-, and (1 \longrightarrow 4')-Linked Polysaccharides

The stiffness of a polysaccharide chain is often characterized by $\sigma^2 = \langle r^2 \rangle_0 / \langle r^2 \rangle_{0f}$, where $\langle r^2 \rangle_0$ is the unperturbed mean square end-to-end distance and $\langle r^2 \rangle_{0f}$ is that calculated from a model assuming free rotation of the sugar residues about the interunit glycosidic bonds. Benoit¹ first calculated the free-rotational dimension for cellulose, considering the polysaccharide chain having N glucose residues as a chain consisting of $2N$ vectors. These methods were later extended by Eliezer and Hayman² to a general case of (1 \longrightarrow 4')-linked polysaccharides and by Cleland³ to chains of disaccharide units. However, these methods cannot be used to calculate the unperturbed dimensions of hindered polysaccharide chains. Recently we have followed a different approach for calculating the dimensions of both hindered and freely rotating polysaccharides by treating the chain comprising N sugar units as a sequence of N virtual bonds of constant length l_v joining the successive bridge oxygen atoms.⁴⁻⁶ The values of $C_f = \langle r^2 \rangle_{0f} / Nl_v^2$ obtained for (1e \longrightarrow 4'e) (cellulose, xylan, mannan, etc.) and (1a \longrightarrow 4'e) (amylose) types of polysaccharides following the virtual bond treatment are in agreement with the values obtained by the earlier methods.^{1,2}

Recently, when this work was being completed, C_f values, also following the earlier procedures,³ were reported for (1e \longrightarrow 3'e) and (1e \longrightarrow 2'e) types of polysaccharides. However, the available data on these few types of polysaccharides are limited to one or two values of the angle τ at the linking oxygen atom. In view of the observed variation of this angle from 111° to 122°,^{7,8} we undertook a systematic study to compute values of C_f using the "virtual bond" approach for various types of polysaccharides as a function of the τ . Such data not only elucidate the effect of the nature of the linkage on the free-rotation dimensions, but on comparison with the experimental values also furnish information about the stiffness of the various polysaccharide chains.

The monomer residues of all the polysaccharide chains studied in the present work were fixed in the C1(D) chair conformation with the bond lengths and bond angles reported by Hybl et al.,⁹ for all the α -D-sugar residues and the average values reported by Ramachandran et al.¹⁰ for the β -D-sugar residues. The definition of free rotation implies that all the orientations of a sugar residue are equally probable and, as a consequence, the values of the free-rotation dimensions are determined entirely by the geometry of the sugar residue and the mode of linkage and are independent of the nature and orientation of the side groups. Hence the polysaccharides may be classified according to the type of linkage and the spatial disposition of interunit glycosidic bonds by the nomenclature suggested by Sundaralingam,⁷ for the discussion of the free-rotation dimensions.

The general expression for calculating the characteristic ratio of an unperturbed infinitely long polysaccharide chain is given by^{4,6}

$$\langle r^2 \rangle_0 / Nl_v^2 = [(\mathbf{E} + \langle \mathbf{T} \rangle)(\mathbf{E} - \langle \mathbf{T} \rangle)^{-1}]_{22} \quad (1)$$

where $\langle \mathbf{T} \rangle$ is the statistical mechanical average matrix and is expressed as

$$\langle \mathbf{T} \rangle = \frac{\sum_{\phi_i} \sum_{\psi_i} \mathbf{T}_i(\phi_i, \psi_i) \exp \{ -V(\phi_i, \psi_i) / RT \}}{\sum_{\phi_i} \sum_{\psi_i} \exp \{ -V(\phi_i, \psi_i) / RT \}} \quad (2)$$

The various parameters occurring in eqs. (1) and (2) have the significance defined in previous papers.^{4,6}

Since in a freely rotating polysaccharide chain all the orientations of the monomer units are equally probable, the characteristic ratios of such a chain may be calculated by using the eqs. (1) and (2) by giving equal statistical weights to all the conformational states. The values of C_f thus computed for various types of polysaccharides for different values of τ are given in Table I. The C_f values given in column 2 and 5 of Table I

TABLE I
Calculated Values of the Characteristic Ratio C_f
of Freely Rotating Linear Polysaccharide Chains

Type of polysaccharide ^a	Value of C_f for different values of angle τ					
	110°	114°	116°	117.5°	119°	122°
(1e → 4'e)	1.96	2.26	2.44	2.58	2.73	3.07
(1e → 4'a)	1.21	1.25	1.26	1.28	1.29	1.31
(1a → 4'a)	1.61	1.80	1.91	2.00	2.10	2.32
(1a → 4'e)	1.11	1.13	1.14	1.14	1.15	1.16
(1e → 3'e)	1.51	1.62	1.68	1.72	1.76	1.85
(1e → 3'a)	1.38	1.47	1.51	1.54	1.58	1.65
(1a → 3'a)	1	1	1	1	1	1
(1a → 3'e)	1.33	1.41	1.45	1.47	1.51	1.56
(1e → 2'e)	1.17	1.20	1.22	1.23	1.24	1.26
(1e → 2'a)	1.13	1.61	1.17	1.71	1.18	1.19
(1a → 2'a)	1.87	2.15	2.30	2.43	2.57	2.88
(1a → 2'e)	1.16	1.19	1.21	1.21	1.22	1.24

^a The nomenclature has been suggested to distinguish the nature of the glycosidic linkages in carbohydrates.⁷ The equatorial and axial orientations of the glycosidic bonds are denoted e and a, respectively, immediately after the numerals which indicate the type of linkage. For instance, (1a → 4'e) means the orientation of the glycosidic bonds C₁—O and C₄—O in axial and equatorial positions, respectively, in the (1 → 4') linked type.

for the τ angles 110° and 117.5° for the (1e → 4'e), (1e → 4'a), (1a → 4'e), (1a → 4'a), (1e → 3'e), and (1e → 2'e) polysaccharides agree well with the values obtained by the earlier approach.¹⁻³ Table I shows that among (1 → 4')-linked polysaccharides, those having (1e → 4'e) (cellulose, xylan, mannan, etc.) and (1a → 4'a) (pectic acid) linkages have higher values of C_f compared to (1a → 4'e) (amylose) or (1e → 4'a) (*lupinus albus* galactan) types. This indicates that C_f is sensitive to the orientation of the interunit glycosidic bonds. Variations in C_f values are also seen in (1 → 3') and (1 → 2') linkages. In the case of the (1 → 3') linked group of polysaccharides, (1e → 3'e), (1e → 3'a), and (1a → 3'e) types have higher values of C_f than the (1a → 3'a) type has. Similarly, chains with (1a → 2'a) linkages have high values of C_f compared to the others in the (1 → 2') linked group. It is interesting to note that the value of C_f computed for $\tau = 110^\circ$ for several types of polysaccharides varies considerably and the values fall between 1 and 2. This happens because the angle between the virtual bonds varies (even though the angle τ is kept constant) when the pyranose units are rotated about the glycosidic bonds. Thus the chain formed by the virtual bonds tends to attain the character of a freely jointed chain. But the extent to which this angle (between the virtual bonds) varies depends on the nature of the linkage and hence leads to different values of C_f for different types of polysaccharides. In fact, in the case of (1a → 3'a) polysaccharides the angle between the virtual bonds vary to such an extent that the chain formed by joining the virtual bonds attains almost the character of an unhindered statistical chain. Hence the calculated value of C_f is not only unity but also becomes independent of τ . Thus the low values of C_f obtained for $\tau = 110^\circ$ for most of the polysaccharide chains are explained. Table I also shows that an increase in C_f with increase in τ is pronounced in (1e → 4'e), (1a → 4'a), (1e → 3'e), (1e → 3'a), (1a → 3'e), and (1a → 2'a) polysaccharides compared to other types. It is thus shown that free-rotational dimensions of polysaccharide chains depend not only on the nature of glycosidic linkage but also on the value of the bridge oxygen angle. Calculations have also been made on

(1e \rightarrow 4'e), (1a \rightarrow 4'e), (1a \rightarrow 4'a), (1e \rightarrow 3'e), (1a \rightarrow 3'a), (1a \rightarrow 3'e), and (1a \rightarrow 2'a) polysaccharides using both^{9,10} the sets of bond angles and bond distances for fixing the pyranose ring in the C1(D) chair conformation, and the values of C_f evaluated differ only in the second decimal place. This indicates that the slight variations in the bond lengths and bond angles of the sugar residue may not affect the values of C_f significantly.

This work was supported by a grant from the Council of Scientific and Industrial Research.

References

1. H. Benoit, *J. Polym. Sci.*, **3**, 376 (1948).
2. I. Eliezer and H. J. G. Hayman, *J. Polym. Sci.*, **23**, 387 (1957).
3. R. L. Cleland, *Biopolymers*, **9**, 811 (1970).
4. V. S. R. Rao, N. Yathindra, and P. R. Sundararajan, *Biopolymers*, **8**, 325 (1969).
5. N. Yathindra and V. S. R. Rao, *Biopolymers*, **9**, 783 (1970).
6. N. Yathindra and V. S. R. Rao, *Biopolymers*, in press.
7. M. Sundaralingam, *Biopolymers*, **6**, 189 (1968).
8. H. M. Berman, *Acta Cryst.*, **B26**, 290 (1970).
9. A. Hybl, R. E. Rundle, and D. E. Williams, *J. Amer. Chem. Soc.*, **87**, 2779 (1965).
10. G. N. Ramachandran, C. Ramakrishnan, and V. Sasisekharan, in *Aspects of Protein Structure* G. N. Ramachandran, Ed., Academic Press, London, 1963, p. 121.

N. YATHINDRA
V. S. R. RAO

Centre of Advanced Study in Physics
University of Madras
Madras-25, India

Received October 12, 1970

The *Journal of Polymer Science* publishes results of fundamental research in all areas of high polymer chemistry and physics. The *Journal* is selective in accepting contributions on the basis of merit and originality. It is not intended as a repository for unevaluated data. Preference is given to contributions that offer new or more comprehensive concepts, interpretations, experimental approaches, and results. Part A-1 *Polymer Chemistry* is devoted to studies in general polymer chemistry and physical organic chemistry. Contributions in physics and physical chemistry appear in Part A-2 *Polymer Physics*. Contributions may be submitted as full-length papers or as "Notes." Notes are ordinarily to be considered as complete publications of limited scope.

Three copies of every manuscript are required. They may be submitted directly to the editor: For Part A-1, to C. G. Overberger, Department of Chemistry, University of Michigan, Ann Arbor, Michigan 48104; and for Part A-2, to T. G. Fox, Mellon Institute, Pittsburgh, Pennsylvania 15213. Three copies of a short but comprehensive synopsis are required with every paper; no synopsis is needed for notes. Books for review may also be sent to the appropriate editor. Alternatively, manuscripts may be submitted through the Editorial Office, c/o H. Mark, Polytechnic Institute of Brooklyn, 333 Jay Street, Brooklyn, New York 11201. All other correspondence is to be addressed to Periodicals Division, Interscience Publishers, a Division of John Wiley & Sons, Inc., 605 Third Avenue, New York, New York 10016.

Detailed instructions on preparation of manuscripts are given frequently in Parts A-1 and A-2 and may also be obtained from the publisher.

Coming soon from Wiley-Interscience—

The Second Edition of the Most Comprehensive Book in the Field of Polymer Science

TEXTBOOK OF POLYMER SCIENCE

Second Edition

By FRED W. BILLMEYER, JR., *Rensselaer Polytechnic Institute*

In the last 50 years, the field of polymer science has developed into a discipline essential to most aspects of our modern technology. Because this development has been so rapid, it has been difficult for educational systems and texts to keep pace. *Textbook of Polymer Science* was originally published in 1962 to help fill this gap, and this new Second Edition continues to supply up-to-date information on the field.

To up-date the original treatment of the theory and practice of all major phases of polymer science, engineering, and technology, the author has made extensive revisions and additions throughout the entire work.

Part I:

An introduction to concepts and characteristics of macromolecules, Part I now includes material on solubility parameters, free-volume theories of polymer solution thermodynamics, gel-permeation chromatography, vapor-phase osometry, and scanning electron microscopy.

Part II:

The advances gained from new data on the crystalline nature of polymers are now treated in a thorough discussion of the structure and properties of bulk polymers.

Part III:

The format and content of Part III, concerned with polymerization kinetics, have been revised to include recent advances and new references, as well as further data and explanations of recently discovered processes.

Part IV:

The material on commercially important polymers has been rearranged, and now includes information on aromatic heterochain, heterocyclic, ladder, and inorganic polymers.

Part V:

The comprehensive discussion of polymer processing in Part V now includes many new references for plastics, fiber, and elastomer technology.

1971 In Press



WILEY-INTERSCIENCE

a division of JOHN WILEY & SONS, Inc.

605 Third Avenue, New York, New York 10016

In Canada: 22 Worcester Road, Rexdale, Ontario